(1)

FINAL TECHNICAL REPORT

LOW LOSS SUBSTRATES FOR MICROWAVE APPLICATIONS AND SOL-GEL PROCESSING OF SUPERCONDUCTORS

September 1, 1990, to March 31, 1994

Advanced Research Projects Agency

and The Office of Naval Research

Order No. N00014-90-J-4140

L. Eric Cross

Rustum Roy

Amar S. Bhalla

PENNSTATE

1855

THE MATERIALS RESEARCH LABORATORY

UNIVERSITY PARK, PA

FINAL TECHNICAL REPORT

LOW LOSS SUBSTRATES FOR MICROWAVE APPLICATIONS AND SOL-GEL PROCESSING OF SUPERCONDUCTORS

September 1, 1990, to March 31, 1994

Advanced Research Projects Agency
and The Office of Naval Research

Order No. N00014-90-J-4140

L. Eric Cross
Rustum Roy
Amar S. Bhalla

Materials Research Laboratory
The Pennsylvania State University
University Park, PA 16802

ABSTRACT

This document is a final technical report of a research program entitled "Low Loss Substrates for Microwave Applications and Sol-Gel Processing of Superconductors." This program was funded through the Advanced Research Projects Agency and The Office of Naval Research under grant No.: N00014-90-J-4140. The grant was for the period September 1, 1990, through March 31, 1994.

Systematic studies on low κ oxide substrate materials suitable for epitaxial deposition of high Tc superconducting (HTSC) yttrium barium cuprate (YBCO) films and their microwave applications have been carried out. Several promising new hosts such as $Sr(Al_{1/2}Ta_{1/2})O_3$, $Sr(Al_{1/2}Nb_{1/2})O_3$, and $Ba(Mg_{1/3}Ta_{2/3})O_3$ in complex oxide perovskite family have been developed. The crystals of these compositions and their associated solid solutions provide new options for ultra low loss, low permittivity substrates with close structural and thermal properties matching to the YBCO. Studies were extended to the twin free perovskites (e.g., modified complex perovskites) with low congruent melting temperatures and alternative compositions with lower dielectric constants (e.g., in spinel, magnetoplumbite, and fluorite structures).

The unique capabilities of a laser heated pedestal growth (LHPG) system have been utilized for test-growth of candidate materials in single crystal fiber form to determine structure, thermal, and dielectric properties and to make positive identification of twin free systems.

Dielectric properties, thermal expansion coefficients, melting temperatures and growth feasibility were tested for a wide range of substrate materials and solid solutions. This knowledge base is important for the projected work and for the fundamental materials research.

Systematic study on the surface crystallographic compatibility and epitaxial relations with the YBCO provided further guidelines for substrates selection and film deposition design.

Development on the predictive capability of the dielectric constant of ionic solids, by improving ion polarizability additivity model (Shannon's approach), may provide a base for the selection of new compositions for further study.

The unusual concentration of talent in the crystal chemistry of oxide insulators, and particularly in perovskite structure crystals, has been brought to bear upon the problem of devising new alternative compositions and twin free perovskites with low congruent melting temperatures, matching thermal expansion from the YBCO processing temperatures down to the liquid nitrogen working temperature and excellent chemical compatibility. New substrates developed and the technology base built in the program have stimulated collaborations among Penn State and other elements in ARPA superconductor programs. New substrate materials have been transferred to the Rockwell International Science Center for the growth of large single crystals.

This final report summarizes significant results produced from this program through successful combination of our experimental and crystal chemistry approaches in this field.

TABLE OF CONTENTS

LIST OF TABLES

LIST OF APPENDICES

1. INTRODUCTION

This document is a final technical report of a research program entitled "Low Loss Substrates for Microwave Applications and Sol-Gel Processing of Superconductors." This program was funded through the Advanced Research Projects Agency and The Office of Naval Research under grant No.: N00014-90-J-4140. The grant was for the period September 1, 1990 through March 31, 1994.

The focus of this program has been upon developing and identifying new substrate materials with perovskite structures primarily, for the deposition of high Tc superconducting (HTSC) yttrium barium cuprate (YBCO) films, in microwave device applications.

Materials issues on the selection of substrates for depositing HTSC films are addressed from a crystal chemistry point of view and on broad range experimental and theoretical approaches. Crystallographic structures (particularly the selected crystal planes for film deposition), dielectric properties (dielectric constants and loss tangents), thermal expansion coefficients, melting and growth behaviors of a large family of candidate substrate materials are presented in Section 3 and Section 4.

The unique capabilities of a laser heated pedestal growth (LHPG) growth system have been utilized for test-growth of candidate materials in single crystal fiber form to determine structure, thermal, and dielectric properties and make positive identification of twin free systems.

We have found from earlier studies, and from the widespread use of "buffer layers" that simple epitaxy does not explain the widespread occurrence of highly oriented films. Clarification of terminology currently ambiguously used in HTSC film field were given and description can be found in Section 5.1 (and Appendix 1).

It became increasingly clear to us that the demand on the substrates to have a close "lattice match" was in many cases less appropriate. Similarity in structure is a higher

order criterion than simply lattice parameter matching though they are not independent. Crucial effort was conducted to establish the proper links between crystallography, ionic groupings in surfaces and the details of the deposition process which control their oriented overgrowths. This work is addressed in Section 5.2 (and Appendix 2). An ongoing wide range search for new low permittivity candidate materials using the predictive capability of the phenomenological ionic polarizability arguments is briefly described in Section 5.3 (and Appendix 3).

2. TOPICS OF STUDY

The objectives of this investigation includes (i) to screen various complex oxide materials to identify suitable HTSC substrate materials; (ii) to test the feasibility of single crystal growth by utilizing a laser heated pedestal crystal growth (LHPG) technique; and (iii) to "tune" the properties of complex perovskites for substrate applications using crystal chemical skills.

This program explored a wide range of materials, mostly of oxide compounds and solid solutions where the atomic/ionic arrangement in the lattice can be directly related to that of the preferred 'c' face of the YBCO superconductor.

High density ceramics were fabricated to explore bulk properties including dielectric and thermal expansion behavior and to test chemical compatibility with YBCO.

Bulk single crystal and monocrystal fibers of the most promising compositions were grown to determine thermal, chemical and dielectric properties and make positive identification of twin free systems. The laser heated pedestal growth apparatus in MRL permited the growth of crystals of new substrate materials.

2.1 Criteria of Suitable Microwave Substrates

Superconductor device applications demand that the substrate materials for HTSC meet several requirements:

- twin-free single crystal with matching lattice (or matching atomic structure) to the HTSC for oriented or ideal epitaxial films.

- thermal compatibility in terms of thermal expansion matching over the temperature range of film processing and operating (90K to >650^{o}C), no structural phase transition.
- suitable dielectric properties (dielectric constants and loss tangent) at liquid nitrogen temperature and microwave frequency.
- chemically inert: at high deposition temperature and O_2 annealing; high stability over time and in the ambient.
- no cleavage property in the surface plane of interface; mechanically strong and scratch resistant.

In addition to satisfy the general requirements, substrates to be used in microwave devices must be twin-free single crystals with potential to be grown in large size (2-4" wafer). Congruent melting compositions with modest melting temperatures are therefore favorable. The dielectric constant influences the propagation speed and the package dimensions therefore a moderately low dielectric constant (<25) is required. Because the conductor loss of the superconductor is diminished, the role of the dielectric loss becomes critically important. Very low dielectric loss ($<10^{-4}$) is therefore demanded.

The potential application of YBCO superconductor to the development of ultra high density interconnect systems for a new generation of high speed high density multichip modules dictates new requirements for the substrate design. An essential feature is the geometry of the X and Y layers of HTSC lines that must have geometries in cross section of order 2 x 1 μ meters thus necessitating a current carrying capability for the HTSC of ~10^{6} A/cm^{2}. For this current capability clearly the YBCO must be highly grain oriented very near to single crystal, so that the whole multilayer structure is in the form of very highly oriented overgrowths on a single crystal substrate. Impedance characteristics for the interconnect structure dictate that the dielectrics used must be of low permittivity (ideally <10) if the geometry is to be preserved. Highly oriented thin films (2 μm or above) will be needed for the separation of strip line and ground plane

structures. Dielectric loss requirements are a little less stringent than those required for the microwave applications; however, $\tan\delta < 0.001$ is highly desirable at the 77K working temperature.

2.2 Overview of Current Available Substrates

All the currently available substrates present some compromises. $SrTiO_3$ crystals of high quality and large sizes, though they are readily available and yield the best quality epitaxial thin films (primarily due to their close interatomic structure matching to the HTSC), have high dielectric constant (>300) arising from the phase transition near the working temperature (~110K). Al_2O_3 sapphire single crystal substrates, which have low dielectric constant κ and low loss at microwave frequencies, require a buffer layer to avoid chemical interactions with the YBCO. One of the substrates, probably the one most used currently, $LaAlO_3$, though good in lattice matching and of reasonable dielectric properties, is heavily twinned and goes through a ferroelastic phase transition at ~435°C.[1] Table 1 lists some of the most commonly used substrates for comparison purposes.

3. NEW SUBSTRATE MATERIALS: PROCESSING AND CHARACTERIZATION

3.1 New Materials Processing

3.1.1 Solid State Ceramic Synthesis

Ceramic samples were prepared by solid state reaction, using conventional techniques. Calcining and sintering conditions were optimized through the study. Differential thermal analysis (DTA) was used to determine the minimum calcining temperature to achieve the desired phases and to select sintering temperatures. X-ray diffraction was used extensively to characterize the crystallographic phases and to adjust the processing conditions. Ceramic processing parameters are listed in Appendices addressing individual material.

3.1.2 Single Crystal Growth by LHPG Technique

The LHPG technique has several unique features that are of special importance for this program. These advantages include containerless crystal growth and therefore the capability of growing refractory materials (that have low dielectric losses in general); capability of growing both incongruently and congruently melting compositions; and rapid growth rates. Fiber geometry also provides one dimensional dielectric material that may by itself meet microwave antenna requirements for some special device applications.[2]

Table I. Most commonly used high Tc superconductor substrates.

Substrates	Symmetry, Lattice Constants (Å)	Dielectric Constant κ (at RT)	Thermal Expansion α (x10^{-6}/°C)	Comments
$YBa_2Cu_3O_{7-\delta}$	Ortho. a=3.836 b=3.883 c=11.68 (Ref. [3])		α_a=14 α_b=9 α_c=19 (Ref. [4])	
$SrTiO_3$	Cubic a=3.905	>300	10.6	Good epitaxial YBCO film; high dielectric constant
$LaAlO_3$	Rhomb. a=3.789 α=90.12°	23	~10	Structural phase transition at ~435°C; heavy twinning
Al_2O_3	Rhomb. a,b=4.7586 c=12.9897 γ=120°	κ_a=9.34 κ_c=11.54	6	Poor lattice matching; poor thermal expansion matching; chemical interactions with YBCO (buffer layer often required).
MgO	Cubic a=4.2114	9.65	10.4	Reasonable cost; easy to cleave; large lattice mismatching.
YSZ $(Zr_{0.72}Y_{0.28}O_{1.862})$	Cubic a=5.16(2)	26	4.5	Chemical interactions with YBCO, $BaZrO_3$ forms at the interface (buffer layer often required).

The laser heated pedestal growth (LHPG) method has been shown to be a powerful method for rapidly growing small diameter single crystals, particularly oxides of high melting temperature, for both property studies and fiber devices.[5,6] The LHPG equipment used in this investigation consisted of a power source (water cooled, tunable flowing gas CO_2 55W laser), an optical layout, and a growth section. The molten zone temperature during a stable growth was monitored using an optical pyrometer with a linear dimension resolution of 0.1mm. Additional details are provided in Appendices 4 and 5.

3.1.3 Solution Sol-Gel Powder and Thick Film Processing

The solution-sol-gel (SSG) method, which was pioneered at Penn State more than 40 years ago,[7] consists three parts: (i) mixing various components in solution, often with the use of metal organic precursors; (ii) forming a sol and causing it to gel as the key step in the process to retain chemical homogeneity during desiccation; and (iii) shaping during or after gelation into essentially final shape before firing. The atomic scale homogeneity and low temperature processing, besides simplicity and low cost are the major advantages of the SSG method.

Compared to the extensive work on a wide variety of deposition methods employed for oxide superconductors, only a small effort has so far gone into the SSG method for superconducting films.[8,9,10,11] The preliminary results obtained so far are encouraging and further effort is justified.

We have demonstrated in this program that it is possible to grow oriented films of several materials on suitable substrates by this method at very modest temperature. High sinterability and high reproducibility are important for these low κ substrate materials. Wet chemical methods are effective for attaining these characteristics.

By using modified solution sol-gel process SAT, SAN, and BMT thin films and high density ceramics were made and the properties are shown to be very good as suitable material for substrates application.

3.2 Structure and Property Characterization

3.2.1 Crystal Structures and Chemical Composition

Crystallographic structures of new candidate materials were studied extensively by x-ray diffraction.

Crystal quality and twinning were studied using polarized optical microscope and Laue back reflection photography. Scanning electron microscopy was also used for microstructure studies.

Chemical compositions of ceramic and crystal materials were analyzed quantitatively using electron probe micro-analysis (EPMA, CAMECA, SX-50) with spatial resolution of 2μm on the surface area and 0.2μm in depth. Relative analytic accuracy was ±2%.

3.2.2 Dielectric Properties: at Microwave and RF

Radio frequency dielectric constants and the tangent loss were measured using a General Radio 1621 Capacitance Measurement System. Dielectric properties at microwave frequency were measured using resonance techniques equipped with an HP8510A network analyzer. Post resonance technique (the Hakki and Coleman technique) was used to measure the dielectric constants of the ceramic samples. Cavity perturbation technique was used for the measurements on samples of thin rod (e.g., single crystal fiber samples) or bar-shaped. The Q factors (of microwave frequency) at liquid nitrogen temperature were measured by a transmission resonance technique.

Detailed description of dielectric measurement apparatus and methods are included in Appendix 4 (for RF measurement) and Appendices 6, 7, and 8 (for microwave measurement).

3.2.3 Thermal Properties

Thermal property compatibility of the substrates with HTSC films is critical for epitaxial film growth, in terms of determining the deposition and annealing temperatures,

possibility of producing thick films, and reducing the degradation process in films and devices under working conditions.

Thermal expansion coefficients of new substrate materials were measured and compared to the thermal properties of the YBCO superconductor. The measurement was carried out from room temperature up to about 800°C by using a vertical push-rod dilatometer equipped with a high sensitivity linear variable differential transformer (LVDT). The heating and the cooling rates for thermal expansion measurements were regulated at 1 or 1.5°C/min using a microprocessor based temperature controller.

3.2.4 Growth Behavior and Melting Temperatures

The melting point was determined rather simply using a strip furnace, with two operators using two separate optical pyrometers and averaging several readings per sample.

The heating element consisted of a V-shaped ribbon of iridium metal clamped between two water-cooled brass electrical contacts. The current through the strip as controlled by two variable AC transformers connected in a vernier arrangement for better temperature control. The notch of the V acts as a black body cavity.

The samples, after determined to be a single phase by x-ray diffraction, were placed in the notch of the strip in form of small amount of granular powder. The onset of a melting process can be directly observed using optical pyrometer

Growth behavior and the molten zone temperature of a crystal sample during a stable growth by LHPG method were monitored simultaneously using a CCD camera and using an optical pyrometer.

4. WIDE RANGE SEARCHING FOR CANDIDATE MATERIALS

4.1 Complex Oxide Perovskites

The family of substrates with the perovskite structure is most important as those materials are among the most obvious candidates for epitaxial growth of YBCO films. Substrates of perovskite structure usually have the ideal cubic (such as $SrTiO_3$),

double cell cubic (such as Ba_2YSbO_6), hexagonal distorted pseudo cubic (such as $LaAlO_3$) or other pseudo-cubic cells (such as $NdGaO_3$ that has the [$GdFeO_3$] structure with orthorhombic symmetry). $SrTiO_3$ crystals of high quality and large sizes, though are readily available and yield the best epitaxial quality thin films (primarily due to their close interatomic structure matching to the HTSC), have high dielectric constant (>300) arising from the phase transition near the working temperature (~110K). Another probably the most used substrate currently, $LaAlO_3$, though good in lattice matching and of reasonable dielectric properties, is heavily twinned and goes through a ferroelastic phase transition at ~435°C.[12] These macroscopic defects in the crystals are not tolerable in substrates used for complex microcircuits.

4.1.1 $Ba(Mg_{1/3}Ta_{2/3})O_3$ (BMT)

Ceramics of complex perovskite oxides $A(B1_{1/3}B2_{2/3})O_3$ type have been explored previously as the candidate materials with excellent microwave dielectric properties.[13] $Ba(Mg_{1/3}Ta_{2/3})O_3$ (BMT), in particular, was reported to have a dielectric constant κ~25 and dielectric Q~16,800 (one of the highest in the oxide family) at 10.5 GHz, in samples with 1 mol% Mn additive as a sintering aid.[14] BMT compound is one of the most refractory oxides known thus the growth of single crystals is difficult. A single crystal of BMT was grown from a BaF_2 flux. It yielded a significantly higher dielectric constant (~200),[15] presumably attributable to the flux contamination.

BMT single crystal fibers were grown successfully using our LHPG technique. It grows congruently from the melt in the temperature range of 2900-3100°C. A high temperature phase of simple cubic perovskite was obtained at room temperature, in comparison to the hexagonal ordered perovskite structure usually obtained in ceramics. Dielectric properties of both the ceramic and the single crystal BMT were studied. BMT ceramic samples have ultra low dielectric loss (<$1x10^{-5}$ at 90K and 10kHz) and good thermal compatibility (α ~ $9.0x10^{-6}$/°C) with the YBCO superconductors. The single crystal BMT has a cubic lattice parameter a=4.0877Å. The dielectric constant increases and saturates as the bulk density approaches the theoretical density. Dielectric loss reduces with the enhancement of the ordering of the

B-site. Single crystals of high temperature disordered cubic form preserve a moderate dielectric constant (26.0 at 10GHz) and low dielectric loss tanδ (2.78×10^{-4} at room temperature and 10kHz and $<10^{-5}$ at 90K) that make this material unique for microwave device applications.

The BMT lattice parameter of a=4.0877Å, represents a lattice mismatch of 5.3% to the b-axis of YBCO (b=3.883Å); this seems less ideal as a substrate for YBCO. However, there has been no clear cut-off for lattice parameter matches for "epitaxial" (or highly oriented) film deposition of YBCO. "Epitaxial" YBCO thin films on MgO single crystals (with mismatch of 8.5%) have been reported.[16] A BMT single crystal has a twin-free cubic perovskite structure that is advantageous as a substrate compared to some of the heavily twinned substrates, e.g., $LaAlO_3$ and $NdAlO_3$. High temperature BMT single crystal grown by LHPG is twin free, of moderate dielectric constant, low dielectric loss, and good thermal expansion matching and is therefore identified to be a potentially suitable substrate for the HTSC thin film deposition.

Additional details are to be found in Appendix 4.

4.1.2 $Sr(Al_{1/2}Ta_{1/2})O_3$ (SAT) and $Sr(Al_{1/2}Nb_{1/2})O_3$ (SAN)

The compounds of $Sr(Al_{1/2}Ta_{1/2})O_3$ (SAT) and $Sr(Al_{1/2}Nb_{1/2})O_3$ (SAN) were first prepared and tested to learn their crystallographic phases and melting behavior by the group at the AT & T Bell Labs.[17] Ceramic samples were identified to have double cell cubic perovskite structure with a=7.795Å and melting temperatures of 1900°C and 1790°C for SAT and SAN, respectively. On the basis of our understandings of the crystal chemistry-dielectric property relation of various oxide perovskites, and the reports by the Bell Labs group that showed both the SAN and SAT melt congruently and produce a single phase of the perovskite structure after melting, we selected the SAT and SAN as primary candidates in the $A(B1_{1/2}B2_{1/2})O_3$ complex oxide perovskite family for crystal growth and to investigate their properties in relation to substrate applications.

$Sr(Al_{1/2}Ta_{1/2})O_3$ (SAT) and $Sr(Al_{1/2}Nb_{1/2})O_3$ (SAN) are grown using the LHPG growth technique. Their crystallographic structures are found to be simple cubic perovskite

with lattice parameters a=3.8952Å (SAT) and a=3.8995Å (SAN) that are of close lattice matching to the YBCO superconductors. No structural phase transitions or twins have been found and the average coefficients of the thermal expansion are in good matching with the YBCO superconductor materials. SAT currently represents one of the best potential HTSC substrate materials for microwave applications. The unique feature of this material is that it has desired dielectric properties (dielectric κ~12, loss factor $\tan\delta<10^{-4}$) at the microwave frequencies with twin-free lattice and good thermal expansion matching along with chemical compatibility with the YBCO superconductors.

Our experimental results on the SAT composition along with the earlier report on the congruent melting nature of the SAT and SAN compounds, have stimulated research works in the thin film area. MOCVD-derived SAT films grown at 850°C on $LaAlO_3$ were found to have exclusively (001) growth with in-plane orientation.[18] Using SAT polycrystalline materials as targets in a pulsed laser deposition process, Findikoglu *et al* [19,20] have reported high quality epitaxial (c-axis orientation) growth of thin films of SAT and multilayers of YBCO/SAT on (001) $LaAlO_3$ and MgO substrates. Dielectric constants of the SAT films (~100-390nm thick), however, were reported to be ~23-30, notably higher than the value (κ~12) found in bulk ceramic materials. The deviations from perfect cation stoichiometry in films may be one of the causes for the discrepancy in value of the dielectric constants as the Al/Ta ratio in SAT films was found to be ~0.8 rather than the stoichiometric ratio of unity.[12,13] No dielectric loss data has been reported for the SAT films therefore direct comparison between the dielectric constants of the film and that of the bulk SAT sample is not intended.

Additional details are provided in Appendix 5.

4.2 Solid Solution of Ternary and Complex Perovskite Oxides

Further modification of the SAN and SAT compositions has been carried out to fine tune their properties, particularly reducing their melting temperatures (SAT: 1900~(1908±25), and SAN:1790~(1739±10))[17,21] for easier fabrication of the crystals and better control of the reduction problem of the Nb^{5+} and Ta^{5+}. This modification was

also an attempt to overcome the twinning problem and to stabilize the cubic phase at room temperature in $LaAlO_3$ crystals.

$LaAlO_3$ has a rhombohedrally distorted perovskite ($A^{3+}B^{3+}O_3$ type) structure. Although the La^{3+} ion generally prefers the 12-coordination-site, it has a tendency for 9-coordination. The distortion in the LaO_{12} polyhedron is brought about by a slight displacement of the oxygen atoms away from the ideal positions of the cubic perovskite-form, that is more clearly shown in other [rear-earth]$^{3+}AlO_3$ family members when the A-site cation radii become even smaller, e.g., in the case of $PrAlO_3$.[22,23] In fact, no ideal cubic perovskite structure but the rhombohedral [$LaAlO_3$] and the orthorhombic [$GdFeO_3$] structure have been reported in ternary compounds of the $[A]^{3+}[B]^{3+}O_3$ type.[24] For aluminate compounds, rhombohedral symmetry is found when A-site is occupied by the largest A^{3+} cation, La^{3+}, and other $[A]^{3+}[Al]^{3+}O_3$ compounds have even lower symmetry.

Our approach following this direction was to introduce "balanced" cation substitution simultaneously in the A- and B-sites to increase the average cation size at the A-site, hence to stabilize the 12-coordination of that position and consequently the cubic perovskite structure. The solid solution of ternary $LaAlO_3$ and complex oxides of $Sr(Al_{1/2}Ta_{1/2})O_3$ or $Sr(Al_{1/2}Nb_{1/2})O_3$ was chosen for investigation.

Single crystal fibers of modified strontium aluminum tantalum oxide $(1-x)Sr(Al_{1/2}Ta_{1/2})O_3$:$xLaAlO_3$ (SAT:LA) and $(1-x)Sr(Al_{1/2}Ta_{1/2})O_3$:$xNdGaO_3$ (SAT:NG), and modified strontium aluminum niobium oxide $(1-x)Sr(Al_{1/2}Nb_{1/2})O_3$:$xNdGaO_3$ (SAN:NG) and $(1-x)Sr(Al_{1/2}Nb_{1/2})O_3$:$xLaAlO_3$ (SAN:LA) were grown using a laser heated molten zone growth technique.[25] 0.7SAT:0.3LA grows congruently and remains twin free simple cubic perovskite structure (as the SAT) when cooled down to room temperature. 0.7SAT:0.3LA crystals have moderate dielectric constant (κ=21.7) and low dielectric loss ($\tan\delta=7.5\times10^{-5}$) at 10 kHz and 90K. The reduction problem of Ta^{5+} is eliminated (which is common in the case of SAT growth). 0.7SAT:0.3NG and 0.7SAN:0.3NG have lower melting temperatures and crystal growth is easier. $NdGaO_3$ addition to the SAT and SAN enhances the potential of SAT and SAN as large area

substrates for HTSC growth. However, the dielectric constants increased from κ~12 to κ~16 (0.7SAT:0.3NG) and from κ~18 to κ~23 (0.7SAN:0.3NG) as a result of $NdGaO_3$ incorporation.

The ideal cubic perovskite structure can be stabilized in the case of ternary $LaAlO_3$ by forming a crystalline solution composition with cubic $Sr(Al_{1/2}Ta_{1/2})O_3$ and $Sr(Al_{1/2}Nb_{1/2})O_3$. The mechanism of this type of stabilization is through introducing the compensated cation substitution in the form of $[2La^{3+}]+[Al^{3+}] \rightarrow [2A^{2+}]+[B^{5+}]$ with the A^{2+} cation having a radius larger than that of La^{3+} and therefore stabilizing the 12-coordinated A-site. Crystalline solutions of SAT-LA maintained or improved most of the dielectric and thermal properties of $LaAlO_3$ and gained the advantage of forming a twin-free simple cubic structure and improved lattice compatibility. $NdGaO_3$ is shown to be an effective end member to decrease the melting temperature of SAN and SAT without disturbing their simple cubic (twin-free) crystal structure. Dielectric constants of SAN and SAT with addition of the $NdGaO_3$ were increased; however, the dielectric loss factor still remained less than $5x10^{-4}$. The results suggesting that SAT-LA and SAN-LA are better candidates as substrate materials than $LaAlO_3$ because the latter is intrinsically twinned. The growth of SAT-NG and SAN-NG are comparatively convenient as they have relatively low melting temperatures together with the relatively lower dielectric constants and the ideal lattice constants and thermal compatibility with the YBCO superconducting materials.

The property parameters of the newly proposed substrate materials of oxide perovskite family are summarized in Table II. $LaAlO_3$ and $NdGaO_3$ are also listed for comparison.

Further details can be found in Appendix 9.

4.3 Other Families

Works were extended to other substrate candidates such as $La(Mg_{2/3}Ta_{1/3})O_3$,[26] $La(Mg_{1/2}Ti_{1/2})O_3$ (Appendix 10),[27] $(Ca,Sr)(Ga,Nb)O_3$ (Appendix 11)[28] and a family of materials of the magnetoplumbite structures,[29] spinel, gahlinite families, and the fluoride perovskites. It is essential to first prepare high quality ceramics of these

compositions, then to use the LHPG technique to produce single crystal for detailed dielectric, thermal expansion, lattice parameter and optical studies. These crystals, particularly the fluorides and magnetoplumbites and their associated solid solutions provide several new options for ultra low loss, low permittivity, and twin free structures.

Dielectric properties, melting temperatures, and thermal expansion properties a large family of new candidate substrate materials are summarized in Tables III, IV, and V.

Further investigation in these families is in progress under the new ARPA grant.

TABLE II. Properties of Some Newly Proposed Oxide Perovskite Substrate Materials

Compo-sition	symmetry	Lattice Constant (Å)	κ 10kHz 90K	tanδ 10kHz 90K	α ($\times 10^{-6}$/°C) (@~300K)	Melting Point (°C) *
BMT (crystal)	Cubic	4.0877	25.9	$<10^{-5}$	9.0	(>2800)
SAT	Cubic	3.8952	11.8	4.2×10^{-5}	9.7	1908±25
SAN	Cubic	3.8995	18.7	2.2×10^{-4}	8.5	1739±10
SAT-LA	Cubic	3.8727	21.7	7.5×10^{-5}	7.7	1830±22
SAN-LA	Cubic	3.8634	25.7	2.8×10^{-4}	9.5	1705+20
SAT-NG	Cubic	3.8866	16.0	4.3×10^{-4}	8.8	1767±31
SAN-NG	Cubic	3.8790	23.0	5.2×10^{-4}	10.8	1582±20
$LaAlO_3$ (crystal)	Rhomb.	a=3.789 a=90.12°	23	7.5×10^{-5}	8.2//[1$\bar{1}$0] 6.4//[001]	2040±9
$NdGaO_3$ (crystal)	Ortho.	a=5.426 b=5.502 c=7.706	23 (77K,10GHz)	3.2×10^{-4}		1484±24

Table III. DIELECTRIC PROPERTIES OF POTENTIAL SUBSTRATES

Substance	@ 10KHz, 90K	
	κ	D
$LaAlO_3$	21.5	7.47×10^{-5}
$Ba(Mg_{1/3}Ta_{2/3})O_3$		
hot-pressed ceramic	25.0	1.93×10^{-5}
ceramic	24.7	$<1 \times 10^{-5}$
crystal fiber	25.0*	$<1 \times 10^{-5}$
$(Ba_{0.9}Sr_{0.1})(Mg_{1/3}Ta_{2/3})O_3$	26.04	2.34×10^{-4}
$(Ba_{0.8}Sr_{0.2})(Mg_{1/3}Ta_{2/3})O_3$	26.6	1.96×10^{-4}
$MgLaAl_{11}O_{19}$	14.0	1.51×10^{-4}
$MgNdGaAl_{10}O_{19}$	15.6	1.75×10^{-4}
$CaGa_6Al_6O_{19}$	20.9	3.20×10^{-4}
$CaGa_{12}O_{19}$	9.4	1.81×10^{-4}
$Sr(Al_{1/2}Nb_{1/2})O_3$	18.7	2.20×10^{-4}
$Sr(Al_{1/2}Nb_{1/2})O_3$, Sol-Gel	17.2	6.57×10^{-4}
$0.7SAN:0.3LaAlO_3$	25.7	2.79×10^{-4}
$0.7SAN:0.3NdGaO_3$	23.0	5.15×10^{-4}
$Sr(Al_{1/2}Ta_{1/2})O_3$	11.8	4.24×10^{-5}
$Sr(Al_{1/2}Ta_{1/2})O_3$, Sol-Gel	11.5	6.05×10^{-4}
$0.7SAT:0.3LaAlO_3$	21.7	7.47×10^{-5}
$0.7SAT:0.3NdGaO_3$	16.0	4.25×10^{-4}
$1/3SAN:1/3SAT:1/3NdGaO_3$	22.3	5.11×10^{-4}
$La(Mg_{2/3}Ta_{1/3})O_3$	23.4	4.22×10^{-4}
$La(Mg_{1/2}Ti_{1/2})O_3$	27.1	1.82×10^{-4}
$La(Al_{1/4}Mg_{1/2}Ta_{1/4})O_3$	24.1	1.17×10^{-4}
$YBa_2Al_2TaO_9$	11.2	8.33×10^{-4}
$KMgF_3$	5.8	1.65×10^{-4}

Table IV. MELTING TEMPERATURES OF POTENTIAL SUBSTRATES

Composition	M.P. (°C) by Strip Furnace	Molten Zone Temp. (±0.5%) (°C) LHPG
$Ba(Mg_{1/3}Ta_{2/3})O_3$		2912-3155
$LaAlO_3$	2040±9	
$La(Mg_{2/3}Ta_{1/3})O_3$		2035
$La(Mg_{1/2}Ti_{1/2})O_3$	1999±18	2003
$LaAlO_3$:$BaZrO_3$	1965±17*	
$BaSnO_3$	1932±27*	
$SrSnO_3$	1926±12*	
$Sr(Al_{1/2}Ta_{1/2})O_3$	1908±25	2049
$La(Al_{1/2}Ga_{1/2})O_3$	1874±14	
$MgLaAl_{11}O_{19}$		1863
$La(Li_{1/2}Ta_{1/2})O_3$	1831±6	
$MgNdGaAl_{10}O_{19}$		1830

Composition	M.P. (°C) by Strip Furnace	Molten Zone Temp. (±0.5%) (°C) LHPG
0.7SAT:0.3$LaAlO_3$	1830±22	1946
$Gd(Mg_{1/2}Ti_{1/2})O3$	1799±25	
0.7SAT:0.3$NdGaO_3$	1767±31	1832
$Sr(Al_{1/2}Nb_{1/2})O_3$	1739±10	1862
0.7SAN:0.3$LaAlO_3$	1705+20	
$CaGa_6Al_6O_{19}$		1887
$CaGa_{12}O_{19}$		1662
$LaGaO_3$	1659±23	
SAN:0.3$NdGaO_3$	1582±20	1775
$NdGaO_3$	1484±24	
$(Ca_{1/2}Sr_{1/2})$-$(Ga_{1/2}Nb_{1/2})O_3$		1590

Table V. **COEFFICIENTS OF THERMAL EXPANSION MEASURED BY DILATOMETRY TECHNIQUE (RT-800°C)**

(* denotes literature value)

Substance	α (x10^{-6}/°C) (near room temperature)	Substance	α (x10^{-6}/°C) (near room temperature)
*YBC (untwined single crystal at 300K)	14 (α_a) 9 (α_b) 19 (α_c) 42 (α_v)	$Sr(Al_{1/2}Ta_{1/2})O_3$	9.7
		$0.7Sr(Al_{1/2}Ta_{1/2})O_3$: $0.3LaAlO_3$	7.7
YBC ceramic	10.9	$0.7Sr(Al_{1/2}Ta_{1/2})O_3$: $0.3NdGaO_3$	9.0
$LaAlO_3$	6.4 (//[100]) 8.2 (//110)	$NdAlO_3$	7.8
		*SiO_2	0.5
$Ba(Mg_{1/3}Ta_{2/3})O_3$	9.2	*Corning 7059	5
		*YSZ	4.5
$CaGa_6Al_6O_{19}$	7.8	*$SrTiO_3$	10.6
$CaGa_{12}O_{19}$	5.2	*$LaGaO_3$	10.6
$La(Mg_{2/3}Ta_{1/3})O_3$	10.5	*Y_2BaCuO_5	14.3
		*Si	3
$MgLaAl_{11}O_{19}$	9.7	*Sapphire	6
$MgNdGaAl_{10}O_{19}$	7.4	*MgO	10.4
		*$BaTiO_3$	7
$Sr(Al_{1/2}Nb_{1/2})O_3$	8.8		

5. SYSTEMATIC SEARCH FOR CANDIDATE SUBSTRATES

5.1 CLARIFICATION: ORIENTED GROWTH OR EPITAXY

It is obvious from earlier studies, and from the widespread use of "buffer layers" that simple epitaxy does not explain the widespread occurrence of highly oriented films. We believe that a key problem is to establish the proper links between crystallography, ionic groupings in surfaces and the details of the deposition process which control their oriented overgrowths. For the superconductor quality what matters is the quality of the HTSC film, not what it is sitting on. This quality can be quantified in four steps, the first three describing the degree of orientation in none (random-orientation), one (growth direction), or two (in film plane) crystallographic directions. The fourth is the degree of continuity of the film or absence of grain boundaries (i.e., a 100% perfectly oriented set of separated islands with grain boundaries will clearly be considerably poorer than a continuous (single) phase).

We proposed that instead of the term "epitaxial" one should focus only on the degree of orientation and continuity of the "oriented film." The phase immediately contiguous to the film should be designated true substrate. (The so-called buffer layers are the substrates.) Any phase below such a substrate ("buffer layer") is structurally and chemically insignificant (to the YBCO growth), although it may be necessary to obtain the oriented "buffer layer." Such phase should be designated as carriers, not substrates.

Discussions on the approaches to be adapted are provided in Appendix 1.

5.2 SURFACE CRYSTALLOGRAPHIC COMPATIBILITY OF SUBSTRATES

During our ongoing search for microwave device and integrated circuit substrates for HTSC thin films, it became increasingly clear to us that the demand on the substrates to have a close "lattice match" was in many cases more misleading than appropriate. Highly oriented polycrystalline YBCO films (sometimes epitaxial films) have been reportedly deposited on a wide variety of substrates of various symmetries and

structural families, using various deposition techniques. In many cases there involved "misfits" considerably exceeding 15% and often occurred on non-crystalline phases. To gain further insight on the crystallographic interactions of the film and substrate, we felt that there was a need to look into the relation with the substrate structure one step beyond the level of lattice symmetry and structural parameters. The sub-level of a structure that can be precisely quantified are the interatomic distances between the anions (mainly oxygen) and cations and between the anions distributed in the structure. In other words our argument was that any similarity in the periodicity in any lattice planes in the electrostatic charge pattern in any lattice planes in these ionic structure may be significant.

Taking advantages of an available database on the crystallographic structures in our preliminary study, we have examined large number of substrate materials in comparison to the ionic structure of the YBCO. This first approach was from purely the crystallographic point of view without relating to possible chemical interactions (or temperature effects) that may in many cases govern the growth of the film.

The case study on a commonly used buffer layer CeO_2 revealed that not only the bonding length but also the bonding angles on and immediately beneath the contacting surface could be vital for the epitaxial relations found in the buffer-YBCO system. Our investigation also indicated the possible relation of the film orientation with the chemical balance at the nucleation stage.

Complete details on the correlation of surface crystallographic structures with the YBCO are presented in Appendix 2.

5.3 Ion Polarizability Additivity Model: Dielectric Constants Prediction

Recently, Shannon[30] has derived a set of 61 ion dielectric polarizabilities from a least square refinement procedure using the ion additivity rule and calculated dielectric constants for about a hundred compounds in conjunction with the Clausius-Mosotti equation. Excellent agreement between the polarizability values calculated and those

experimentally measured was shown for many ternary systems including borates, aluminates, gallates, silicates, germanates, phosphates, and vanadates.

It is of great interest for us to apply the ion polarizability additivity rule to the family of substrate or potential substrate materials. We have gathered fair amount of dielectric and structural data that were previously unavailable. It is specially interesting to examine if Shannon's model and the ion polarizability data can be used to predict the dielectric constant of new materials and to identify the "abnormal" behavior in a material if present. Comparison of calculated and experimental dielectric constants using the ion polarizability additivity rule can be found in Appendix 3. We found that good agreements are usually seen in cases of substances containing cations having high valence and small sizes, while large discrepancies are common in ternary systems that involve large cations in high coordination sites. Poor agreements are also apparent in materials contains d^0 ions (Nb, Ta) such as $Ba(Mg_{1/3}Ta_{2/3})O_3$, $Sr(Al_{0.5}Ta_{0.5})O_3$, and $Sr(Al_{0.5}Nb_{0.5})O_3$ and cations of rare-earth family such as $LaAlO_3$ and $LaGaO_3$.

The work has already been undertaken to improve the fit to experimental values by taking account of the apparent bonding valence and its correlation to bonding distance in providing a normalized ionic polarizability in a given structural configuration. The method is applicable to oxides, fluorides and oxyfluorides and will provide a base for the selection of new compositions for further study. This modification approach improved the accuracy of dielectric constant prediction significantly particularly for compounds containing d^0 elements, alkali earth elements and rare-earth elements.

6. COLLABORATION AMONG ARPA PROJECTS

A simplified block diagram of the linkages which has been established from the Penn State Program is outlined in Fig. 1. Work addressing bulk single crystal growth has been in close cooperation with Dr. R. R. Neurgaonkar and his team at the Rockwell International Science Center. The laboratory has worked effectively with Rockwell for more than 25 years and communication is excellent. For the film studies we are establishing similar cooperation with The Ceramic Processing Research Laboratory

PENN STATE SUBSTRATE PROGRAM AND ACTIVE INTERACTIONS WITH OTHER ARPA PROGRAMS

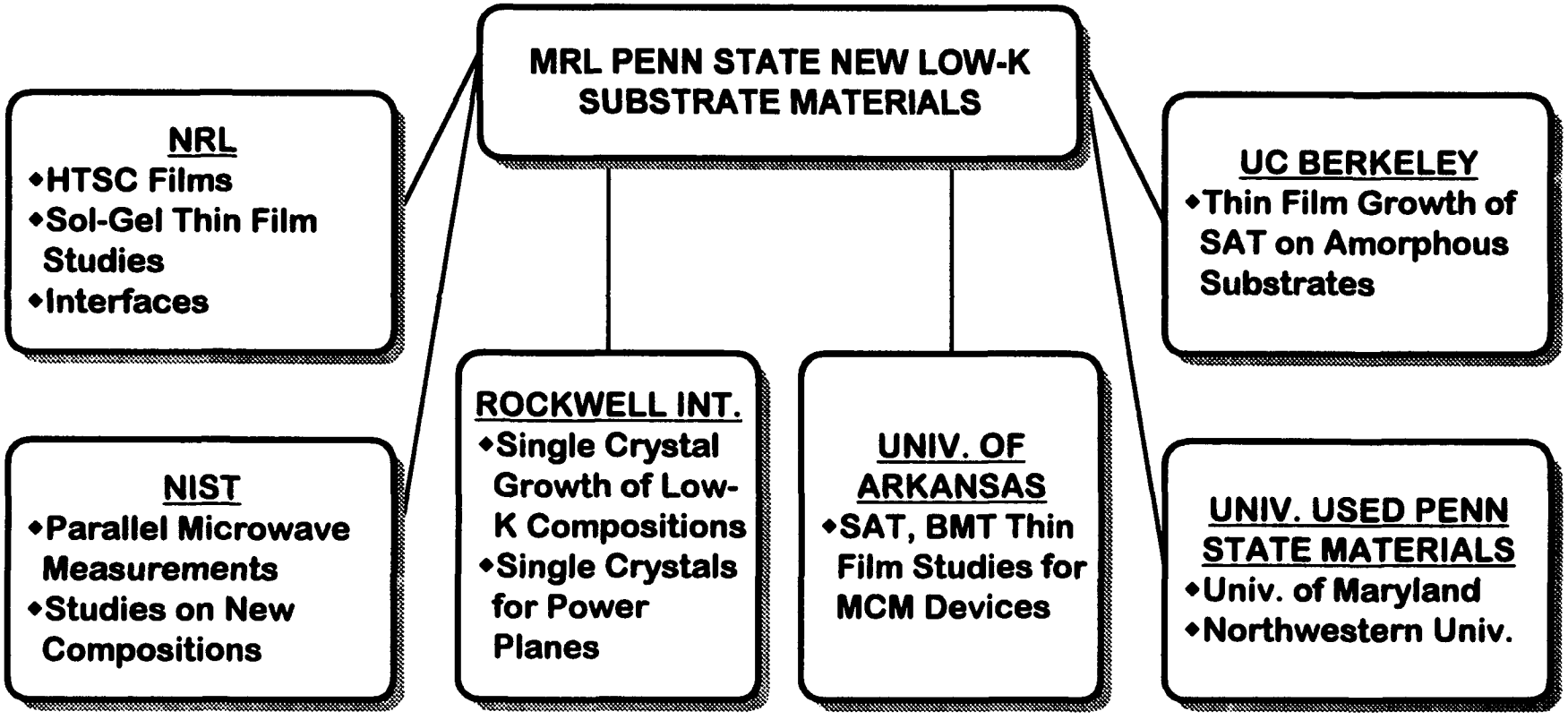

group at MIT (Cima, Sonnenberg, Chang, Ng, McIntyre, Ressler) particularly for orientation and interfacial studies, and with the Berkeley group (R. Russo), Northwestern (Tobin Marks), and Arkansas University (Greg Salamo) for new composition studies in film form.

7. FUTURE DIRECTIONS

New requirements which have emerged during this contract period are concerned with the potential application of YBCO superconductor to the development of ultra high density interconnect systems for a new generation of high speed high density multichip modules. The potential application of YBCO superconductor to the development of ultra high density interconnect systems for a new generation of high speed high density multichip modules dictates new requirements for the substrate design. An essential feature is the geometry of the X and Y layers of HTSC lines that must have geometries in cross section of order 2 x 1 μ meters thus necessitating a current carrying capability for the HTSC of ~10^6 A/cm^2. For this current capability clearly the YBCO must be highly grain oriented very near to single crystal, so that the whole multilayer structure is in the form of very highly oriented overgrowths on a single crystal substrate. Impedance characteristics for the interconnect structure dictate that the dielectrics used must be of low permittivity (ideally <10) if the geometry is to be preserved. Highly oriented thin films (2 μm or above) will be needed for the separation of strip line and ground plane structures. Dielectric loss requirements are a little less stringent than those required for the microwave applications; however, tanδ < 0.001 is highly desirable at the 77K working temperature.

Our future approach will concentrate on meeting these goals. We will improve and revise Shannon's model to take into account the apparent bond valence and its correlation to the bonding distance to derive the "universal" or "normalized" ionic polarizability and compare with the experimentally measured values. Potential dielectric substrate materials can be enlisted. These materials then will be tried for the single crystal growth feasibility study. In our new upgraded LHPG facilities (with CO_2

laser power upto 150W), we should be able to grow the materials (fiber shape) in diameters ranging from a few hundred micrometers to several mm (bulk crystal).

Further development of the surface crystallographic correlation of substrates with HTSC is also intended. Two dimensional relations taking into considerations on both the bonding distances and the bonding angles will be studied in detail for oriented overgrowth.

Films of potential substrates will be tested by using laser ablation to optimize the growth parameters, to study the dielectric properties of the films, the effect of annealing, thermal cycling, interfacial and oxygen diffusion.

We intend to keep active interaction and close collaboration with other elements of ARPA programs and continue to maintain strong standing as a knowledge base in substrate materials science and technology.

8. REFERENCES

[1] E.A. Wood, *Amer. Min.* **36**, 768 (1951).
[2] R.J. Dinger and D.J. White, *IEEE Trans. Antennas Propagat.* **38**(8), 1313 (1990).
[3] W. Wong-Ng, F.W. Gayle, D.L. Kaiser, S.F. Warkins, and F.R. Fronczek, *Phys. Rev. B* **41**(7), 4220 (1990).
[4] Hoydoo You, U. Welp, and Y. Fang, *Phys. Rev.* **B43** (4), 3660 (1991).
[5] J.S. Haggerty, W.P. Menashi and J.F. Wenckus, *Method for Forming Refractory Fibers by Laser Energy*, U.S. Patent 3,944,640, March 16, 1976 and *Apparatus for Forming Refractory Fibers*, U.S. Patent 4,012,213, March 15, 1977.
[6] R.S. Feigelson, *MRS Bull.* **13**, 47 (1988).
[7] R. Roy, Science, 238, 1664 (1987).
[8] S.A. Kremer, G. Kordas, J. McMillan, G.C. Hilton, and D.S. Van Harligen, *Appl. Phys. Lett.*, **53**, 156 (1988).
[9] S.A. Khan, P. Barboux, B.G. Bagley, and J.M. Tarascan, *Appl. Phys. Lett.*, **53**, 700 (1988).
[10] P. Barboux, J.M. Tarascan, L.H. Coreene, G.W. Hull, and B.G. Bagley, *J. Appl. Phys.*, **63**, 2725 (1988).
[11] P. Ravindranathan, S. Komameni, A.S. Bhalla, and R. Roy, Presented at the MRS Meeting, Boston, MA (November 1989).
[12] E.A. Wood, *Amer. Min.* **36** 768 (1951).
[13] K. Wakino, *Ferroelectrics* **91** 69 (1989).
[14] S. Nomura, K. Toyama, and K. Kaneta, *Jpn. J. Appl. Phys.* **21**(10) L624 (1982).
[15] F. Galasso and J. Pinto, *Nature* vol. **207** No. 4992, 70 (1965).
[16] e.g., T. Terashima, K. Iijima, K. Yamamoto, K. Irata, Y. Bando, and T. Takada, *Jpn. J. Appl. Phys.* **28**, L987 (1989).
[17] C.D. Brandle and V.J. Fratello, *J. Mater. Res.* **5**(10), 2160 (1990).

[18] B. Han, D. A. Neumayer, B.H. Goodreau, T. J. Marks, H. Zhang, and V.P. Dravid, *Chem. Mater.* **6**, 18-20 (1994).
[19] A.T. Findikoglu, C. Doughty, S. Bhattacharya, Qi Li, X.X. Xi, T. Venkatesan, R.E. Fahey, A.J. Strauss, and J. M. Phillips, *Appl. Phys. Lett.* **61** 1718 (1992).
[20] A.T. Findikoglu, S. Bhattacharya, C. Doughty, M.S. Pambianchi, Qi Li, X.X. Xi, S.M. Anlage, R.E. Fahey, A.J. Strauss, J.M. Phillips, and T. Venkatesan, *IEEE Trans. Appl. Superconductivity*, **3**(1) 1425 (1993).
[21] R. Guo, A.S. Bhalla, J. Sheen, F. Ainger, E.C. Subbarao, S. Erdei, and L.E. Cross, *J. Mat. Res.* (in press, 1994).
[22] R.D. Burbank, *J. Appl. Cryst.* **3** 112 (1970).
[23] O. Muller and R. Roy, in "*The major ternary structural families*" (Springer-Verlag, Berlin, Heidelberg, New York 1974) p.215.
[24] F.S. Galasso, in "*Structure, properties and preparation of perovskite-type compounds*" (Pergamon Press, Oxford, London, Edinburgh, Now York, Toronto, Sydney, Paris, Braunschweig 1969) p.10.
[25] R. Guo, P. Ravindranathan, U. Selvaraj, A.S. Bhalla, L.E. Cross, and R. Roy, *J. Mater. Sci.* (Oct. 1994).
[26] P. Ravindranathan and A.S. Bhalla *et al.* (to be published).
[27] G. Harshe, A.S. Bhalla, and L.E. Cross, *Materials Letters* **18**(4), 173 (1994)
[28] S. Erdei, L.E. Cross, F.W. Ainger, and A.S. Bhalla, *J. Cryst. Growth* **139**, 54-66 (1994).
[29] R. Guo and A.S. Bhalla (to be published).
[30] R. D. Shannon, *J. Appl. Phys.* **73**(1), 348 (1993).

9. PUBLICATIONS

(1) Jyh Sheen, Ruyan Guo, A.S. Bhalla, and L.E. Cross, "Measurements of Dielectric Constant and Quality Factor of $Ba(Mg_{1/3}Ta_{2/3})O_3$ at X Band Frequencies," *Ferroelectrics Letters* **16** (1/2), 33-41 (1993).

(2) Jyh Sheen, Ruyan Guo, A.S. Bhalla, and L.E. Cross, "Microwave Dielectric Properties Measurements of Potential HTSC Substrate Materials," *Ferroelectrics*, **145**, 15-22 (1993).

(3) Jyh Sheen, "Microwave Dielectric Properties Measurements by Various Resonance Techniques on the Potential Substrate Materials for High Tc Superconductor Thin Films," Ph.D. Thesis, Penn State University (Dec. 1993).

(4) Ruyan Guo, A. S. Bhalla, and L.E. Cross, "$Ba(Mg_{1/3}Ta_{2/3})O_3$ Single Crystal Fiber Grown by Laser Heated Pedestal Growth Technique," *J. Appl. Phys.* **75**(9) 4704-4708 (1994).

(5) Rustum Roy, Ruyan Guo, A.S. Bhalla, and L.E. Cross, "'Oriented Film Growth", Not 'Epitaxy' in HTSC Film Growth," *J. Vac. Sci. Technol. A* **12**(2) 269-273 (1994).

(6) Jyn Sheen, A.S. Bhalla, and L.E. Cross, "A Modification to a Simple Field Model to the $TE_{01\delta}$ Mode of the Parallel-Plate Open Dielectric Resonator," *Microwave and Optical Technology Letters*, **7**(5), 226 (1994).

(7) Ruyan Guo, A.S. Bhalla, L.E. Cross, and Rustum Roy, "Surface Crystallographic Structure Compatibility between Substrates and High Tc (YBCO) Thin Films," *J. Mater. Res.* **9**(7), 1644-1656 (1994).

(8) G. Harshe, A.S. Bhalla, and L.E. Cross, "Synthesis and Dielectric Properties of a Cubic Perovskite Material: $La(Mg_{1/2}Ti_{1/2})O_3$," *Materials Letter* **18**(4), 173 (1994).

(9) Ruyan Guo, P. Ravindranathan, U. Selvaraj, A.S. Bhalla, L.E. Cross, and R. Roy, "Modified Mixed Oxide Perovskite for High Tc Superconductor Substrate Applications," *J. Materials Science* **29**(19) (Oct. 1, 1994).

(10) Ruyan Guo, A.S. Bhalla, R. Roy, and L.E. Cross, "Ion Polarizability Additivity Rule and Its Application on HTSC Substrate Materials," *Ferroelectrics* **155** (1-4) (Proceedings of the Eighth International Meeting on Ferroelectrics), 43-48, (1994).

(11) S. Erdei, L.E. Cross, F.W. Ainger, and A. Bhalla, "Ca-Sr-Ga-Nb Mixed System for HTSC Substrate Applications," *J. Crystal Growth* **139**, 54-66 (1994).

(12) Ruyan Guo, A.S. Bhalla, Rustum Roy and L.E. Cross, "Candidate HTSC Film Substrates of Complex Oxide Perovskite Compositions," *Epitaxial Oxide Thin Films and Heterostructures, Proceedings of the MRS Spring Meeting* SPIE 1994 (Sept. 1994).

(13) Ruyan Guo, J. Sheen, A.S. Bhalla, F.W. Ainger, S. Erdei, E.C. Subbarao, and L.E. Cross, "Strontium Aluminum Tantalum Oxide and Strontium Aluminum Niobium Oxide as Potential Substrates for HTSC Thin Films," *J. Materials Research* (in printing).

(14) P. Ravindranathan, U. Selvaraj, A.S. Bhalla, and L.E. Cross, "Solution Sol-Gel Processing of $Ba(Mg_{1/3}Ta_{2/3})_{1-x}Sn_xO_3$ [x=0.0, 0.2] as Substrates for High Tc Superconductors," *J. Mat. Res.* (to be published).

10. PRESENTATION AT NATIONAL AND INTERNATIONAL MEETINGS

(1) R. Guo, J. Sheen, A.S. Bhalla, F. Ainger, E.C. Subbarao, and L.E. Cross, "Low Loss Single Crystal Fiber Dielectric Substrates of Cubic Perovskites," International Symposium on Application of Ferroelectrics, Aug. 30-Sept. 2, 1992, Greenville, South Carolina.

(2) R. Guo, A.S. Bhalla, L.E. Cross, and Rustum Roy, "Potential Substrates for High Tc Superconductors," The America Ceramic Society 95th Annual Meeting, April 18-22, 1993, Cincinnati, Ohio.

(3) R. Guo and A.S. Bhalla, "Materials of Magnetoplumbite Structure for High Tc Superconductor Substrates," The America Ceramic Society 95th Annual Meeting, April 18-22, 1993, Cincinnati, Ohio.

(4) R. Guo, A.S. Bhalla, L.E. Cross, and Rustum Roy, "Searching Candidate Materials for High Tc Superconductor Thin Film Substrates," The 8th International Meeting on Ferroelectrics, Aug. 1993, Geithersburg, Maryland.

(5) S. Erdei, F.W. Ainger, L.E. Cross, and A. Bhalla, "New Low Melting Oxide Substrate Material For HTSC Applications," Ninth American Conference on Crystal Growth, Aug. 1-6, 1993, Baltimore, Maryland.

(6) G. Harshe, A.S. Bhalla, and L.E. Cross, "Dielectric Properties of a New Perovskite Materials $La(Mg_{1/2}Ti_{1/2})O_3$," The America Ceramic Society 95th Annual Meeting, April 18-22, 1993, Cincinnati, Ohio.

(7) Ruyan Guo, A.S. Bhalla, Rustum Roy and L.E. Cross, "Experimental and Theoretical Approaches for HTSC Substrate Materials," Materials Research Society 1994 Spring Meeting, April 4-8, 1994, San Francisco, California.

(8) (*invited*) A. S. Bhalla, "Structure and Property of Substrate Materials for HTSC Films," World Congress on Superconductivity, June 27-July 1, 1994, Orlando, Florida.

(9) S. Afonso, Y.Q. Tang, K.Y. Chen, G.J. Salamo, F.T. Chan and R. Guo, "$Sr(Al_{.5}Ta_{.5})O_3$ as a New Dielectric Material for YBCO/Dielectric/YBCO Trilayer Thin Films," The American Physical Society Annual Meeting (1994).

(10) Ruyan Guo, A.S. Bhalla, Rustum Roy and L.E. Cross, "Modified Ionic Polarizability Additivity Model and Its Application in Dielectric Property Studies

of Ionic Materials," The Ninth IEEE International Symposium on the Applications of Ferroelectrics, Aug. 7-10, 1994, University Park, Pennsylvania.

(11) Ruyan Guo, A.S. Bhalla, Rustum Roy and L.E. Cross, "Studies of Oxide Crystals for HTSC Film Substrates Microwave Applications," The Ninth IEEE International Symposium on the Applications of Ferroelectrics, Aug. 7-10, 1994, University Park, Pennsylvania.

11. PARTICIPANTS

Name	Status	Remarks
L. Eric Cross	Evan Pugh Professor of Electrical Engineering	Co-PI
Rustum Roy	Evan Pugh Professor of Solid State Science	Co-PI
Amar S. Bhalla	Prof. of Solid State Science & Senior Scientist	Co-PI
Ruyan Guo	Faculty Research Associate	
Jyn Sheen	Research Assistant	Ph.D. (1991-1993)
Sandor Erdei	Faculty Research Associate	
Frank W. Ainger	Senior Scientist	Visiting Faculty
E.C. Subbarao	Senior Scientist and Professor of Materials	Visiting Faculty
P. Ravindranathan	Post-Doctoral Research Associate	(1992-1993)
U. Selvaraj	Post-Doctoral Research Associate	(1992)
Girish Harshe	Post-Doctoral Research Associate	(1993)

12. APPENDICES

Appendix 1.

"'Oriented Film Growth', Not 'Epitaxy' in HTSC Film Growth,"
J. Vac. Sci. Technol. A 12(2) 269-273 (1994).

Rustum Roy
Ruyan Guo
A.S. Bhalla
L.E. Cross

"Oriented film growth," not "epitaxy" in HTSC film growth

Rustum Roy, Ruyan Guo, A. S. Bhalla, and L. E. Cross
Materials Research Laboratory, The Pennsylvania State University, University Park, Pennsylvania 16802

(Received 1 October 1993; accepted 4 December 1993)

A survey of the literature reveals that the following materials have been used as the substrates for "epitaxial" deposition of YBCO high T_c superconducting (HTSC) thin films: $SrTiO_3$, ZrO_2 (or YSZ), MgO, $LaAlO_3$, Si and Al_2O_3 (with or without buffer layers), SiO_2, Pt, $MgAl_2O_4$, even noncrystalline substrates. An analysis of the structural relations between the substrate and HTSC phase is presented. It is obvious that the term "epitaxy" is misapplied in many of these cases. We analyze the evidence for actual crystal structural control from the substrate influencing the oriented growth of the desired phase and find it nonexistent in many cases, very weak in others, and persuasive in a few cases. For the superconductor quality what matters is the quality of the HTSC film, not what it is sitting on. This quality can be quantified in four steps, the first three describing the degree of orientation in none (random-orientation), one (growth direction), or two (in film plane) crystallographic directions. The fourth is the degree of continuity of the film or absence of grain boundaries (i.e., a 100% perfectly oriented set of separated islands with grain boundaries will clearly be considerably poorer than a continuous (single) phase). We propose that instead of the term epitaxial one should focus only on the degree of orientation and continuity of the "oriented film." The phase immediately contiguous to the film (including many so-called buffer layers) should be designated substrate. Any phase below such a substrate is structurally and chemically insignificant (to the YBCO growth), although it may be necessary to obtain the oriented "buffer layer." Such phases should be designated as carriers, not substrates.

I. INTRODUCTION

Due to the high anisotropy of the high T_c superconducting materials and the very short coherence length, randomly oriented polycrystalline samples have very low critical current densities at 77 K and behave even worse when an external magnetic field is applied.[1] In contrast, current densities as high as 10^6 A/cm^2 have been reported in textured thin films that also appeared to a large extent less sensitive to the magnetic fields.[2] A high quality epitaxial high-T_c superconducting (HTSC) film is the mid- or long range goal to realize various device applications, particularly in electronic integration package applications. Excellent properties, such as high J_c, high T_c, less magnetic field dependence, support without deterioration of the further steps in device fabrication process or patterning, and minimal degradation over time and thermal cycle, are likely to be maximized in single crystal films however realized. Therefore a worldwide competition among numerous groups has appeared for controlling the growth of high-quality thin films, using the whole variety of available deposition techniques.[3] High critical current density in "textured" films (i.e., having one crystallographic axis normal to the substrate plane) or, better, in "epitaxial" films (i.e., having their three crystallographic axes related to those of a single crystal substrate) have been obtained. Since the selection of useful substrate materials is clearly of foremost importance in the case of epitaxial growth, the group at the Pennsylvania State University is currently active in searching for ideal substrate materials for epitaxial growth of HTSC films for microwave applications, with the financial support from Defense Advanced Research Projects Agency (DARPA).

Through a survey of the Chemical Abstracts database (from 1987 to August, 1993), we have found a total of 1631 articles including patent applications in the literature describing researches on HTSC films in conjunction with substrate materials. Our particular interests were drawn to the pool of 270 publications in which "epitaxy"(or "epitaxial" HTSC film(s) on specific "substrate(s)" were specified in the title, the key words, or the abstract. We found that a rather large "array" of substrates, listed in Table I, had been used allegedly for epitaxial growth of the HTSC films. However, in most of the cases the term epitaxy appeared to us to have been far too loosely used without adequate experimental evidence. In this article, we attempt to improve the terminology in use.

II. TERMINOLOGICAL CONSIDERATIONS

The term epitaxy does not appear in the index of any of the dozen best known textbooks of crystal physics or crystal chemistry. Since the term was introduced by Royer,[4] it has endured among the small community of crystal growers to mean (loosely) control of the orientation of a growing phase by the crystal structure of a preexisting solid substrate. One outstanding example of genuine ideal epitaxy in modern solid state technology, in the growth of ferrimagnetic garnets by liquid phase epitaxy (LPE), is from a melt using a paramagnetic garnet structure substrate. Here the term epitaxy is universally validated. The garnet structure of the substrate determines the structure and orientation and perfection of the magnetic phase. Of even more general significance is the epitaxial seeding of every single Czochralski pulled crystal. Some hundreds of tons of single crystal quartz are grown homoepitaxially on to oriented single crystal wafers. In the semiconductor world, vapor phase epitaxy of diamond structured phases of varying compositions on to diamond structured substrates of similar composition is universally recognized.

 0734-2101/94/12(2)/269/5/$1.00

TABLE I. Survey result of "epitaxy HTSC films on various substrates" (1987–August 1993).

Number of publications found	Substrates specified
total 270	Epitaxy HTSC film on substrates
17	with buffer layer
69	$SrTiO_3$
47	ZrO_2 or YSZ
57	MgO
45	$LaAlO_3$
35	Si
30	Al_2O_3
6	$MgAl_2O_4$
3	SiO_2
3	Amorphous
1	Pt

When the compositions of the two phases (host and growing phase) are different (albeit sometimes very slightly so), the term heteroepitaxy has come into general use. Thus also for example GaAs may be grown heteroepitaxially on Si: identical crystal orientation but chemically different. But as Fang and Roy[5] pointed out in some cases clearly epitaxial crystals may also be grown when there is little or no resemblance in the bulk crystal structure. Thus Buckley's classic case of growing NH_4I crystals on a mica substrate from aqueous solution are "hetero" concerning both composition and structure. Two explanations accepted for this have been that the K^+–K^+ spacing in the 0001 mica structure are very close to the $(NH_4)^+$–$(NH_4)^+$ spacing in NH_4I. Obviously whatever structural control is exercised on the mica substrate, it can only be from the surface. No three-dimensional crystal structural affinities of any kind exist between the bulk crystal structures of mica and NH_4I. "Epi" means surface and etymologically one need not imply any control other than between the two surfaces.

Since the advent of semiconductor technology and the need to grow crystallographically oriented films on other even noncrystalline substrates the definition of epitaxy has become fuzzier and fuzzier. Givargizov[6] in a book devoted to the subject of epitaxial growth of crystalline semiconductors on amorphous substrates, which may at first appear to be an oxymoron, summarizes the enormously wide range of meanings that have become attached to the term (see Ref. 6, pp. 8, 9). He notes that 3700 epitaxial system pairs are to be found in the 1970 Landolt–Börnstein. He lists six radically different "ideas and manifestations of epitaxy" and comments that: "These regularities in epitaxy being empirical in origin are based mainly on ideas of geometric correspondence on the atomic scale. However many experimental facts in the field of epitaxy cannot be explained in terms of these ideas." His own book is largely concerned with the huge literature on graphoepitaxy on glassy substrates that could fit no chemical or crystallographic control whatever.

A useful summary of traditional structure mediated control is found in Ref. 7. A great deal of the literature is concerned with the detailed, often mathematical models of mechanism of nucleation of the very first few atoms, islands, linear chains (Frank and van de Merwe[8]). As Venables and Price note in Chap. 4 of the Matthews compilation[7] in referring to the applicability of the Stranski–Krastanov (2D and 3D combination[9]): "...there are many unknown features and a quantitative theory has not been given. In particular it is unknown whether nucleation processes within or on top of the first few layers determine the observed structures or whether they are homogeneous or defect-induced." They go on "Little has been done toward a quantitative theory of nucleation at defect sites. ...the variety of possible influences is so vast that a comprehensive treatment would be virtually useless."

This article has a much more limited and modest objective. We attempt herein merely to clarify the net qualitative structural relationships of the deposited bulk (10 nm–10 μm) film to the bulk structure of the nearest neighbor substrate. We do not address the difficult and much studied issues of nucleation of the first few atoms or clusters with <10 nm of the interfaces.

III. CLASSIFICATION OF FILM PERFECTION

It is known that oxide films have a greater propensity for textured growth than those of semiconductors and metals. This may be understood in terms of the strong and directional bonds which oxides make in contrast to covalent or metallic bonds. Hartman and Perdok[10] long ago showed that the morphology of a growing crystal is governed by chains of strong bonds running through the structure. The YBCO film exhibits a strong tendency to orient itself with the c-axis perpendicular to the substrate surface (strong bonds within the plane, weak between planes gives rise to large growth anisotropy), which results in the platy structure of this material. The growth rate within the $a-b$ plane has been observed to be ten times higher than along the c direction.[11] Thus even on any surface, noncrystalline and polycrystalline substrates, a preferred orientation of the c axis perpendicular to the substrate has been observed.[12] A sharp fall off in the critical current was reported for high grain boundary mismatches in the $a-b$ plane of YBCO thin films (angles >10),[13] while textured films with in plane a- and b-axes controls have been reported to have high current density ($J_c \sim 6\times10^5$ A/cm^2, Ref. 14 and $J_c \sim 4.3\times10^5$ A/cm^2, Ref. 15 at 77 K).

To characterize the HTSC properties the information concerning how well oriented the crystallites are with respect to each other is needed. Classification of the perfection of films, we propose, should quantify this degree of orientation. It could consist of four steps. The schematic (simplified) definition of each step is illustrated in Fig. 1. Substrates are defined as the solid immediately underneath the deposited film. The phases may be single crystal isostructural materials, such as $SrTiO_3$ or $LaAlO_3$. They could include the so-called buffer layers such as CeO_2, MgO, and YSZ (whenever used as "buffer"). Crystalline materials supporting a buffer layer but neither structurally nor chemically essential to the film growth are defined to be carriers. Thus the Si or Al_2O_3 wafers used on which the substrate (buffer) layers are applied should be called carriers. Such carrier materials may be necessary to allow oriented films of the substrate layer to be formed and contribute to the dielectric properties of the integrated module. However, the carrier phase does not play any direct role in the orientation of the film. A simple single

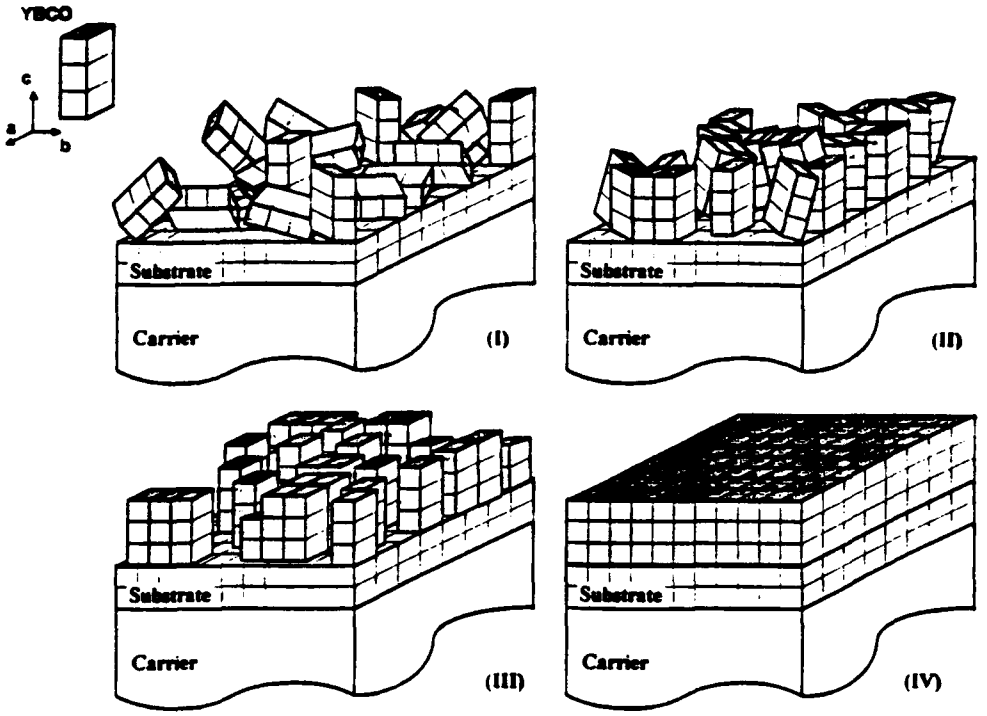

FIG. 1. Illustration of the film classification on basis of orientation and perfection.

layer YBCO unit is shown in the drawings to illustrate the crystallographic relation with the substrate. The substrate shown in Fig. 1 is assumed to be an ideal crystalline single crystal substrate with its (001) plane facilitating the deposition of the film. Films in cases (I), (II), and (III) are all polycrystalline. In Fig. 1 case (I) only randomly oriented (in all directions) assemblies are found in the films. In case (II) we find strong orientation in one dimension (along the film deposition direction). There is no crystalline orientation or correlation within the plane of growth in association with the substrate. Modest misalignment along the growth direction is also shown in this case as is often found in real films. Films of case (II) may be viewed as having (very) high angle grain boundaries that cause drastic degradation of the critical current. Films of case (III) are still polycrystalline. Although the individual grains are very well oriented in both the *c* and the *a*, *b* directions, they are not connected in the plane. Case (IV) is ideal case of (perfect) single crystal film having full in plane alignment together with the formation of a continuous film throughout large areas. The difference between the films of case (III) and case (IV) is very significant in their superconducting properties even though they both have excellent in-plane and out-of-plane orientations. Polycrystalline films (case III) may have considerably higher tolerance for lattice mismatch than single crystal films (case IV) because of the buildup of mismatch over several unit cells. Films of case (III) may also contain mosaic and diverse growth regions and various defects such as cracks, voids, tunnels, growth twins, antiphase boundaries, ferroic twins, steps, and phase or composition deviations. Steps (as shifted fractions of the structural repeat unit) in the *c* direction and the *a* or *b* directions due to nucleations at different contact sections of the unit cell,[16] are also illustrated in the drawing of case (III). Fig. 1. In contrast to this categorization, in the current literature many such oriented films have been ambiguously categorized as epitaxial films.

IV. FILM QUALITY CHARACTERIZATION

Characterization of the film qualities requires various techniques. X-ray (or electron) diffraction is adequate for determining the crystallographic orientation within the film. Randomly oriented films and the one dimensionally oriented films can be distinguished easily in a powder pattern and the orientation direction can be semiquantitatively characterized. Rocking curves are useful to quantify (by detailed comparison of the intensity among diffraction peaks) the level of the one dimensional orientation. Scanning electron microscopy (SEM) is essential to get a gross picture and large angle grain boundaries in the assemblage of crystallites and the continuity or island structure of the film. Images of the electron channeling patterns of the crystallographic microstructure of the film also obtained by SEM can be used to provide more detailed information on orientation relative to the incident beam and to view the high and low angle grain boundaries. The crystallographic information available in the SEM electron channeling pattern is analogous to that which can be obtained by x-ray diffraction of solid specimens with the advantage of the simultaneous combination of imaging and orientation information.

Films of case (II), one dimensionally oriented, and case (III), with in-plane two dimensional orientations added, are, in fact, indistinguishable from standard x-ray diffraction (XRD) data alone, using the Bragg–Brentano usual configu-

ration. To provide additional information about the crystal orientation in its plane parallel to the substrate surface, reflection high energy electron diffraction (RHEED), Rutherford backscattering spectroscopy (RBS) channeling, pole figures, Seeman–Bohlin XRD configurations are required. It has been reported that the use of a standard Weissenberg camera is an efficient, fast, inexpensive, nondestructive, and easy to use method to study the film orientation in its plane.[17] In oscillating photographs, a case (II) film will show diffraction rings, in addition to the reflection spots that indicate a strong c-axis orientation. In contrast, well-defined spots with full alignment of the a- and b-crystal directions of the YBCO unit cell with the unit cell axes of the substrates are to be expected for a case (III) film. The diffraction spots of the film are not broadened when compared to those of the single crystal substrate when the possible misalignments are kept within a fraction of degree. Quantitatively, the a- and b-lattice constants can be calculated using the inter-row distance. Transmission electron microscope (TEM) or high resolution transmission electron microscope (HRTEM) does not serve the purpose of identifying the in-plane orientation well. TEM is most useful for detailed observations of cross sections of the film and the substrate to estimate the degree of epitaxy. A helpful indicator is the FWHM of the rocking curve. Case (III) films (two dimensionally oriented in growth plane and along the growth directions) give the narrowest peaks in XRD (in the order of minutes to seconds of arc). Studying the rocking curves corresponding to the various hkl diffraction may even reflect the quality of the film at various depth thicknesses from the surfaces. In a true three-dimensional film, FWHM for various hkl should correspond to the theoretical calculated values.

All the above techniques used to identify the case (III) film is of course essential for establishing that one has a case (IV) film. To distinguish between true single crystal film and a film formed from a mosaic of small, perfectly aligned single crystals, either optical microscopy or electromagnetic spectroscopy is to be applied. TEM needs the destruction of the film and could induce some cracks related to interfacial strain relief or some related surface modifications during specimen preparation, and therefore is not recommended. SEM and optical microscopy analysis on films of etched surfaces can provide images of the grain distribution and perfection of a film. Finally, the superconductor properties (such as high critical current density) are themselves the best correlate of film quality, which reflect the degree of continuity of orientation in three directions.

Table II summarizes the film perfection classification and the techniques required to adequately characterize the films. The suggested techniques are the most commonly used among other techniques though the classification is clearly different from other schemes used in today's literature.

TABLE II. Classification and characterization techniques for oriented HTSC film growth.

Film classification on basis of orientation	Characterization technique
(I) Polycrystalline Random orientation	XRD J_c measurement
(II) Polycrystalline One-dimensional orientation//(growth direction) (No in-plane orientation)	XRD SEM channeling J_c measurement
(III) Polycrystalline Two (or three) in-plane and in growth directions orientation (Not continuous)	Rocking curve Pole figure RBS channeling Weissenberg camera SEM channeling J_c measurement
(IV) Single crystal Three-dimensional orientation and continuous film	(All the above in (III)) Optical microscopy SEM J_c measurement

V. CONCLUDING REMARKS

Our reconsideration of terminology used to describe HTSC films suggests that the term epitaxy be abandoned in general, since it is usually unproved and in any case of no value. The film grower is interested in the quality of the film produced. Is it a true single crystal? Or is it highly oriented in two, or (only) in one dimension, or none? That is the salient parameter for HTSC properties. We recommend that the term substrate (especially epitaxial substrate) always be used to designate only the solid phase immediately contiguous to the film. Any solid phase below that should be designated as the (substrate) carrier phase. There is no doubt considerable empirical value in designating which carriers provide for the creation of particular substrates. The structural relationship of film to the substrate is of seemly value. It is usually unknown. And even the extremely tedious and costly cross-section TEM cannot provide any definitive answer on the quality of the large area film, by establishing any crystallographic relation between substrate and film. Hence our recommendation that the phenomenon being studied be called generically oriented film growth. The film can then be categorized successfully as to degree of orientation (in polycrystalline films) in none (random), one, and two dimensions, or as truly single crystal with continuous perfection.

ACKNOWLEDGMENT

This work was supported by the Defense Advanced Research Projects Agency (DARPA) under the Contract No. DN 00014-90-J-4140.

[1] J. W. Ekin, A. J. Panson, A. I. Braginski, M. A. Janocke, M. Hong, J. Kwo, S. H. Liou, D. W. Capone II, and B. Flandermeyer, *Proceedings of Symposium S, 1987 Spring Meeting of the Materials Research Society*, Anaheim, CA, April, 1987, edited by D. U. Gubser and M. Schluter (Materials Research Society, Pittsburgh, PA, 1987), p. 223.
[2] H. Isozaki, S. Tanaka, K. Higaki, and S. Yazu, Phys. C 1155, 153 (1988).
[3] A. Perrin and M. Sergent, *Studies of High Temperature Superconductors*, edited by A. Narlikar (Nova Science, New York, 1991), Vol. 7.
[4] L. Royer, Bull. Soc. Fr. Mineral. Cryst. 51, 7 (1928).
[5] C. S. Fang and Rustum Roy, J. Cryst. Growth 60, 182 (1982).
[6] E. I. Givargizov, *Oriented Crystallization on Amorphous Substrates* (Plenum, New York, 1991).
[7] *Epitaxial Growth part A and B*, edited by J. W. Matthews (Academic, New York, 1975).

[8]F. C. Frank and J. H. van der Merwe. Proc. R. Soc. London Ser. A 198. 216 (1949).
[9]I. N. Stranski and L. Krastanov. Acad. Math.-Nat. KIIIb. Deut. 146. 797 (1938).
[10]P. Hartman and W. G. Perdok. Acta Crystallogr. 8. 49 (1955).
[11]C. W. Nieh. L. Anthony. J. Y. Josefowicz. and F. G. Krajenbrink. Appl. Phys. Lett. 56. 2138 (1990).
[12]D. P. Norton. D. H. Lowndes. J. D. Budai. D. K. Christen. E. C. Jones. J. W. McCamy. T. D. Ketcham. D. St. Julien. K. W. Lay. and J. E. Tkaczyk. J. Appl. Phys. 68. 223 (1990).
[13]D. Dimos. P. Chaudhari. F. K. Mannhart. and LeGoves. Phys. Rev. Lett. 61. 219 (1988).
[14]R. E. Russo. presented at the HTS Materials Research Meeting. Falls Church. VA. March 1993 (unpublished).
[15]Y. Iijima. K. Onabe. N. Futaki. N. Tanabe. N. Sadakata. O. Kohno. and Y. Ikeno. IEEE Trans. Appl. Supercond. AS-3. 1510 (1993).
[16]R. Guo. A. S. Bhalla. L. E. Cross. and Rustum Roy. J. Mater. Res. (in press).
[17]A. Perrin. M. G. Karkut. M. Guilloux-Viry. and M. Sergent. Appl. Phys. Lett. 58. 412 (1991).

Appendix 2.

"Surface Crystallographic Structure Compatibility between Substrates and High Tc (YBCO) Thin Films,"

J. Mater. Res. 9(7), 1644-1656 (1994).

Ruyan Guo

A.S. Bhalla

L.E. Cross

Rustum Roy

Surface crystallographic structure compatibility between substrates and high T_c (YBCO) thin films

Ruyan Guo, A. S. Bhalla, L. E. Cross, and Rustum Roy
Materials Research Laboratory, The Pennsylvania State University, University Park, Pennsylvania 16802

(Received 30 September 1993; accepted 24 March 1994)

A review and some case studies on the interatomic distances of candidate substrates in comparison to the high T_c superconductor (HTSC) phase $YBa_2Cu_3O_{7-\delta}$ (YBCO) is presented, in an attempt to enhance the basis for substrate selection for YBCO film epitaxy. This preliminary study was carried out by examining a variety of interatomic distances in the structure rather than merely matching the lattice parameters. Interatomic structure matching planes of selected YBCO orientations in contact with substrates were identified. The surface termination of the substrate was found to be a crucial parameter in determining the oriented or epitaxial growth. Possible composition dependence of the orientation of the films at the nucleation stage was also anticipated depending on the comparison. Several currently most commonly used substrates are discussed in some detail.

I. INTRODUCTION

There is great interest worldwide in many research groups focused on growing high quality thin films of high T_c superconductors (HTSC), using a whole variety of available deposition techniques. The selection of useful substrate materials is of first importance and is subjected to a number of constraints such as thermal and chemical stability under the conditions used in the film process and use, reasonable lattice constant matching, thermal compatibility in terms of thermal expansion matching over the temperature range of film processing and annealing down to the operating temperature (90 K), physical properties (for instance, the dielectric constant and loss) suitable for specific use, commercial availability, and, if possible, low cost. An enormously valuable and comprehensive survey of recent experimental work has been provided by Perrin and Sergent.[1]

In the general case most such films are referred to as "epitaxial films." It is arguable that this term is misapplied in many cases.[2] The understanding of the term epitaxy has come a long way, and detailed crystallographic guidelines for successful epitaxy are still to be sorted out. At the beginning of this century, without the help of x-ray diffraction, scientists knew that epitaxy was more likely to occur if the molecular volumes of the two intergrowing alkali halides were nearly equal (i.e., low misfit).[3] The discovery of x-ray diffraction made it possible to examine the effect of the geometry of crystal structure on the phenomenon. It was found largely for growth from liquid solutions that "epitaxy" (oriented growth) occurs only when it involves the parallelism of two lattice planes that have networks of identical or quasi-identical structure and of closely similar spacing.[4] The experiments indicated that epitaxy occurs only if the "misfit" between "lattices" of substrate and growing phase is no more than about 15%.[4] This vague belief about epitaxy remains prominent to this day. A classic introduction to the history of epitaxy was given by Pashley.[5]

Since the time of Royer's pioneering work, progress in the subject has been dominated by the influence of new experimental techniques, including a variety of growth techniques (mainly from the vapor, and even solid state), and making structural observations on crystals. With the appearance of various electron microscopes, extremely detailed information on the nucleation, growth, and structure of oriented crystalline deposits can be analyzed in layers of much less than one monolayer. The experimental evidence, however, is at total variance with the simplistic views on what is demanded of an epitaxial substrate. Obviously Barker and Royer's criteria are not met by such classic cases of "silicon on sapphire." Highly oriented films of dozens of materials have been prepared on noncrystalline glasses. Mysterious "buffer layers" are involved between a substrate and epitaxial film. There has been little real progress toward the understanding of what really determines the occurrence of "epitaxy" or more generally oriented overgrowth, because of this terminological confusion.[2] In actuality, the dominant factor in today's film deposition field is really not the intelligent selection of the substrates, for the selection criteria are not clear, it is the availability of any single crystal substrates which can be empirically tested. Part of our task has been to try to integrate the application of crystal chemical principles into the search for new substrates.

During our ongoing search for microwave device and integrated circuit substrates for HTSC thin films, it became increasingly clear to us that the demand on the substrates to have a close "lattice match" was in many cases more misleading than appropriate. Highly oriented polycrystalline YBCO films (sometimes epitaxial films) have been reportedly deposited on a wide variety of substrates of various symmetries and structural families, using various deposition techniques. In many cases the reported growths involved "misfits" considerably exceeding 15%[1] and often occurred on noncrystalline phases. To gain further insight on the crystallographic interactions of the film and substrate, there was a need to look into the relation with the substrate structure one step beyond the level of lattice symmetry and lattice parameters. The sublevel of a structure that can be precisely quantified are the interatomic distances between the anions (mainly oxygen) and cations and between the anions themselves in the structure. In other words our argument was that any similarity in the periodicity in the electrostatic charge pattern in any lattice planes of these ionic structures may be significant.

Taking advantage of an available database on the crystallographic structures, large numbers of substrate materials have been examined in comparison to the ionic structure of the YBCO. This approach is purely from the crystallographic point of view without relating to possible chemical interactions (or temperature effects) that may in many cases govern the growth of the film.

II. INTERATOMIC DISTANCES: THE DATABASE

The Inorganic Crystal Structure Database (ICSD),[9] produced by the Fachinformationszentrum–Karlsruhe, was used as our major source for the crystallographic parameters. This database is a compilation of crystal structures of 35 005 entries (as of April 1993). Most of the structural information used had been tested for their reliability level. Besides the symmetry and lattice parameters, the interatomic distances between the corresponding ions and the angles between ion pairs in the structure can be derived using the database. The interatomic distances of nearest neighbors, between an oxygen ion (or fluorine ion) and a cation and between two oxygen ions (or fluorine ions) were obtained. Each pair of distances was compared with the interatomic distances in the YBCO structure. Because the misfit between a substrate and the deposited-layer requires the knowledge of the actual crystal planes involved, the comparison was made to various selected cross sections of YBCO in the growth orientation under the consideration.

All the materials chosen for this study were substrates which have been considered for use for HTSC film deposition or have been reported as effective substrates for HTSC thin films. The listed relative differences of interatomic distances in tables (Tables II, III, and IV) were calculated using the equation:

$$\Delta(\text{interatomic distance})\% = 100 \times (\text{Dist.}_{\text{Subs.}} - \text{Dist.}_{\text{YBCO}})/\text{Dist.}_{\text{YBCO}} \quad (1)$$

A set criterion, $|\Delta(\text{interatomic distance})| < 6\%$, was applied for listing in the following tables (Tables II, III, and IV) to avoid excessively long listings.

III. THE YBCO STRUCTURE AND INTERATOMIC DISTANCES

The crystallographic structure of the single crystal high T_c superconductor $YBa_2Cu_3O_{7-\delta}$ ($\delta = 0.3$) is shown in Fig. 1 with all the atomic positions labeled. Several cross sections in the planes of (0, 0, 1) (at $z = 0$, $0.159c$, $0.378c$, and $0.5c$), (1, 0, 0) (at $x = a$ and $0.5a$), (010) (at $y = b$ and $0.5b$), and (110) (at $x = a$, $y = b$ and $x = 0.5a$, $y = 0.5b$), where a, b, and c are the lattice parameters of the structure, are singled out in particular to identify the interatomic spacing that is exposed on the surface. Interatomic distances among these atoms are presumably crucial for epitaxial overgrowth and therefore must be matched.

Table I(a) summarizes the interatomic distances (oxygen-oxygen and oxygen-cation), their appearance on the specific surfaces (and the abbreviated identifiers), and the corresponding effective lattice parameters when a specific growth orientation is considered. Cation-cation distances are often equivalent to the lattice edges that are reflected in the column of effective lattice parameters and are omitted in the calculation. The interatomic distances listed in Table I(a) are used in the calculations to compare the differences in a substrate to that in the YBCO superconductors.

Table I(b) lists all the angles between any two of the nearest oxygen ions for any distinct cation in the YBCO crystallographic structure, for interatomic distance less than 1.2 times the combined radius of the cation and the oxygen ion. Because the O–O distances in most close-packed structures are of similar dimensions, a two-dimensional model of the contact surface with the YBCO film, not just a one-dimensional model, is needed to identify the structure unit on the surface that can act as a nucleus for overgrowth. The interatomic distances and the angles have to be evaluated in considering the potential epitaxy planes.

IV. SUBSTRATES OF HIGH T_C SUPERCONDUCTING THIN FILMS

Tables II, III, and IV present the detailed comparison of the interatomic distances between a substrate and the YBCO. The fourth and fifth columns list the oxygen-oxygen distances and the oxygen-cation distances in a

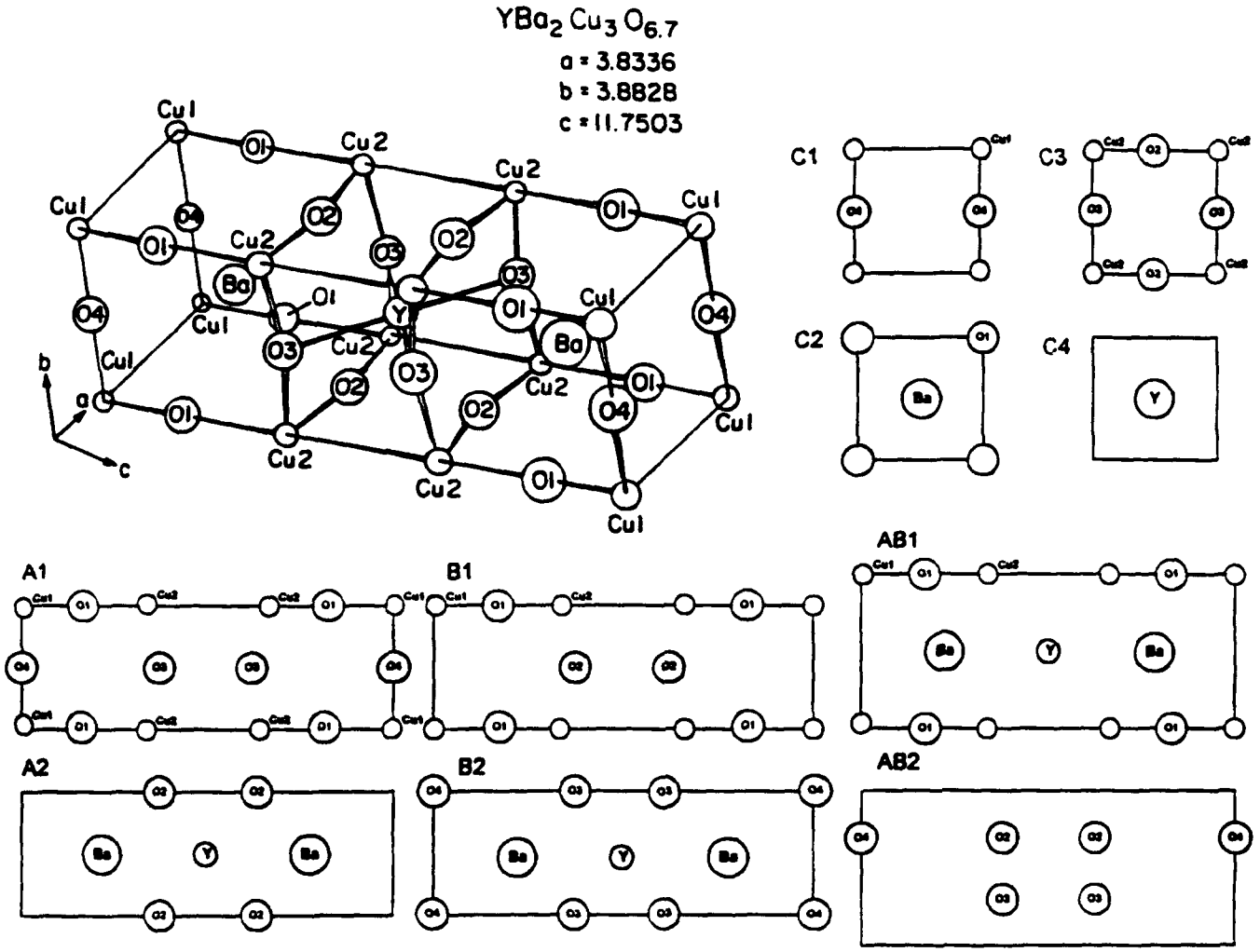

FIG. 1. Crystal structure of the high T_c superconductor YBCO.

substrate, respectively, with the sixth column showing the cations referred to. Values appearing in a row (from the 7th to 10th column for oxygen-oxygen distance and from the 11th to the 21st column for oxygen-cation distance) are the calculated relative differences between the substrate (column 4 or column 5 in the same row) and the individual distance (as the title of the column suggests) in the YBCO. Relative differences of interatomic distances which equal or exceed ±6% are not listed in the table for the sake of clarity. The very last column lists the suggested overgrowth planes in YBCO [abbreviated identifiers used as in the Table I(a)] in contact with the substrate where the match in interatomic distances is found within a tolerance of ±6%. Additional epitaxial planes in contact are also suggested (listed in bracket) when the tolerance range is expanded to ±15%.

The orientation of the substrate is not specified in Tables II, III, and IV but can be derived from the knowledge of crystal structure of the substrates using the matching requirement for both the interatomic distances listed in Table I(a) and the angles shown in Table I(b). A few examples for such analysis are given in related discussions though a comprehensive analysis is the topic of a separate publication.[8]

A. Ternary phases with the perovskite structure

This family of substrates is of the most importance as those materials are among the most obvious candidates for epitaxial growth of YBCO films. Substrates of perovskite structure usually have the ideal cubic (such as $SrTiO_3$), double cell cubic (such as Ba_2YSbO_6), hexagonally distorted pseudo cubic (such as $LaAlO_3$), or other pseudo cubic cells (such as $NdGaO_3$ that has the $GdFeO_3$ structure with orthorhombic symmetry). Some of the fluoride perovskites are also listed together with the oxides as they have lower dielectric constants (~6–8) in comparison to most of the oxide perovskites, which is advantageous for integrated circuit applications.

TABLE I(a). Interatomic distances (Å) in the YBCO.

Materials	Lattice	Orient.	I.D.	Coord. Plane	Effec. Cell	O2–O3	O3–O3	O1–O4	O2–O2	O4–Cu1	O2–Cu2	O3–Cu2	O1–Cu1	O1–Ba	O2–Ba	O2–Y	O1–Cu2	O3–Y	O3–Ba	O4–Ba	Y–Y
YBCO $\delta = 0.3$	$a = 3.8336$		C1	0.0.*c*	3.8336, 3.8828					1.941											
	$b = 3.8828$	(001)	C2	0.0.0.1586*c*	3.8336, 3.8828									2.751 (2.729)							
Symm.	$c = 11.7503$		C3	0.0.0.3782*c*	3.8336, 3.8828	2.728					1.933	1.957									
Pmmm	$c/3 = 3.917$		C4	0.0.0.5*c*	3.9336, 3.8828																3.834, 3.883
		(100)	A1	*a*, 0.0	3.8828, 11.7503		2.862	2.691		1.941		1.957	1.864				2.3357				
			A2	0.5*a*, 0.0	3.8828, 11.7503				2.858						2.959	2.411					
		(010)	B1	0, *b*, 0	3.8336, 11.7503				2.858		1.933		1.864				2.3357				
			B2	0.0.5*b*, 0	3.8336, 11.7503		2.862											2.392	2.941	2.928	
		(110)	AB1	*a*, *b*, 0	5.4564, 11.7503								1.864	2.751 (2.729)			2.3357				
Ref. 7			AB2	0.5*a*, 0.5*b*, 0	5.4564, 11.7503	2.728	2.862		2.858												

TABLE I(b). Bonding angles (degree) in the YBCO.

∠(O–Ba–O)		∠(O–Y–O)		∠(O–Cu1–O)		∠(O–Cu2–O)	
∠(O1–Ba–O1)	165.40	∠(O3–Y–O3)	179.98	∠(O1–Cu1–O1)	180.00	∠(O2–Cu2–O2)	165.32
	88.36		73.49				
	89.79		106.51				
∠(O1–Ba–O4)	111.11	∠(O3–Y–O2)	110.77	∠(O1–Cu1–O4)	90.00	∠(O2–Cu2–O3)	89.08
	56.47		69.23				
∠(O1–Ba–O3)	69.04	∠(O2–Y–O2)	107.30	∠(O4–Cu1–O4)	180.00	∠(O3–Cu2–O3)	165.64
	123.41		72.70				
			180.00				
∠(O1–Ba–O2)	123.99					∠(O1–Cu2–O3)	97.18
	68.46						

B. Binary oxides and fluorides

Simple oxides and fluorides are of importance because good crystals are often readily available: moreover, their dielectric constants are low. MgO and Al_2O_3 are among the first substrates that have been used as substrates for YBCO. Yttrium stabilized cubic zirconia (YSZ) crystals have also been tested as YBCO substrates. CeO_2 is another substrate material that has been frequently used as a "buffer layer" between, e.g., Al_2O_3 and the YBCO, allegedly to interrupt the chemical interactions. Interatomic distances for such binary oxides in comparison with that of the YBCO are listed in Table III.

C. Substrates of other structures

Representatives of potential substrates of a variety of structure types, including gehlenite, spinel, garnet, and magnetoplumbite, are included in Table IV. These structures are interesting because they are high symmetry structures with a common feature containing oxygen octahedra as their main building blocks that tend to allow reasonable matches with the YBCO perovskite-like structure. Moreover, as noted above, many of them are obtainable in large single crystal form and have low dielectric constants (in comparison to many of the oxide crystals of perovskite structure).

V. DISCUSSION

All the above comparisons have been performed using crystallographic data at ambient temperatures, and therefore thermal expansion corrections are required for elevated deposition temperatures particularly for substrates where there may be large differences in thermal expansion properties with the YBCO. As the average thermal expansion of YBCO nonlinearly increases at temperatures higher than ~500 °C[9] (due to the orthorhombic-tetragonal phase transition at a temperature ~600 °C), any mismatch of positive sign will be relieved and negative sign will be worsened. Thermal expansion isotropy found in most of the substrates of high symmetry versus the anisotropy in the YBCO structure is also a critical concern not to be ignored for thermal expansion corrections.

YBCO film orientations used for comparison in the calculation are those with their planes perpendicular to the [001], [100], [010], and [110] directions. Other higher-indexed planes such as the (103) plane[10] are also possible but have not been tested. The last

TABLE II. Comparison of interatomic distances in substrates of perovskite structure with the YBCO.

Substrates			Interatomic distances (Å)			Relative interatomic distance mismatch with the YBCO (%)														Matching YBCO plane
Composition	Symm.	Lattice (Å)	O–O (F–F)	O–Cat. element (F–Cat. element)		O2–O3	O3–O3	O1–O4	O2–O2	O4–Cu1	O2–Cu2	O3–Cu2	O1–Cu1	O1–Ba	O2–Ba	O2–Y	O1–Cu2	O3–Y	O3–Ba	O4–Ba	<6% (<15%)
$SrTiO_3$	*Pm3-m*	3.905	2.761	2.761	Sr	1.2	−3.5	2.6	−3.4					1.2						−5.7	C1, C2, C3, C4,
Ref. 11				1.952	Ti					0.6	1.0	−0.3	4.7								AB2 (+A2, B2)
$LaAlO_3$	*R3m*	a = 3.789	2.676	1.895	Al	−1.9		−0.6		−2.4	−2.0	−3.2	1.7								C1, C2, C3, C4
		α = 90.12°	2.682	2.676	La	−1.7		−0.3						−1.9							(All)
				2.682	La									−1.7							
Ref. 12				1.894	Al					−2.4	−2.0	−3.2	1.6								
$YAlO_3$	*Pnma*	a = 5.330	2.666	2.237	Y	−2.3		−0.9									−4.2				C1, C3, C4, A1,
		b = 7.375	2.681	2.306	Y	−1.7		−0.4								−4.4	−1.3	−3.6			B1, AB2
		c = 5.180	2.724	2.284	Y	−0.1	−4.8	1.2	−4.7							−5.3	−2.2	−4.5			(+C2, AB1)
			2.725	2.481	Y	−0.1	−4.8	1.3	−4.7							2.9		3.7			
			2.709	1.901	Al	−0.7	−5.3	0.7	−5.2	−2.0	−1.7	−2.9	2.0								
				1.910	Al					−1.6	−1.2	−2.4	2.5								
				1.921	Al					−1.0	−0.6	−1.8	3.1								
Ref. 13				2.569	Y									−5.9							
$NdGaO_3$	*Pbn2*$_1$	a = 5.44	2.792	1.756	Ga	2.3	−2.4	3.8	−2.3				−5.8								C1, C2, C3, C4,
		b = 5.50	2.296	2.003	Ga					3.2	3.6	2.4									A1, B1, AB1,
		c = 7.71	2.612	1.776	Ga	−4.3		−2.9					−4.7								AB2
			2.652	2.546	Nd	−2.8		−1.4								5.6					(All)
			2.684	2.133	Nd	−1.6		−0.3													
			2.713	2.206	Nd	−0.5	−5.2	0.8	−5.1								−5.6				
			2.759	2.600	Nd	1.1	−3.6	2.5	−3.5					−4.7							
			2.760	2.609	Nd	1.2	−3.6	2.6	−3.4					−4.4							
			2.762	2.172	Ga	1.2	−3.5	2.6	−3.4												
				2.070	Ga							5.8									
				2.269	Ga							5.7									
				2.654	Nd									−2.7							
				2.870	Nd									5.2	−3.0				−2.4	−2.0	
				2.986	Nd										0.9				1.5	2.0	
				2.944	Nd										−0.5				0.1	0.5	
Ref. 14				2.971	Nd										0.4				1.0	1.5	
$KTaO_3$	*Pm3-m*	3.9885	2.827	2.827	K	3.6	−1.2	5.1	−1.1												C1, C2, C3, C4,
Ref. 15				1.994	Ta					2.7	3.2	1.9									AB2 (+A1,
																					B1, AB1)
$LaGaO_3$	(undet.)	3.86	2.729	2.729	La	0.0	−4.7	1.4	−4.5					0.0							C1, C2, C3, C4,
Ref. 16				1.930	Ga					−0.6	−0.2	−1.4	3.5								AB2
																					(+A2, B2)
$LiNbO_3$		a,b = 5.1473	2.731	2.050	Li	0.1	−4.6	1.5	−4.4	5.6		4.8									C1, C4, AB2
	R3c	c = 13.85614	2.803			2.7	−2.1	4.2	−1.9												(+C3, A1, B1)
		γ = 120°	2.838			4.0	−0.8	5.5	−0.7												
Ref. 17			2.872			5.3	0.3		0.5												
$LiBaF_3$	(undet.)	3.988	2.8199	2.8199	Ba	3.4	−1.5	4.8	−1.3					3.3	−4.7				−4.1	−3.7	C1, C2, C3, C4,
Ref. 18				1.994	Li					2.7	3.2	1.9									AB2
																					(+B1, B2, AB1)
$KZnF_3$	*Pm3-m*	4.055	2.867	2.027	Zn	5.1	0.2		0.3	4.4	4.9	3.6									C1, C2, C3, C4,
				2.028	Zn					4.5	4.9	3.6									AB2
Ref. 19				2.867	K									5.1	−3.1				−2.5	−2.1	(+A1, B1, AB1)
Ba_2YSbO_6	*Fm3-m*	8.414	2.975	2.103	Ba		3.9		4.1												None
				2.104	Ba																
Ref. 20				2.975	Y/Sb										0.5				1.2	1.6	(C1, C3, C4, A1, B1, AB2)
$KMgF_3$	*Pm3-m*	3.98	2.814	2.814	K	3.2	−1.7	4.6	−1.5					3.1	−4.9				−4.3	−3.9	C1, C2, C3, C4,
Ref. 21				1.990	Mg					2.5	2.9	1.7									AB2
																					(+A1, B1, AB1)
$BaZrO_3$	*P*23	4.1815	2.957	2.957	Ba		3.3		3.5						−0.1				0.5	1.0	None
Ref. 22				2.091	Zr																(All)

TABLE III. Comparison of interatomic distances in substrates of simple oxides and fluorides with the YBCO.

Substrates			Interatomic distances (Å)			Relative interatomic distance mismatch with the YBCO (%)														Matching YBCO planes
Composition	Symm.	Lattice (Å)	O–O (F–F)	O–Cat. (F–Cat. | Element Element)	O2–O3	O3–O3	O1–O4	O2–O2	O4–Cu1	O2–Cu2	O3–Cu2	O1–Cu1	O1–Ba	O2–Ba	O2–Y	O1–Cu2	O3–Y	O3–Ba	O4–Ba	(<6% ,<15%)
MgO	*Fm3-m*	4.2114	2.978	2.1057	Mg		4.1		4.2												None
Ref. 23																					(C1, C3, C4, A1, B1, AB2)
Al_2O_3	*R3-c*	*a*, *b* = 4.7586	2.540	1.852	Al			−5.6		−4.6	−4.2	−5.4	−0.6								C1, C3, C4, AB2 (+ −)
		c = 12.9897	2.623	1.975	Al	−3.8		−2.5		1.8	2.2	0.9	6.0								
		γ = 120°	2.722			−0.2	−4.9	1.2	−4.8												
			2.857			4.7	−0.2		−0.0												
Ref. 24																					
CeO_2	*Fm3-m*	5.389	2.694	2.334	Ce	−1.2	−5.9	0.1	−5.7							−3.2	−0.1	−2.4			AB2, C4
			2.695	2.343	Ce	−1.2	−5.8	0.1	−5.7							−2.8	0.3	−2.0			(+C2)
			2.706			−0.8	−5.5	0.6	−5.3												
Ref. 25																					
CaF_2	*Fm3-m*	5.45279	2.726	2.361	Ca	−0.1	−4.8	1.3	−4.6							−2.1	1.1	−1.3			AB2, C4
Ref. 26																					(+C2)
$Zr(Y)O_2$ (+12.0.28 1.862)	*Fm3-m*	5.16(2)	2.580	2.234	Zr/Y	−5.4		−4.1									−4.4				C4 (+AB2)
Ref. 27																					
SiO_2	$P6_222$	*a*, *b* = 4.9977	2.409	1.565	Si																AB2 (+C4)
		c = 5.4601	2.318	1.635	Si																
		γ = 120°	2.539					−5.6													
			2.567			−5.9		−4.6													
			2.571			−5.8		−4.5													
			2.611			−4.3		−2.9													
			2.616			−4.1		−2.8													
			2.624			−3.8		−2.5													
			2.720			−0.3	−5.0	1.1	−4.8												
Ref. 28			2.886			5.8	0.8		1.0												
MgF_2	$P4_2/mnm$	*a*,*b* = 4.615	2.570	1.978	Mg	−5.8		−4.5		1.9	2.3	1.1									C1, C3
		c = 3.043	2.807	1.992	Mg	2.9	−1.9	4.3	−1.8	2.6	3.1	1.8									(+C4, AB2)
Ref. 29																					

column in Tables II, III, and IV lists the interatomic distance-matched planes in the YBCO structure, though the specific planes in the substrate that contain the required matching distances need to be worked out in each case, and are not listed in the above tables.

Interatomic distance comparisons led to a suggestion that the substrate's surface termination (that exposes required interatomic spacing), not only the substrate orientation, is a crucial parameter both in determining the epitaxial growth and the orientation of the films. This understanding emphasizes the role played by the substrate's surface structure (the interatomic distances and the ion distribution). This consideration has not received the attention it deserves. Evidence was reported[38] that YBCO films prepared on (001) $KTaO_3$ single crystals are *c*-axis oriented when deposited on as-grown (001) surfaces and *a*-axis oriented when deposited on (001) cleaved surfaces. The interatomic distance comparison showed that [001] and [110] orientations of YBCO have sections with matching interatomic distances with the $KTaO_3$ within ±6%, and additional directions include [100] and [010] when ±15% matching is allowed. The [001] growth (through contact plane C4 or C2) is the favored growth direction for substrate surface terminated with K and O as shown in Fig. 2(a). When the oxygen ions and Ta are the terminating ions to the surface (the cleaved surface in $KTaO_3$), the [110] (through the contact plane AB2), [001] (through the contact planes of C3 or C1), and [100] (through the contact plane of A1) orientations are possible. This situation is illustrated in Fig. 2(b). Further characteristics of the atomic termination layers are needed to identify which of the orientations is the most favored from energy argument.

A point needed to be emphasized is that the considerations of epitaxial growth of superconducting films must start at levels of atomic structure and arrangements of atoms on the surface (not only the crystallographic unit cell). Even if the film may have excellent in-plane and out-of-plane orientations, steps and antiphase boundaries can occur from nucleation at different points on the surface of the substrate and with different sections (or horizon levels) of the YBCO structure, resulting in clusters with the structural repeat unit out of phase in both in- and out-of-plane directions.[2] The superconduct-

TABLE IV. Comparison of interatomic distances in substrates of miscellaneous structure types with the YBCO.

Substrates			Interatomic distances (Å)			Relative interatomic distance mismatch with the YBCO (%)														Matching YBCO plane
Composition	Symm.	Lattice (Å)	O–O	O–Cat.	element	O2–O3	O3–O3	O1–O4	O2–O2	O4–Cu1	O2–Cu2	O3–Cu2	O1–Cu1	O1–Ba	O2–Ba	O2–Y	O1–Cu2	O3–Y	O3–Ba	O4–Ba	<6% (<15%)
$CaNdAlO_4$	$I4/mmm$	$a, b = 3.688$	2.593	2.430	Ca/Nd	−4.9		−3.6								0.8	4.0	1.6			C1, C2, C3.
	(K_2NiF_4)	$c = 12.15$	2.608	2.608	Ca/Nd	−4.4		−3.1						−4.4							C4, AB1
		$\gamma = 120$		2.593	Ca/Nd									−5.0							(All)
				1.822	Al						−5.7		−2.3								
Ref. 30				1.844	Al					−5.0	−4.6	−6.0	−1.1								
$Ca_2Al_2SiO_7$	$P\bar{4}2_1m$	$a, b = 7.6770$	2.643	2.437	Ca	−3.1		−1.8								1.1	4.3	1.9			C4, AB2
(Gehlenite)		$c = 5.0594$	2.799	2.418	Ca	2.6	−2.2	4.0	−2.1							0.3	3.5	1.1			(All)
			2.848	2.440	Ca	4.4	−0.5	5.8	−0.4							1.2	4.5	2.0			
			2.900	2.559	Ca		1.3		1.5												
			2.830	1.693	Al/Si	3.7	−1.1	5.2	−1.0												
			2.660	1.748	Al	−2.5		−1.2													
				1.694	Al/Si																
				1.656	Al/Si																
Ref. 31				2.826	Ca																
$Ca_2Ga_2(SiO_4)O_1$		$a, b = 7.797$	2.708	2.440	Ca	−0.7	−5.4	0.6	−5.2							1.2	4.5	2.0			C4, B1,
	$P\bar{4}2_1m$	$c = 5.132$	2.829	2.523	Ca	3.7	−1.2	5.1	−1.0							4.6		5.5			AB1, AB2
	(Gehlenite)		2.687	2.401	Ca	−1.5		−0.1	−6.0							−0.4	2.8	0.4			(All)
			2.957	2.573	Ca		3.3		3.5					−5.7							
			3.019	1.738	Ga/Si		5.5		5.6												
			2.941	1.620	Ga/Si		2.8		2.9												
			2.983	1.789	Ga/Si		4.2		4.4				−4.0								
				1.818	Ga						−6.0		−2.5								
Ref. 32				2.854	Ca									4.6	−3.5				−3.0	−2.5	
Ba_2SiO_4	$Pmcn$	$a = 5.772$	2.676	2.796	Ba	−1.9		−0.6						2.5	−5.5				−4.9	−4.5	C2, C4, A2,
		$b = 10.225$	2.512	2.823	Ba									3.4	−4.6				−4.0	−3.6	B2, AB2
		$c = 7.513$	2.697	2.331	Ba	−1.1	−5.8	0.2	−5.6							−3.3	−0.2	−2.6			(All)
			2.678	2.733	Ba	−1.8		−0.5						0.1							
			2.943	2.898	Ba		2.8		3.0						−2.1				−1.5	−1.0	
				2.648	Ba									−3.0							
				1.610	Si																
				1.674	Si																
				2.661	Ba									−2.5							
Ref. 33				2.794	Ba									2.4	−5.6				−5.0	−5.0	
$BaAl_2O_4$	$P6_3$	$a, b = 10.470$	2.727	2.748	Ba	−1.0	−4.7	1.3	−4.6					0.7							C1, C2, C4,
		$c = 8.819$	2.759	2.622	Ba	1.1	−3.6	2.5	−3.5					−3.9							AB2
			2.782	3.017	Ba	2.0	−2.8	3.4	−2.7						2.0				2.6	3.0	(All)
			2.895	2.796	Ba		1.2		1.3					2.5	−5.5				−4.9	−4.5	
			2.751	2.973	Ba	0.8	−3.9	2.2	−3.7						0.5				1.1	1.5	
			2.760	2.826	Ba	1.2	−3.6	2.6	−3.4					3.6	−4.5				−3.9	−3.5	
			2.801	3.003	Ba	2.7	−2.1	4.1	−2.0						1.5				2.1	2.6	
			2.802	2.761	Ba	2.7	−2.1	4.1	−2.0					1.2						−5.7	
			2.893	2.919	Ba		1.1		1.2						−1.4				−0.7	−0.3	
				3.007	Ba										1.6				2.2	2.7	
				1.775	Al								−4.8								
				1.844	Al					−5.0	−4.6	−5.8	−1.1								
				1.759	Al								−5.6								
				1.790	Al								−4.0								
				1.747	Al																
				1.834	Al					−5.5	−5.1		−1.6								
				1.669	Al																
				1.749	Al																
				1.732	Al																
				1.762	Al								−5.5								
				1.717	Al																
				1.729	Al																
				1.750	Al																
Ref. 34				1.748	Al																

TABLE IV. (continued)

Substrates			Interatomic distances (Å)			Relative interatomic distance mismatch with the YBCO (%)														Matching YBCO plane
Composition	Symm.	Lattice (Å)	O–O	O–Cat.	element	O2–O3	O3–O3	O1–O4	O2–O2	O4–Cu1	O2–Cu2	O3–Cu2	O1–Cu1	O1–Ba	O2–Ba	O2–Y	O1–Cu2	O3–Y	O3–Ba	O4–Ba	<6% (<15%)
$Y_3Fe_3Ga_2O_{12}$			2.490	2.211	Y												−5.4				C1, C3, A1, B1, AB2 (+C2, C4, AB1)
	Ia3-d	11.5	2.645	2.366	Y	−3.0		−1.7								−1.9	1.3	−1.1			
	(Garnet)		2.711	1.627	Fe/Ga	−0.6	−5.3	0.7	−5.1												
			2.737	1.894	Fe/Ga	0.3	−4.3	1.7	−4.2	−2.4	−2.0	−3.2	1.6								
			2.747			0.7	−4.0	2.1	−3.9												
Ref. 35			2.794			2.4	−2.4	3.8	−2.2												
$MgAl_2O_4$	*Fd3m*	8.0806(5)	2.587	1.926	Al	−5.2		−3.9		−0.8	−0.4	−1.6	3.3								C1, C3, AB2 (+C4)
Ref. 36	(Spinel)		2.863	1.922	Mg	4.9	0.0		0.2	−1.0	−0.6	−1.8	3.1								
$LaMgAl_{11}$-	$P6_3/mmc$	a = 5.590	2.543	1.771	Al/Mg			−5.5					−5.0								C1, C2, C3, C4, A1, B1 AB1, AB2 (All)
O_{19}	(Magneto-	b = 5.590	2.550	1.846	Mg			−5.2		−4.9	−4.5	−5.7	−1.0								
	plumbite)	c = 21.968	2.576	1.847	Al	−5.6		−4.3		−4.8	−4.4	−5.6	−0.9								
		γ = 120°	2.577	1.848	Al	−5.5		−4.2		−4.8	−4.4	−5.6	−0.9								
			2.600	1.864	Al	−4.7		−3.4		−4.0	−3.6	−4.8	0.0								
			2.683	1.865	Al	−1.7		−0.3		−3.9	−3.5	−4.7	0.1								
			2.684	1.873	Mg/Al	−1.6		−0.3		−3.5	−3.1	−4.3	0.5								
			2.715	1.877	Al	−0.5	−5.1	0.9	−5.0	−3.3	−2.9	−4.1	0.7								
			2.743	1.882	Al	0.6	−4.2	1.9	−4.0	−3.0	−2.6	−3.8	1.0								
			2.769	1.972	Mg/Al	1.5	−3.2	2.9	−3.1	1.6	2.0	0.8	5.8								
			2.795	2.445	La	2.5	−2.3	3.9	−2.2							1.4	4.7	2.2			
			2.796	2.587	La	2.5	−2.3	3.9	−2.1					−5.2							
			2.799	2.681	La	2.6	−2.2	4.0	−2.1					−1.8							
			2.800	2.957	La	2.6	−2.2	4.1	−2.0						−0.1				0.5	1.0	
			2.801	2.799	La	2.7	−2.1	4.1	−2.0					2.6	−5.4				−4.8	−4.4	
			2.875	2.810	La	5.4	0.5		0.6					3.0	−5.0				−4.5	−4.0	
			2.904	2.382	Mg/Al		1.5		1.6							−1.2	2.0	−0.4			
			3.010	1.961	Al		5.2		5.3	1.0	1.5	0.2	5.2								
				1.962	Al					1.1	1.5	0.3	5.3								
				1.944	Al					0.2	0.6	−0.7	4.3								
				1.945	Al					0.2	0.6	−0.6	4.3								
Ref. 37				1.978	Al					1.9	2.3	1.1									

ing properties such as the critical current density, J_c, will be affected significantly by the antiphase boundaries and stacking faults in otherwise "perfect epitaxial" films.[39]

Interatomic distance comparison also indicates a possible dependence of the orientation of the films at the nucleation stage on composition during deposition.

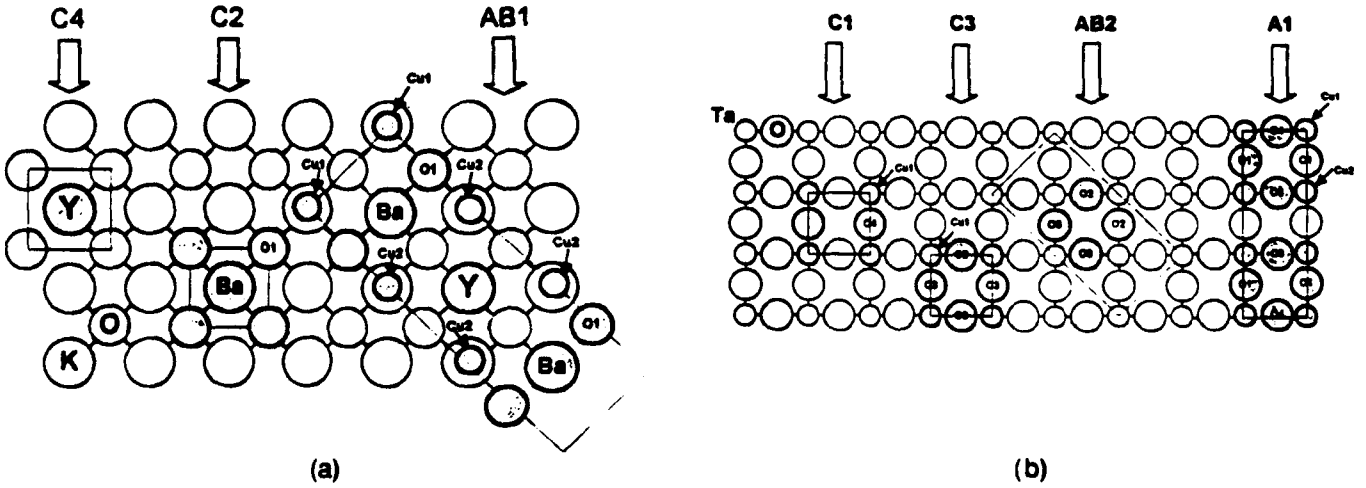

FIG. 2. Epitaxial relations of the $KTaO_3$ with the YBCO for different cleavage planes: (a) (001) $KTaO_3$ substrate terminated with K and O, and (b) (001) $KTaO_3$ substrate terminated with Ta and O. The shaded circles are the matching sites in the YBCO planes. The plane identifiers are shown above the hollow arrows.

For instance, rich in Cu or rich in Ba may very well determine the film orientation to be [100] as the interatomic distances of O4–Cu1, O3–Cu2, O1–Cu1, and O1–Cu2 are essential to fulfill (or [010] as O2–Cu2, O1–Cu1, and O1–Cu2 matching are needed) or [001] as the distance of O1–Ba is required. This type of composition dependence was indeed observed by Oh *et al.*[40] in YBCO films deposited on (100) $KTaO_3$ substrate. The Ba-poor films tend to be *a*-axis oriented, whereas Ba-rich films are usually *c*-axis oriented. This phenomenon appears to suggest the Ba (or Y) might be the key in some cases in determining *c*-axis films (both Ba and Y may result in *c*-axis films though nucleated in different horizon), because of its large size. Orientation dependence on composition could be useful to control undesired orientations, chemically, in a deposition process when several competing orientations of growth are present. The role of defects in the substrates and any surface contaminations will then undoubtedly affect the intended epitaxial deposition of the YBCO films.

A number of other substrates with the perovskite structure (both oxides and fluorides) can be analyzed as has been done for $KTaO_3$. In fact, it is true that the lattice parameters are often sufficient considerations in epitaxial film growth only when the cubic or pseudo cubic structures are considered.

For simple oxides or fluorides listed in Table III, the lattice parameters are all larger than that of the YBCO (*b*-axis) with the MgO representing the smallest mismatch at ~8.5%. Interatomic distance-matching planes can be found when a ±15% mismatch is allowed to identify the most probable direction of overgrowth. MgO has been tested quite extensively and either highly textured or epitaxial films have been reported. Using distance calculations, there is no atomic distance matching within the ±6% for MgO substrates. This result agrees with the experimental observations that, in general, YBCO thin films grown on (001) MgO are highly oriented polycrystalline films with the *c*-axes parallel between grains and perpendicular to the substrate surface.[41] However, if a ±15% mismatch is allowed, all studied YBCO directions become possible, on specific surfaces of the substrate. YBCO films of both [001] and [100] growths were reported, and "epitaxy quality" is reportedly obtained depending mainly on the substrate temperature. YBCO thin films deposited on (100) MgO substrates at 650 °C, although fully *c*-axis oriented, do not exhibit much in-plane orientation as evidenced by oscillating photographs.[42] However, epitaxial growth of the YBCO with *a*- and *b*-axes parallel to those of the substrate was reported for growth temperature at 700 °C. It is our speculation that the thermal expansion of the YBCO at the higher temperatures (near the orthorhombic-tetragonal phase transition) might have resulted in much less severe mismatches, overlapped with the normal effects of monotonically increased thermal activation energy, and an epitaxial relation might therefore be obtained.

CeO_2 has been reported as one of the most versatile "buffer layers" in various cases for the HTSC thin film depositions. Using the distance comparison as seen in Table III, a (001) CeO_2 substrate terminated with O has a close interatomic distance match with the YBCO and can result in the film of [110] growth direction through the contact plane of AB2, as shown in Fig. 3(a), or the film of [001] growth direction through the contact plane of C4 by rotating the CeO_2 lattice 45° about the *c*-axis, on (001) CeO_2 terminated with only Ce, as shown in Fig. 3(b). Two other possible contact planes in the YBCO can be identified as C3 and C1, as also shown in

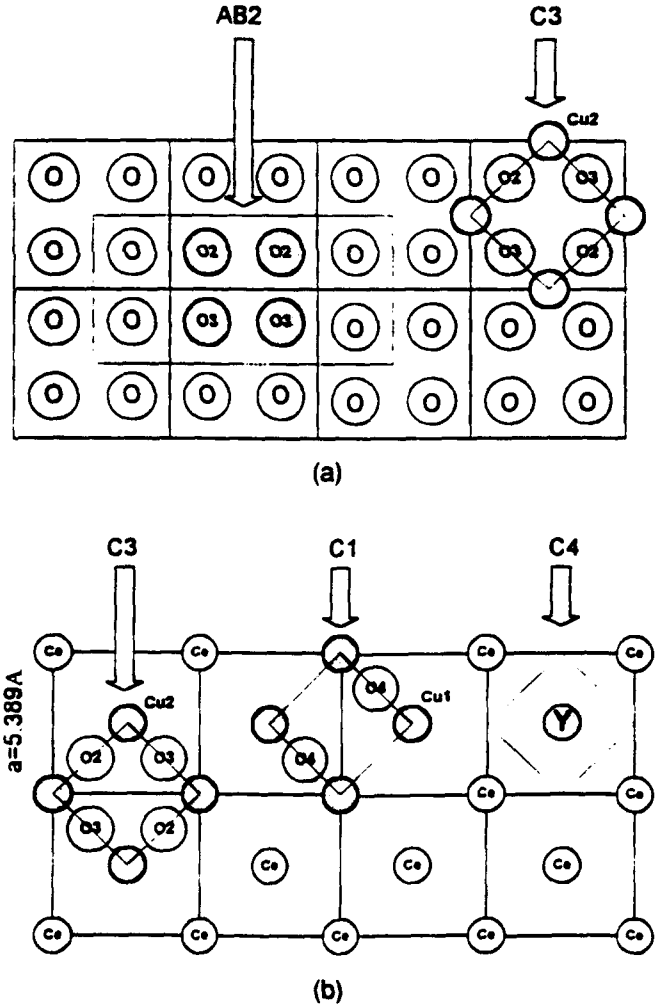

FIG. 3. Possible epitaxy relations in substrate (001) CeO_2 for the YBCO film: (a) (110) and (001) YBCO films deposited on (100) CeO_2 substrate terminated with oxygen ions through AB2 contact plane and C3 contact plane ($z = 0.3782c$), respectively; and (b) (001) YBCO film on the (100) CeO_2 substrate terminated with Ce ions through the C1 ($z = 0$), C3 ($z = 0.3782c$), and C4 ($z = 0.5c$) contact planes, respectively. AB2 and C4 planes are the probable epitaxy planes with overall good interatomic distance matches.

Figs. 3(a) and 3(b). The C3 and C1 contact situations, however, exclude the O4–Cu1 or O2–Cu2, and O3–Cu2 interatomic distances match as there are no oxygen sites on the substrate surface and are therefore hypothetical. Further detailed comparison between the angles of the ∠(O–Ce–O) (in CeO_2) and the ∠(O–Y–O) in YBCO [listed in Table I(b) for YBCO] shows clearly an excellent match at the horizon of $z = 0.5c$ (C4) contact plane for a (001) YBCO film when its *a*- (or *b*-) axis is aligned along the [110] direction of the CeO_2 unit cell. Besides the interatomic distance mismatch less than ~3%, the mismatches in angles are found to be less than 3°. The epitaxial relation of CeO_2 and YBCO (when the contact plane is the C4) is schematically shown in Fig. 4.

Epitaxial (001) YBCO films prepared by pulsed laser deposition on the (001) CeO_2 buffer layer on $(1\bar{1}02)$ sapphire have been reported ($J_c = 1.3 \times 10^6$ A/cm^2 at 84 K) and the cross section of the substrate/buffer layer/YBCO film was studied by TEM and HRTEM.[43] The in-plane relation was found to be ⟨100⟩ YBCO ‖ ⟨110⟩ CeO_2 ‖ [$\bar{2}$021] Al_2O_3. This result clearly confirms the proposed in-plane alignment situation depicted in Fig. 4; however, it does not render further judgment on whether the O–O distance matching [without the Cu-site matching in the case of C3 shown in Fig. 3(a)] or Y–Y distance matching [C4 in Fig. 3(b)]

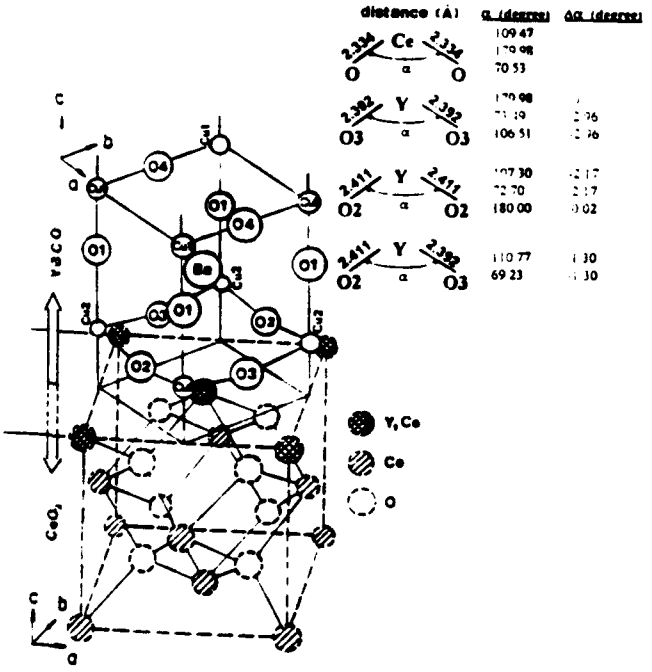

FIG. 4. Schematic illustration of the epitaxy relations for the (001)CeO_2/(001)YBCO system through contact plane C4 ($z = 0.5c$) in YBCO. Part of the YBCO unit cell is drawn. A comparison of the atomic structure similarities (distance and angles) between the YBCO and the CeO_2 is also given.

is responsible for the growth. Similar crystallographic matching relations in other crystals such as YSZ and CaF_2 of the fluorite structure have also been found. However, due to the reactive nature of Ce, it is not clear if this type of overgrowth can be generalized for other materials of similar structures. The strain misfit at the Al_2O_3/CeO_2 interface is as high as 14% and a disordered layer of ~0.5 nm (two atomic rows in a 13 nm thick CeO_2 layer) thick was observed by HRTEM.[43] The reason CeO_2 is successful despite such a large lattice misfit is still unclear. Epitaxial films of (001) YBCO on (100) $LaAlO_3$ or (100) YSZ using CeO_2 as buffer layers have also been reported.[44] Convincing in-plane evidence for the above cases that identifies the plane(s) of CeO_2 that allow(s) the overgrowth of the (001) YBCO films, the epitaxial mechanisms on the contact plane, and the strain level the film may tolerate, is still lacking. Similar arguments may be applied to the CaF_2, MgF_2, and yttria-stabilized-zirconia that all share the fluorite structure with CeO_2.

Sapphire has some specially interesting features as a substrate: availability as large-sized wafers, low cost, and very low dielectric loss. Its application as a substrate for HTSC, however, has been hindered by the chemical reaction with the YBCO to form $BaAl_2O_4$ at high temperature. Oriented YBCO films generally were reported deposited on the $(1\bar{1}02)$ plane. Comparing the interatomic distances of Al_2O_3 with the YBCO, the possible contact planes in the YBCO are found to be the C1, C3, C4, and AB2. No clear atomic site matching can be found by examining the surface structure of the $(1\bar{1}02)$ sapphire with oxygen layer termination (the plane marked A in Fig. 5). However, for the plane marked B in the Al_2O_3 structure that is terminated with Al only, a tolerable matching relation for fluorite-type structures such as CeO_2 (distance mismatch for 5.389 Å in CeO_2 is 5.1–13.2%) and YSZ (distance mismatch for 5.162 Å in YSZ is 8.5–0.7%) could be identified as a unit area 4.759 Å wide and 5.128 Å long enclosed in thick solid lines in Fig. 5(a). It was reported that the (001) YBCO films deposited on a $(1\bar{1}02)$ Al_2O_3 substrate (without buffer layers) were obtained only in a narrow substrate-temperature window of 650–670 °C.[45] Degraded YBCO properties were attributed to severe lattice mismatch between the sapphire $(1\bar{1}02)$ plane and the YBCO *a*-*b* plane. The *c*-axis misalignment of the YBCO/Al_2O_3 film was reported to be substantial (4° of the *c*-axis of YBCO about the sapphire [$1\bar{1}02$] direction). Some in-plane alignments [the [100] and [010] of YBCO aligned with ⟨$2\bar{2}01$⟩ in the $(1\bar{1}02)$ plane of Al_2O_3, similar as reported in the case where CeO_2 buffer layer was used[43]] with considerable distribution in orientation were also reported. The possible YBCO/Al_2O_3 overgrowth relation is illustrated in Fig. 5(a), following the work of Boyce

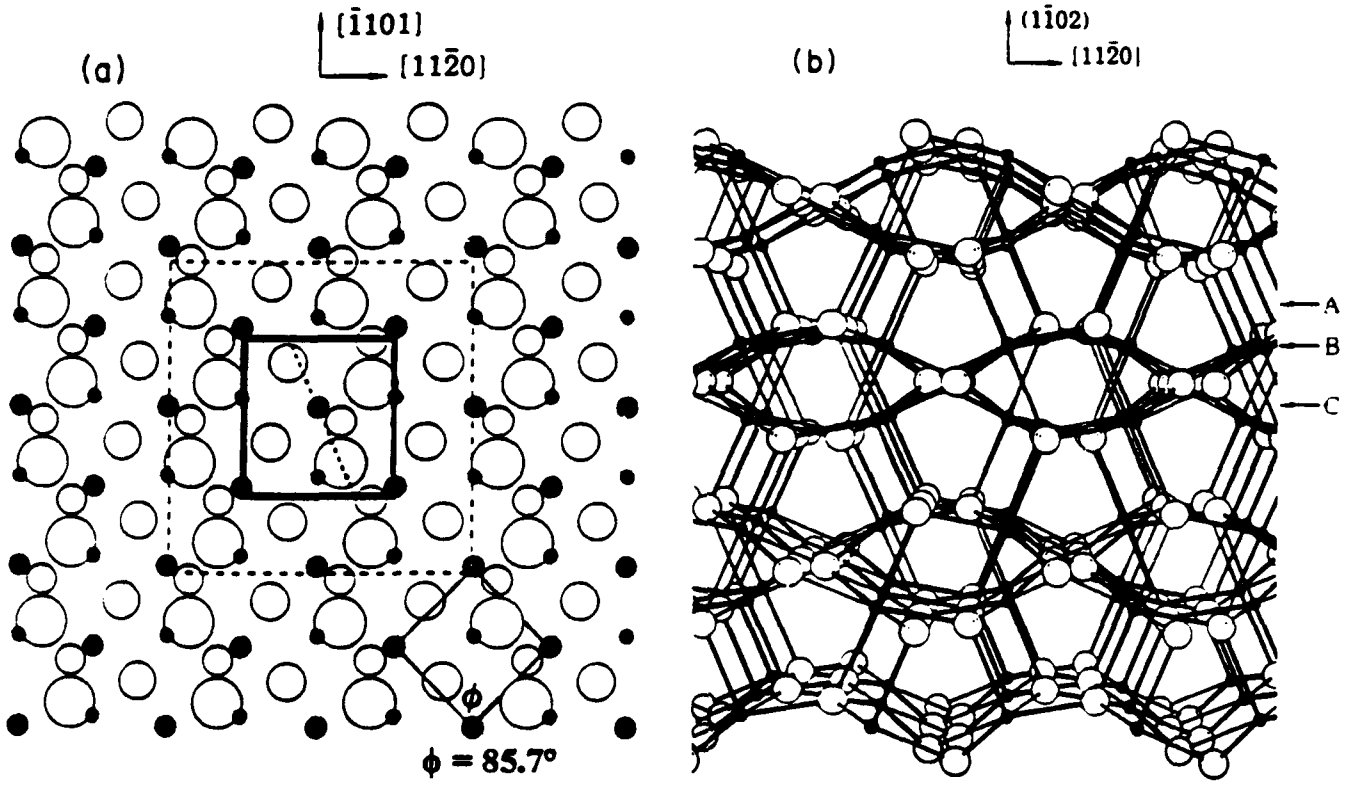

FIG. 5. Sapphire (1$\bar{1}$02) surface[46]: (a) top view of one surface building block made up of five atomic layers of O–Al–O–Al–O. The deeper the atom below the top layer, the smaller the radius. The open circles label O atoms. The large and small filled circles label Al atoms on the top and the bottom layers. The unit mesh area, 4.759 Å wide and 5.128 Å long, is enclosed by the dark solid lines. The fine solid lines enclose an area of side length 3.498 Å. The dashed circle is the lateral boundary of the cluster. (b) Side view along the [$\bar{1}$101] direction. The three arrows labeled A, B, and C indicate the three different (1$\bar{1}$02) planes.

et al.,[45] as the area (3.498 Å in each side) enclosed in fine solid lines. The interatomic distance mismatch for YBCO (a = 3.8336 Å and b = 3.8828 Å) is about 10–11% and the angles ∠(Al–Al–Al) are several degrees off 90°. It is suggested, therefore, that YBCO films deposited on a (1$\bar{1}$02) sapphire substrate (which is terminated in general with an oxygen layer as that presenting a lowest cleavage energy for this orientation[46]) will not, in general, have the (001) epitaxial quality. The so-called buffer layers, such as CeO_2 and YSZ, are entirely responsible for the reported (001) epitaxial quality films. Direct overgrowth of YBCO films on a (1$\bar{1}$02) sapphire substrate may be possible in a narrow substrate-temperature window; however, the in- and out-of-plane orientations will not be perfect.

Though the detailed substrate-film orientation relations may be considerably complicated for some of the substrates of the [K_2NiF_4], gehlenite, [$BaAl_2O_6$], spinel, garnet, and the magnetoplumbite structures, the primary adaptability of those materials as a host for overgrowth of the YBCO is due to their similarity in having the identical building blocks (oxygen octahedra) as are present in the perovskite structure of YBCO. YBCO films have been deposited on some of these materials, and the films reportedly have good superconductivity.[47]

VI. SUMMARY

From these preliminary considerations and supported by experimental evidence from a variety of sources, it is clear to us that the "lattice match" ideology used in discussing epitaxy is inaccurate and sometimes misleading. Similarity in structure is a higher order criterion than simply lattice matching though they are not independent. By analyzing a variety of substrate structures, it has been shown that it is the similarities in interatomic structure, which includes the ionic distributions and distances, that is the primary consideration for substrate selection. With this understanding, the range of potential HTSC substrates can be considerably broadened.

Interface layers suitable for "epitaxial" growth of YBCO thin films have been found empirically for many substrates of various structures of miscellaneous symmetries. Very rarely do authors report the quality (degree of orientation) of the buffer layer (e.g., CeO_2), which is in fact the directing substrate. Indeed, it

is not clear what orientations would result in with nearly zero structural interaction with the substrate. Consideration of control of morphology by strong bond chains, the so-called PBC (periodic bond chain) vectors of Hartman and Perdok,[48] may be particularly significant here. Noncrystalline oxides, fluorides, and glasses would serve as good testing cases.

A very important point to emphasize is, in the interatomic distance and angle calculations and analysis, the "ideal" surface termination was studied and the atomic arrangements that lie just on the surface of the crystal were assumed to be indistinguishable to that inside the bulk. It must be noted, however, the atoms on or very near a clean surface of a crystal need not maintain the atomic positions found in the bulk because atoms on the surface interact with atoms below the surface plane but not above. Deviations from the bulk atomic positions can cause changes either with [reconstruction-type, as for examples found in the case of Si(001)[49]] or without (relaxation-type in which the symmetry of the atoms on or near the surface is maintained, but the distances change between the successive planes of atoms parallel to the surface plane) the change in symmetry of atoms. The further detailed study requires knowledge of symmetry of the surface structure resolved from LEED (low-energy electron diffraction) patterns (or combinations with reflection electron microscopy or reflection high-energy electron diffraction techniques, etc.) by a LEED intensity analysis. Except in a few cases, such as Si and Al_2O_3, this type of information is very scarce for substrates of interest to us. This study is but a preliminary evaluation that gives a new perspective from which to look for potential substrates from the surface interatomic structure matching point of view, one step beyond the lattice matching consideration. It can be used to evaluate or screen potential substrates and to design an ideal deposition experiment.

ACKNOWLEDGMENTS

The authors would like to thank Professor D. K. Smith of Penn State University, for encouraging discussions and critical reading of the manuscript. His interests and expertise on the subject are greatly appreciated. The authors also thank Dr. D. J. Lam of the Argonne National Laboratory for discussions on ceramic epitaxy.

This work was supported by the Defense Advanced Research Projects Agency (DARPA) under the Contract No. DN 00014-90-J-4140.

REFERENCES

1. A. Perrin and M. Sergent, *Studies of High Temperature Superconductors*, edited by A. Narlikar (Nova Science Publishers, Commack, NY, 1991), Vol. 7.
2. R. Roy, R. Guo, A. S. Bhalla, and L. E. Cross, J. Vac. Sci. Technol. A **12** (2), 269 (1994).
3. T. V. Barker, J. Chem. Soc. Trans. **89**, 1120 (1906); Mineral. Mag. **14**, 235 (1907); and Z. Kristallogr. **45**, 1 (1908).
4. L. Royer, Bull. Soc. Fr. Mineral. Crist. **51**, 7 (1928).
5. D. W. Pashley, *Epitaxial Growth*, edited by J. W. Matthews (Academic Press, New York, San Francisco, London, 1975).
6. The Inorganic Crystal Structure Database (ICSD), copyrighted by Fachinformationszentrum-Karlsruhe, D-7514 Eggenstein-Leopoldshafen 2, Karlsruhe, West Germany.
7. W. Wong-Ng, F. W. Gayle, D. L. Kaiser, S. F. Watkins, and F. R. Fronczek, Phys. Rev. B **41** (7), 4220–4223 (1990).
8. R. Guo and D. K. Smith (unpublished research).
9. R. Guo, J. Povoa, and A. S. Bhalla (unpublished research).
10. T. Terashima, Y. Bando, K. Iijima, K. Yamamoto, and K. Hirata, Appl. Phys. Lett. **53**, 2232 (1988).
11. G. M. Meyer, R. J. Nelmes, and J. Hutton, Ferroelectrics **21**, 461–462 (1978).
12. S. A. Fedulov, Y. N. Venevtsev, and D. F. Dzhmukhadze, Kristallografiya **7**, 408–411 (1962).
13. R. Diehl and G. Brandt, Mater. Res. Bull. **X**, 85–90 (1975).
14. H. Brusset, H. Gillier-Pandraud, and J. L. Berdot, Bull. Societe Chimique de France **1967**, 2886–2890 (1967).
15. P. Vousden, Acta Crystallogr. **4**, 68 (1951); Acta Crystallogr. **4**, 373 (1951).
16. T. Moeller and G. L. King, J. Am. Chem. Soc. **75**, 6060–6061 (1953).
17. S. C. Abrahams and P. Marsh, Acta Crystallogr. B **42**, 61–68 (1986).
18. W. L. W. Ludekens and A. J. E. Welch, Acta Crystallogr. **5**, 841 (1952).
19. K. Knox, Acta Crystallogr. **14**, 583–585 (1961).
20. U. Wittmann, G. Rauser, and S. Kemmler-Sack, Z. Anorg. Allg. Chemie **482**, 143–153 (1981).
21. R. C. DeVries and R. Roy, J. Am. Chem. Soc. **75**, 2479–2484 (1953).
22. H. D. Megaw, Proceedings of the Physical Society, London **58**, 133–152 (1946).
23. N. G. Schmahl, J. Barthel, and G. F. Eikerling, Z. Anorg. Allg. Chemie **332**, 230–237 (1964).
24. P. Thompson, D. E. Cox, and J. B. Hastings, J. Appl. Crystallogr. **20**, 79–83 (1987).
25. G. Brauer and H. Gradinger, Z. Anorg. Allg. Chemie **277**, 89–95 (1954).
26. D. N. Batchelder and R. O. Simmons, J. Chem. Phys. **41**, 2324–2329 (1964).
27. H. Horiuchi, A. J. Schultz, P. C. Leung, and J. M. Williams, Acta Crystallogr. **40**, 367–372 (1984).
28. A. F. Wright and M. S. Lehmann, J. Solid State Chem. **36**, 371–380 (1981).
29. G. Vidal-Valat, J. P. Vidal, C. M. E. Zeyen, and K. Kurki-Suonio, Acta Crystallogr. B **35**, 1584–1590 (1979).
30. J. P. Oudalov, A. Daoudi, J. C. Joubert, G. leFlem, and P. Hagenmueller, Bull. Societe Chimique France **1970**, 3408–3410 (1970).
31. M. Kimata and N. Ii, Neues Jahrbuch fur Mineralogie Abhandlungen (Band-NR) **143**, 254–267 (1982).
32. P. Korczak and F. Raaz, Anzeiger der Oesterreichischen Akademie der Wissenschaften, Mathematisch-Naturwissenschaftliche Klasse **104**, 383–388 (1967).
33. H. Uchikawa and K. Tsukiyama, J. Ceram. Assoc. Jpn. **73**, 100–104 (1965).
34. W. Hoerkner and H. Müller-Buschbaum, Z. Anorg. Allg. Chem. **451**, 40–44 (1979).
35. G. Amthauer, V. Guenzler, S. S. Hafner, and D. Reinen, Z. Kristallogr. **161**, 167–186 (1982).
36. T. Yamanaka and Y. Takeuchi, Z. Kristallogr. **165**, 65–78 (1983).

37. V. A. Efremov, N. G. Chernaya, V. K. Trunov, and V. F. Pisarenko, Sov. Phys. Crystallogr. **33** (1), 19–22 (1988).
38. R. Feenstra, L. A. Boatner, J. D. Budai, D. K. Christen, M. D. Galloway, and D. P. Poler, Appl. Phys. Lett. **54**, 1063 (1989).
39. D. M. Hwang, T. Venkatesan, C. C. Chang, L. Nazar, X. D. Wu, A. Inam, and M. S. Hegde, Appl. Phys. Lett. **54**, 1702 (1989).
40. B. Oh, M. Naito, S. Arnason, P. Rosenthal, R. Barton, M. R. Beasley, T. H. Geballe, R. H. Hammond, and A. Kapitulnik, Appl. Phys. Lett. **51**, 852 (1987).
41. Y. Gao, K. L. Merkle, G. Bai, H. L. M. Chang, and D. J. Lam, Ultramicroscopy **37**, 326–340 (1991).
42. A. Perrin, M. G. Karkut, M. Guilloux-Viry, and M. Sergent, Appl. Phys. Lett. **58** (4), 412 (1991).
43. M. W. Denhoff and J. P. McCaffrey, J. Appl. Phys. **70** (7), 3986–3988 (1991).
44. X. D. Wu, R. C. Dye, R. E. Muenchausen, S. R. Foltyn, M. Maley, A. D. Rollett, A. R. Garcia, and N. S. Nogar, Appl. Phys. Lett. **58**, 2165–2167 (1991).
45. J. B. Boyce, G. A. N. Connell, D. K. Fork, D. B. Fenner, K. Char, F. A. Ponce, F. Bridges, J. Tramontana, A. M. Viano, S. S. Laderman, R. C. Taber, S. Tahara, and T. H. Geballe, SPIE **1187**, 136–147 (1989).
46. J. Guo, D. E. Ellis, and D. L. Lam, Phys. Rev. B **45** (23), 13647–13656 (1992).
47. G. C. Xiong, G. J. Lian, X. Zhu, J. Li, Y. J. Li, and Z. Z. Gan, IEEE Trans. Appl. Superconductivity **3** (1), 1429 (1993).
48. P. Hartman and W. G. Perdok, Acta Crystallogr. **8**, 165 (1955).
49. G. Burns and A. M. Glazer, *Space Groups for Solid State Scientists*, 2nd ed. (Academic Press, New York, 1990).

Appendix 3.

"Ion Polarizability Additivity Rule and Its Application on HTSC Substrate Materials," *Ferroelectrics* **155** (1-4) (Proceedings of the Eighth International Meeting on Ferroelectrics), 43-48, (1994).

Ruyan Guo

A.S. Bhalla

R. Roy

L.E. Cross

Ferroelectrics, 1994, Vol. 155, pp. 43–48
Reprints available directly from the publisher
Photocopying permitted by license only

ION POLARIZABILITY ADDITIVITY RULE AND ITS APPLICATION ON HTSC SUBSTRATE MATERIALS

RUYAN GUO, A.S. BHALLA, R. ROY AND L.E. CROSS
Materials Research Laboratory, The Pennsylvania State University
University Park, PA 16802 USA

(Received August 9, 1993, in final form October 31, 1993)

Abstract An ion polarizability additivity rule (R.D. Shannon)[1] was applied to calculate the dielectric constants of a large family of substrate materials (for HTSC films) and to compare with the measured dielectric constant values. The applicability and the limitations of the model were examined in light of experimental results of new substrate materials. The suitability and the limitations of the ion polarizability additivity rule in predicting dielectric constants of ionic materials were discussed. Possible causes of discrepancies found between the calculated and experimental values of the dielectric polarizabilities and dielectric constants were examined and modifications on the current additivity approach were proposed.

1. INTRODUCTION

Dielectric constant of substrates for HTSC thin films is an important selection criteria in addition to the suitability of the substrate for oriented film growth. To be used in microwave resonator applications where the substrates act as passive dielectrics, the suitable dielectric constant κ' values should be 20~25 and the dielectric loss tangent must be low ($<10^{-4}$). To be used for integrated circuits as the dielectric plane between the patterning, the κ' must be ~10 or less in order to accommodate the HTSC thin films (~1μm in thickness).

The macroscopic dielectric constant and the molecular polarizability are connected through the Clausius-Mosotti relation:

$$\alpha_D = \frac{3}{4\pi} V_m \frac{\kappa'-1}{\kappa'+2} \qquad (1)$$

where α_D is the dielectric polarizability and V_m is the molar volume in $Å^3$. Much of the effort in this field has been, rather than trying to resolve the local field of each complex substance, to utilize the increasing pool of dielectric polarizabilities of substances with various compositions and structures. Dielectric polarizabilities and hence the dielectric constants of new materials/compounds whose dielectric constants have not been measured are potentially predictable by linear addition of the molecular polarizabilities of simpler substances (molecular polarizability additivity rule)[2,3,4] or ion polarizabilities of individual ions (ion polarizability additivity rule).[3,4] Review and comments about the application of polarizability additivity rules can be found in Shannon's paper.[1]

Recently, molecular polarizabilities were used to calculate the dielectric constants of several substrate materials ($CaYAlO_4$, $CaNdAlO_4$, and $SrLaAlO_4$) of K_2NiF_4 structure and the comparison between the calculated and observed polarizabilities shown to have good agreement.[6] Shannon[1] has derived a set of

61 ion dielectric polarizabilities from a least square refinement procedure using the ion additivity rule and calculated dielectric constants for about a hundred compounds in conjunction with the Clausius-Mosotti equation. Excellent agreement between the polarizability values calculated and those experimentally measured was shown for many ternary systems including borates, aluminates, gallates, silicates, germanates, phosphates, and vanadates.

The research team at the Materials Research Laboratory, Pennsylvania State University, has been active in HTSC substrates study for the last two years and had proposed number of materials for potential substrate applications.[7,8] New materials such as $Sr(Al_{1/2}Ta_{1/2})O_3$ and $Sr(Al_{1/2}Nb_{1/2})O_3$,[9] $La(Mg_{2/3}Ta_{1/3})O_3$,[10] $La(Mg_{1/2}Ti_{1/2})O_3$,[11] and a family of materials of the magnetoplumbite structures[12] have been fabricated and their dielectric properties studied. It is of great interest for us to apply the ion polarizability additivity rule to the family of substrate or potential substrate materials for those we have gathered fair amount of dielectric and structural data that are previously unavailable.

In this paper we report the application of Shannon's model to the substrate materials; then the discrepancies between the experimental and the predicted dielectric polarizabilities (and the dielectric constants) are discussed. A new approach, applying apparent bond valence and its correlation to the bonding distance to derive "universal" or "normalized" (to its electrostatic bond valence) ionic polarizability, is proposed to modify current ion polarizability additivity approach. The derivation of the normalized ionic polarizability and the comparison of the experimental results to the predicted values obtained using the preliminary set of normalized ionic polarizabilities will be published elsewhere.[13]

2. SHANNON'S ION POLARIZABILITY AND THE ADDITIVITY MODEL

The method to obtain the ion polarizability data and the basic approach to predict the dielectric constants described by Shannon are schematically shown in Fig. 1. Several assumptions were applied by Shannon in the approach that include: Polarizabilities of cations and fluorine are independent of the compound in which the ions are found; Polarizability of oxygen was assumed to depend exponentially on the volume occupied by an oxide ion V_{ox}. This dependence can be disregarded for $V_{ox}<2.5\AA^3$; Polarizability of B^{3+} (in B_2O_3) was chosen to be $0.05\AA^3$ that gave the polarizability of O^{2-} to be $2.01\AA^3$.

3. COMPARISON OF EXPERIMENTAL AND PREDICTED VALUES

The calculation results using Shannon's ion polarizability data[1] (Table III, second column) and the ion polarizability additivity rule are shown in Table 1. Comparison of the calculated and experimental molar polarizability and dielectric constants are tabulated. All the materials chosen for this study were substrates which have been considered for use for HTSC film deposition or have been reported as effective substrate for HTSC thin films. Some materials which appeared in Shannon's database or calculation are also included for the sake of completeness. Most of the structural data, symmetry parameters and the

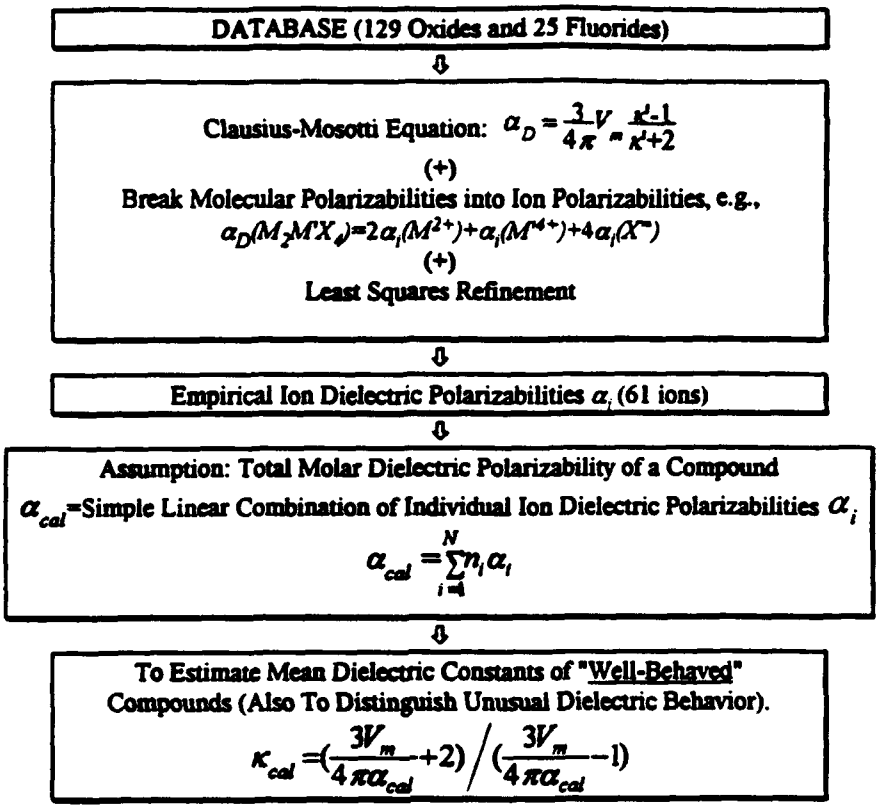

FIGURE 1. Schemetic approach of the ion polarizability additivity rule applied by Shannon.[1]

molar volume (V_m), are reasonably well established and the refined single crystal structure information used may be found in The Inorganic Crystal Structure Database (ICSD).[14] Crystal structures and the molar volumes of new substrate materials are determined on available single crystal samples (grown by a laser heated pedestal growth technique) by x-ray diffraction. Ceramic samples of new substrate materials are also used, only for those well sintered samples having high density and cubic or pseudocubic symmetries. The experimental value of the dielectric constants were taken from Shannon's database wherever available, otherwise the reference is given in the table. Dielectric constants of new substrate materials are measured using a high precision capacitance measurement system (Gen Rad 1621) in frequency range 10^3-10^5 Hz at room temperature and resonance technique or cavity perturbation techniques at the microwave frequencies (GHz). Details regarding the synthesis, preparation, and properties of new substrate materials may be found in the referred publications.

Several observations on the results listed in Table 1 are worth mentioning for further discussions. First, it is strikingly apparent that small discrepancies in molar polarizability can many times cause large discrepancies in dielectric constant prediction that indicates the V_m value in dielectric constant prediction plays a significant role. Second, good agreements are usually seen in case of substances containing cations having high valence and small sizes, while large discrepancies are common in ternary systems

that involve large cations in high coordination sites. Third, poor agreements are found in materials containing Nb or Ta ions such as $Ba(Mg_{1/3}Ta_{2/3})O_3$, $Sr(Al_{0.5}Ta_{0.5})O_3$, and $Sr(Al_{0.5}Nb_{0.5})O_3$ and cations of rare-earth family such as $LaAlO_3$.

TABLE I. Comparison of Calculated and Experimental Dielectric Constants Using Ion Polarizability Additivity Rule.[1]

Substance	Space Gr. or Sym.	V_m	κ'_{exp}	κ'_{cal}	$\Delta\alpha$%
Al_2O_3	R3ch	42.45	9.34, 9.34, 11.54	10.05	0.06
CaF_2	Fm3m	40.75	6.81	6.77	0.23
MgO	Fm3m	18.68	9.65	9.86	-0.61
Ba_2YSbO_6	Cubic	139.53	25.0	23.71	0.63
$Sr(Ga_{.5}Ta_{.5})O_3$	Cubic	61.58	26.9	31.54	-1.60
MgF_2	P42/mnm	32.40	5.50	5.31	1.73
$(Sr_{0.5}Ca_{0.5})(Ga_{0.5}Nb_{0.5})O_3$	Cubic	58.64	32.0	25.41	2.32
SiO_2 (quartz syn)	P6222	39.37	4.42, 4.41, 4.6	4.26	3.10
$Zr_{0.72}Y_{0.28}O_{1.862}$	Pm3m	34.35	29	21.43	3.60
$BaZrO_3$	P23	73.10	43.0	27.59	3.72
$NdGaO_3$ (NG)	Pbn21	57.68	20-25	31.66	-3.80
$CaYAlO_4$	Tetra	79.85	21.44,21.44,16.12	15.54	3.80
1/3SAN-1/3SAT-1/3NG	Cubic	63.30	22.8	17.13	4.08
$Nd_{.39}Sr_{.61}Al_{.695}Ta_{.305}O_3$		56.76	24.04	39.20	-4.79
$La(MgAl_{11})O_{19}$	Hex	296.86	13.50	10.81	5.03
$GdAlO_3$		51.87	19.50	29.17	-5.03
$LiBaF_3$	Cubic	63.40	11.71	14.98	-5.40
$0.7Sr(Al_{.5}Nb_{.5})O_3$-$0.3NdGaO_3$	Cubic	63.30	23.50	16.06	5.49
$0.7Sr(Al_{.5}Nb_{.5})O_3$-$0.3LaAlO_3$	Cubic	63.28	25.90	17.02	5.63
$SrLaAlO_4$	Tetra	88.99	16.70,16.70,20.02	28.30	-6.19
$Sr(Al_{.5}Nb_{.5})O_3$ (SAN)	Cubic	59.09	17.30	27.08	-6.19
$KMgF_3$	Pm3m	63.00	5.98	6.97	-6.66
$KZnF_3$	Pm3m	66.70	8.85	7.20	6.85
$0.7Sr(Al_{.5}Ta_{.5})O_3$-$0.3LaAlO_3$	Cubic	58.08	21.9	45.52	-7.08
$La(Mg_{2/3}Ta_{1/3})O_3$	Hex	74.33	24.1	14.56	7.30
$Nd(MgGaAl_{10})O_{19}$	Hex	296.50	14.9	10.60	7.37
$0.7Sr(Al_{.5}Ta_{.5})O_3$-$0.3LaAlO_3$	Cubic	57.89	21.9	47.94	-7.44
$PrAlO_3$	R3-mr	53.25	25.0	64.81	-7.45
$SmAlO_3$	Pbnm	52.30	19.0	38.53	-8.03
$BaSnO_3$	P23	69.40	18.0	36.06	-8.37
$LaGaO_3$	[$GdFeO_3$]	59.10	25.0	81.33	-8.45
$(Ba_{0.8}Sr_{0.2})(Mg_{1/3}Ta_{2/3})O_3$	Cubic	67.48	25.9	91.67	-8.46
$(Ba_{0.9}Sr_{0.1})(Mg_{1/3}Ta_{2/3})O_3$	Cubic	67.84	25.3	123.65	-9.66
$CaGa_{12}O_{19}$	Hex	301.48	9.70	15.12	-9.83
$Ba(Mg_{1/3}Ta_{2/3})O_3$	Hex	68.59	24.6	138.91	-10.31
$La(Mg_{.5}Ti_{.5})O_3$	Cubic	60.10	26.5	355.40	-10.83
$NdAlO_3$	R3ch	52.80	17.50	46.89	-10.93
$CaGa_6Al_6O_{19}$	Hex	302.00	18.2	10.72	11.43
$0.7Sr(Al_{.5}Ta_{.5})O_3$-$0.3NdGaO_3$	Cubic	57.90	16.3	42.22	-11.49
$LaAlO_3$	R3mr	54.40	23.8	406.86	-10.96
$YAlO_3$	P63/mmc	61.69	16.83,16.83,15.94	8.79	14.13
$Sr(Al_{.5}Ta_{.5})O_3$ (SAT)	Cubic	59.09	11.78	37.36	-18.09
CeO_2	Fm3m	78.25	7.0	4.59	18.33

4. DISCUSSION

Origin of Large Discrepancy in Predicted Dielectric Constants Values

Obviously any inaccuracy in dielectric constant measurements or structure parameter determinations are the up front cause for the discrepancies. All the data used in our calculation are believed to be the most reliable data available.

Besides experimental errors, large deviations from additivity rule using Shannon's ion polarizability data can sometimes be traced to, as pointed out by Shannon, unusual properties of the compounds such as ionic or electronic conductivity, the presence of dipolar impurities, or piezo- or ferroelectricity. However, above mentioned irregularities are presumably non existent in the substrate materials in current study.

After taking into consideration the oxygen polarizability dependence of the volume, V_{ox}, the calculation in table 1 was repeated using the refined ion polarizabilities given by Shannon[1] (Table III, first column). The improvement is insignificant and discrepancy is largely non corrected.

A critical question needed to be answered after examining the ion polarizability calculation is whether the assumption is valid that cation (and fluorine) polarizability is independent of the compound in which it is found.

There seems to be enough indication that suggests the answer to the this question is no. Evidence was presented by Safford and Silverman[15] that a change of coordination of an ion alters the molar refraction contribution of the ion or more correctly of the group immediately surrounding the ion. Fajans and co-workers[16] showed that the coordination number of Zn^{2+} is related to the molar volume (of Zn^{2+}) and demonstrated a relationship between molar refraction and molar volume (of the cation). These authors showed that the Al^{3+} in fourfold coordination in glass or in certain crystals has a molar refraction contribution of 12.3 (calculated for Al_2O_3), whereas in sixfold coordination it is 10.5. Kreidl[17] first indicated that MgO may assume both "basic" and "acidic" properties in glass. Difference in molar refractions were found for Mg^{2+} in sixfold coordination such as in periclase MgO where R=4.538, and in fourfold coordination such as in spinel $MgAl_2O_4$ where R=5.18.[18] For ions preferably found only in the same coordination, the dielectric polarizability of the ion remains relatively constant and the additivity rule applies well. Molar volumes of the compounds in these cases are all one need to calculate total polarizabilities of the compounds. Examples of this type would be the silicates and borates. For substances that contain cations which are found in different coordination, the difference in the dielectric polarizability is averaged when enough (unbiased) substances are used in the least square fitting process and therefore good or fair additivity application can be obtained. Examples of this type may be identified as aluminates, and gallates. However, for cations like Cu^{2+}, Ba^{2+}, RE^{3+}, Sb^{3+}, As^{3+}, Nb^{5+}, Ta^{5+}, the ion polarizability data are scarce and single crystal data are not available, the uncertainties are larger because the ratio of the number of observed molar polarizabilities to refined ion polarizabilities is rather low and the observed total polarizabilities have larger errors (as also noted by Shannon).

Modification Proposed on Current Additivity Approach

Following the above discussion, if the dielectric polarizability of a cation is dependent on individual compound, can a set of generally constant ion polarizability data be found and valid for use by the additivity rule for a broad range of compounds with various coordination combinations or crystallographic senses? Following the work of O'Keeffe[19] and Brown and Altermatt[20] on the apparent bond valences and their relations to bond lengths, we suggest reformulating of the ion polarizability additivity rule by normalizing each ion polarizability to its electrostatic valence status. This new approach defines the normalized ion polarizability which is applicable for estimation of the dielectric constants with higher precision once the refined crystal structure is known. The derivation of the modified ion polarizability data and the preliminary examination on ionic materials of broad range is in progress.

ACKNOWLEDGMENT

This work was supported by the Defense Advanced Research Projects Agency (DARPA) under the contract DN 00014-90-J-4140.

REFERENCES

[1]R.D. Shannon, *J. Appl. Phys.* 73(1), 348 (1993).
[2]A. Heydweiller, *Z. Phys.* 3, 308 (1920).
[3]D.A.A.S. Narayana Rao, *Proc. Ind. Acad. Sci.* 30A, 317 (1949).
[4]A.C. Lasaga and R.T. Cygan, *Amer. Mineral.* 67, 328 (1982).
[5]R. Roberts, *Phys. Rev.* 76, 1215 (1949).
[6]R.D. Shannon, R.A. Oswald, J.B. Parise, B.H.T. Chai, P. Byszewski, A. Pajaczkowska, and R. Sobolewski, *J. Solid State Chemistry* 98, 90-98 (1992).
[7]R. Guo, A.S. Bhalla, and L.E. Cross, *J. Appl. Phys.* (to be published).
[8]L.E. Cross, R. Roy, A.S. Bhalla, R. Guo, J. Sheen, S. Erdei, F.W. Ainger, and E.C. Subbarao, presented at the Defense Advanced Research Projects Agency 3rd Annual High Temperature Superconductor Workshop, Seattle, Washington, Sept.30-Oct.2 (1991).
[9]R.Guo, A.S. Bhalla, J. Sheen, S. Erdei, F.W. Ainger, E.C. Subbarao, and L.E. Cross, *J. Mater. Res.* (to be published).
[10]P. Ravindranthan el al. (to be published).
[11]G. Harshe et al. (to be published).
[12]R.Guo and A.S. Bhalla, (to be published).
[13]R. Guo, A.S. Bhalla, R. Roy, and L.E. Cross, *J. Appl. Phys.* (to be published).
[14]The Inorganic Crystal Structure Database (ICSD), copyrighted by Fachinformationszentrum-Karlsruhe, D-7514 Eggenstein-Leopoldshafen 2, Karlsruhe, West Germany.
[15]H.W. Safford and A. Silverman, *J. Am. Ceram. Soc.*, 30, 203 (1947).
[16]K. Fajans and N.J. Kreidl, *J. Am. Ceram. Soc.*, 31, 105 (1948); K. Fajans and G. Joos, *Z. Physik*, 23, 1 (1923).
[17]N.J. Kreidl, *Glastchn. Ber.*, 7, 313 (1929).
[18]Rustum Roy, *J. Am. Chem. Soc.*, 72, 3307 (1950).
[19]M. O'Keeffe, *Structure and Bonding*, 71 (Springer-Verlag, Berlin Heidelberg, 1989) p.163-190.
[20]I.D. Brown and D. Altermatt, *Acta Cryst.* B41, 244 (1985).

Appendix 4.

"$Ba(Mg_{1/3}Ta_{2/3})O_3$ Single Crystal Fiber Grown by Laser Heated Pedestal Growth Technique,"

J. Appl. Phys. **75**(9) 4704-4708 (1994).

Ruyan Guo

A. S. Bhalla

L.E. Cross

$Ba(Mg_{1/3}Ta_{2/3})O_3$ single crystal fiber grown by the laser heated pedestal growth technique[a)]

Ruyan Guo, A. S. Bhalla, and L. E. Cross
Materials Research Laboratory, The Pennsylvania State University, University Park, Pennsylvania 16802

(Received 22 July 1993; accepted for publication 26 January 1994)

The preparation of $Ba(Mg_{1/3}Ta_{2/3})O_3$ (BMT) ceramics and the first successful growth of BMT single crystals by the laser heated pedestal growth technique (LHPG) is reported. The single crystal has a simple cubic perovskite structure in comparison to the ordered hexagonal structure normally found in ceramics of the same phase. The dielectric properties of single crystals are examined, the dielectric Q value increases with the increase in B-site ordering, while the dielectric constant κ is relatively independent of ordering. Our results also show that BMT is a candidate substrate for high T_c superconductor thin films as it has one of the highest Q values known for the oxide perovskite family, along with its matching thermal expansion coefficient $\alpha = 9.0 \times 10^{-6}$/ °C and twin-free cubic perovskite structure with $a = 4.0877$ Å. BMT single crystals grown by the LHPG technique are probably the highest melting oxide compounds grown to date.

I. INTRODUCTION

Ceramics of complex perovskite oxides $A(Ba1_{1/3}B2_{2/3})O_3$ type were previously explored in search of candidate materials with excellent microwave dielectric properties.[1] $Ba(Mg_{1/3}Ta_{2/3})O_3$ (BMT), in particular, was reported to have a dielectric constant $\kappa \sim 25$ and a dielectric $Q \sim 16\,800$ (one of the highest in the oxide family) at 10.5 GHz in samples with a 1 mol % Mn additive as a sintering aid.[2] However, the reported Q values in BMT are widely scattered (5000~50 000), presumably due to differences in B-site ordering and the density of the ceramic body. Sintering additives, such as Mn[2] or Sn[3] or rapid sintering methods,[4] have been used to obtain dense ceramics with improved microwave properties in this poorly sinterable compound. It has been reported that Q values increase with increases in B-site ordering and bulk density of the ceramic,[4] although the individual effects of density and ordering on the dielectric Q have not been determined since variations in density and ordering occur simultaneously in these ceramics.

BMT is one of the most refractory oxide dielectrics; therefore single crystal growth is quite difficult. A BMT single crystal was grown from a BaF_2 flux and yielded a significantly higher dielectric constant (~200),[5] presumably attributable to flux contamination. No detailed study on the properties of a single crystal BMT is currently available.

Motivated by a search for suitable substrate materials for high T_c superconducting (HTSC) thin films for microwave device applications, various mixed perovskite oxides were studied. BMT, with a high dielectric Q, was a promising candidate. Single crystal growth was attempted without the use of flux utilizing the laser heated pedestal growth (LHPG) technique. BMT ceramic preparation, the first successful growth of BMT single crystals by the LHPG technique, and their characterization are presented. The single crystal has a simple cubic perovskite structure as opposed to the ordered hexagonal structure normally obtained in well-sintered ceramics.[6] The dielectric properties of single crystals were examined: the Q value increased with increased B-site ordering, while the dielectric constant κ was more dependent on the density of the sample. Our results also establish BMT as a potential HTSC thin film substrate since it has one of the highest Q values known for the oxide family, in addition to its moderate dielectric constant, good thermal expansion coefficient matching, and twin-free cubic structure with acceptable lattice misfit to the $YBa_2Cu_3O_{1-\delta}$ (YBCO) superconductor.

II. EXPERIMENT

A. Preparation of ceramic preforms

In addition to preparing ceramic samples for dielectric characterization, ceramic processing was also necessary to provide ceramic seed and feed rods for crystal fiber growth using the LHPG technique.

Ceramic specimens were prepared by solid state reaction using conventional techniques. Differential thermal analysis (DTA) was used to determine the minimum calcining temperature and select sintering temperatures. Powder x-ray diffraction was used extensively to characterize the crystallographic phases and adjust processing conditions. High purity magnesium oxide (3N5), tantalum pentoxide (4N) and barium carbonate (Grade 1) were used as starting chemicals. The ground mixture was calcined in an alumina crucible at 1500 °C for 3 h. The sintering time varied from 3 to 35 h at temperatures from 1600 to 1670 °C.

The sintered pellet ($\phi \sim 35$ mm) was sliced into wafers approximately 2 mm thick, ground to 0.4–0.8 mm thick, then cut into square rod preforms.

Ceramic disks used for low frequency dielectric measurement were prepared using the same process. Sputtered gold electrodes were used for all rf dielectric property measurements.

[a)]Part of this work was first presented at the DARPA 3rd Annual High Temperature Superconductor Workshop, Sept. 30–Oct. 2, 1991, Seattle, Washington. Related presentations were also made at the DARPA/ONR Workshop on Substrate Materials for High T_c Superconductors, Feb. 5–7, 1992, Williamsburg, Virginia.

 0021-8979/94/75(9)/4704/5/$6.00

B. Laser heated pedestal growth

The laser heated pedestal growth technique is a powerful tool for rapid growth of small-diameter single crystals (particularly high melting temperature oxides) for both property study and fiber devices.[7] The LHPG equipment used in this investigation consisted of a power source (water cooled, tunable flowing gas CO_2 55 W laser), an optical layout, and a growth section. The circular laser radiation of the TEM_{00} mode was transformed into an annulus by a reflaxicon.[8] The annulus was directed onto a parabolic mirror that focused the radiation back to its focal point, forming the hot zone. The pulling heads were high precision five-phase microstepper motors, with a single step increment of 25 μm. The growth chamber was a stainless steel vacuum chamber enclosing the reflaxicon and the internal optics to minimize air current disturbances and allow growth to take place in reducing or oxidizing atmospheres. A further description can be found elsewhere.[9,10]

C. Dielectric measurements

The rf dielectric constants and loss tangents were measured using a General Radio 1621 capacitance measurement system. Three-terminal measurements were conducted using a shielded sample holder. The accuracy of the measurements was in the range of $\pm$(10–50) ppm for capacitance and $\pm$(0.1+1 step in least significant decade) for conductance. The stray capacitance, lead, and contact resistances were corrected during measurement by taking open circuit measurements. Edge corrections of the measurement results were made using an empirical equation obtained from the measurement results for a family of fused silica samples,

$$C_e=\left(0.02798\times \ln\left(\frac{P}{t}\right)-0.05922\right)P, \qquad (1)$$

where C_e is the edge capacitance, P and t are the perimeter and the thickness, respectively, of the sample in cm.

III. RESULTS AND DISCUSSION

After calcination at 1500 °C for 3 h, powder x-ray diffraction showed the crystallographic phase to be single-phase pseudocubic perovskite with a weak superlattice diffraction, indicating a lack of grain growth and absence of a long range order of B-site (Mg,Ta) ions [see Fig. 1(a)]. The material developed strong ordering with hexagonal symmetry and lattice parameters of $a=5.7731(6)$ Å and $c=7.0941(2)$ Å after sintering at 1655 °C for 5 h, as seen in Fig. 1(b). Lattice parameters of $a=5.782$ Å and $c=7.067$ Å in BMT have been previously reported.[6]

The crystallographic structure of BMT is known to be similar to that of $Ba(Sr_{1/3}Ta_{2/3})O_3$, based on the $P\bar{3}m1$ space group. The perovskite structure consists of close-packed layers of Ba and oxygen ions perpendicular to [111], with Mg and Ta ions occupying the octahedral holes between the layers. When fully ordered, the Mg^{2+} and Ta^{5+} ions form planes parallel to the close-packed layers with a three-layer repeat sequence (two layers of Ta^{5+} ions and one layer of Mg^{2+} ions). The ordering parameter S is defined as follows:

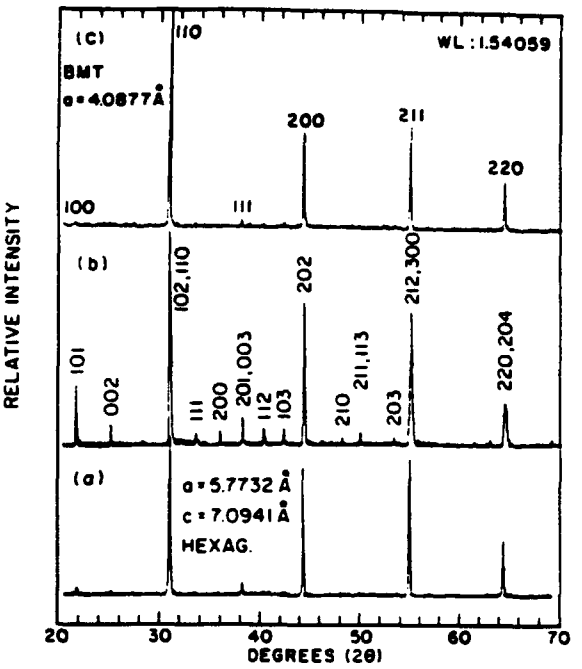

FIG. 1. Typical x-ray diffraction pattern of $Ba(Mg_{1/3}Ta_{2/3})O_3$: (a) ceramic powder calcined at 1500 °C for 3 h showing weak ordering; (b) ceramic sintered at 1655 °C for 5 h showing strong B-site ordering; and (c) single crystal (powder) grown by LHPG showing an ideal simple cubic perovskite structure with $a=4.0877$ Å. BMT ceramic XRD patterns are indexed as a hexagonal perovskite structure with $a=5.7731(6)$ Å and $c=7.0941(2)$ Å.

$$S=\sqrt{\frac{(I_{100}/I_{110})_{obs}}{(I_{100}/I_{110})_{order}}}, \qquad (2)$$

where $(I_{100}/I_{110})_{obs}$ is the ratio of observed intensities between the superstructure 100 and the simple cubic 110 diffraction peaks. The ratio of intensities for a completely ordered structure $(I_{100}/I_{110})_{order}$ is calculated to be 8.3/100. The value of S varies from 0 for disordered to 1 for complete ordered powder. The ordering was found to be nearly 100% in the case of Fig. 1(b).

Various sintering conditions were evaluated to obtain high density ceramic samples. Samples sintered at 1600 °C for 3 h were 91.8% of theoretical density. Successive improvements in density were obtained for sintering temperatures above 1650 °C for prolonged times. A highly densified sample was obtained after sintering at 1655 °C for 35 h while the sample was embedded inside a prefired (at 1670 °C) $Sr(Al_{1/2}Ta_{1/2})O_3$ powder.[10] Well-sintered ceramic pellets with a 99.7% theoretical density and a 5–10 μm grain size were produced. The sintered BMT disks were translucent, with a light yellowish color.

Single crystal fibers of BMT were difficult to grow. Since there was no single crystal available to be used as a seed, both feed material and the pulling seed were ceramics, prepared as previously described. The primary difficulty was due to the extremely high temperature necessary to sustain stable growth from the melt. The actual molten zone temperature was observed to be as high as 3100 °C. At such high temperatures, vaporization of residues of simple oxides such as MgO could take place at the hot spot, due to the temperature gradient and nonuniformity (if present) of the molten

zone. Therefore, careful alignment of the sample and precise control of the molten zone shape were critical.

A single crystal BMT was grown using ceramics as the feeding rod (~0.45 mm^2 in cross section) and pulling seed (~0.12 mm^2 in cross section). A mass conservation relation was used to adjust the growth parameters,

$$R_f d_f^2 S^2 = R_s d_s^2, \tag{3}$$

where R_f and R_s are the translational rates of the feed rod (f) and the seed rod (s), d_f and d_s are the linear dimensions of the feed and seed rods, respectively, and S is the ratio of linear shrinkage between the ceramic and crystal (this needs to be experimentally determined for individual materials). BMT single crystal fibers, ranging from 300–1000 μm in diameter and 1–2 cm in length using pulling rates (R_s) of 0.5 to 1 mm/min were grown. The S ratio was determined for each batch of ceramic preforms and was found to vary between 0.697 and 0.714. The molten zone temperature during a growth run was measured to be 2960–3112 °C, with an accuracy of ±30 °C.

A powder x-ray diffraction pattern of the BMT crystal fiber grown by LHPG [Fig. 1(c)] reveals a simple cubic symmetry with unit cell parameters $a=4.0877$, $V=68.301$ Å^3, $Z=1$ and $\rho=7.635$ (g/cm^3), and no B-site ordering. The high temperature phase persisted to room temperature as the B-site ordering is inhibited during fiber growth due to quenching effects produced by the high growth rates and steep axial temperature gradients employed in LHPG growth. The high temperature disordered phase has not been previously reported. This high temperature phase is very stable and no appreciable B-site ordering was found after annealing the crystal at 1600 °C in air for 3 h.

As-grown BMT crystals were colorless and transparent. No clear facet can be seen in a fiber of a 500 μm diameter. The [112] was found to be the growth direction (parallel to the fiber pulling direction) by Laue back-reflection photography. A Laue photograph of a single crystal BMT fiber with the beam parallel to the fiber growth direction is presented in Fig. 2. This pattern does not have a twofold symmetry axis normal to the plane. The [011] direction is 30° from the [112] towards the [110]. The [001] direction is 35°16′ from the [112] towards the [$\bar{1}\bar{1}$2].

Ceramic and single crystal BMT samples were analyzed quantitatively for their chemical compositions using electron probe microanalysis (EPMA, CAMECA SX-50) with spatial resolutions of 2 μm in surface area and 0.2 μm in depth. The relative analytic accuracy was ±2%. Chemical analysis showed that single crystal BMT grows congruently within the stoichiometric composition. The resultant composition of a BMT single crystal fiber as grown was found to be $Ba_{1.003\pm0.006}(Mg_{0.313\pm0.006}Ta_{0.672\pm0.003})O_3$. Light colored regions of 1–2 μm in size in less perfect crystals (typically, at the beginning of the fiber growth) were found to be Mg-deficient, although no interruption in crystal growth continuity was found (within the resolution limit of the microscope). The Ba:Ta:O ratio in these Mg-deficient regions was close to 5:4:15. It is therefore hypothesized that $Ba_5Ta_4O_{15}$,[11] a five-layer high temperature ABX_3 hexagonal structure deviating from ABX_3 stoichiometry, may have formed because some

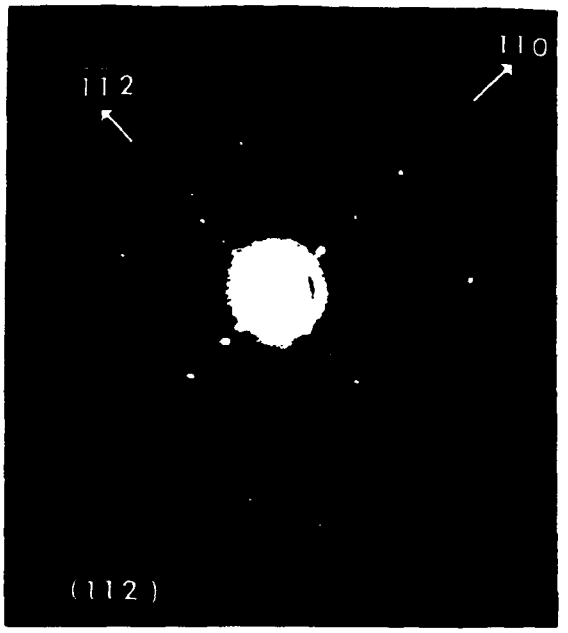

FIG. 2. Laue back-reflection photograph of a single crystal BMT fiber with the beam parallel to the fiber growth direction (distance=3 cm). Beam is approximately parallel to [112].

face-sharing octahedral sites are unoccupied. The fiber surface does not show enhanced Mg deficiency, nor do fibers obtained from stable growth. It is postulated that MgO vaporization may have taken place during the initial stage of growth when the molten zone is neither uniform nor stabilized. It was reported that an intermediate $BaTa_2O_6$ phase forms during the sintering process.[12] Similar phases were not found in our ceramic or single crystal samples, by either x-ray diffraction or EPMA.

Dielectric properties of ceramic and single crystal samples were examined as functions of temperature in the rf region. The dielectric constant κ of a single crystal BMT is presented as a function of temperature in the low frequency region in Fig. 3. Table 1 summarizes the dielectric properties of both ceramics and single crystals. It is a general trend that both the dielectric constant and the Q factor in bulk ceramic samples increase with increasing density, as does B-site or-

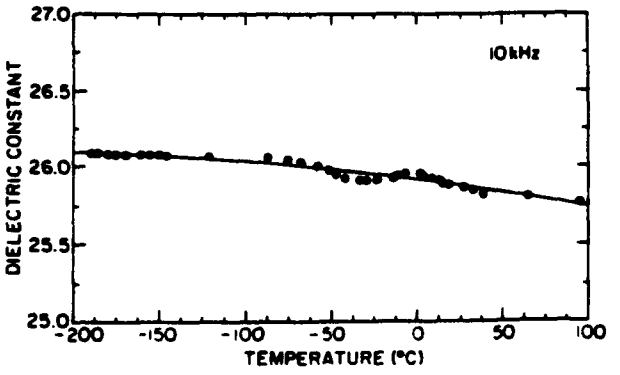

FIG. 3. Dielectric constant measured as a function of temperature for single crystal $Ba(Mg_{1/3}Ta_{2/3})O_3$.

TABLE I. Dielectric properties of BMT ceramics and single crystals synthesized under various processing conditions.

BMT sample No.	Sintering conditions	% x-ray density	Order parameter S	κ (10 kHz.RT)	Q (10 kHz.RT)
1	1600 °C 3 h	91.8	0.85	21.17	277
2	1630 °C 10 h	97.0	0.92	22.91	3012 ~5980
3	1655 °C 5 h	99.5	~1	23.33	9296
4	1655 °C 35 h	99.7	~1	24.97	30,536 ~47,600
Crystal fiber	(LHPG)	(Crystal)	0	25.9 (at 10 kHz) 26.50 (at 10 GHz)[a]	3597

[a]After Ref. 13.

dering. Although the dielectric loss maintained a very low value (2.78×10^{-4} at ambient temperature and $<10^{-5}$ at 80 K and 10 kHz) in cubic single crystals, the highest Q values (up to 35 000 at room temperature and 10 kHz) were obtained in high density hexagonal ceramic samples. The dielectric constant κ of the single crystal sample was measured by a cavity perturbation technique at microwave frequencies[13] and found to be comparable to the high density ceramic samples. Thus the individual effects of densification and B-site ordering on the dielectric properties of BMT can be determined. The dielectric constant increases with increases in bulk density, while Q essentially increases with the enhancement of B-site ordering.

Thermal expansion measurements were conducted from room temperature to about 800 °C using a vertical push-rod dilatometer equipped with a high-sensitivity linear variable differential transformer (LVDT). The heating and cooling rates for thermal expansion measurements were regulated at 1 or 1.5 °C/min using a microprocessor based temperature controller. The thermal expansion coefficients of BMT were measured in comparison to those of the YBCO superconductor. As seen in Fig. 4, the thermal strain in BMT is a close match to the average thermal strain in a ceramic YBCO sample. No structural phase transition is found within the measured temperature region. Thermal property matching of BMT is important for its potential application as a microwave substrate material for HTSC epitaxial films.

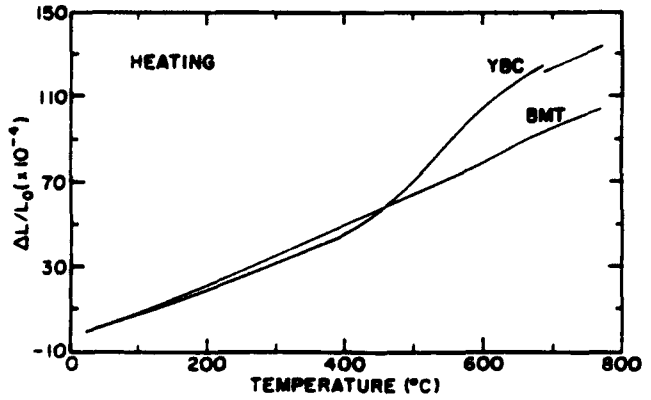

FIG. 4. Thermal expansion of $Ba(Mg_{1/3}Ta_{2/3})O_3$ and YBCO ceramic samples measured by the push-rod linear voltage differential transformer method.

An attempt was made to study the dielectric properties of BMT at different ordering levels by quenching the fully ordered ceramic samples at various conditions. The results, however, were not conclusive, primarily due to the poor quenching effectiveness of the sample.

There has been no study reported previously on the melting behavior of the BMT ternary compound. BMT has an apparent melting temperature (as measured by optical pyrometer during LHPG growth) that surpasses its simple oxides end members (BaO, M.P.=1923 °C; MgO, M.P. =2800 °C; and Ta_2O_5, M.P.=1800 °C). This seems logical, as experimental results show BMT to be a congruent melting compound. It must be noted, however, that the molten zone temperature reported for stable single crystal growth represents the upper-bounds of the melting temperature. Actual melting most probably takes place at a somewhat lower temperature. No oxide single crystals, to our knowledge, have been grown at such elevated temperatures directly from the melt. The feasibility of growing highly refractory material illustrates the unique advantage of the LHPG technique, as there is practically no limit on growth temperature because no crucible is needed nor is contamination introduced by means of a flux.

The disordered BMT single crystal with high temperature symmetry is not a "well-behaved" material from a dielectric characteristic point of view. The random distribution of B-site cations causes an overall reduction of 0.42% in molecular volume. The larger Mg^{2+} cation (0.86 Å)[14] is forced into a compressed state and the smaller Ta^{5+} cation (0.78 Å)[14] into a "rattling" state. The lower dielectric Q values obtained for single crystal samples compared to dense, and fully B-site ordered, ceramics is evidence of an overall increase (due to the 1:2 Mg^{2+}:Ta^{5+} ratio) in ionic polarizability arising from the rattling Ta^{5+} cations. On the basis of classical dielectric dispersion theory, the loss factor D is approximately proportional to the damping constant. The damping constant is characteristic of the interaction of electromagnetic waves and electric dipoles associated with lattice vibrations, and attributable to lattice anharmonic interactions and lattice imperfections including impurities, dislocations, and local strains.[15] It is therefore reasonable that the disordered single crystal BMT samples have a higher loss factor than fully ordered ceramics, even though their dielectric constants are comparable.

The BMT lattice parameter of $a=4.0877$ Å represents a lattice mismatch of 5.3% to the b axis of YBCO ($b=3.883$ Å), seemingly a less than ideal substrate for YBCO. However, there has been no clear cutoff established for lattice parameter matches for "epitaxial" (or highly oriented) YBCO film deposition. Epitaxial YBCO thin films on MgO single crystals (with a mismatch of 8.5%) have been reported.[16] BMT single crystals have a twin-free cubic perovskite structure that is advantageous as a substrate, compared to some of the heavily twinned substrates (e.g.,

$LaAlO_3$ and $NdAlO_3$). High temperature BMT single crystals grown by LHPG are twin free, of moderate dielectric constant, low dielectric loss, and good thermal expansion matching and are therefore identified as potentially suitable substrates for HTSC thin film deposition.

The application of BMT as a substrate, in addition to its crystal fibers for microwave antenna applications, may be restricted due to growth difficulties. The skull melting growth technique[17] could presumably be used to grow BMT crystals of adequate size. The high melting temperature of BMT will not be a crucial issue when the material is used as an insulating layer between YBCO films in a multichip-module integrated structure because vapor phase deposition techniques (e.g., laser ablation and metal-organic chemical vapor deposition) rather than liquid phase growth methods will be utilized.

IV. SUMMARY

BMT single crystal fibers were grown successfully for the first time using the LHPG technique. Congruent growth from the melt was observed in the temperature range of 2900–3100 °C. A simple cubic perovskite high temperature phase was obtained at room temperature compared to the hexagonal ordered perovskite structure usually obtained in ceramics. Dielectric properties of both a ceramic and a single crystal BMT were studied. BMT ceramic samples have ultra low dielectric loss ($<1\times10^{-5}$ at 90 K and 10 kHz) and good thermal compatibility ($\alpha\sim9.0\times10^{-6}$/ °C) with YBCO superconductors. A single crystal BMT has a cubic lattice parameter $a=4.0877$ Å, representing an acceptable misfit for epitaxial growth of high T_c YBCO superconducting films. Dielectric constants increase and saturate as the bulk densities approach the theoretical values. Dielectric loss decreases with an increase in the B-site ordering. Single crystals of the high temperature disordered cubic form maintain a moderate dielectric constant (26.5 at 10 GHz) and low dielectric loss (tan $\delta=2.78\times10^{-4}$ at room temperature and at 10 kHz and $<10^{-5}$ at 90 K), making this material unique for microwave device applications.

ACKNOWLEDGMENTS

The authors would like to acknowledge Professor Rustum Roy for his important comments, Professor D. K. Smith for helpful discussions on XRD and crystal structures, Dr. Russell P. Brodeur for critical reading of the manuscript, and Professor F. W. Ainger, Professor E. C. Subbarao, Dr. S. Erdei, and Dr. J. Sheen for their suggestions and discussions. This work was supported by the Defense Advanced Research Projects Agency (DARPA) under Contract No. DN00014-90-J-4140.

[1] K. Wakino, Ferroelectrics **91**, 69 (1989).
[2] S. Nomura, K. Toyama, and K. Kaneta, Jpn. J. Appl. Phys. **21**, L624 (1982).
[3] H. Tamura, H. Matsumoto, and K. Wakino, Jpn. J. Appl. Phys. Pt. 1, **28**, 21 (1989).
[4] K. Matsumoto, T. Hiuga, K. Takada, and H. Ichimura, *Proceedings of the Sixth IEEE International Symposium on Applications of Ferroelectrics* (IEEE, New York, 1986), p. 118.
[5] F. Galasso and J. Pinto, Nature **207**, 70 (1965).
[6] F. Galasso and J. Pinto, Inorg. Chem. **2**, 482 (1963).
[7] R. S. Feigelson, Mater. Res. Soc. Bull. **13**, 47 (1988).
[8] M. A. Saifi and M. J. Andrejco, Proc. SPIE **668**, 158 (1986).
[9] J. K. Yamamoto and A. S. Bhalla, Mater. Res. Bull. **24**, 761 (1989).
[10] R. Guo, A. S. Bhalla, J. Sheen, F. W. Ainger, S. Erdei, E. C. Subbarao, and L. E. Cross, J. Mater. Res. (to be published).
[11] O. Muller and R. Roy, *The Major Ternary Structural Families* (Springer, Berlin, 1974), p. 202.
[12] K. Kakegawa, T. Wakabayashi, and Y. Sasaki, J. Jpn. Chem. Soc. **1**, 25 (1988).
[13] J. Sheen, R. Guo, A. S. Bhalla, and L. E. Cross, Ferroelectrics Lett. **16**, 33 (1993).
[14] R. D. Shannon and C. T. Prewitt, Acta Crystallogr. B **25**, 925 (1969); Acta Crystallogr. B **26**, 1046 (1970).
[15] B. D. Silverman, Phys. Rev. **125**, 1921 (1962).
[16] See, e.g., T. Terashima, K. Iijima, K. Yamamoto, K. Irata, Y. Bando, and T. Takada, Jpn. J. Appl. Phys. **28**, L987 (1989).
[17] H. R. Harrison and J. M. Honig, Bull. Mater. Sci. **3**, 247 (1981).

Appendix 5.

"Strontium Aluminum Tantalum Oxide and Strontium Aluminum Niobium Oxide as Potential Substrates for HTSC Thin Films,"

J. Materials Research (in printing)

Ruyan Guo

J. Sheen

A.S. Bhalla

F.W. Ainger

S. Erdei

E.C. Subbarao

L.E. Cross

STRONTIUM ALUMINUM TANTALUM OXIDE AND STRONTIUM ALUMINUM NIOBIUM OXIDE AS POTENTIAL SUBSTRATES FOR HTSC THIN FILMS*

Ruyan Guo, A.S. Bhalla, Jyh Sheen, F.W. Ainger, S. Erdei, E.C. Subbarao, and L.E. Cross

Materials Research Laboratory, The Pennsylvania State University

University Park, PA 16802 USA

ABSTRACT

Single crystal fibers of $A(B1_{1/2}B2_{1/2})O_3$ perovskites type with compositions $Sr(Al_{1/2}Ta_{1/2})O_3$ (SAT) and $Sr(Al_{1/2}Nb_{1/2})O_3$ (SAN) were grown successfully for the first time, using a laser heated pedestal growth (LHPG) technique. Their crystallographic structures were found to be simple cubic perovskite with lattice parameters a=3.8952Å (SAT) and a=3.8995Å (SAN) that are close lattice matches to the YBCO superconductors. No structural phase transitions or twins have been found, and the average coefficients of the thermal expansion match well with the YBCO superconductor materials. We report that SAT is one of the most promising substrates to date for the epitaxial growth of HTSC thin films suitable for microwave device applications as it has low dielectric constants (κ~11-12, at 100Hz-10GHz and 300K) and low dielectric loss (~4×10^{-5} at 10kHz and 80K), together with lattice parameter matching, thermal expansion matching and chemical compatibility with the high Tc superconductors (YBCO).

* Part of this work was first presented at DARPA 3rd Annual High Temperature Superconductor Workshop, Sept. 30-Oct.2, 1991, Seattle, Washington. Related presentations were also made at DARPA/ONR Workshop on Substrate Materials for High Tc Superconductors, Feb.5-7, 1992, Williamsburg, Virginia.

1. INTRODUCTION

The rise of electronic technology utilizing high temperature oxide superconducting materials requires at the very least the mastering of processing of the epitaxial thin films of high Tc superconducting (HTSC) materials on suitable substrates and the understanding of their properties. Superconductor device applications demand that the substrate materials for HTSC meet several requirements: lattice matching (or atomic structure matching)[1] to the HTSC materials for ideal epitaxial films; thermal compatibility in terms of thermal expansion matching over the temperature range of film processing and annealing (>900K) down to the operating temperature (90K); low dielectric constants for integrated circuit designs (<25 or ideally less than 10); very low dielectric loss ($\leq 10^{-4}$) at microwave frequencies (~10GHz) and at low temperatures (90K) for microwave device applications; chemical inertia and compatibility with the HTSC thin film deposition; mechanically strong and scratch resistant. As a single crystal substrate is most desirable (as large as 4" in diameter), it is also vital that the crystal should be available at a reasonable cost. All the currently available substrates present some compromises. $SrTiO_3$ crystals of high quality and large sizes, though they are readily available and yield the best quality epitaxial thin films (primarily due to their close interatomic structure matching to the HTSC), have high dielectric constant (>300) arising from the phase transition near the working temperature (~110K). Al_2O_3 sapphire single crystal substrates, which have low dielectric constant κ and low loss at microwave frequencies, require a buffer layer to avoid chemical interactions with the YBCO. One of the substrates, probably the one most used currently, $LaAlO_3$, though good in lattice matching and of reasonable dielectric properties, is heavily twinned and goes through a ferroelastic phase transition at ~435°C.[2] Table 1 lists some of the most commonly used substrates for comparison purposes.

The objective of our investigation was to screen various complex oxide materials to identify suitable HTSC substrate materials and to test the feasibility of single crystal growth by utilizing a laser heated pedestal crystal growth (LHPG) technique. The LHPG technique has several unique features that are of special importance for this task. These advantages include containerless crystal growth and therefore the capability of growing refractory materials (that have low dielectric losses in general); capability of growing both incongruently and congruently melting compositions; and rapid growth rates. Fiber geometry also provides one dimensional dielectric material that may by itself meet microwave antenna requirements for some special device applications.[5]

The compounds $Sr(Al_{1/2}Ta_{1/2})O_3$ (SAT) and $Sr(Al_{1/2}Nb_{1/2})O_3$ (SAN) were first prepared and tested to learn their crystallographic phases and their melting behavior by the group at the AT & T Bell Labs.[6] Ceramic samples were identified to have double cell cubic perovskite structure with a=7.795Å and melting temperatures of 1900°C and 1790°C for SAT and SAN, respectively. On the basis of our understanding of the crystal chemistry-dielectric property relationships of various oxide perovskites, and the reports by the Bell Labs group that showed both the SAN and SAT melt congruently and produce a single phase of the perovskite structure after melting, we selected SAT and SAN as primary candidates in the $A(B1_{1/2}B2_{1/2})O_3$ complex oxide perovskite family for crystal growth and investigated their properties in relation to substrate applications.

This paper reports two single crystals. $Sr(Al_{1/2}Ta_{1/2})O_3$ (SAT) and $Sr(Al_{1/2}Nb_{1/2})O_3$ (SAN), both of $A(B1_{1/2}B2_{1/2})O_3$ complex oxide perovskite formula, grown by the laser heated pedestal growth technique. Their preparation, chemical analysis, crystal structures and dielectric and thermal expansion properties are reported. They have twin-free simple cubic

perovskite structures and attractive dielectric properties. They have potential to be used as microwave substrates for YBCO superconducting thin films.

2. EXPERIMENTAL PROCEDURE

2.1. *Ceramic Preform Preparation*

Ceramic samples were prepared by solid state reaction, using conventional techniques. Several batches with various calcining and sintering conditions were prepared and the procedure was somewhat optimized through the study. Differential thermal analysis (DTA) was used to determine the minimum calcining temperature to achieve the desired phases and to select sintering temperatures. X-ray diffraction was used extensively to characterize the crystallographic phases and to adjust the processing conditions. Some of the processing parameters used are summarized in Table 2.

2.2. *Laser Heated Pedestal Growth: The Instrument*

The laser heated pedestal growth (LHPG) method has been shown to be a powerful method for rapidly growing small diameter single crystals, particularly oxides of high melting temperature, for both property studies and fiber devices.[7,8] The LHPG equipment used in this investigation consisted of a power source (water cooled, tunable flowing gas CO_2 55W laser), an optical layout, and a growth section. The molten zone temperature during a stable growth was monitored using an optical pyrometer with a linear dimension resolution of 0.1mm. A schematic diagram of the LHPG station is shown in Fig. 1. Additional details can be found elsewhere.[9]

2.3. *Dielectric Measurements*

Radio frequency dielectric constants and the loss tangent were measured using a General Radio 1621 Capacitance Measurement System. Three-terminal measurements were carried

out using a shielded sample holder. The accuracy of the measurement was in the range of ±(10 ~ 50) ppm for capacitance measurement and ±(0.1+1 step in the least significant decade) for conductance measurement. The stray capacitance. lead and contact resistance were corrected during measurement by taking an open circuit measurement. The edge corrections of the measurement results were made using an empirical equation derived from the measurements on a family of fused silica samples:

$$C_e = (0.02798 \cdot Ln(\frac{P}{t}) - 0.05922) \cdot P \qquad (1)$$

where C_e is the edge capacitance. P and t are the perimeter and the thickness of the sample in cm.

Dielectric properties at microwave frequency were measured using resonance techniques equipped with an HP8510A network analyzer. Post resonance technique (the Hakki and Coleman technique[10]) was used to measure the dielectric constants of the ceramic samples. Cavity perturbation technique[11] was used for the measurements on samples of thin rod (e.g., single crystal fiber samples) or bar-shaped. The Q factors (of microwave frequency) at liquid nitrogen temperature were measured by a transmission resonance technique.

3. RESULTS AND DISCUSSION

3.1. *Crystallographic Phases in Ceramics*

3.1.1. $\underline{Sr(Al_{1/2}Ta_{1/2})O_3}$

The presence of an intermediate phase. $SrTa_2O_6$, was noticed in ceramic powders for calcining temperature between 1250°C and ~1550°C. and the phase disappeared after calcination at 1550°C. Another intermediate phase. $SrAl_2O_4$, could also form and remain in the ceramic powder until the melting point (~1960°C)[12] when excess Al was present. This intermediate phase could be harmful for single crystal growth. and therefore repeated grinding

followed by calcining was performed. A MgO crucible (instead of Al_2O_3 crucible) was used to avoid excess Al diffusion into the compound during the calcination process. The x-ray diffraction pattern for the SAT ceramics sintered at 1655°C for 5 hours is shown in Fig. 2 (a). The crystallographic phase of the SAT powder is a double cell cubic perovskite as reported by Brandle and Fratello.[6] with a lattice parameter a=7.7772Å. The sharp (111), (311), (331), and (333) diffraction peaks indicate that the SAT has a strong tendency to form a B-site ordered (Al:Ta=1:1) perovskite structure.

3.1.2. $\underline{Sr(Al_{1/2}Nb_{1/2})O_3}$

As in the case of SAT, the presence of an intermediate phase, $SrNb_2O_6$, was found in the powder at a calcining temperature T~1150°C. This intermediate phase reacted with the remaining SrO and Al_2O_3 to form pure SAN phase at a higher temperature (~1570°C). The SAN phase was found to be an ordered perovskite cubic phase with a lattice parameter a=7.7824Å. The x-ray diffraction pattern for the SAN ceramics sintered at 1570°C for 24 hours is shown in Fig. 2 (b).

3.2. *Single Crystal Fiber Growth and Crystallographic Phases*

Single crystals of SAN and SAT were grown successfully using the LHPG technique. Both the feeding rods (~0.45mm² in cross section) and the pulling seeds (~0.12mm² in cross section) were ceramics prepared as described in Section 2.1. SAN and SAT single crystal fibers of ~500 μm in diameter and up to 3 cm in length (not limited) were grown using a pulling to feeding ratio of 1.5~2. All growths were performed in air. The stable molten zone temperatures during the crystal fiber growth were obtained using an optical pyrometer and were typically 1862°C and 2030°C for SAN and SAT, respectively, with an estimated accuracy of ±30°C.

As grown SAT and SAN crystals were both chemically reduced. The SAN fiber was dark gray due to the reduction of Nb^{5+} to Nb^{4+}. No clear facet was observed for SAN fibers 500μm in diameter. As grown SAT fiber showed a bluish color. Facets on SAT fibers ~500μm in diameter can be seen. Fig. 3 shows a Laue photograph of a single crystal SAT fiber with the x-ray beam approximately parallel to [110], normal to the cleavage plane, and hitting the crystal in the direction perpendicular to the growth direction. The crystal fiber growth direction was found to be along $[\bar{1}\,\bar{1}\,1]$, 54°44' from the [001].

X-ray diffraction patterns, as shown in Fig. 4, revealed that the SAN and SAT crystal fibers grown by LHPG do not show B-site long range ordering (with only weak diffractions of the superlattice peaks) and as a result, have simple cubic symmetry. The crystallographic data for SAN and SAT single crystal fibers as determined by x-ray diffraction are: a=3.8995Å, volume=59.295Å^3, Z=1 and ρ=5.4758 g/cm^3 (for SAN), and a=3.8952Å, volume=59.109Å^3, Z=1, and ρ=6.7306 g/cm^3 (for SAT). Their cubic lattices closely match the high Tc superconductor YBCO that has an orthorhombic symmetry with lattice parameter b=3.883Å.[3]

The high temperature (disordered) phases existed to room temperature as the B-site orderings were inhibited during the fiber growth process because of the quenching effect produced by the high growth rates and steep axial temperature gradients employed in the LHPG growth. The high temperature disordered phases have not been reported previously in either SAN or SAT. The SAN fibers became colorless after annealing at 1630°C for 10 hours in air (no annealing effect was observed at 1000°C for 24 hours in flowing O_2). SAT became transparent after annealing in flowing O_2 at 1000°C for 24 hours. However, annealing treatments at these conditions did not cause significant or conclusive changes in the disorderedness of the structure as examined by x-ray diffraction. This observation suggested that their high temperature ideal cubic perovskite phases are stable.

3.3. *Chemical Composition Analysis*

Ceramic and single crystal SAN and SAT samples were analyzed quantitatively for their chemical compositions by using electron probe microscopic analysis (CAMECA, SX-50 with spatial resolution of 2μm on surface area and 0.2μm in depth). Relative analytic accuracy is ± 2%. Chemical analysis showed that the single crystals SAN and SAT grow congruently within the stoichiometric composition. The assigned composition of an as grown SAT single crystal fiber was $Sr_{1.022\pm0.001}(Al_{0.496\pm0.001}Ta_{0.493\pm0.001})O_3$ and was uniform across the entire surface. As mentioned in the ceramic processing section, excess Al in the compound may cause formation of an intermediate phase $SrAl_2O_4$. Electron probe microscopic analysis detected $SrAl_2O_4$ grains in the SAT ceramic sample. It is evident from the microscope study that the $SrAl_2O_4$ phase (a hexagonal stuffed tridymite structure with a=5.10Å, c=8.49Å, M.P~1960°C)[13] is formed before the densification temperature is reached as the $SrAl_2O_4$ grains are fully enclosed by SAT grains. Crystal fibers of SAT, however, are not affected by the intermediate phase as the growth zone temperature is higher than the melting temperature of the intermediate phase. Improvement in crystal quality is expected after the powder preparation process is modified to avoid the $SrAl_2O_4$ phase.

The composition of an as grown SAN single crystal fiber was found to be $Sr_{0.931\pm0.006}(Al_{0.463\pm0.005}Nb_{0.550\pm0.004})O_3$, in comparison to the composition, $Sr_{0.940}(Al_{0.477}Nb_{0.538})O_3$, found in the SAN ceramic sample. The reason for the off stoichiometry on the cation ratio for both the ceramic and single crystal samples is not yet clear; however the congruent melting and growth behaviors were confirmed through the similarity between the ceramic sample and the crystal sample. Avoiding the formation of the intermediate $SrAl_2O_4$ phase in ceramics may be more important for improving the

stoichiometry and quality of SAN single crystals than for SAT, because SAN crystals were grown at relatively lower temperatures.

3.4. *Dielectric Properties*

Dielectric properties of the SAN and SAT samples were examined as functions of temperature and frequency. Table 3 summarizes the dielectric properties of high density SAN and SAT ceramic samples. Their dielectric constants as functions of temperature in the low frequency range and as functions of frequency at room temperature are shown in Fig. 5 and Fig. 6.

Dielectric constant as low as 11~12 for the SAT sample is of special significance for substrate applications as, we believe, it is one of the lowest dielectric constants reported for the complex oxide perovskite family. It is the oxygen ionic polarizability that sets the baseline limitation to the dielectric polarizability in the oxide perovskite family. SAT, therefore, seems to be a special example in complex oxide perovskite compounds of cubic structure for further studies on polarization mechanisms.

More study on the effect of B-site ordering on various properties including dielectric properties is required. On the basis of our experimental results on another oxide perovskite, $Ba(Mg_{1/3}Ta_{2/3})O_3$,[14] the dielectric constant increases with the increase in the bulk density (does not strongly depend on the B-site ordering); while dielectric loss factor decreases with the enhancement in B-site ordering.

3.5. *Thermal Expansion Behavior*

Thermal expansion coefficients of SAN and SAT were measured and compared to the thermal properties of the YBCO superconductor. The measurement was carried out from room temperature up to about 800°C by using a vertical push-rod dilatometer equipped with a

high sensitivity linear variable differential transformer (LVDT). The heating and the cooling rates for thermal expansion measurements were regulated at 1 or 1.5°C/min using a microprocessor based temperature controller.

Good thermal expansion match was found in both SAT and SAN samples (the thermal expansion coefficients. α= 9.7x10^{-6}/°C (SAT) and α=8.8x10^{-6}/°C (SAN)) compared to that of the YBCO single crystals (α_a=14. α_b=9. and α_c=19x10^{-6}/°C).[4] No structural phase transition was found in the measured temperature region. Fig. 7 shows the average linear thermal strains of SAN. SAT, and YBCO ceramic samples as a function of temperature. Thermal property compatibility of the substrates with HTSC films is critical for epitaxial film growth, in terms of determining the deposition and annealing temperatures, possibility of producing thick films, and reducing the degradation process in films and devices under working conditions.

3.6. *Microhardness*

Vickers hardness on the single crystals SAN and SAT grown by the LHPG technique was measured by using a Leitz Miniload Hardness Tester. The side of a single crystal fiber perpendicular to the fiber growth direction was ground and optically polished. The indentation diameter resulting from the diamond indentor was measured using a micrometer scale etched into the microscope eyepiece. Five indentations were measured for each different load (200 to 500 gram) and the resulting values were averaged.

The Vickers hardness was calculated by a formula: $H_v(10^9\ N\ m^2) = 18.1854\,P\,d^2$, where P is the measuring force in grams and d is the mean value of the indentation diagonal in μm. Preliminary results of the microhardness measurements are given in Table 4. Comparative studies on the hardness were also performed under the identical conditions on the single crystal Al_2O_3 and quartz. for those are well characterized for their high value of hardnesses.

The literature values of their hardness are also given.

It is not surprising that both SAT and SAN have high values of hardness. High bonding strength in the ionic compounds and the small size of cations on both A and B-sites may be responsible for these high values.

3.7. *General Comments*

Comparing SAN and SAT, it is interesting to notice the similarities and dissimilarities in the Nb- and Ta-compounds. In spite of all the similarities of SAN and SAT (e.g., identical structure type, similar lattice parameters, similar thermal expansion properties), there are a number of distinct differences between them. SAT has a higher melting temperature, higher hardness, lower dielectric constant, lower dielectric loss over broad ranges of temperature and frequency, and less reduction problem during growth. These differences between SAT and SAN are not unique to these two materials, but are common to all Nb-compounds and their analogous Ta-compounds. It is impossible to explain the reason of those differences by, for instance, simply considering the bonding strength (as they have the same valence and coordination numbers), or on the basis of available ionic polarizability data[15] ($\alpha_i^{Ta^{5+}}$=4.73Å^3 and $\alpha_i^{Nb^{5+}}$=3.97Å^3 that would predict a lesser polarizability for SAN than SAT). It seems to us that the electronic structure differences may have caused the Ta-O bonding to be less ionic in nature and somehow enhanced the bonding strength. Detailed understandings and modeling are beyond the scope of this paper.

Considering all the suitable substrate requirements, SAT seems more desirable primarily due to its low dielectric constant. The drawbacks are the difficulty in crystal growth as SAT has higher melting temperature. The (110) cleavage plane in the SAT crystals does not seem to present a problem as cleavage is primarily determined by crystal structure and is only secondarily related to chemical composition.

Chemical compatibility of SAN and SAT substrates with YBCO was tested by spin coating YBCO films on SAN and SAT ceramic disks using the sol-gel technique.[16] No chemical interactions were observed, and the YBCO film formed was of good crystal quality with T_c~90K. Therefore it is concluded that the chemical compatibility of SAN and SAT with YBCO is good.

We believe that further modification of the SAN and SAT compositions to fine tune their properties, particularly reducing their melting temperatures, will lead to easier fabrication of the crystals and better control of the reduction problem of the Nb^{5+} and Ta^{5+}. Work following this direction will be the content of separate publications.

Using SAT polycrystalline materials as targets in a pulsed laser deposition process, Findikoglu et al.[17,18] have reported high quality epitaxial (c-axis orientation) growth of thin films of SAT and multilayers of YBCO/SAT on (001) $LaAlO_3$ and MgO substrates. Dielectric constants of the SAT films (~100-390nm thick), however, were found to be ~23-30, notably higher than the value (κ~12) found in bulk ceramic materials. The deviations from perfect cation stoichiometry in the films may be one of the causes for the discrepancy in the value of the dielectric constants as the Al/Ta ratio in SAT films was found to be ~0.8 rather than the stoichiometric ratio of unity.[17,18] No dielectric loss data was reported for the SAT films therefore direct comparison between the dielectric constants of the film and the bulk SAT samples is not possible. The dielectric properties (κ~12, $\tan\delta \leq 10^{-3}$ at room temperature and 1KHz) of SAT ceramic samples are reproducible. Consistent results have also been given by independent dielectric property measurements on the same SAT ceramic samples.[19]

4. SUMMARY

We have investigated single crystals of $Sr(Al_{1/2}Nb_{1/2})O_3$ and $Sr(Al_{1/2}Ta_{1/2})O_3$ as substrate materials for epitaxial thin film fabrication of the high Tc superconductors. Single crystal

fibers of SAN and SAT were grown using a laser heated pedestal growth technique. Crystal structures, dielectric properties, thermal expansion properties, and hardness test results are reported. Both SAN and SAT are of ideal cubic perovskite structure with a lattice parameter in close match to YBCO and can be explored further for device applications. SAT currently represents one of the best potential HTSC substrate materials for microwave applications. The unique feature of this material is that it combines desired dielectric properties (dielectric $\kappa \sim 12$, loss factor $\tan\delta < 10^{-4}$) at microwave frequencies with a twin-free lattice and good thermal expansion matching along with chemical compatibility.

ACKNOWLEDGMENTS

The authors like to thank Professor Rustum Roy for his important comments, and thank Dr. E. Breval for her help in microhardness measurement. This work was supported by the Defense Advanced Research Projects Agency (DARPA) under the contract DN No. 00014-90-J-4140.

REFERENCES

1. Ruyan Guo, A.S. Bhalla, L.E. Cross, and Rustum Roy, *J. Mater. Res.* 9(7), 1644-1656 (1994).
2. E.A. Wood, *Amer. Min.* **36**, 768 (1951).
3. W. Wong-Ng, F.W. Gayle, D.L. Kaiser, S.F. Warkins, and F.R. Fronczek, *Phys. Rev. B* **41**(7), 4220 (1990).
4. Hoydoo You, U. Welp, and Y. Fang, *Phys. Rev.* **B43** (4), 3660 (1991).
5. R.J. Dinger and D.J. White, *IEEE Trans. Antennas Propagat.* **38**(8), 1313 (1990).
6. C.D. Brandle and V.J. Fratello, *J. Mater. Res.* **5**(10), 2160 (1990).
7. J.S. Haggerty, W.P. Menashi and J.F. Wenckus, *Method for Forming Refractory Fibers by Laser Energy*, U.S. Patent 3,944,640, March 16, 1976 and *Apparatus for Forming Refractory Fibers*, U.S. Patent 4,012,213, March 15, 1977.
8. R.S. Feigelson, *MRS Bull.* **13**, 47 (1988).
9. J. Yamamoto and A.S. Bhalla, *Mat. Res. Bull.* **24**, 761 (1989).
10. B.W. Hakki and P.D. Coleman, *IRE Trans. Microwave Theory Tech.* **MTT-8**, 402 (1960).
11. D.C. Dube, M.T. Lanagan, J.H. Kim, and S.J. Jang, *J. Appl. Phys.* **63**, 2466 (1988).
12. F. Ganits, T. Yu. Chemekova, and Yu. P. Udalov, *Zh. Neorg. Khim.* **24(2)**, 471 (1979); *Russ. J. Inorg. Chem. (Engl. Transl.)* **24**(2), 260 (1979).
13. F.P. Glasser, L.S. Dent Glasser, *J. Am. Ceram. Soc.* **46**, 377 (1963).
14. Ruyan Guo, A.S. Bhalla, and L.E. Cross, *J. Appl. Phys.* **75**(9), 4704-4708 (1994).
15. R.D. Shannon, *J. Appl. Phys.* **73**(1), 348 (1993).
16. P. Ravindranathan *et al.* (unpublished results).
17. A.T. Findikoglu, C. Doughty, S. Bhattacharya, Qi Li, X.X. Xi, T. Venkatesan, R.E. Fahey, A.J. Strauss, and J. M. Phillips, *Appl. Phys. Lett.* **61**, 1718 (1992).
18. A.T. Findikoglu, S. Bhattacharya, C. Doughty, M.S. Pambianchi, Qi Li, X.X. Xi, S.M. Anlage, R.E. Fahey, A.J. Strauss, J.M. Phillips, and T. Venkatesan, *IEEE Trans. Appl. Superconductivity*, **3**(1), 1425 (1993).
19. F.I. Mopsik, National Institute of Standards and Technology (private communication).
20. E. Breval, G.C. Dodds, and N.H. Macmillan, *Mat. Res. Bull.* 20, 413 (1985).

TABLE CAPTIONS

Table 1. Most commonly used high Tc superconductor substrates.

Table 2. Ceramic processing conditions for $Sr(Al_{1/2}Nb_{1/2})O_3$ and $Sr(Al_{1/2}Ta_{1/2})O_3$.

Table 3. Dielectric properties of $Sr(Al_{1/2}Nb_{1/2})O_3$ and $Sr(Al_{1/2}Ta_{1/2})O_3$

Table 4. Vickers hardnesses data for $Sr(Al_{1/2}Nb_{1/2})O_3$ and $Sr(Al_{1/2}Ta_{1/2})O_3$ single crystal fibers (on planes perpendicular to the growth direction).

FIGURE CAPTIONS

Fig. 1. Schematic diagram of the laser heated pedestal growth station.

Fig. 2. X-ray diffraction patterns of (a) SAT ceramic sintered at 1655°C for five hours and (b) SAN ceramic sintered at 1570°C for 24 hours.

Fig. 3. Lauè photograph of a single crystal SAT fiber with the x-ray beam hitting the crystal in direction perpendicular to the growth direction at the cleavage plane.

Fig. 4. X-ray (powder) diffraction patterns of single crystal: (a) SAT and (b) SAN.

Fig. 5. Dielectric constants of SAN and SAT ceramics at 10 kH^{-} as functions of temperature.

Fig. 6. Dielectric constants of SAN and SAT ceramics as functions of frequency at room temperature.

Fig. 7. Thermal strain measured by using vertical push rod linear voltage differential transformer dilatometer.

Table 1. Most commonly used high Tc superconductor substrates.

Substrates	Symmetry, Lattice Constants (Å)	Dielectric Constant κ (at RT)	Thermal Expansion α ($x10^{-6}/°C$)	Comments
$YBa_2Cu_3O_{7-\delta}$	Ortho. a=3.836 b=3.883 c=11.68 (Ref. [3])		α_a=14 α_b=9 α_c=19 (Ref. [1])	
$SrTiO_3$	Cubic a=3.905	>300	10.6	Good epitaxial YBCO film; high dielectric constant
$LaAlO_3$	Rhomb. a=3.789 α=90.12°	23	10	Structural phase transition at ~435°C; heavy twinning
Al_2O_3	Rhomb. a,b=4.7586 c=12.9897 γ=120°	κ_a=9.34 κ_c=11.54	6	Poor lattice matching; poor thermal expansion matching; chemical interactions with YBCO (buffer layer often required).
MgO	Cubic a=4.2114	9.65	10.4	Reasonable cost; easy to cleave; large lattice mismatching.
YSZ $(Zr_{0.72}Y_{0.28}O_{1.862})$	Cubic a=5.16(2)	26	4.5	Chemical interactions with YBCO, $BaZrO_3$ forms at the interface (buffer layer often required).

Table 2. Ceramic processing conditions for $Sr(Al_{1/2}Nb_{1/2})O_3$ and $Sr(Al_{1/2}Ta_{1/2})O_3$.

Composition	Starting Chemicals (purity)	Calcination Condition	Sintering Condition	Density (g/cm^3)
$Sr(Al_{1/2}Nb_{1/2})O_3$	$SrCO_3$ (4N) Al_2O_3 (3N5) Nb_2O_5 (4N)	1570°C for three hours	1600°C for three hours	5.051 (91.7% theoretical)
$Sr(Al_{1/2}Ta_{1/2})O_3$	$SrCO_3$ (4N) Al_2O_3 (3N5) Ta_2O_5 (4N)	1600°C for three hours	1620°C for four hours	6.537 (96.6% theoretical)

Table 3. Dielectric properties of $Sr(Al_{1/2}Nb_{1/2})O_3$ and $Sr(Al_{1/2}Ta_{1/2})O_3$

Composition	Room Temperature				Low Temperature, 77K			
	10kHz		Microwave (GHz)		10kHz		Microwave	
	κ	tanδ ($x10^{-4}$)	κ	tanδ ($x10^{-4}$)	κ	tanδ ($x10^{-4}$)	κ	tanδ ($x10^{-4}$)
SAT (97% density)	11.8	16.8	10.7 (11.0GHz)	3.64 (7.64GHz)	11.8	0.42	-	2.09 (7.64GHz)
SAN (92% density)	18.6	31.8	18.3 (9.61GHz)	9.26 (6.08GHz)	18.7	2.20	-	5.56 (6.08GHz)

Table 4. Vickers hardness data for $Sr(Al_{1/2}Nb_{1/2})O_3$ and $Sr(Al_{1/2}Ta_{1/2})O_3$ single crystals (on planes perpendicular to the growth direction).

Material	H_v (GPa) (averaged for P=0.2-0.5N)
SAT Crystal Fiber (⊥ Growth Direction)	15.1±3.3
SAN Crystal Fiber (⊥ Growth Direction)	9.1±1.2
Sapphire Crystal Fiber(⊥c)[20]	18.1±2.1
Quartz (//c)[20]	9.3±1.2

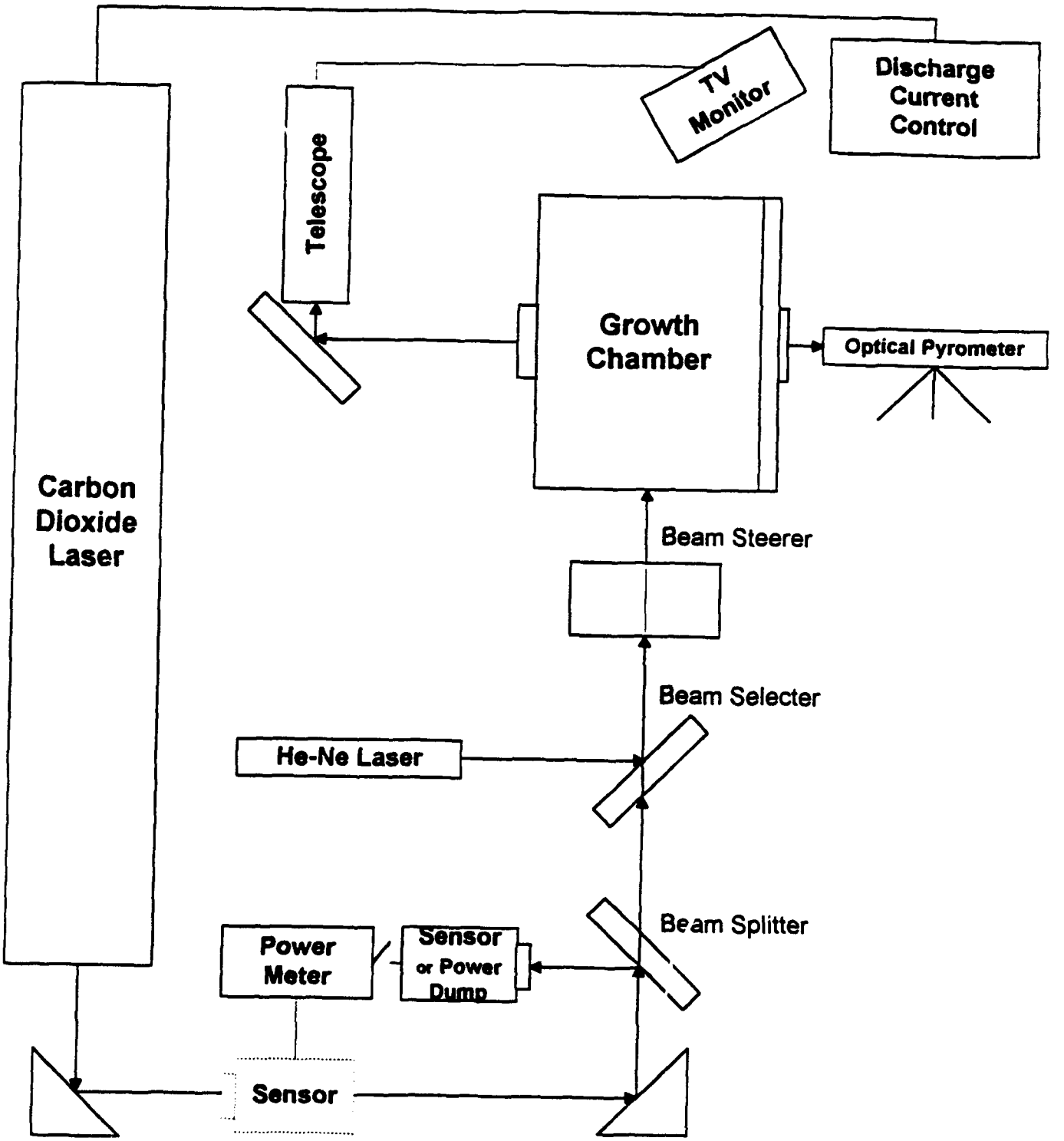

Schematic Drawing of the Laser-Heated Pedestal Growth Station.

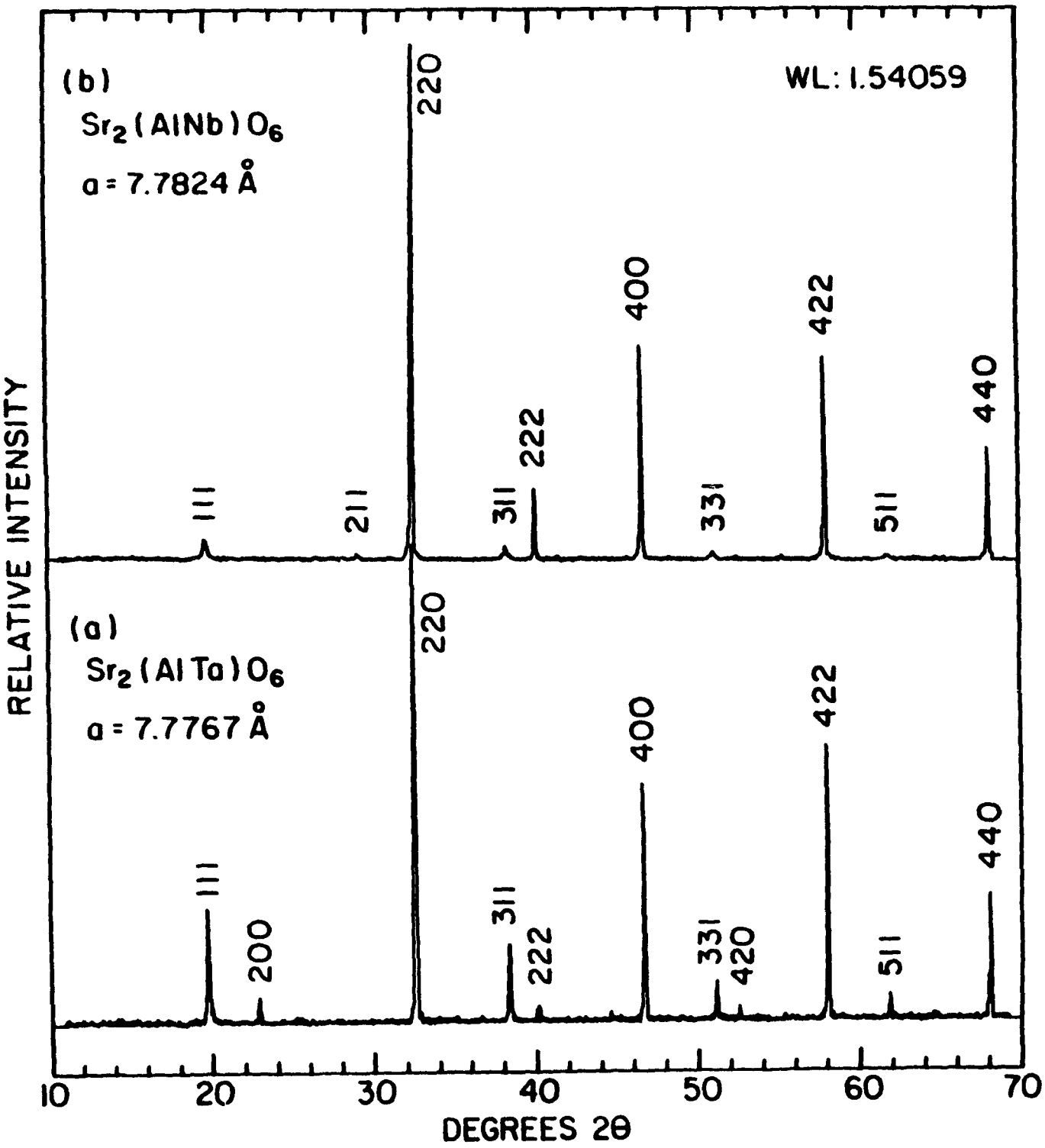
(b)
$Sr_2(AlNb)O_6$
a = 7.7824 Å
WL: 1.54059
220
400
422
440
111
211
311
222
331
511
(a)
$Sr_2(AlTa)O_6$
a = 7.7767 Å
220
400
422
440
111
200
311
222
331
420
511
RELATIVE INTENSITY
10
20
30
40
50
60
70
DEGREES 2θ

Fig. 2

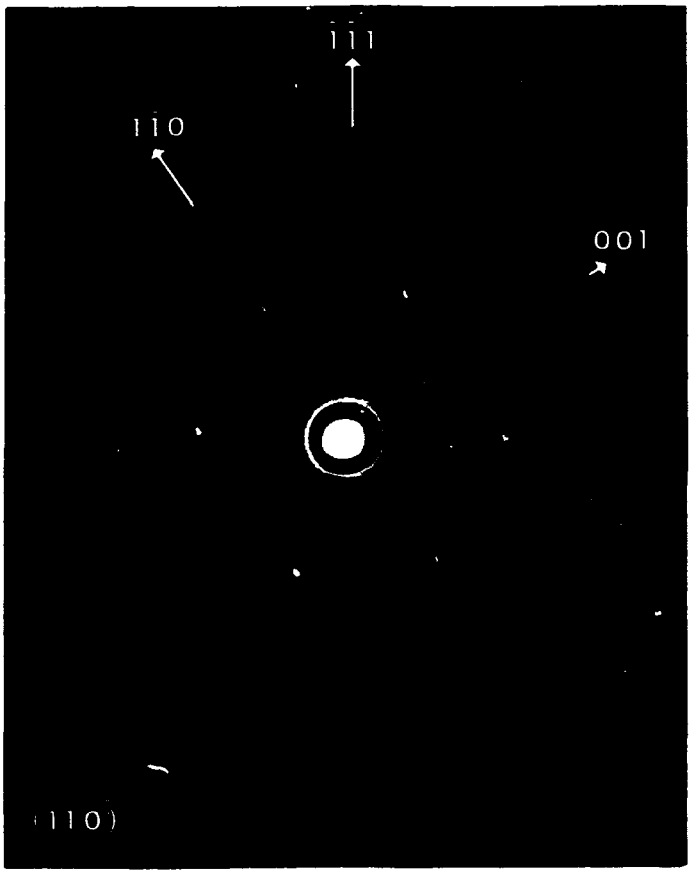
111
110
001
(110)

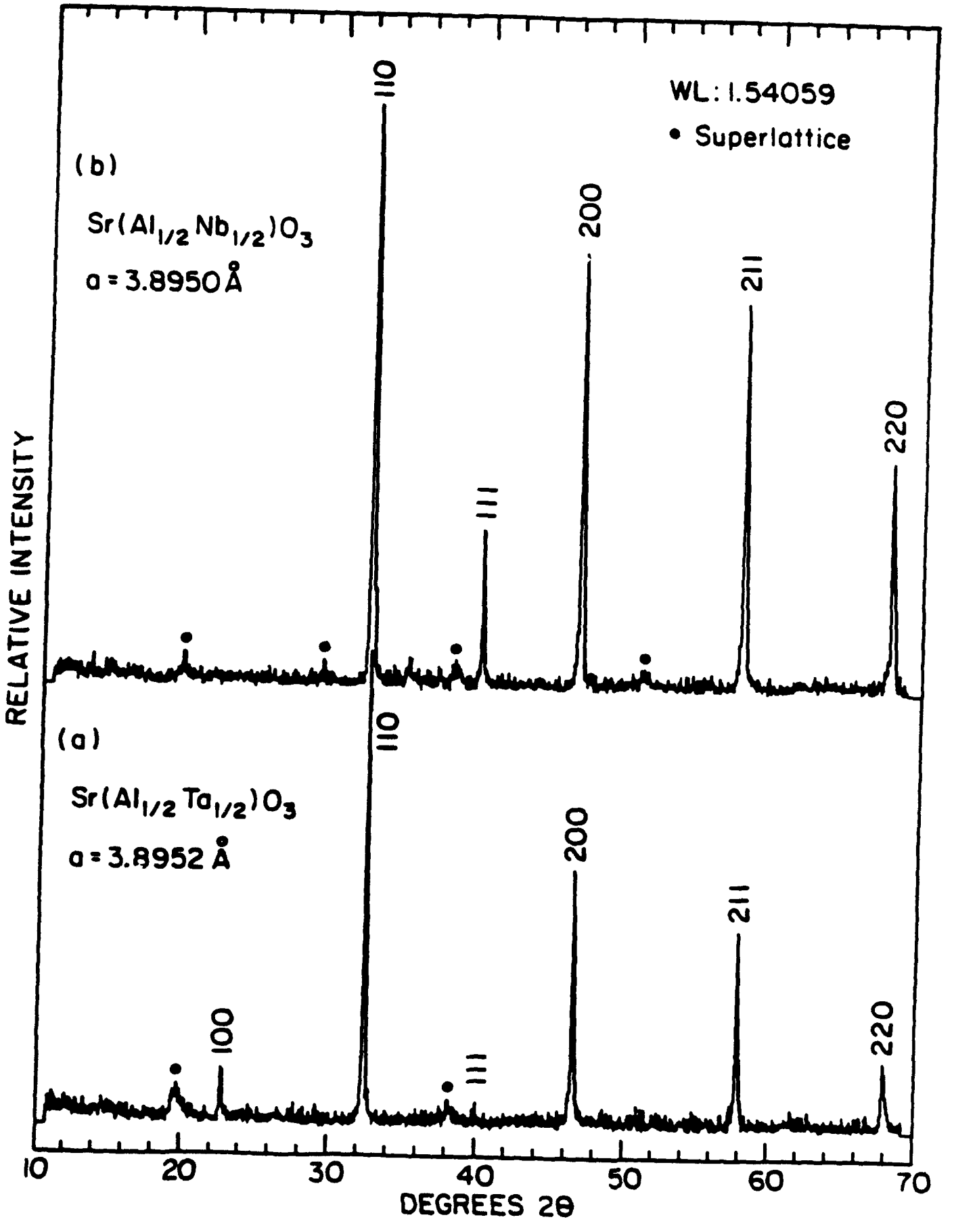
WL: 1.54059
• Superlattice
(b)
Sr(Al1/2 Nb1/2)O3
a = 3.8950 Å
110
200
211
220
111
(a)
Sr(Al1/2 Ta1/2)O3
a = 3.8952 Å
110
200
211
220
100
111
RELATIVE INTENSITY
10
20
30
40
50
60
70
DEGREES 2θ

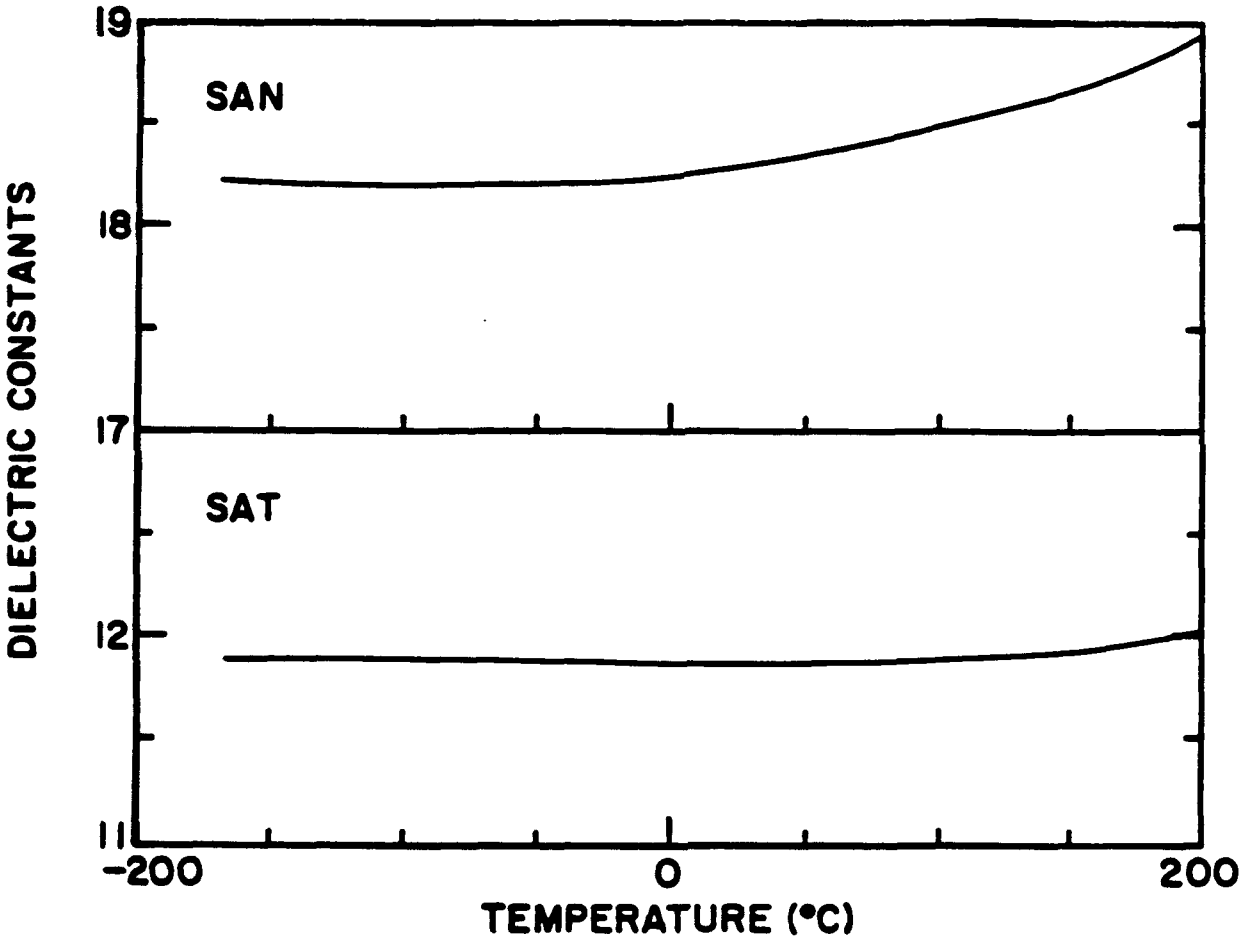
19
18
17
12
11
SAN
SAT
DIELECTRIC CONSTANTS
-200
0
200
TEMPERATURE (°C)

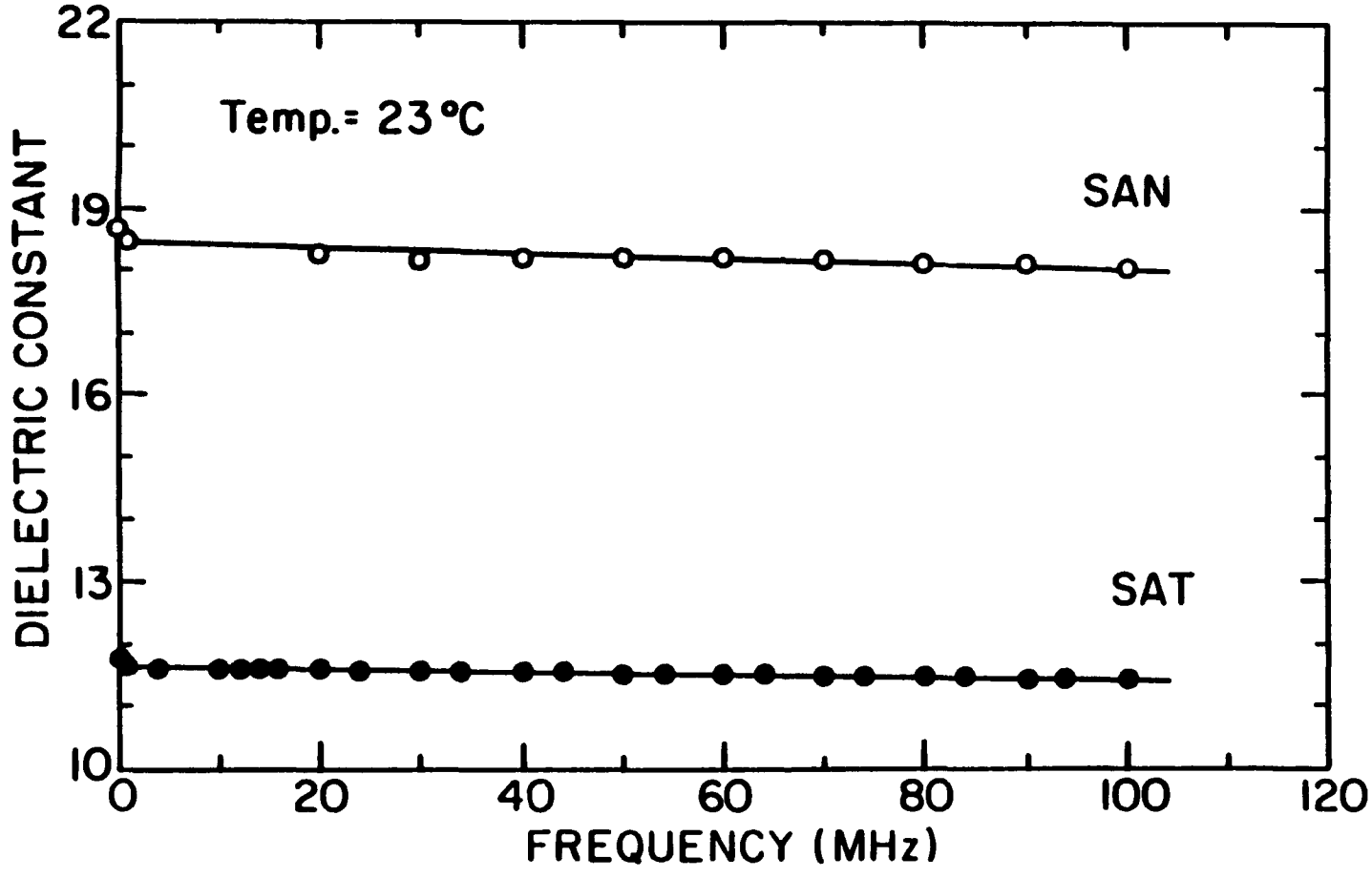
Temp.= 23°C
SAN
SAT
DIELECTRIC CONSTANT
FREQUENCY (MHz)
22
19
16
13
10
0
20
40
60
80
100
120

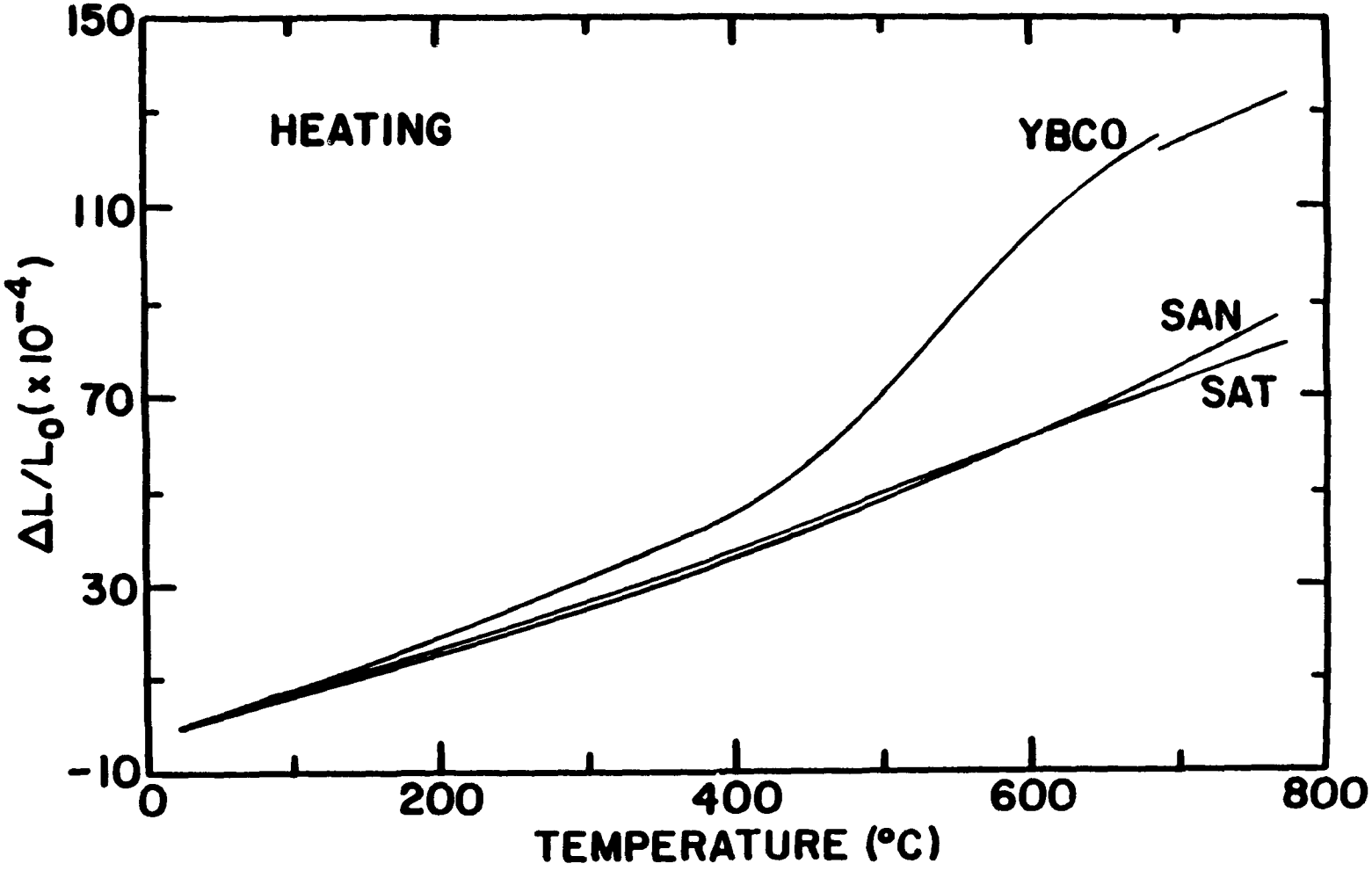
150
110
70
30
-10
HEATING
YBCO
SAN
SAT
$\Delta L/L_0 (\times 10^{-4})$
0
200
400
600
800
TEMPERATURE (°C)

Appendix 6.

"Measurements of Dielectric Constant and Quality Factor of $Ba(Mg_{1/3}Ta_{2/3})O_3$ at X Band Frequencies,"

Ferroelectrics Letters **16** (1/2), 33-41 (1993)

Jyh Sheen

Ruyan Guo

A.S. Bhalla

L.E. Cross

Ferroelectrics Letters, 1993, Vol. 16, pp. 33-41
Reprints available directly from publisher
Photocopying permitted by license only

MEASUREMENTS OF DIELECTRIC CONSTANT AND QUALITY FACTOR OF $Ba(Mg_{1/3}Ta_{2/3})O_3$ AT X BAND FREQUENCIES

JYH SHEEN, RUYAN GUO, A. S. BHALLA, AND L. E. CROSS

Materials Research Laboratory, The Pennsylvania State University, University Park, Pennsylvania 16802, U.S.A.

(Received for Publication June 25, 1993)

ABSTRACT Dielectric properties of $Ba(Mg_{1/3}Ta_{2/3})O_3$ in forms of ceramic, single crystal fiber, and polyethylene composite at microwave frequencies were measured. The dielectric constants 23.33, 24.30, and 26.50 and the quality factors 8,050, 6,430, and larger than 2,000 at 10 GHz were measured for the ceramic, hot pressed ceramic and the fiber respectively. The powder was studied by forming composites of $Ba(Mg_{1/3}Ta_{2/3})O_3$ - Polyethylene. It is found that the experimental dielectric constant values at X band frequencies fit reasonably well to the logarithmic mixture rule. A newly reported mixing equation by Wakino et al. was studied by comparing with our experimental results.

I. INTRODUCTION

The $A(B'_{1/3}B''_{2/3})O_3$ ($A=Ba^{2+},Sr^{2+}$, $B'=Mg^{2+},Zn^{2+},Mn^{2+}$, $B''=Nb^{5+},Ta^{5+}$) perovskite compounds have been reported for the application of microwave dielectric resonator [1]. These materials have dielectric constants 22 to 41 and low dielectric losses. $Ba(Mg_{1/3}Ta_{2/3})O_3$(BMT) is one of the perovskite compounds which has been reported with dielectric constant about 25 and Q values 5,000 to 30,000 at 10 GHz [2-4] (Table1). The single crystal of BMT is recently identified to be one of the potential substrate materials for high Tc superconducting thin film at microwave applications [5]. It is cubic with a lattice constant a= 0.4088nm comparing to the YBCO superconductor a= 0.3820nm, b= 0.3892nm. The dielectric constant 25 is suitable for many microwave device applications. Its very low loss makes it a good candidate for substrate and support structure for superconductor antenna [6].

Communicated by Dr. G. W. Taylor

TABLE I Reported Microwave Dielectric Properties of BMT Ceramics.

f(GHz)	ε'	Q	Ref.
10	25.4	5,000-30,000	[2]
10.5	25	16,800	[3]
7	25	10,200	[4]

In this paper, we report the dielectric properties of BMT samples prepared in various forms at microwave frequencies. Dielectric constants and quality factors of the ceramic, hot pressed ceramic, and single crystal fiber of BMT were systematically studied using different microwave measurement techniques.

The dielectric constants of 0:3 composite samples, xBMT: (1-x)Polyethylene (PE) made by various volume percentages of PE and BMT powders were measured at X band frequencies. The experimental results were then compared with the logarithmic mixture rule and a newly reported mixing equation by Wakino et al. [7]. It is found that the experimental data fit reasonably well with the logarithmic rule and Wakino's equation. By extrapolating the measured values of dielectric constant, the dielectric constant of pure BMT are also estimated.

II. EXPERIMENT

(1) Sample Preparation

(a) Ceramic Sample

Ceramic specimens of BMT were prepared by solid state reaction using conventional techniques. Weighted from high purity magnesium oxide(3N5), tantalum penta oxide(4N), and barium carbonate(grade 1), the starting powders were mixed, ball milled, dried, and ground. Well mixed fine powders were calcined in an alumina crucible at 1,500°C for three hours. Calcined BMT powder was characterized by XRD to confirm the single phase(Hexagonal, a= 0.5773nm, c=

0.7094nm). The powder with added nonaqueous binder were pressed using a hydraulic uniaxial press into circular pellets. The binder was burned out at 550°C for about 3 hours. The binder-free green pellets were sintered at temperature between 1,600 to 1,670°C for various soaking time. Well sintered sample with high density and fully ordered hexagonal perovskite phase were produced.

The hot pressed BMT ceramic sample was provided by Dr. W. Wersing of the Siemens Company. The ceramic sample was prepared essentially using the similar process with additional grain growth and densification by means of hydrostatic pressing at elevated temperatures.

(b) Single Crystal Fiber

The laser heated pedestal growth technique was used to grow the BMT single crystal fiber [5]. A molten zone was formed on the BMT feed rod by a CO_2 laser and supported by the surface tension. A seed crystal was placed in contact with the molten zone and the fiber was grown by pulling out of the molten zone with the feedrod moving simultaneously into the molten zone. The pulling and feed rates were controlled in range of 0.5 to 1 mm/min with relative 1:2 reduction ratio. Both the feed rod(0.7mm^{x}0.7mm in cross section) and the seed rod(0.35mm^{x}0.35mm in cross section) were cut from the ceramic pellet. A [112] oriented as grown BMT single crystal fiber with diameter 0.48 mm was used for measurement.

(c) Composite Sample

The ordered and single phase BMT ceramic powder and high purity and low density(0.915 g/cm^3) PE powder with reported dielectric constant 2.25 and quality factor 2,500 at 10 GHz [8] were used for preparing the composite samples. Suitable amounts of PE and BMT powders were mixed using alcohol as a solvent with ZrO_2 balls in a plastic jar by ball milling for more than 10 hours. After the well mixed suspension was stirred and evaporated to almost dry state, it was then baked in at 80°C in an oven for 4 to 5 hours to obtain the complete dried powder mixture. The mixture was then pressed using a steel die at a temperature of 125°C(the melting point of PE is 115°C) and under a pressure ~7,000 lb/in^2 to make slab samples.

(2) Mixture Rules for the Composite Samples

A series of studies on the mixture rules are available in the literature [9]. The logarithmic mixture rule is one of the most suitable mixing rules. The logarithmic mixture rule applies well in the case of high dielectric constant phase dispersed in a low dielectric constant matrix which is adequate in the present case of BMT dispersed in the PE matrix. In addition, the logarithmic mixture has the advantage of having a very simple relation for deriving the extrapolated dielectric constant values from the measured results. Recently, Wakino et al. [7] reported a new mixing equation,

$$\varepsilon_r^{(V_1-V_0)} = V_1 \varepsilon_{r1}^{(V_1-V_0)} + V_2 \varepsilon_{r2}^{(V_1-V_0)} \qquad (1)$$

where ε_r, ε_{r1}, and ε_{r2} are dielectric constants of composite, materials 1 and 2 and V_1 and V_2 are the volume fractions of materials 1 and 2 respectively. The V_0 is about 0.35. For $V_1=V_0$, this equation is the same as the logarithmic mixture rule. They claimed that this new equation is by far the best among the other equations reported till now.

In this paper, the logarithmic and the new mixture rules are used to compare with our measured dielectric constant values of composite samples. The predicted dielectric constant of BMT by extrapolating the dielectric constants of various composite compounds is also given. We found our measured data fit well to the logarithmic rule and to the new reported equation. The predicted dielectric constant of BMT by using the log rule to extrapolate the measured values to 100% BMT volume percentage is ~23.

Because the surface conditions(roughness and porosity) of the composite samples could not be precisely controlled the quality factors($Q \approx 1/\tan\delta$) of the samples are not of very precise values. The estimation of Q values by this powder mixing method is not adequate without solving the surface condition problems.

(3) Measurement Methods

The dielectric constant of the two BMT ceramic samples were measured by the Hakki and Coleman post resonance technique [10] and the quality factor was measured by a cavity resonator transmission method [11]. The dielectric properties of fiber were measured by the cavity perturbation technique [12,13]. The dielectric constants of composite samples were measured by the cavity perturbation technique and the S11 and S21 transmission and reflection method [14]. Since the bad surface conditions of the composite samples as mentioned before, two different methods were used to ensure accurate results.

III. EXPERIMENTAL RESULTS AND DISCUSSIONS

(1) Ceramic and Fiber Samples

The dielectric constants and quality factors of the BMT ceramic and fiber samples are listed in table2. The fiber sample has the highest dielectric constant followed by the hot pressed ceramic and the ceramic samples. However, the ceramic sample has a higher quality factor than that of the hot pressed sample. This agrees with the results on BMT reported by K. Matsumoto et al. [2]. They found the dielectric constant increases with increasing the relative density but the quality factor does not always increase with increasing relative density. Quality factors of both ceramic samples agree with the reported values. The quality factor of BMT fiber is higher than the capability that our perturbation method can measure where the highest Q value can be accurately measured is about 2,000 [13].

TABLE 2 Dielectric Properties of BMT at 10 GHz.

	ε'	Q
Ceramic	23.33	8,050
Hot pressed ceramic	24.30	6,430
Fiber	26.50	> 2,000

(2) Composite Samples

The dielectric constants of composite samples with various volume percentages were measured by the S11 & S21 technique and the cavity perturbation technique. Good agreement between the measured results obtained from these two techniques was desired to ensure correct measurement results. Fig.1 shows the results measured by the S11 & S21 technique at X band frequencies. Table3 shows the average dielectric constant values at X band frequencies plotted in Fig.1 and the results measured by the perturbation technique at 10 GHz. The measurement results by the two techniques have differences <5%. The average dielectric constant value by these two methods was used for extrapolation on estimating the dielectric constant of pure BMT. In Fig.2, the measured results are compared with the Wakino's equation, and the logarithmic rule. It was found the measured results fit well to the logarithmic rule and to the equation (1). By using the logarithmic mixture rule, the extrapolately estimated dielectric constant value of pure BMT ceramic is ~23. Comparing to the reported dielectric constant ~25 on BMT [2-4], the difference is 8%. However, if we compare this value with the values of table2, the differences are 1.4% and 5.3% respectively.

TABLE 3 Dielectric Constants of the BMT-PE Composite Samples.

Volume %	ε'	
	S11 & S21	Perturbation
100% PE	2.25	2.29
9.05% BMT	3.09	3.16
19.3% BMT	4.10	4.01
37.5% BMT	6.09	5.91
58.1% BMT	8.53	8.48

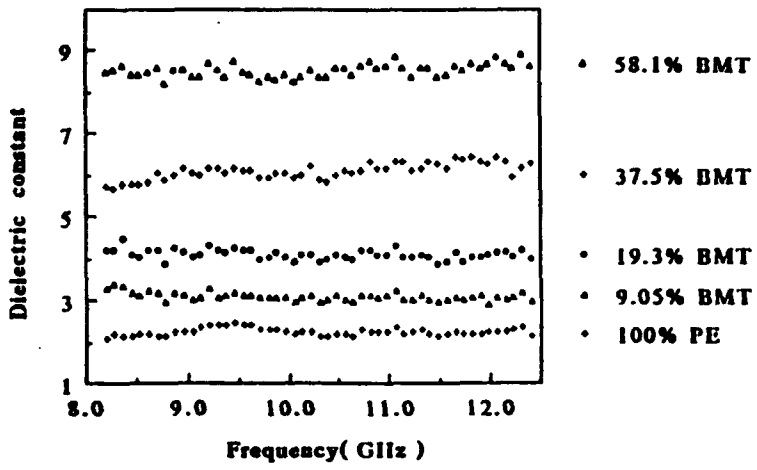

FIGURE 1 Dielectric Constants of BMT-PE Composites Measured by the S11 and S21 Technique.

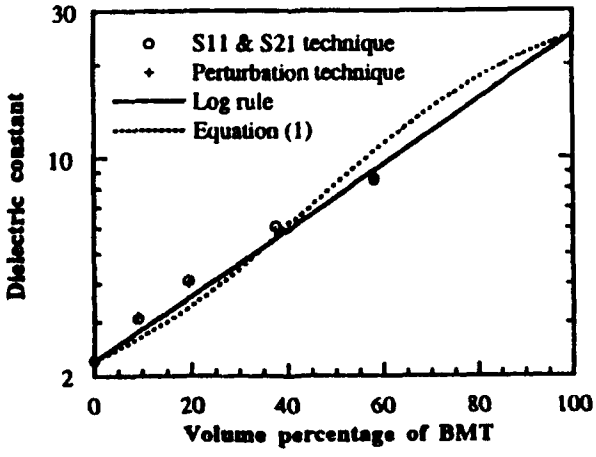

FIGURE 2 Comparsion of Experimental Data and Theoretical Expressions.

VI. CONCLUSION

The dielectric properties of BMT of various forms are reported in this paper. Due to the moderate dielectric constant and very low loss value in this material, it is a very attractive material for various microwave applications. Our measurements on the dielectric properties of ceramic samples are close to the reported values. Single crystal fiber has shown higher dielectric constant value than that of ceramic samples.

Dielectric constant of composite materials with various mixture volume percentages of BMT and PE have been investigated in X band frequencies. We found our measured results agree with the new reported equation and with the logarithmic rule. With the estimation on the dielectric constant of 100% volume percentage BMT by the logarithmic mixture rule, this powder mixture method gave a reasonable prediction on the dielectric constant of BMT ceramic at X band frequencies.

ACKNOWLEDGEMENTS:

The authors like to thank Dr. C.J. Peng for his help during the preparation of composite samples and Dr. W. Wersing, Siemens Company, for supplying the hot pressed ceramic sample. This work was supported by the Defense Advanced Research Projects Agency under the contract # DN 00014-90-J-4140.

REFERENCES:

[1] S. Nomura, Ferroelectrics, 49, 61 (1983).
[2] K. Matsumoto, T. Hiuga, K. Takata, and H. Ichimura, IEEE 1986 6th Inter. Sym. on Appl. of Ferroelectrics, 118.
[3] S. Nomura, K. Toyama, and, K. Kaneta, Jpn. J. Appl. Phys., 21, 624 (1982).
[4] H. Tamura, T. Konoike, Y. Sakabe, and K. Wakino, Commun. Am. Ceram. Soc., C59 (1984).
[5] Ruyan Guo, A.S. Bhalla, and L.E. Cross, To be published.
[6] R.J. Dinger and D.J. White, IEEE Trans. Antennas Propagat., 38, 1313 (1990).
[7] K. Wakino, T. Okada, N. Yoshida, and K. Tomono, Reported at the Am. Ceram. Soc. Meeting, Cincinnati, Ohio, Apr. 1993.
[8] D.M. Pozar, "Microwave Engineering," (Addison Wesley, New York, 1990), p.715.

[9] W.R. Tinga, W.A.G. Voss, and D.F. Blossey, J. Appl. Phys., 44, 3897 (1973).
[10] Y. Kobayashi, and M. Katoh, IEEE Trans. Microwave Theory Tech., MTT-33, 586 (1985).
[11] H. Tamura, H. Hatsumoto, and K. Wakino, Jpn. J. Appl. Phys., 28, Suppl. 28-2, 21 (1989).
[12] ASTM D 2520-86, 210 (1986).
[13] D.C. Dube, M.T. Lanagan, J.H. Kim, and S.J. Jang, " J. Appl. Phys., 63, 2466 (1988).
[14] Hewlett-Packard, Product Note 8510-3.

Appendix 7.

"Microwave Dielectric Properties Measurements of Potential HTSC Substrate Materials,"

Ferroelectrics, **145**, 15-22 (1993)

Jyh Sheen

Ruyan Guo

A.S. Bhalla

L.E. Cross

Ferroelectrics, 1993, Vol. 145, pp. 15–22
Reprints available directly from the publisher
Photocopying permitted by license only

MICROWAVE DIELECTRIC PROPERTIES MEASUREMENTS OF POTENTIAL HTSC SUBSTRATE MATERIALS

JYH SHEEN, RUYAN GUO, A. S. BHALLA and L. E. CROSS
Materials Research Laboratory, The Pennsylvania State University, University Park, PA 16802, USA

(Received June 25, 1993)

The dielectric properties of some potential substrate materials for the high-T_c superconducting film were measured at 5 to 11 GHz by using different microwave resonance techniques at 300 K and 77 K. The dielectric constants and quality factors of ceramics $Ba(Mg_{1/3}Ta_{2/3})O_3$, $Sr(Al_{1/2}Ta_{1/2})O_3$, $Sr(Al_{1/2}Nb_{1/2})O_3$, $Sr(Ga_{1/2}Ta_{1/2})O_3$, and their solid solutions with $NdGaO_3$ and $LaAlO_3$ were measured. These materials have shown dielectric constants in the range 10.7 to 26.9 and quality factors 1,750 to 35,200 at 77 K. Discussions about the suitable microwave measurement techniques are also given. The accuracies for both the dielectric constant and the quality factor measurements are within 2%.

Keywords: Substrate, microwave measurement, dielectric constant, dielectric loss

I. INTRODUCTION

The discovery of the high T_c superconductors (HTSC) opened up the possibility of superconducting devices which can be operated with liquid nitrogen as the refrigerant. The low conductor loss and low dispersion characteristics of the superconducting films make it very attractive in many microwave devices. The requirements on the dielectric properties of substrate material at microwave frequencies for the superconducting film depend on the characteristic of the desired device. An UHF circuit requires a dielectric constant of 20 to 25; a low dielectric constant is not preferred as the package volume will be increased. However, for the application as the interconnects for a high speed system, low dielectric constant will be desired to increase the propagation speed. Generally, a quality factor (Q = 1/tan δ) larger than 1,000 would be required. For certain applications,[1] the requirement on quality factor may be as high as on the order of 10,000 or more.

Recently, $Ba(Mg_{1/3}Ta_{2/3})O_3$ (BMT), $Sr(Al_{1/2}Ta_{1/2})O_3$ (SAT), $Sr(Al_{1/2}Nb_{1/2})O_3$ (SAN), and $Sr(Ga_{1/2}Ta_{1/2})O_3$ (SGT) were found to have good or adequate lattice matching and thermal expansion matching at the deposition temperatures with the high T_c YBCO superconductor.[2] In this paper, we report the microwave dielectric properties of the above materials and their solid solutions along with other two widely used substrate materials $NdGaO_3$ (NG) and $LaAlO_3$ (LA) for HTSC film. These materials have shown good potential as the substrates for the HTSC film.

We adopted four different microwave measurement techniques in our studies. Two of them are for quality factor measurements: i) the transmission type and ii) the reflection type method. The theoretical accuracy of these two techniques was given by M. Sucher.[3] Kajfez and Crnadak have compared experimental and the-

oretical accuracies.[4] They used a dielectric resonator inside a cylindrical cavity and measured both the transmission and reflection signals in the same cavity to calculate the Q factors of the dielectric resonator. They reported the major error for these two methods came from the amplitude resolution ability of the network analyzer and the errors are between 1% and 2%. Instead of using a same cavity, we adopted two different setups in the reflection and transmission methods respectively to compare the differences in Q factor measurement. We found our major error was not from the amplitude resolution ability of the network analyzer but from the uncertainty of the measurements. The advantages and disadvantages of these two methods will be discussed which are based on the critical analysis of measurements on various samples. Two more methods, i) the Hakki and Coleman post resonance technique and ii) the cavity perturbation technique, were used for the dielectric constant measurements. Good agreement of the measured dielectric constants and Q factors from different methods can ensure accuracy of our measurements. By using single method or single setup, the results of the microwave dielectric properties can sometime be difficult to rely upon. Especially for the Q factor measurement, a standard is not always available.

II. MEASUREMENT TECHNIQUES

A. Room Temperature Measurements

Four microwave resonance techniques were used in our studies. Setups of these methods included a HP8510A network analyzer for testing. A cylindrical cavity dielectric resonance technique as shown in Figure 1 was used to measure the Q-factors. The transmission signal was tested. This method has been used for Q factor measurements on high Q materials.[5,6] Kobayashi *et al.* gave a detailed study on the theoretical background of this technique.[7] The specimen under test is put inside a copper cavity with inner diameter 3.0 cm and height 1.7 cm and on a styrofoam support of 6 mm height. It has been tested that the styrofoam support does not influence the measurements. By using supports with various sizes the results didn't show significant changes (<0.5%). The TE_{018} mode was used for measurements. The formula used for the quality factor calculation is

$$\frac{1}{Q} = \frac{1}{Q_0} - \frac{1}{Q_c} \tag{1}$$

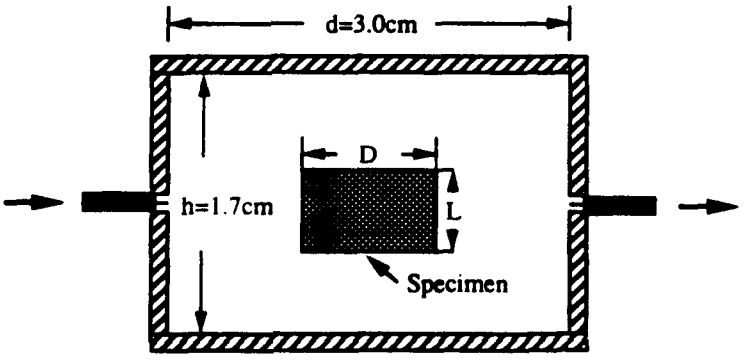

FIGURE 1 Transmission dielectric resonance method.

where Q_0 is the measured unloaded quality factor and Q_c is from the conductor loss. A DRESV31 program obtained from the University of Mississippi, USA, was used for the calculation of conductor loss. No program was used for the precise computation of the dielectric constant values. Generally, the conductor loss can be neglected when the dimension ratios d/D and h/L are larger than 3.[8]

In contrast to the cylindrical cavity dielectric resonance technique where the transmission signal was taken by the network analyzer, a reflection cavity dielectric resonance technique was used in which case the reflection signal was measured. The setup is shown in Figure 2. Like the transmission technique, this method has also been used for high Q factor measurements.[9,10] The support is made by the

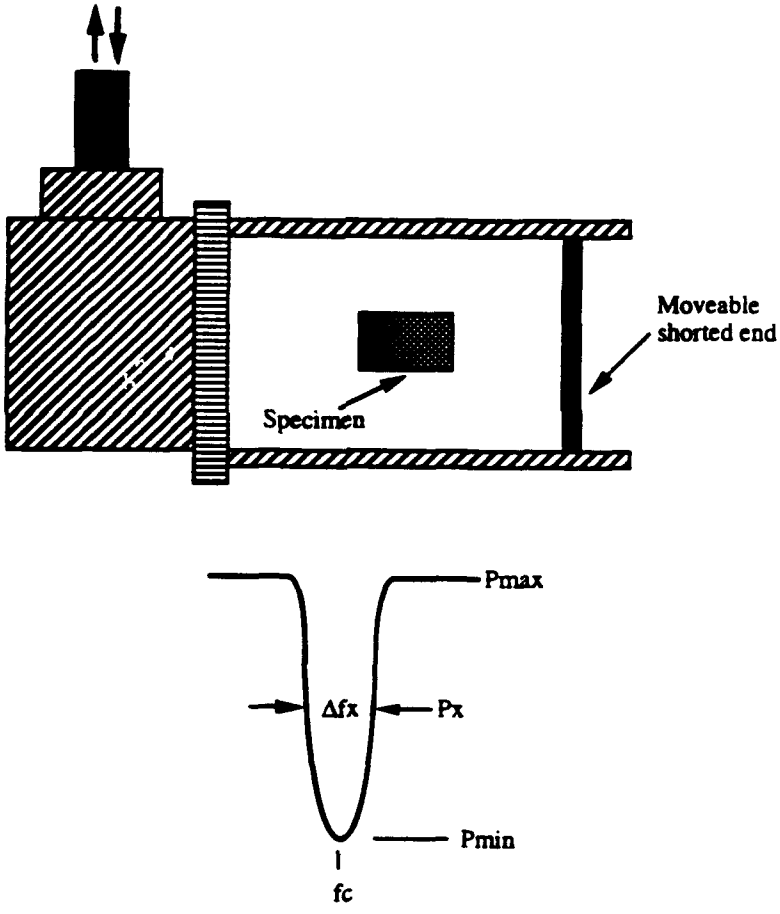

FIGURE 2 Reflection dielectric resonance method.

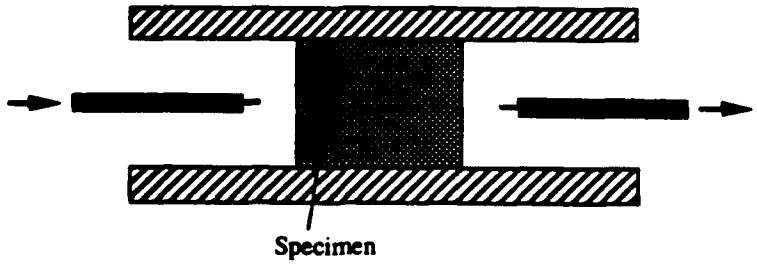

FIGURE 3 Hakki & Coleman post resonance method.

styrofoam layer of 8 mm thick. The cavity is made by a *C*-band copper cavity with a shorted end. The position of this end is adjustable to have a best resolution of the resonance signal. The unloaded Q was calculated by using the expression,[3]

$$Q_0 = \left(\frac{P_x - P_{\min}}{P_{\max} - P_x}\right)^{1/2} \frac{2}{2 \pm \sqrt{P_{\min}} - \sqrt{P_{\max}}} \frac{f_c}{\Delta f_x} \tag{2}$$

the $\pm$ sign accounts for the undercoupled case(+) and overcoupled case(−). Expression for the dielectric constant is not available for this method. TE_{018} mode was also used for this technique. The conductor loss is on the same order as that of the cylindrical cavity resonance technique.

The Hakki and Coleman dielectric resonance technique[11] shown in Figure 3 was used to measure the dielectric constants of the ceramic samples. It is also a transmission type method. An unelectroded cylindrical shaped sample was put between two highly polished brass plates like posts. The formulae used for calculation of the dielectric constant are given as follows[12]:

$$\alpha \frac{J_0(\alpha)}{J_1(\alpha)} = -\beta \frac{K_0(\beta)}{K_1(\beta)} \tag{3}$$

$$\beta^2 = \left(\frac{\pi D}{\lambda_0}\right)^2 \left[\left(\frac{\lambda_0}{2L}\right)^2 - 1\right] \tag{4}$$

$$\varepsilon' = \left(\frac{\lambda_0}{\pi D}\right)^2 (\alpha^2 + \beta^2) + 1 \tag{5}$$

This technique can also be used to measure the Q factor and the expression used for calculation is similar to Equation (1). The TE_{011} mode was used for this method. A computer program developed in our laboratory was used for the calculations of dielectric constant and quality factor. Because the sample surfaces are in contact with the two metal plates, the conductor loss in this method is much higher than that of the above two techniques. For a material with Q factor larger than 2,000, the conductor losses are of the same order as of the dielectric loss, which influence very much the accuracy of the Q factor measurement.[12] For this reason, we did not use this technique to measure the quality factor. For simplification, we called the three techniques shown in Figures 1, 2, and 3, as transmission, reflection, and post resonance techniques respectively in this paper.

The cavity perturbation technique was used for the measurements on the thin rod or bar samples as shown in Figure 4. The specimen was put inside a *X* band rectangular copper cavity. This method has been widely studied and used for the microwave dielectric property measurements.[13-16] The dielectric constant is calculated by using the formula:

$$\varepsilon' = \frac{V_c(f_c - f_s)}{2V_s f_s} + 1 \tag{6}$$

where V_c and V_s are the volumes of the cavity and sample, and f_c and f_s are the resonant frequencies without and with the specimen in the cavity. Thin bars of BMT and SAN cut out of ceramic blocks were measured by the perturbation method

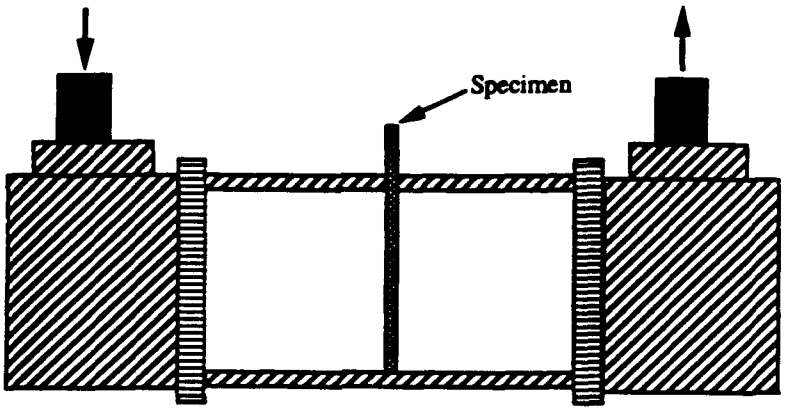

FIGURE 4 Cavity perturbation method.

to compare with the results obtained from the post resonance technique. The quality factors were not measured by this method because the Q factor measurement is limited to about $Q < 2{,}000$ for our cavity.[14]

B. *Measurements at Liquid Nitrogen Temperature*

The Q factors at liquid nitrogen temperature were measured by the transmission resonance technique. The opened cavity was directly immersed inside a container of liquid nitrogen. Dried nitrogen gas was introduced in the container to assure a negligible humidity around the specimen. The cavity was then covered and sealed and the liquid nitrogen was finally poured into the container to cool down the cavity to liquid nitrogen temperature.

C. *Error Analysis for the Q Factor Measurements*

There are four major sources of errors for the Q factor measurements. The first error ($E1$) is the frequency bandwidth measurement error. For the HP8510A network analyzer $E1$ is about 0.5%. The second error ($E2$) is from the amplitude resolution error (ΔA in dB). The error can be calculated by using the expressions[3]:

$$E2 = 0.23\Delta A \qquad \text{with 3 dB bandwidth measured, and}$$

$$E2 = 0.115\,\frac{1+\gamma}{\gamma}\,\frac{\gamma P_{\max} + P_{\min}}{P_{\max} - P_{\min}}\,\Delta A, \qquad \gamma = \frac{P_x - P_{\min}}{P_{\max} - P_x}$$

for the transmission and the reflection techniques respectively. For the transmission technique, the $E2$ is about 0.23% where ΔA is about 0.01 dB for HP8510A. The amplitude resolution of the reflection method depends on how sharp the trough is. $E2$ for reflection method varies from 0.5% to 1.0% for the depth of the trough changing from 5 dB to 40 dB. Another error ($E3$) is from the loss on the styrofoam support and the calculation error on the conductor loss. Since both of them are pretty small, the combined error is less than 0.5%. The total errors from the above three sources are less than 0.8% and 1.3% for transmission and reflection methods respectively. The last one ($E4$) is due to the uncertainty of measurements. This

error may come from different reasons: Temperature and humidity instability, bends on the measuring cables, exact position and imperfection of the specimen, and other unexpected reasons. The uncertainty of measuring the power level is an important factor in the reflection method which is calculated from,[3]

$$E4 = 0.5 \frac{(1 + \gamma)^{3/2}}{\gamma} \frac{(\gamma P_{max} + P_{min})^{1/2}}{P_{max} - P_{min}} \Delta P$$

A 1% power level error can cause the uncertainty error $E4$ on the level of 1.5% or higher for the reflection method.

III. EXPERIMENTAL RESULTS AND DISCUSSIONS

A. *Measurement Techniques*

The results are listed in Table I. The errors at room temperature for the repeated measurements on the Q factors for the transmission resonance and reflection resonance techniques on individual samples were less than 2% and 3 to 6% respectively. The 2% error for the transmission technique is a reasonable value when comparing with the theoretical value where the total error is ~0.8% for frequency error ($E1$), amplitude resolution error ($E2$), and $E3$. The 1.2% difference may come from the uncertainty error ($E4$). It was also found the large error for the reflection method come from the uncertainty error in the power level. The resonance trough was very sensitive to the positions of the sample and the short end which caused the error in reproducibility. In order to reduce the uncertainty error in the reflection method to measure the Q factor, many measurements were made and the average values were calculated. The resulted Q factors for individual materials from the reflection method are higher than those obtained from the transmission technique. The differences are less than 9%. This result is reasonable because lower resonance frequencies were encountered in the reflection method and Q factors usually increase with decreasing frequency. The transmission resonance technique is a better technique for the Q factor measurement because of its

TABLE I

Dielectric properties of the measured materials

Measurement techniques / Materials	Post resonance technique (300 K)		Reflection technique (300 K)		Transmission technique		
	f(GHz)	ε'	f(GHz)	Q	f(GHz)	Q (300 K)	Q (77 K)
BMT	10.9	23.3	6.39	12,600	6.55	12,300	35,200
SGT	10.6	26.9	6.30	7,840	6.50	7,500	8,200
SAT	11.0	10.7	7.55	2,900	7.64	2,750	4,480
.7SAT-.3NG	10.5	20.7	6.15	2,760	6.37	2,620	2,970
SAN	9.61	18.3	5.89	1,170	6.08	1,080	1,800
.7SAN-.3LA	8.06	24.6	5.31	4,160	5.45	4,000	6,500
.7SAN-.3NG	9.66	24.9	5.69	1,500	5.83	1,440	1,750

Cavity perturbation technique:

BMT: ε'= 23.1 at f = 8.59 GHz.

SAN: ε'= 18.5 at f = 10.2 GHz.

lower error factors. The measurements of Q factors at liquid nitrogen temperature by the transmission technique has a deviation of 3%. The higher error than that of the measurement at room temperature may come from the uncertainty of the temperature and humidity. The dielectric constant measurements on BMT and SAN by the post resonance and perturbation techniques have a difference less than 1.5% ($\varepsilon' = 23.3$ and 23.1 for BMT and 18.3 and 18.5 for SAN respectively), which establishes the accuracy of our dielectric constant measurements.

B. Material Characteristics

From the dielectric constant data in Table I, all the values are below 27. Different range of dielectric constants depending upon the applications are desirable. All the Q values of ceramic materials are larger than 1,750 at 77 K. The Q factors of single crystals of these materials could be improved further if the large size samples are available for the measurements. All the materials measured here have shown a potential as the substrate materials for the HTSC film devices in the microwave frequencies.

IV. CONCLUSIONS

Various dielectric resonance techniques have been used in the present study. The measurement errors in Q factor for the transmission technique is less than 2% which agrees well with the theoretical estimated value. We found, the major factor of error arising in the measurements was due to the uncertainty other than the amplitude resolution error reported by Kajfez and Crnadak.[4] It was concluded that the transmission resonance technique is a better method for the Q factor measurements. The reflection method has higher uncertainty error in Q factor measurements. It is suggested that a large number of measurements should be made and averaged to increase the confidence in accuracy of Q factor measurement. The post resonance method is not suggested as suitable for measuring the quality factor of material with Q larger than 2,000 unless the conductor loss can be precisely measured. Both post resonance and cavity perturbation techniques gave accurate measurements of the dielectric constants.

All the suggested materials have suitable dielectric constant and high enough quality factor for the microwave application as substrate for high T_c superconducting film.

V. APPENDIX

TABLE II

Specimen dimensions used in measurements

	BMT	SGT	SAT	0.7SAT-0.3NG	SAN	0.7SAN-0.3LA	0.7SAN-0.3NG
D(cm)	1.148	1.071	1.258	1.258	1.258	1.258	1.258
L(cm)	0.333	0.323	0.547	0.367	0.537	0.471	0.363

ACKNOWLEDGEMENTS

The authors like to thank Dr. Kajfez, Electrical Engineering Department, University of Mississippi, for supplying the DRESV31 program used in our measurements; Dr. S. Erdei, Dr. P. Ravindranathan, and Dr. U. Selvaraj for preparing the samples; Dr. Rustum Roy, Dr. F. W. Ainger, Dr. E. C. Subbarao, and Dr. G. Harshe for useful comments and discussions. This research is supported by the Defense Advanced Research Projects Agency under the contract # DN 00014-90-J-4140.

REFERENCES

1. R. J. Dinger and D. J. White, *IEEE Trans. Antennas Propagat.*, **38**, 1313 (1990).
2. R. Guo, A. S. Bhalla, L. E. Cross and R. Roy, to be published.
3. M. Sucher, in *Handbook of Microwave Measurements*, edited by M. Sucher and J. Fox (Brooklyn Polytechnic Press, New York 1963), **2**, chapter VIII.
4. D. Kajfez and M. Crnadak, *IEEE 1985 Southeastcon.*, 83.
5. H. Tamura, H. Hatsumoto and K. Wakino, *Jpn. J. Appl. Phys.*, **28**(Suppl. 28-2), 21 (1989).
6. T. Konaka, M. Sato, H. Asano and S. Kubo, *J. of Superconductivity*, **4**, 283 (1991).
7. K. Kobayashi, T. Aoki and Y. Kabe, *IEEE Trans. Microwave Theory Tech.*, **MTT-33**, 1361 (1985).
8. J. Delaballe, P. Guillon and Y. Garault, *AEU, Electronics and Communication*, **35**, 80 (1981).
9. M. Onoda, J. Kuwata, K. Kaneta, K. Toyama and S. Nomura, *Jpn. J. Appl. Phys.*, **21**, 1707 (1982).
10. J. K. Plourde, D. F. Linn, H. M. O'Bryan, Jr. and J. Thomson, Jr., *J. Am. Ceram. Soc.*, **58**, 418 (1975).
11. B. W. Hakki and P. D. Coleman, *IRE Trans. Microwave Theory Tech.*, **MTT-8**, 402 (1960).
12. Y. Kobayashi and M. Katoh, *IEEE Trans. Microwave Theory Tech.*, **MTT-33**, 586 (1985).
13. H. M. Altschuler, in *Handbook of Microwave Measurements*, edited by M. Sucher and J. Fox (Brooklyn Polytechnic Press, New York 1963), **2**, chapter IX.
14. D. C. Dube, M. T. Lanagan, J. H. Kim and S. J. Jang, *J. Appl. Phys.*, **63**, 2466 (1988).
15. M. R. Lakshminarayana, L. D. Partain and W. A. Cook, *IEEE Trans. Microwave Theory Tech.*, **MTT-27**, 661 (1979).
16. ASTM D 2520-86, 210 (1986).

Appendix 8.

"A Modification to a Simple Field Model to the TE_{01d} Mode of the Parallel-Plate Open Dielectric Resonator,"

Microwave and Optical Technology Letters, 7(5), 226 (1994).

Jyn Sheen

A.S. Bhalla

L.E. Cross

A MODIFICATION TO A SIMPLE FIELD MODEL OF THE $TE_{01\delta}$ MODE OF THE PARALLEL-PLATE OPEN DIELECTRIC RESONATOR

Jyh Sheen, A. S. Bhalla, and L. E. Cross
Materials Research Laboratory
The Pennsylvania State University
University Park, Pennsylvania 16802

KEY TERMS

Dielectric resonator, field modeling, parallel plate

ABSTRACT

A modification to the field expressions on the simple Itoh and Rudokas model for the $TE_{01\delta}$ mode of the parallel-plate open dielectric resonator is given. This modification is justified by the dramatic improvement in the accuracy of resonant frequency prediction.

1. INTRODUCTION

Different theoretical analyses on the parallel-plate open dielectric resonator (PPODR) in Figure 1 has been reported in several publications [1–9]. The $TE_{01\delta}$ mode is the one always studied and the field expressions are always quite complicated. Examples are the reports by Kobayashi, Fukuoka, and Yoshida [1] and Kobayashi, Aoki, and Kabe [2], where the infinite-series field expressions were used. Because the analysis requires quite complicated formulations, various simplified models have been also published [6–9]. To confirm the accuracy of their analysis, computation of resonant frequency was always accompanied by these publications to compare calculations with the experimental results. The Itoh and Rudokas model [6] is one of the more interesting ones. The accuracy of predicting resonant frequency by this model is

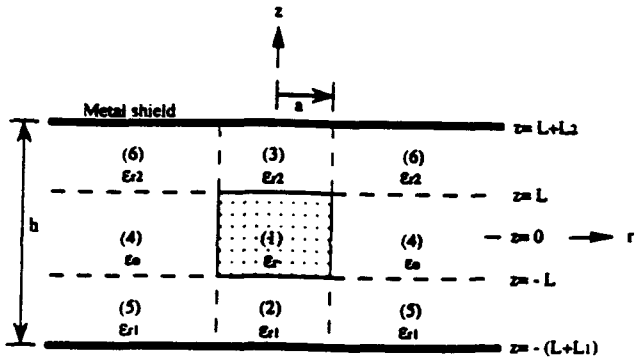

Figure 1 Parallel-plate open dielectric resonator

not very good: however, it has the great advantage of dealing with very simple field expressions.

In this article we tried to improve the simple Itoh and Rudokas model to give more accurate prediction on the resonant frequency of the TE_{011} mode. The validity of this modified model is established by comparing the results with the experimental values.

II. FIELD EXPRESSIONS

By using the Itoh and Rudokas model [6, 10], the electric fields of the TE_{011} mode in regions 1 to 4 (denoted by the subscripts 1 to 4) can be derived as

$$E_{\phi 1} = E_o J_1(k_{ci} r) \cos(\beta_1 z - \phi_1), \tag{1a}$$

$$E_{\phi 2} = E_o \frac{\cos(\beta_1 L + \phi_1)}{\sinh(\alpha_1 L_1)} \times J_1(k_{ci} r) \sinh \alpha_1 (z + L_1 + L), \tag{1b}$$

$$E_{\phi 3} = E_o \frac{\cos(\beta_1 L + \phi_2)}{\sinh(\alpha_2 L_2)} \times J_1(k_{ci} r) \sinh \alpha_2 (L_2 + L - z), \tag{1c}$$

$$E_{\phi 4} = E_o \frac{J_1(k_{ci} a)}{K_1(k_{co} a)} \times K_1(k_{co} r) \cos(\beta_1 z - \phi_1), \tag{1d}$$

where

$$\frac{J_0(k_{ci} a)}{J_1(k_{ci} a)} = -\frac{k_{co} a}{k_{ci} a} \frac{K_0(k_{co} a)}{K_1(k_{co} a)}, \tag{2a}$$

$$k_{co}^2 = \beta_1^2 - k_o^2, \tag{2b}$$

$$\beta_1^2 = k_o^2 \varepsilon_r - k_{ci}^2, \tag{2c}$$

$$k_o = \omega \sqrt{\mu_o \varepsilon_o}, \tag{2d}$$

$$\phi_1 + \phi_2 = 0, \tag{2e}$$

$$\phi_{1,2} = \tan^{-1}\left(\frac{\alpha_{1,2}}{\beta_1} \coth \alpha_{1,2} L_{1,2}\right) - \beta_1 L, \tag{2f}$$

$$\alpha_{1,2}^2 = k_{ci}^2 - k_o^2 \varepsilon_{r1,r2}, \tag{2g}$$

and the J and K are Bessel functions and modified Bessel functions, respectively. The magnetic field components can be easily derived from the above electric fields. Fields in regions 5 and 6 are postulated to be zero. The k_{ci} and k_{co} are obtained by substituting the Eqs. (2b) and (2c) in Eq. (2a).

To increase the accuracy of this simple model, we modified the Eq. (2b) to the following:

$$k_{co}^2 = \beta_{11}^2 - k_o^2, \tag{3a}$$

$$\beta_{11} = \frac{\pi}{h}. \tag{3b}$$

This modification is based on the fact that the distance between the two metal shields should be smaller than one half of the wavelength λ_o to keep the system below cutoff condition [1, 2, 4]. For $h > \lambda_o/2$, the resonator is over the cutoff condition and k_{co} becomes imaginary, as can be seen from Eq. (3). The modified Bessel function would be replaced by the Hankel function and the radiation loss dramatically increased [2]. The k_{co} obtained from Eq. (3) is then substituted into Eq. (2a) to compute k_{ci} by a simple numerical method.

III. COMPUTATIONS AND EXPERIMENTS

To examine the validity of this simply modified model, we conducted computations on the resonant frequencies of three samples to compare with experiments for this PPOD resonator. For all the experimental confirmations in other publications, dielectric constants larger than 35 were always adopted. In our research ceramic specimens with dielectric constants (ε_r) 10, 23, and 37 are used, which have diameter ($2a$, mm) × thickness ($2L$, mm) 11.48 × 3.33, 12.66 × 4.36, and 10.72 × 3.06, respectively. A styrofoam with dielectric constant 1.03 (ε_{r1}) is used as the sample support and the ε_{r2} is equal to 1.0.

The computational and experimental resonant frequencies are shown in Figure 2. The resonant frequencies of the Itoh and Rudokas model were computed by the DRESV2 program [10] (Copyright 1986 D. Kajfez). The modification in Eq. (3) gives dramatic improvement over the Itoh and Rudokas model on computing resonant frequency. The accuracy of this modified model is excellent at L_1, $L_2 < 5$ mm. The results are surprisingly good for such a simple model. This modification method is still not perfect, as the experimental results do not exactly fall on the theoretically calculated solid curves in Figure 2. However, for such a simple model, these results are considered to be quite satisfactory.

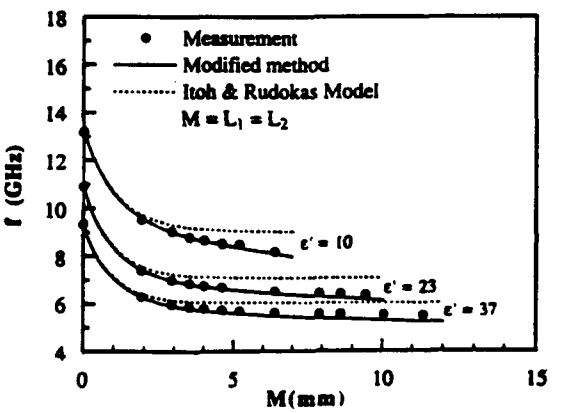

Figure 2 Numerical and experimental results of the resonant frequency

IV. CONCLUSION

The simple Itoh and Rudokas model has been modified in this article. The theoretical resonant frequencies have been computed to compare with the experimental results. Although this modified method is not perfect in comparison with experimental results, this presented method gives a very simple model to analyze the parallel-plate open dielectric resonator and has a much better accuracy in the computation of resonant frequency than that of the nonmodified Itoh and Rudokas model.

ACKNOWLEDGMENT

This work was supported by the Defense Advanced Research Projects Agency under Contract No. DN 00014-90-J-4140.

REFERENCES

1. Y. Kobayashi, N. Fukuoka, and S. Yoshida, "Resonant Modes for a Shielded Dielectric rod Resonator," *Electron. Commun. Jpn.*, Vol. 64-B, Nov. 1981, pp. 44–51.
2. Y. Kobayashi, T. Aoki, and Y. Kabe, "Influence of Conductor shields on the Q-Factors of a TE_{0} Dielectric Resonator," *IEEE Trans. Microwave Theory Tech.*, Vol. MTT-33, Dec. 1985, pp. 1361–1366.
3. P. Guillon and Y. Garault, "Accurate Resonant Frequencies of Dielectric Resonators," *IEEE Trans. Microwave Theory Tech.*, Vol. MTT-25, Nov. 1977, pp. 916–922.
4. M. Jaworski and M. W. Pospieszalski, "An Accurate Solution of Cylindrical Dielectric Resonator Problem," *IEEE Trans. Microwave Theory Tech.*, Vol. MTT-27, July 1979, pp. 639–643.
5. Y. Konishi, N. Hoshino, and Y. Utsumi, "Resonant Frequency of a $TE_{01\delta}$ Dielectric Resonator," *IEEE Trans. Microwave Theory Tech.*, Vol. MTT-24, Feb. 1976, pp. 112–114.
6. T. Itoh, and R. S. Rudokas, "New Method for Computing the Resonant Frequencies of Dielectric Resonators," *IEEE Trans. Microwave Theory Tech.*, Vol. MTT-25, Jan. 1977, pp. 52–54.
7. S. B. Cohn, "Microwave Bandpass Filters Containing High-Q Dielectric Resonators," *IEEE Trans. Microwave Theory Tech.*, Vol. MTT-16, April 1968, pp. 218–227.
8. H. Y. Yee, "Natural Resonant Frequencies of Microwave Dielectric Resonators," *IEEE Trans. Microwave Theory Tech.*, Vol. MTT-13, Feb. 1965, p. 256.
9. M. Pospieszalski, "Cylindrical Dielectric Resonators and their Applications in TEM Line Microwave Circuits," *IEEE Trans. Microwave Theory Tech.*, Vol. MTT-27, July 1979, pp. 233–238.
10. D. Kajfez, in D. Kajfez and P. Guillon (Eds.), *Dielectric Resonators*, Artech House, Dedham, MA, 1986, Chap. 4.

Received 10-20-93

Microwave and Optical Technology Letters, 7/5, 226–228

CCC 0895-2477/94

Appendix 9.

"Modified Mixed Oxide Perovskite for High Tc Superconductor Substrate Applications,"

J. Materials Science **29**(19) (Oct. 1, 1994).

Ruyan Guo

P. Ravindranathan

U. Selvaraj

A.S. Bhalla

L.E. Cross

R. Roy

MODIFIED MIXED OXIDE PEROVSKITES $0.7Sr(Al_{1/2}B_{1/2})O_3$:$0.3LaAlO_3$ AND $0.7Sr(Al_{1/2}B_{1/2})O_3$:$0.3NdGaO_3$ (B=Ta^{5+} or Nb^{5+}) FOR HIGH Tc SUPERCONDUCTOR SUBSTRATE APPLICATIONS

Ruyan Guo, P. Ravindranathan, U. Selvaraj, A.S. Bhalla, L.E. Cross and Rustum Roy

Materials Research Laboratory, The Pennsylvania State University

University Park, PA 16802 USA

ABSTRACT

Single crystal fibers of modified strontium aluminum tantalum oxide $(1-x)Sr(Al_{1/2}Ta_{1/2})O_3$:$xLaAlO_3$ (SAT:LA) and $(1-x)Sr(Al_{1/2}Ta_{1/2})O_3$:$xNdGaO_3$ (SAT:NG), and modified strontium aluminum niobium oxide $(1-x)Sr(Al_{1/2}Nb_{1/2})O_3$:$xNdGaO_3$ (SAN:NG) and $(1-x)Sr(Al_{1/2}Nb_{1/2})O_3$:$xLaAlO_3$ (SAN:LA) were grown using a laser heated pedestal growth technique. 0.7SAT:0.3LA grows congruently and remains twin free simple cubic perovskite structure (as the SAT) when cooled down to room temperature. 0.7SAT:0.3LA crystals have moderate dielectric constant (κ=21.7) and low dielectric loss ($\tan\delta=7.5\times10^{-5}$) at 10 kHz and 90K. The reduction problem of Ta^{5+} is eliminated (which is common in the case of SAT growth). 0.7SAT:0.3NG and 0.7SAN:0.3NG have lower melting temperatures and crystal growth is easier. $NdGaO_3$ addition to the SAT and SAN enhances the potential of SAT and SAN as large area substrates for HTSC growth. However, the dielectric constants increased from κ~12 to κ~16 (0.7SAT:0.3NG) and from κ~18 to κ~23 (0.7SAN:0.3NG) as a result of $NdGaO_3$ incorporation.

1. INTRODUCTION

One of the recent interests in high Tc superconductor thin films has been to develop suitable substrate materials for microwave device applications. The ideal substrate for such application should satisfy the following conditions: [1] 1) the lattice constants (or the atomic arrangement) of the substrate should be closely matched to the high Tc superconducting thin films; 2) the substrates should have a low dielectric constant and dielectric loss at low temperature; 3) the substrates should not have any phase transitions that create micro twins and 4) if possible, the substrates should be readily prepared in large sections. (This often requires materials of moderate melting points suitable for Czochralski growth). Various single crystals such as $SrTiO_3$, $LaAlO_3$, $LaGaO_3$, Al_2O_3, MgO and yttrium-stablized-ZrO_2 (YSZ) have been used as substrates for the high Tc superconducting thin films [2,3,4]. However, these substrates satisfy only part of the above-mentioned conditions.

We have been studying the crystal chemistry of perovskite oxides for quite sometime and we have proposed many complex oxides for substrate applications [5, 6]. The results of our approaches presented in this paper are basically two-fold: (i) to control the twinning problem in $LaAlO_3$ by introducing chemical modification to stabilize the cubic phase at room temperature and (ii) to lower the melting temperatures of the complex perovskite single crystals $Sr(Al_{1/2}Ta_{1/2})O_3$ (SAT) and $Sr(Al_{1/2}Nb_{1/2})O_3$ (SAN) as a follow-up of our previous work [7].

$LaAlO_3$, is a rhombohedrally distorted perovskite ($A^{3+}B^{3+}O_3$ type) with a pseudo-cell of a=3.789Å, γ=90.12° and has a ferroic phase transition at ~435°C [8] that results in highly twinned crystal [9, 10]. Although the La^{3+} ion generally prefers the 12-coordination-site,

there is a trend for the 9-coordination. The distortion in the LaO_{12} polyhedron is brought about by a slight displacement of the oxygen atoms away from the ideal positions of the cubic perovskite-form, that is more clearly shown in other [rear-earth]$^{3+}AlO_3$ family members when the A-site cation radius become even smaller, e.g., in the case of $PrAlO_3$ [11, 12].

In fact, no ideal cubic perovskite structure has been reported in ternary compounds of the $[A]^{3+}[B]^{3+}O_3$ type [13]. Fig. 1 presents a classification of $[A]^{3+}[B]^{3+}O_3$ type compounds according to the constituent ionic radii (8-coordination cation radii were used for A-site cations) focusing on the perovskite region. The [$LaAlO_3$] and [$GdFeO_3$] are the only perovskite-like regions in the figure. For aluminate compounds, the largest A^{3+} cation, La^{3+}, has rhombohedral symmetry and the other $[A]^{3+}[Al]^{3+}O_3$ compounds have even lower symmetry.

It is therefore our approach in this study to introduce "balanced" cation substitution simultaneously in the A- and B-sites by forming crystalline solutions of known end members to increase the average cation size at the A-site to stabilize the 12-coordination of that position and consequently the cubic perovskite structure. Recently, Mateika et al. [14, 4] reported mixed rare-earth aluminum perovskites by coupled substitution of {[Sr,Ca], [Ta,Nb]} and the crystal growth thereof by the Czochralski method. Such mixed crystals are twin-free when the cubic symmetry is obtained. One of the compositions $(La_{0.289}Sr_{0.709})(Al_{0.646}Ta_{0.356})O_3$ they studied may be considered as solid solution of two end members, $LaAlO_3$ and $Sr(Al_{1/2}Ta_{1/2})O_3$. The $Sr(Al_{1/2}Ta_{1/2})O_3$ (SAT). We have reported the growth of single crystal fibers of the latter by the laser heated pedestal growth technique [7].

SAT and SAN, are potential substrates for HTSC and have a near ideal lattice fit to the high Tc superconductors, excellent thermal expansion compatibility and desirable dielectric properties. The dielectric constant κ of SAT was found to be ~12, one of the lowest reported in the oxide perovskite family. However, both of them have relatively high melting temperatures (SAT: 1900~(1908±25), and SAN:1790~(1739±10)) [15, 7] therefore they cannot be grown using the platinum crucibles by Czochralski growth technique. Reduction of Nb^{5+} or Ta^{5+} was also found to be intrinsic, in these crystals grown in air. By forming crystalline solutions with compounds of low melting temperatures, it was hoped that the crystalline solution will result lower melting temperature and consequently avoid the reduction problem and permit growth in platinum. We have measured the melting temperatures of various oxide perovskites [6] and the refractory character of this family is generally well known. $NdGaO_3$, proved to be an exception; it was found to have a melting temperature of ~1484±24°C, and it was therefore selected as an end member of the crystalline solution series with SAT and/or SAN for the present studies. $NdGaO_3$ has the [$GdFeO_3$] structure with orthorhombic symmetry as majority of the $[A]^{3+}[B]^{3+}O_3$ type compounds do (Fig.1). No twinning problems were reported in this material. YBCO thin films of superior quality were deposited on $NdGaO_3$ as compared to the YBCO film deposited on a $LaAlO_3$ substrate. However, the high dielectric loss in the $NdGaO_3$ is a limiting factor for the YBCO film applications in microwave devices and resonator.

This paper reports an approach in which by forming the crystalline solutions between selected end members the specific properties are modified to meet the requirements of the HTSC thin films for microwave device applications. The selected crystalline solution

phases $0.7Sr(Al_{1/2}Ta_{1/2})O_3$-$0.3LaAlO_3$, $0.7Sr(Al_{1/2}Nb_{1/2})O_3$-$0.3LaAlO_3$, $0.7Sr(Al_{1/2}Ta_{1/2})O_3$-$0.3NdGaO_3$, and $0.7Sr(Al_{1/2}Nb_{1/2})O_3$-$0.3NdGaO_3$ (addressed in their short-handed forms as SAT-LA, SAN-LA, SAT-NG, and SAN-NG respectively in the paper) and their single crystal growth, structure and properties are reported in this paper.

2. EXPERIMENTAL

2.1 *Sample preparation*

La $(OH)_3$, $SrCO_3$ and the respective oxides were used as starting materials. The purity of the starting materials was about 99.9% or better.

The starting materials were weighed in the right stoichiometry ratio and thoroughly mixed using a ball mill with a carrier solvent such as ethanol. The resulting mixture was dried at 100°C and fired at 1100°C for 12 hours. The sample was then reground and fired at 1400 °C for additional 12 hours. X-ray powder diffraction (XRD) was used to identify the products after each step of the processing. Finally, the sample was reground and fired at 1500°C for 6 hours.

The calcined powders were sieved through 325 mesh screen. A 2 weight percentage polyvinyl alcohol (PVA) aqueous solution was added as binder. The calcined powders containing PVA binder were then pressed as pellets. The pellets were sintered at 1500°C to 1625°C, depending on the compositions, for 6 hours.

2.2 *Melting Point Determination*

Melting points were determined using a strip furnace and optical pyrometers. The heating element consisted of a V-shaped ribbon of iridium metal clamped between two

water-cooled brass electrical contacts. The current through the strip as controlled by two variable AC transformers connected with a vernier control arrangement for the better temperature control. The notch of the V acts as a black body cavity. This extremely simple furnace designed in 1930, was used extensively in the early work on perovskites in the 1950's [16].

The samples, having been determined to be a single phase by x-ray diffraction, were placed in the notch of the strip in the form of a small amount (pinhead) of granular powder. The temperature of the sample and the strip was monitored simultaneously using three optical pyrometers through which the onset of melting was observed. Each measurement was repeated three times with fresh samples used and refined temperature scales. A total of nine readings were taken for each sample by three independent operators and pyrometers. The average melting temperature was obtained along with the estimation of the precision of these measurements after rejecting the lowest and highest points.

2.3 *Laser Heated Pedestal Growth Technique*

The laser heated pedestal growth (LHPG) method was used to grow single crystal fibers of modified compositions. The LHPG equipment used in this investigation consisted of a power source (water cooled, tunable flowing gas CO_2 55W laser), an optical layout, and a growth section. The alignment, seeding and growths were visually imaged outside the growth chamber by a short focal length telescope, which was in line with a CCD camera. Molten zone temperature during a stable growth was monitored using an optical pyrometer focusing telescope with a resolution of linear dimension of 0.1mm. Further detailed description can be found elsewhere [17, 18].

3. RESULTS AND DISCUSSION

The x-ray powder diffraction patterns of the calcined powder (at 1500°C) showed the presence of only a single phase. All four modified compositions were found to have the ideal simple cubic structure after crystallization as determined by the x-ray powder diffraction techniques on the respective crystals. The crystallographic structure and lattice parameters are listed in Table 1. Ceramic samples of SAT-NG (sintered at 1625°C for six hours) showed an ordered cubic structure that yielded a double cell a=7.7732Å. Similarly, the SAN-NG ceramic sample (sintered at 1575°C for six hours) also has the ordered structure with double unit cell a=7.7647Å. The geometrical density of all the sintered samples was more than 91% of the theoretical density when the sintering temperature was 1600°C.

Our results further confirmed the report of Mateika et. al. [4] that the ideal cubic phase can be formed in (La,Sr)(Al,Ta)O_3 compounds. It is interesting to notice that similar substitutions using [Ca,Ta] instead of [Sr,Ta] did not produce a compound with cubic structure. The average A-site cation radii of the [Ca,Ta] substitution is smaller than that of $LaAlO_3$ (ionic radii of Ca^{2+}, La^{3+}, and Sr^{2+} are 1.14, 1.185, and 1.27Å, respectively), [19] therefore, no stabilization effect on 12-coordination A-site can be expected.

The existence of cubic symmetry for the compound of SAT-NG and SAN-NG may be due to the fact that Ga^{3+} is almost of the same cation size as Ta^{5+}/Nb^{5+}. Slight reduction in the A-site cation size is accompanied by the slight increase of the B-site cation size and thus the cubic structure of SAN or SAT stays intact.

The melting temperatures as determined using the strip furnace melting and the optical pyrometer, along with the observed stable growth zone temperature during the LHPG growth are listed in Table 2. It is especially interesting that $NdGaO_3$ addition to SAT and SAN reduced the melting point as expected.

Single crystals of SAT-LA, SAT-NG, SAN-LA, and SAN-NG were grown by the laser heated pedestal growth technique using the ceramic rods as both seed and feed materials. All growth was performed in air. The temperatures required for the growth of SAT-LA was somewhat lower (~100°C) than that for the growth of SAT; however, the crystals as grown were transparent and colorless. The reduction problems found earlier in SAT growth were eliminated. Crystal fibers of ~500μm in diameter did not show any clear facet and cleavage characteristics. Single crystals of SAT-NG and SAN-NG were likewise easier to grow than to their unmodified forms as their respective melting temperatures were considerably lower and the stable growth melt zone during the LHPG growth was easier to maintain. Crystal fibers of SAT-NG and SAN-NG of ~400-500μm in diameter and 40mm in length were grown. The as grown SAT-NG and SAN-NG both haav a dark color with the SAT-NG being lighter and partially transparent. The color of the crystals is believed to be due to the Ga^{3+} in the compound. As grown SAT-NG and SAN-NG single crystal fibers are shown in Fig. 2.

Dielectric properties of the ceramic samples were measured using a General Radio 1621 Capacitance Measurement System. A 3-terminal measurement was carried out using an environmental controllable sample holder. The stray capacitance, lead and contact resistance were corrected during the measurements by taking into account the open circuit

measurement. The edge corrections were made to the results by using an empirical equation obtained from a family of fused silica samples.

Dielectric constant κ and loss tangent of the modified samples were examined as functions of temperature and frequency. Table 3. summarizes the values obtained on ceramic samples at liquid nitrogen temperature and at 10kHz. Dielectric property of the crystalline solution SAT-LA appeared to have maintained the dielectric features of the $LaAlO_3$ alone, though with the twin-free cubic structure resulted from the SAT end member. All $NdGaO_3$ end member compounds have low dielectric loss ($<5.1x10^{-4}$); however, the dielectric constants of modified compounds appeared to be elevated by the addition of the $NdGaO_3$. In general, all the compounds studied have comparable or smaller dielectric constants and comparable dielectric loss to the rhombohedral $LaAlO_3$ simple perovskite.

Thermal expansion coefficients of the crystalline solution compounds were measured in comparison to the thermal properties of the YBCO superconductor and are listed in Table 4. Good thermal expansion matching was found in all NG-end member compounds. $LaAlO_3$ and modified SAT-LA samples, however, showed thermal expansion coefficients somewhat smaller than the ideal. There has been a report on the thermal expansion coefficient of $LaAlO_3$ as being $10x10^{-6}/°C$ [20] and the reason of the discrepancies between our results and the reported values may be due to the different thermal annealing history of the samples. In our measurements, the $LaAlO_3$ crystal was annealed several times at temperature ~800°C before thermal strain measurements were done and also our results were reproducible. No structural phase transition was found in the measured temperature region for all the compositions listed. Plots of the thermal strains vs. temperature as measured are shown in Fig.3.

4. CONCLUSIONS

The ideal cubic perovskite structure can be stabilized in the case of $LaAlO_3$ by forming a crystalline solution compositions with cubic $Sr(Al_{1/2}Ta_{1/2})O_3$ and $Sr(Al_{1/2}Nb_{1/2})O_3$. The mechanism of this type of stabilization is perhaps through introducing the compensated cation substitution in the form of $[2La^{3+}]+[Al^{3+}] \rightarrow [2A^{2+}]+[B^{5+}]$ with the A^{2+} cation having a radius larger than that of La^{3+} and therefore stabilizing the 12-coordinated A-site. Crystalline solutions of SAT-LA maintained most of the dielectric and thermal properties of $LaAlO_3$ and gained the advantage of forming a twin-free simple cubic structure and improved lattice compatibility. $NdGaO_3$ is shown to be an effective end member to decrease the melting temperature of SAN and SAT without disturbing their simple cubic (twin free) crystal structure. Dielectric constants of SAN and SAT with an addition of $NdGaO_3$ were increased; however, the dielectric loss factor still remained less than $5x10^{-4}$. The results suggesting that SAT-LA and SAN-LA are better candidates as substrate materials than $LaAlO_3$ because they have the twin free cubic structure. Also the growth of SAT-NG and SAN-NG are comparatively convenient as they have relatively low melting temperatures together with the relatively lower dielectric constants and the ideal lattice constants and thermal compatibility with the YBCO superconducting materials.

ACKNOWLEDGMENT

The authors like to thank Dr. S. Erdei and Prof. F.W. Ainger for the discussions on the subject. This work was supported by the Defense Advanced Research Projects Agency (DARPA) under the contract DN 00014-90-J-4140.

REFERENCES

1. H.M. O'BRYAN, P.K. GALLAGHER, G.W. BERKSTREKKER and C.D. BRANDLE, *J.Mater. Res.* **5**(1) (1990) 183.
2. T. VENKATESAN, C.C. CHANG, D. DIJKKAMP, S.B. DGALE, E.W. CHASE, L.A. FARROW, D.M. HWANG, P.F. MICELI, S.A. SCHWARZ, J.M. TERASION, X.D. WU, and A. INAM, *J. Appl. Phys.* **63** (1988) 4591.
3. G. KOREN, A. GUPTA, E.A. GIESS, A. SEGMULLER and R.B. LAIBOWITZ, *Appl. Phys. Lett.* **54** (1989) 1054.
4. D. MATEIKA, H. KOHLER, H. LAUDAN and E. VÖLKEL, *J. Cryst. Growth* **109** (1991) 447.
5. L.E. CROSS, R. ROY, R. GUO, J. SHEEN, A.S. BHALLA, F.W. AINGER, and E.C. SUBBARAO, presented at the Defence Advanced Research Projects Agency (DARPA) 3rd Annual High Temperature Superconductor Workshop, Seattle, Washington, Sept.30-Oct.2 (1991).
6. R. GUO, J. SHEEN, A.S. BHALLA, F. AINGER, E.C. SUBBARAO, and L.E. CROSS, presented at the Defence Advanced Research Projects Agency and Office of Naval Research (DARPA/ONR) Workshop on Substrate Materials for High Tc Superconductors, Colonial Williamsburg, Virginia, Feb.5-7 (1992).
7. R. GUO, A.S. BHALLA, JYH SHEEN, F.W. AINGER, E.C. SUBBARAO, and L.E. CROSS, "Strontium aluminum tantalum and strontium aluminum niobium oxide as potential substrates for HTSC thin films," *J. Mater. Res.* (to be published).
8. E.A. WOOD, *Amer. Min.* **36** (1951) 768.
9. S. GELLER and V.B. BALA, *Acta Crystal.* **9** (1956) 1019.
10. M. DAVIDSON, *Superconductor Industry* **5**(2) (1992) cover page.
11. R.D. BURBANK, *J. Appl. Cryst.* **3** (1970) 112.
12. O. MULLER and R. ROY, in "*The major ternary structural families*" (Springer-Verlag, Berlin, Heidelberg, New York 1974) p.215.
13. F.S. GALASSO, in "*Structure, properties and preparation of perovskite-type compounds*" (Pergamon Press, Oxford, London, Ediburgh, Now York, Toronto, Sydney, Paris, Braunschweig 1969) p.10.
14. S. HAUSSÜHL and D. MATEIKA, *Crystal. Res. Technol.* **26**(4) (1991) 481.
15. C.D. BRANDLE and V.J. FRATELLO, *J. Mater. Res.* **5**(10) (1990) 2160.

16 M.L. Keith and R. Roy, *Amer. Min.*, **39** (1954) 1.

17. J. YAMAMOTO and A.S. BHALLA, *Mat. Res. Bull.* **24** (1989) 761.

18. R. GUO, A.S. BHALLA, and L.E. CROSS, "Barium magnesium tantalum oxide single crystal grown by laser heated pedestal growth technique," *J. Appl. Phys.* (to be published).

19. R.D. SHANNON and C.T. PREWITT, *Acta Cryst.* **B25** (1969) 925; *Acta Cryst.* **B26** (1970) 1046.

20. R. RAMESH, A. INAM, W.A. BONNER, P. ENGLAND, B.J. WILKENS, B.J. MAEGHER, L. NAZAR, X.D. WU, M.S. HEDGE, C.C. CHANG, T. VANKATESAN, and H. PADAMSEE, *Appl. Phys. Lett.* **55** (1989) 1138.

21. R. GUO, J. POVOA, and A.S. BHALLA, "*Thermal Expansion Coefficients of Potential HTSC Substrate Materials*," *Mater. Res. Lett.* (to be published).

22. S. GELLER, *Acta Cryst.* **10** (1957) 243.

23. T. KONAKA, M. SATO, H. ASANO, and S. KUBO, *J. Superconductivity* **4**(4) (1991) 283.

24. HOYDOO YOU, U. WELP, and Y. FANG, *Phys. Rev.* **B43**(4) (1991) 3660.

TABLE CAPTIONS

Table 1. Symmetry and Lattice Parameters of The Modified Compounds Determined by X-ray Diffraction.

Table 2. Melting Temperatures of Modified Complex Perovskites.

Table 3. Dielectric Properties of Modified Complex Perovskites.

Table 4. Coefficient of Thermal Expansion Measured by the Linear Voltage Differential Transformer Dilatometry Technique (RT - ~800°C) [21].

FIGURE CAPTIONS

Figure 1. Structure field map for $A^{3+}B^{3+}O_3$ [perovskites] [12].

Figure 2. Single crystal fibers of (a) SAT-NG and (b) SAN-NG grown by the laser heated pedestal growth technique.

Figure 3. Thermal strains vs temperature as measured using the push rod linear voltage differential transformer dilatometer [21].

TABLE 1. SYMMETRY AND LATTICE PARAMETERS OF THE MODIFIED COMPOUNDS DETERMINED BY X-RAY DIFFRACTION.

Composition	symmetry	Lattice Constant (Å)	Density (g/cm^3)
SAT	cubic	a=3.8952	6.730
SAN	cubic	a=3.8950	5.495
$LaAlO_3$	Rhomb.	a=3.789, γ=90.12°	6.532
$NdGaO_3$	Ortho. [22] $GdFeO_3$ structure	a=5.426, b=5.502, c=7.706 (pseudo cell a_0=3.860)	7.561
SAT-LA	Cubic	a=3.8727	6.628
SAN-LA	Cubic	a=3.8634	5.798
SAT-NG	Cubic	a=3.8866	6.965
SAN-NG	Cubic	a=3.8790	6.1299

Table 2. MELTING TEMPERATURES OF MODIFIED COMPLEX PEROVSKITES

Composition	M.P. (°C) (Strip Furnace)	Molten Zone Temp.(±0.5%)(°C) (LHPG)
$Sr(Al_{1/2}Ta_{1/2})O_3$	1908±25	2049
$Sr(Al_{1/2}Nb_{1/2})O_3$	1739±10	1862
$LaAlO_3$	2040±9	
$NdGaO_3$	1484±24	
$0.7SAT:0.3LaAlO_3$	1830±22	1946
$0.7SAT:0.3NdGaO_3$	1767±31	1832
$0.7SAN:0.3LaAlO_3$	1705+20	
$0.7SAN:0.3NdGaO_3$	1582±20	1775

Table 3. DIELECTRIC PROPERTIES OF MODIFIED COMPLEX PEROVSKITES

Material	at 10kHz, 90K	
	κ	tanδ
$LaAlO_3$	23	7.47×10^{-5}
$NdGaO_3$ (77K,10GHz) [23]	23	3.24×10^{-4}
$Sr(Al_{1/2}Ta_{1/2})O_3$	11.8	4.24×10^{-5}
$Sr(Al_{1/2}Nb_{1/2})O_3$	18.7	2.20×10^{-4}
$0.7SAT:0.3LaAlO_3$	21.7	7.47×10^{-5}
$0.7SAN:0.3LaAlO_3$	25.7	2.79×10^{-4}
$0.7SAT:0.3NdGaO_3$	16.0	4.25×10^{-4}
$0.7SAN:0.3NdGaO_3$	23.0	5.15×10^{-4}
$1/3SAN:1/3SAT:1/3NdGaO_3$	22.3	5.11×10^{-4}

Table 4. COEFFICIENT OF THERMAL EXPANSION MEASURED BY DILATOMETRY TECHNIQUE (RT - ~800°C) [21]

$$\Delta L / L_0 = A_0 + \alpha T + \beta T^2$$

Material	α (x10^{-6}/°C) (@~300K)	α (x10^{-6}/°C), β (x10^{-8}/°C^2) (300-1050K)
YBCO [24] (untwinned single crystal at 300K)	14 (a_a) 9 (a_b) 19 (a_c) 42 (a_v)	
YBCO ceramic	10.9	9.5
$LaAlO_3$ //[1$\bar{1}$0] //[001]	8.2 6.4	
$Sr(Al_{1/2}Ta_{1/2})O_3$	9.7	8.9, 1.1
$Sr(Al_{1/2}Nb_{1/2})O_3$	8.5	6.5, 2.4
$0.7Sr(Al_{1/2}Ta_{1/2})O_3$:$0.3LaAlO_3$	7.7	
$0.7Sr(Al_{1/2}Nb_{1/2})O_3$:$0.3NdGaO_3$	10.8	
$0.7Sr(Al_{1/2}Ta_{1/2})O_3$:$0.3NdGaO_3$	8.8	6.3, 3.6

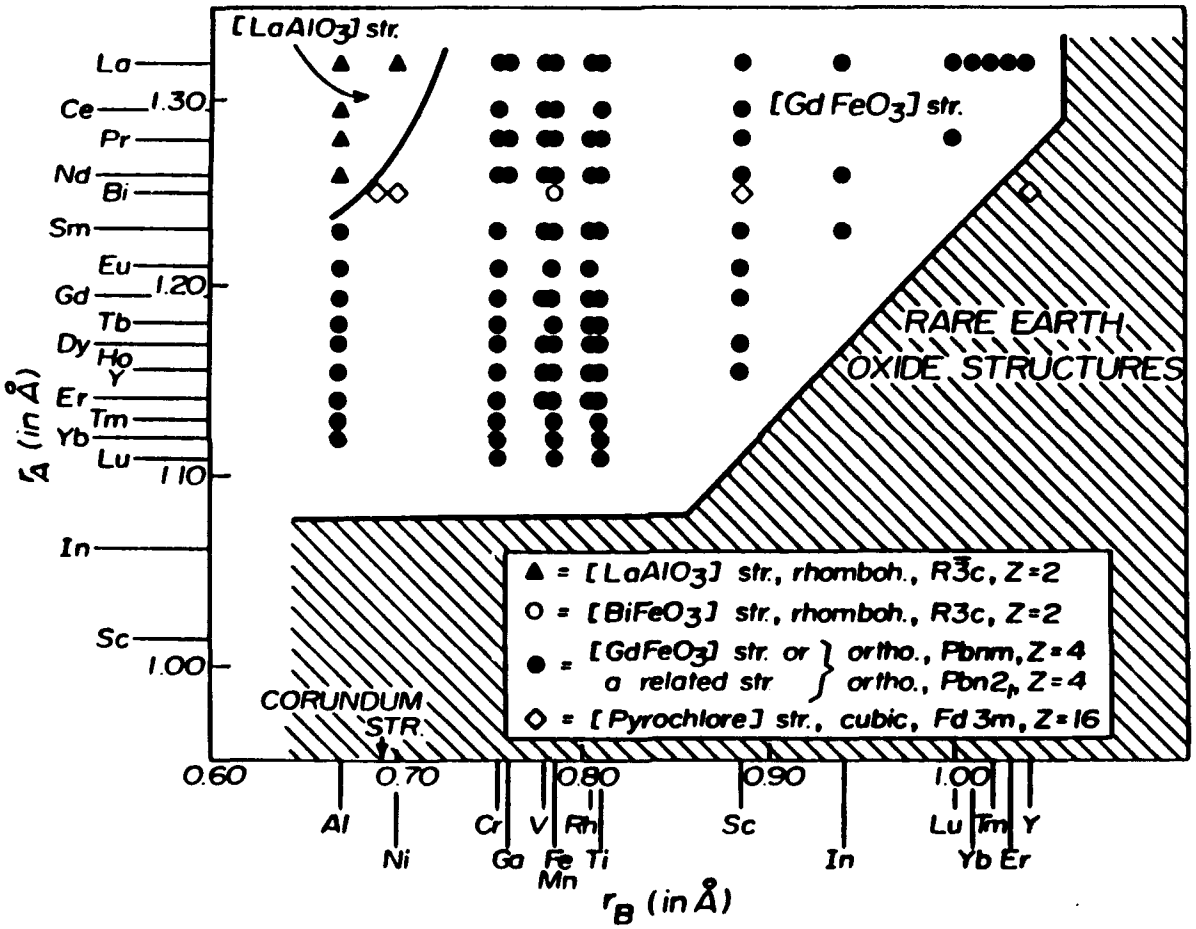
[LaAlO3] str.
[GdFeO3] str.
RARE EARTH OXIDE STRUCTURES
La
Ce
Pr
Nd
Bi
Sm
Eu
Gd
Tb
Dy
Ho
Y
Er
Tm
Yb
Lu
In
Sc
1.30
1.20
1.10
1.00
rA (in Å)
▲ = [LaAlO3] str., rhomboh., R3̄c, Z=2
○ = [BiFeO3] str., rhomboh., R3c, Z=2
● = [GdFeO3] str. or a related str. } ortho., Pbnm, Z=4 / ortho., Pbn2₁, Z=4
◇ = [Pyrochlore] str., cubic, Fd3m, Z=16
CORUNDUM STR.
0.60
0.70
0.80
0.90
1.00
Al
Ni
Cr
Ga
V
Fe
Mn
Rh
Ti
Sc
In
Lu
Tm
Yb
Y
Er
rB (in Å)

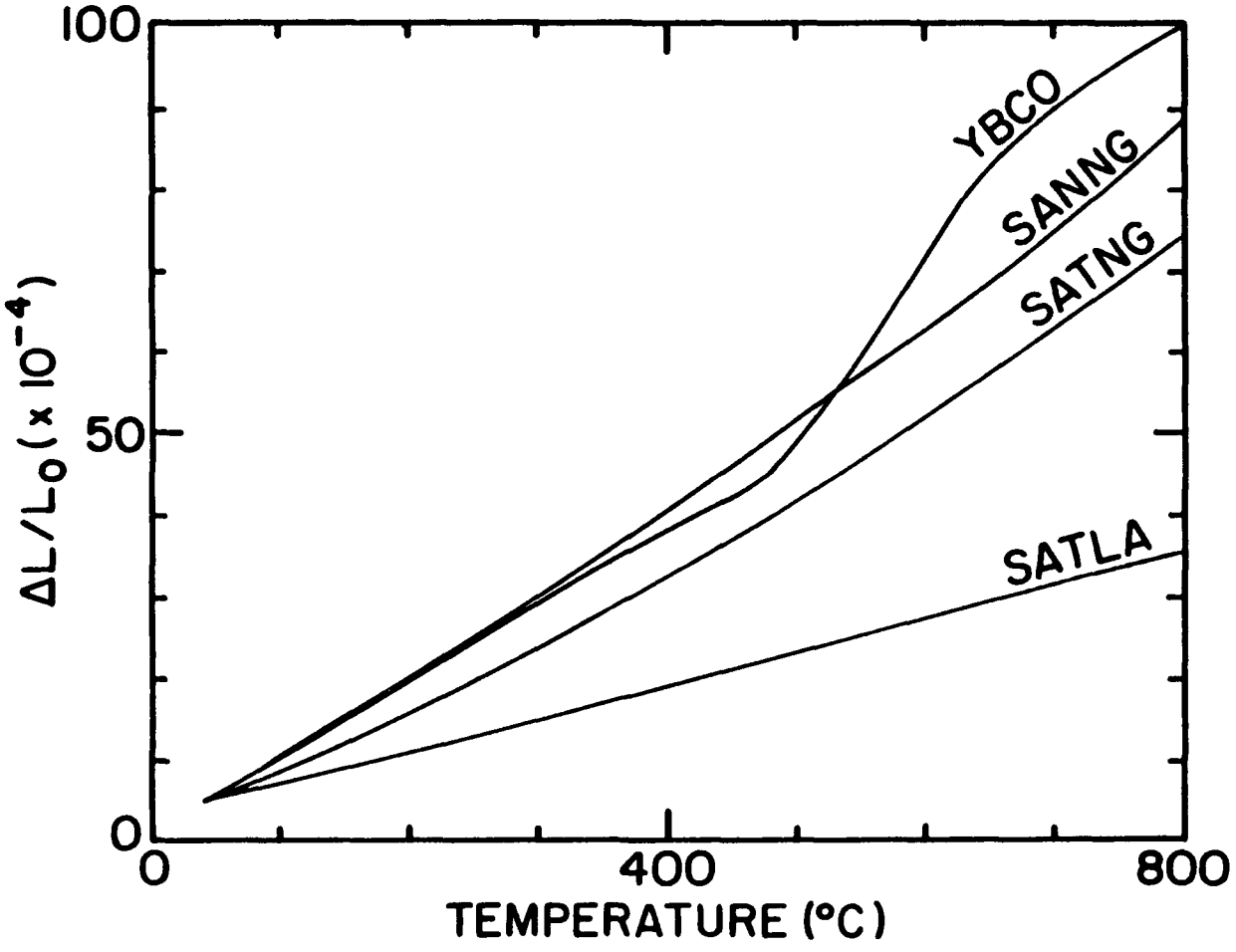
100
50
0
0
400
800
$\Delta L/L_o (\times 10^{-4})$
TEMPERATURE (°C)
YBCO
SANNG
SATNG
SATLA

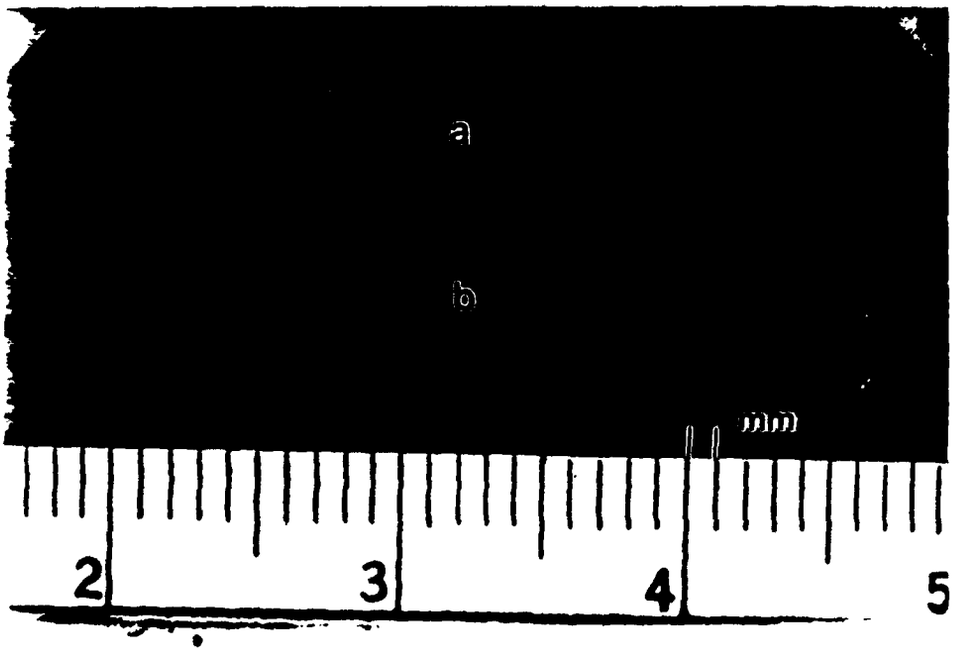
a
b
2
3
4
5

Appendix 10.

"Synthesis and Dielectric Properties of a Cubic Perovskite Material:
$La(Mg_{1/2}Ti_{1/2})O_3$,"
Materials Letter 18(4), 173 (1994).

G. Harshe
A.S. Bhalla
L.E. Cross

Materials Letters 18 (1994) 173–175
North-Holland

MATERIALS LETTERS

Synthesis and dielectric properties of a cubic perovskite: $La(Mg_{1/2}Ti_{1/2})O_3$

Girish Harshé, A.S. Bhalla and L.E. Cross
Materials Research Laboratory, The Pennsylvania State University, University Park, PA 16802, USA

Received 27 September 1993; accepted 29 September 1993

We have prepared a cubic perovskite material of the composition $La(Mg_{1/2}Ti_{1/2})O_3$ which seems to be a suitable candidate as a substrate material for an epitaxial growth of the high-T_c superconductors. The dielectric constant of this material is 27 at 1 MHz, the loss is less than 10^{-3}, and the thermal coefficient of expansion is about 13 ppm, close to that of YBC superconductor.

1. Introduction

New materials with attractive dielectric properties are being evaluated extensively for substrates for multi-chip module (MCM) devices and microwave resonators. These include $LaAlO_3$, $LaGaO_3$, $SrTiO_3$, $NdGaO_3$, $LiNbO_3$, Al_2O_3, MgO, ZrO_2, and many other cation-substituted derivatives of these [1–3]. Depending on the application, the dielectric response requirements can vary. In general very low dielectric constants and low losses are desired of a substrate, however, these requirements are difficult to meet if the substrate is also required to be a single crystal having a melting point lower than 2000°C. Additionally, if a substrate is to be used for the deposition of high-T_c superconductor thin films, it is desirable to have cubic crystal structure with a matching lattice parameter. Considering these requirements, very few materials fully meet the criteria.

Our work on various new perovskite compositions has resulted in many attractive substrate materials [4–6]. One of such materials with cubic perovskite structure, of the composition $La(Mg_{1/2}Ti_{1/2})O_3$ has been characterized and reported in this paper. The dielectric properties have been measured in the temperature range −150 to 100°C. The thermal expansion behavior has been observed over the range 25 to 800°C.

2. Experimental

The powder preparation was done using the solid state reaction method. Starting materials, $La(OH)_3$, MgO and TiO_2 were mixed in the stoichiometric proportions in a ball mill for 24 h in ethyl alcohol. The ball-milled mixture was dried at 80°C and calcined at 1400°C for 6 h in air. The calcined powder was ground and analyzed by X-ray diffraction. The powder was further mixed with 2 wt% of PVA as a binder and pressed at a pressure of about 2000 kg/cm^2. The green pellets were sintered at 1600°C for 6 h in air.

The sintered pellets were polished. The geometrical density of the samples was calculated and compared with the X-ray density. The samples were then electroded with sputtered gold. The dielectric constants of these samples were measured in the range −150 to 100°C at frequencies from 10 kHz to 1 MHz on the 4274A HP and 4275A LCR meters.

The thermal expansion was measured on a TD 716 Harrop dilatometric analyzer. The maximum temperature was 800°C and the rate of heating as well as cooling was 3°C/min.

3. Results and discussion

Fig. 1 shows the XRD pattern of the calcined powder of $La(Mg_{1/2}Ti_{1/2})O_3$ (LMT). It shows the pres-

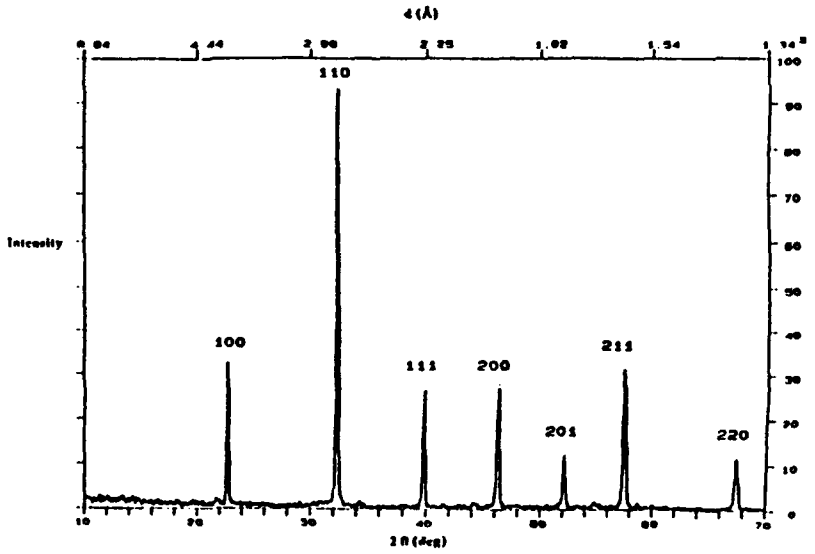

Fig. 1. X-ray diffraction pattern of $La(Mg_{1/2}Ti_{1/2})O_3$ phase after calcination at 1500°C for 4 h.

ence of a single phase with a cubic structure. The calculated lattice parameter of $La(Mg_{1/2}Ti_{1/2})O_3$ is $a=3.9195$ Å and the X-ray density is 6.02 g/cm^3. The LMT composition reported by Negas et al. [7] was orthorhombic, but our XRD analysis did not show any splitting or broadening of cubic peaks to indicate the presence of an orthorhombic phase in the powder. The XRD patterns of the calcined phase and the sintered pellet were indentical.

Fig. 2 shows the dielectric constant, K, for a $La(Mg_{1/2}Ti_{1/2})O_3$ sample as a function of temperature in the range -150 to 100°C at frequencies 100 kHz, 400 kHz and 1 MHz. There is very little variation in K with temperature or frequency in the ranges used for the measurements. The dielectric constant is about 27 and the loss is less than 5×10^{-4} at room temperature at 10 and 100 kHz. These values were confirmed in more precise measurements using a General Radio capacitance bridge.

The melting point of LMT was determined by melting a small quantity of the powder on a heated iridium strip. The temperature was recorded using an optical pyrometer. The melting point was around 1998°C.

The thermal expansion behavior of LMT from room temperature to 800°C is shown in fig. 3. The

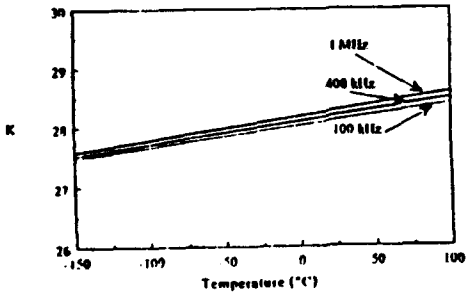

Fig. 2. Dielectric constant of $La(Mg_{1/2}Ti_{1/2})O_3$ as a function of temperature at 100 kHz, 400 kHz and 1 MHz.

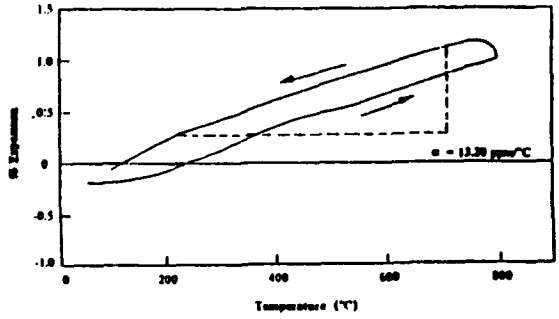

Fig. 3. Thermal expansion behavior of $La(Mg_{1/2}Ti_{1/2})O_3$ from room temperature to 800°C. The heating and cooling rates were 3°C/min.

coefficient of thermal expansion (CTE) in this range is 13.2×10^{-6}/°C. The CTEs of the YBC superconductor are 14×10^{-6}/°C along the *a* axis, 9×10^{-6}/°C along the *b* axis and 19×10^{-6}/°C along the *c* axis. Thus the CTEs of LMT and YBC *a* and *b* axes are matching to facilitate an epitaxial growth of YBC superconductor on a single crystal LMT substrate.

4. Conclusions

The results of an exploratory study of the dielectric properties of a cubic perovskite $La(Mg_{1/2}Ti_{1/2})O_3$, have been reported. The lattice constant determined by XRD is 3.9195 Å. The X-ray density is 6.02 g/cm^3. This material can be sintered at 1600°C for 6 h to achieve a sintered density of about 98%. The melting point of this compound is 1998°C.

The dielectric constant is about 27 in the range −150 to 100°C between 10 kHz and 1 MHz and the loss tangent is less than 5×10^{-4} at 10 and 100 kHz at room temperature.

The coefficient of thermal expansion in this range is 13.2×10^{-6}/°C in the range 25 to 800°C. Thus this material shows promise as a candidate material (in a single crystal form) for substrates for YBC superconductor epitaxial thin films. Studies are in progress to grow a single crystal of this material.

References

[1] D. Mateika, H. Kohler, H. Lauden and E. Völkel, J. Cryst. Growth 109 (1991) 447.
[2] C.D. Brandle and V.J. Fratello, J. Mater. Res. 5 (1990) 2160.
[3] S. Haussühl and D. Mateika, Cryst. Res. Technol. 26 (1991) 481.
[4] R. Guo, A.S. Bhalla and L.E. Cross, in preparation.
[5] P. Ravindranathan, U. Selvaraj, A.S. Bhalla, R. Roy and L.E. Cross, in preparation.
[6] G. Harshé, A.S. Bhalla and L.E. Cross, in preparation.
[7] T. Negas, G. Yeager, S. Bell and R. Amren, in: NIST Special Publication 804 (1991) p. 21.

Appendix 11.

"Ca-Sr-Ga-Nb Mixed System for HTSC Substrate Applications,"
J. Crystal Growth **139**, 54-66 (1994).

S. Erdei
L.E. Cross
F.W. Ainger
A. Bhalla

ELSEVIER

Journal of Crystal Growth 139 (1994) 54–66

JOURNAL OF CRYSTAL GROWTH

Ca–Sr–Ga–Nb mixed oxide system for high temperature superconductor substrate applications

S. Erdei *, L.E. Cross, F.W. Ainger, A. Bhalla

Materials Research Laboratory, The Pennsylvania State University, University Park, Pennsylvania 16802, USA

(Received 27 October 1993; manuscript received in final form 18 November 1993)

Abstract

Twin-free crystals with relatively low melting temperatures are desirable as substrates for high temperature superconductor (HTSC) oxide substrate materials. In the selection of new oxide substrate compositions, special requirements (e.g. suitable dielectric properties for microwave application and perovskite structure with good lattice matching with $YBa_2Cu_3O_{7-\delta}$) were considered. In this study the calcium–strontium gallate–niobate (CSGN) system has been investigated in both ceramic and single crystal samples, focusing on their crystal growth. The CSGN compositions were formed by mixing orthorhombic calcium gallate–niobate (CGN) and cubic strontium gallate–niobate (SGN) complex perovskites. CGN-excess mixtures do not create a single phase, as opposed to SGN-excess compositions, where single phase solid solutions are formed. The SGN-excess compositions can produce twin-free CSGN single crystals, which have excellent room temperature dielectric loss ($\tan\delta \leq 3 \times 10^{-4}$) and reasonably low dielectric constant ($K = 41$) values at 100 kHz. The growth temperature for a 50 mol% SGN starting composition (CSGN1) was about 1600°C, but for a 65 mol% SGN concentration (CSGN2) it increased to 1750°C. A lattice parameter $a = 3.939$ Å was obtained for the CSGN1 crystal increasing with SGN concentration. A significant drawback was observed for the Ca–Sr–Ga–Nb oxide system: the effective distribution coefficient of Ca^{2+} is very small ($k_{eff}(Ca^{2+}) \approx 0.4$). This can cause crystal growth difficulties due to constitutional supercooling phenomena.

1. Background

Since the discovery of the $YBa_2Cu_3O_{7-\delta}$ (YBCO) high temperature superconductor (HTSC) [1,2], there were numerous attempts to find the most suitable single crystal substrate for the deposition of epitaxial YBCO layers. The major substrate requirements are as follows:

- good lattice matching [41] and similar thermal expansion [40] with YBCO (Table 5);
- twin-free crystallization;
- low dielectric constant ($K < 30$–40) and low dielectric loss ($\tan\delta < 10^{-3}$) in the microwave regime;
- relatively low melting temperature for crystal growth.

Previous studies were mainly focused on $SrTiO_3$, $LaAlO_3$, $NdGaO_3$ and related crystals [3–7].

$SrTiO_3$ [3–5,8] has good lattice matching with YBCO, since its lattice constant is 3.905 Å, causing about 1% misfit with the YBCO unit cell. However, the dielectric constant (K) and dielec-

* Corresponding author.

SSDI 0022-0248(93)E0732-M

tric loss (tan δ) of $SrTiO_3$ are too high ($K \approx 300$, tan $\delta > 2 \times 10^{-3}$) and the crystal has twinning problems caused by structural phase transitions. Its melting temperature is 1920°C.

$LaAlO_3$ [3,7,8] single crystals have acceptable lattice matching ($a = 3.793$ Å, 2% misfit) with good dielectric properties ($K = 15$, tan $\delta = 6 \times 10^{-4}$). However, they have severe twin formation and high melting temperature (2100°C), limiting their HTSC applications.

In the case of $NdGaO_3$ [3,6,8], the lattice constant is $a = 3.86$ Å, giving a very good matching (0.27%) with YBCO. The dielectric constant is 26 and the dielectric loss is 3×10^{-4}. Its melting point is not too high (1750°C), but twin formation still exists as a disadvantage for $NdGaO_3$ in spite of techniques reported for elimination of this unwanted phenomenon [9,10,12].

In the search for new substrate compositions, Mateika et al. reported mixed perovskite crystals for HTSC applications [11]. They grew a large number of solid solution crystals from mixtures of $LaAlO_3$ and $Sr(Al_{1/2}Ta_{1/2})O_3$, as well as $LaAlO_3$ and $Sr(Al_{1/2}Nb_{1/2})O_3$ compounds. For substitution of A-site elements, Ca^{2+},Nd^{3+} and others have also been investigated. The dielectric properties of these crystals were acceptable ($K = 13.4–21.3$, tan $\delta \leq 10^{-3}$) for HTSC substrate application. Some crystals in this series were grown without twinning, crystallizing mainly as cubic perovskites. The lattice constants varied from 3.78 to 3.88 Å for crystals grown at about 1800°C.

2. CSGN selection from the oxide perovskites for HTSC substrate

In order to find other suitable candidate substrate compositions for high T_c superconductors, oxide perovskites were classified into ten groups (three simple and seven complex). This classification was primarily based on the valency of A, B or AA′, BB′ site cations, along with additional restrictions based on lattice parameters and electroconductivity properties. Unit cell parameters of 3.80–4.00 Å or 7.70–7.90 Å (double cell) are preferred, which significantly reduces the number of compounds. Compounds possessing undesirable semiconducting and conducting properties were also rejected. Consequently, compounds consisting of only transition metal (including lanthanide) cations in A–B, A–B–B′ (or A–A′–B) sides (e.g. YVO_3 [13], $LaCoO_3$ [8], $La(Zn_{1/2}Ru_{1/2})O_3$ [8,21], etc.) were not investigated due to possible conductivity problems. In spite of the above-mentioned restrictions, a large number of

Table 1
Simple perovskite groups

Group No.	Perovskite group	Typical compounds	Unit cell type	Cell parameters (Å)			Dielectric properties [a], K and tan δ	Melting temperature T_{MP} (°C)	References
				a	b	c			
1	$A^{1+}B^{5+}O_3$	$NaNbO_3$	Orthorhombic	5.512	5.577	3.885	Ferroelectric	1412	[26,27,8]
		$KTaO_3$	Cubic	3.9885			Ferroelectric	1370	[28–30,8]
								1357	[3]
2	$A^{2+}B^{4+}O_3$	$BaTiO_3$	Tetragonal	3.989		4.029	Ferroelectric	1610	[25,8]
		$SrTiO_3$	Cubic	3.904			$K = 200$	2080	[25,8]
				3.905			$K = 300$	1920	[3]
							tan $\delta > 2 \times 10^{-3}$		
3	$A^{3+}B^{3+}O_3$	$LaAlO_3$	Rhombohedral	3.788	$\alpha = 90°4'$			2075–2080	[25,8]
				3.793			$K = 15$	2100	[3]
							tan $\delta = 6 \times 10^{-4}$		
		$NdGaO_3$	Orthorhombic	5.426	5.502	7.706			[31]
				3.86			$K = 26$	1750	[3]
							tan $\delta = 3 \times 10^{-4}$		

[a] K is dielectric constant and tan δ is dielectric loss.

Table 2
Complex perovskite groups

Group No.	Perovskite group	Typical compounds	Unit cell type	Cell parameters (Å)			Dielectric properties [a] K and tan δ	Melting temperature T_{MP} (°C)	References
				a	b	c			
4	$A^{2+}(B^{3+}_{1/2}B'^{5+}_{1/2})^{4+}O_3$	$Sr(Al_{1/2}Ta_{1/2})O_3$	Cubic (double)	7.795				1900	[23]
			Cubic	3.895			$K = 11.9$ $\tan\delta = 1.68\times10^{-3}$	2030	[18]
		$Sr(Al_{1/2}Nb_{1/2})O_3$	Cubic (double)	7.795				1790	[23]
			Cubic	3.895			$K = 18.6$ $\tan\delta = 3.18\times10^{-3}$	1862	[18]
5	$A^{2+}(B^{2+}_{1/3}B'^{5+}_{2/3})^{4+}O_3$	$Ba(Mg_{1/3}Ta_{2/3})O_3$	Hexagonal	5.774		7.095	$K = 25$ $\tan\delta = 5.95\times10^{-5}$		[24]
			Hexagonal	5.782		7.067			[8]
			Cubic	4.0877			$K = 25.9$ $\tan\delta = 2.78\times10^{-4}$	3100	[19]
6	$A^{2+}(B^{1+}_{1/4}B'^{5+}_{3/4})^{4+}O_3$	$Sr(Na_{1/4}Ta_{3/4})O_3$	Cubic	4.055					[32]
7	$A^{3+}(B^{2+}_{1/2}B'^{4+}_{1/2})^{3+}O_3$	$La(Mg_{1/2}Ti_{1/2})O_3$	Cubic (double)	7.868					[33]
			Cubic	3.932				1735 [b]	[22]
							$K \le 56$ $\tan\delta \le 5\times10^{-4}$		[34]
		$Nd(Mg_{1/2}Ti_{1/2})O_3$	Orthorhombic	5.587	7.768	5.460			[33]
8	$A^{3+}(B^{1+}_{2/3}B'^{5+}_{1/3})^{3+}O_3$	$La(Mg_{2/3}Ta_{1/3})O_3$	Hexagonal				$K = 22.4$ $\tan\delta = 2.4\times10^{-3}$	≈ 2000	[35]
9	$A^{3+}(B^{1+}_{1/2}B'^{5+}_{1/2})^{3+}O_3$	$La(Li_{1/2}Ta_{1/2})O_3$	Monoclinic	5.619 $\beta = 89.6°$	5.778	7.952			[36]
		$La(Li_{1/2}Nb_{1/2})O_3$	Orthorhombic	5.64	5.76	7.95			[37]
10	$(A^{1+}_{1/2}A'^{3+}_{1/2})^{2+}B^{4+}O_3$	$(K_{1/2}La_{1/2})TiO_3$	Cubic	3.914				1360 [b]	[22]

[a] K is dielectric constant and tan δ is dielectric loss.
[b] Incongruent.

oxide perovskites can be synthesized from the following elements: Li, Na, K, Mg, Ca, Sr, Ba, Ln, Ti, Zr, Nb, Ta, Al, and Ga.

Three simple perovskite groups, listed in Table 1, can be created from this selection technique. Perovskites in $A^{1+}B^{5+}O_3$ (No. 1) are ferroelectrics (e.g. $NaNbO_3$ [14,15,8], $KTaO_3$ [16,8], etc.). Group No. 2 ($A^{2+}B^{4+}O_3$) is a transitional dielectric group, which may be ferroelectric (e.g. $BaTiO_3$ [17]) or paraelectric with high dielectric constants (e.g. $SrTiO_3$ [8]). One of the most frequently investigated groups for HTSC substrates is the $A^{3+}B^{3+}O_3$ family (e.g. $LaAlO_3$, $NdGaO_3$, etc.) (No. 3) due to their excellent dielectric properties.

Seven complex perovskite groups were selected based on previously-mentioned requirements (see Table 2). In these groups, B-site cations generally consist of two different elements to form $A(BB')O_3$ type perovskites. Numerous compounds of these series have excellent dielectric properties [24], in ceramic form. Crystal growth technologies (although there have been some attempts [18,19]) have not been developed yet for complex perovskite compounds, probably because of their high melting temperatures (e.g. $Ba(Mg_{1/3}Ta_{2/3})O_3$) or incongruent melting (e.g. $(K_{1/2}La_{1/2})TiO_3$ [22]). $Ba(Mg_{1/3}Ta_{2/3})O_3$, in the No. 5 group, has excellent room temperature dielectric loss ($\tan\delta = 2.78 \times 10^{-4}$) and good dielectric constant ($K = 25.9$) at 10 kHz for crystal fiber grown by the laser heated pedestal growth (LHPG) technique [19]. However, its melting temperature is about 3000°C. With the exception of $A^{2+}(B^{3+}_{1/2}B^{5+}_{1/2})O_3$ (No. 4), very limited data were reported for complex perovskite groups (see Table 2). The No. 4 perovskites were originally investigated by Brandle and Fratello [23] without characterization of dielectric properties. Some data from their work can be seen in Table 3. In subsequent attempts, some compounds in this series, $Sr(Al_{1/2}Nb_{1/2})O_3$ (SAN) and $Sr(Al_{1/2}Ta_{1/2})O_3$ (SAT) have been grown by the LHPG technique in single crystal fiber form by Guo et al. [18] and characterized for dielectric properties.

Surveying the present position, it is obvious from the list of classified perovskite compounds that there are three different approaches for obtaining new oxide perovskite HTSC substrate candidates:

(1) Development of twin-free crystal growth technique for the widely investigated $A^{3+}B^{3+}O_3$ compounds (e.g. by using optimized axial temperature gradient or special dopants [12,9,10]).

(2) Find twin-free compounds with suitable di-

Table 3
$A^{2+}(B^{3+}_{1/2}B^{5+}_{1/2})O_3$-type complex perovskites (No. 4)

Compound	Unit cell type	Cell parameters (Å)				Melting temperature T_{MP} (°C)	Ref.
		Observed			Calculated		
		a	*b*	*c*	*a*		
Ca_2GaNbO_6	Orthorhombic	5.441	5.498	7.724	7.95	1510	[23] [a]
Ca_2GaTaO_6	Orthorhombic	5.437	5.527	7.730	7.95	1710	[23] [a]
Ca_2AlNbO_6	Orthorhombic	5.377	5.421	7.624	7.86	1675	[23] [a]
		5.382	5.408	7.614			[38]
Ca_2AlTaO_6	Orthorhombic	5.382	5.427	7.631	7.86	1835	
		5.381	5.407	7.612			[38]
Sr_2GaNbO_6	Cubic	7.895			8.08	1720	[23] [a]
Sr_2GaTaO_6	Cubic	7.898			8.08	1820	[23] [a]
$Sr(Ga_{1/2}Ta_{1/2})O_3$	Cubic	3.947			3.95	1720	[39]
Sr_2AlNbO_6	Cubic	7.795			7.98	1790	[23] [a]
$Sr(Al_{1/2}Nb_{1/3})O_3$	Cubic	3.895				1862	[18]
Sr_2AlTaO_6	Cubic	7.795			7.98	1900	[23] [a]
$Sr(Al_{1/2}Ta_{1/2})O_3$	Cubic	3.895				2030	[18]

[a] Data published by Brandle and Fratello [23].

electric properties in the complex perovskite groups, which can be grown by the Czochralski technique. They must also possess acceptable melting temperatures. Possible candidates are compounds of the $A^{2+}(B^{3+}B^{5+})O_3$ group (e.g. SAN, SAT).

(3) Combinations of the above-mentioned perovskite compounds to obtain optimized substrate parameters and crystal quality. This technique provides the broadest range of substrate compositions; however, it includes possible crystal growth difficulties due to the complexity of these systems. In these cases the effective distribution coefficient for all cations needs to approach unity, which becomes an especially important factor.

In order to find the lowest melting compositions with optimized dielectric parameters, the third method was utilized in our present work. Preliminary selection of numerous ceramic samples focused our attention on the $Ca(Ga_{1/2}Nb_{1/2})O_3$–$Sr(Ga_{1/2}Nb_{1/2})O_3$ (CSGN) system. In addition, it was found that some other mixtures can also form single phase compositions (e.g. $(K_{1/4}Nd_{3/4})(Mg_{1/4}Ti_{3/4})O_3$ from $\frac{1}{2}Nd(Mg_{1/2}Ti_{1/2})O_3$–$\frac{1}{2}(K_{1/2}Nd_{1/2})TiO_3$ or $(Sr_{1/3}La_{2/3})(Mg_{1/3}Ti_{2/3})O_3$ from $\frac{1}{3}(SrTiO_3)$–$\frac{2}{3}La(Mg_{1/2}Ti_{1/2})O_3$), whereas others cannot (e.g. $(Ca_{1/2}Nd_{1/2})(Mg_{1/2}Nb_{1/2})O_3$ from $\frac{1}{2}Ca(Mg_{1/3}Nb_{2/3})O_3$–$\frac{1}{2}Nd(Mg_{2/3}Nb_{1/3})O_3$).

Combination of low-melting temperature $KTaO_3$ with low dielectric loss $La(Mg_{2/3}Ta_{1/3})$ [35] allowed single phase $(K_{1/2}La_{1/2})(Mg_{1/2}Ta_{2/3})O_3$ to be produced; however, it was not investigated in more detail due to its unsuitable dielectric properties. For combinations of these and other samples different mixing ratios (1/2 : 1/2; 1/3 : 2/3; 2/3 : 1/3; 1/4 : 3/4; 3/4 : 1/4 mole ratios) were considered. The ceramic samples were analyzed for structure, dielectric and melting characteristics.

Since Ca-based compounds in the $A^{2+}(B^{3+}_{1/2}B^{5+}_{1/2})O_3$ group (Table 3) have orthorhombic unit cells and Sr-based compounds have cubic unit cells with acceptable lattice matching to YBCO, it was expected that the mixture with excess Sr-based compound would retain its cubic unit cell with limited cell parameter modifications. The combination of lowest melting (T_{MP} = 1510°C) $Ca(Ga_{1/2}Nb_{1/2})O_3$ (CGN) of the Ca-based compounds and the lowest melting (T_{MP} = 1720°C) $Sr(Ga_{1/2}Nb_{1/2})O_3$ (SGN) of the Sr-based compounds of No. 4 perovskite group promised low melting compositions with acceptable dielectric properties. Twin-free crystallization was also expected, since other niobates (SAN) and tantalates (SAT) have been grown without twins [18].

3. Experimental procedure

3.1. CSGN ceramic preparation

Calcium–strontium gallate–niobate (CSGN) ceramic samples were prepared by conventional ceramic processing techniques. High purity $SrCO_3$, Ga_2O_3, Nb_2O_5 (99.99%) and CaO (99.95%) (Johnson Matthey Alfa Chemicals) were weighed in 0.5:0.5, 0.33:0.67, 0.67:0.33 and 0.45:0.55 molar ratios of $Ca(Ga_{1/2}Nb_{1/2})O_3$: $Sr(Ga_{1/2}Nb_{1/2})O_3$ for 1/30 mole CSGN batches. The weighed powders were mixed with 50 ml alcohol and Al_2O_3 grinding media at 120 rpm for 8 h in 125 ml high density polyethylene bottles. After drying at 80°C for 8 h, the powder mixtures were pressed into 34 × 4 mm diameter size discs without binder, and fired at 1100°C for 6 h on alumina plates. Subsequently, the fired samples were reground and re-pressed into 12 × 2 mm diameter size discs. A second firing at optimized temperatures (1280–1350°C) for 6 h was conducted in order to obtain single-phase high-density ceramic samples.

3.2. Characterization of CSGN ceramic samples

X-ray powder diffraction (XRD) (Scintag PAD-V) was used for characterization of phase relations, crystallographic structure, and lattice parameters (see Fig. 1a).

Dielectric measurements were performed at 10 and 100 kHz on polished gold-sputtered electroded samples from −50 to 120°C using a computer-controlled multifrequency LCR meter (Hewlett Packard 4275). Data for CSGN are presented in Fig. 6.

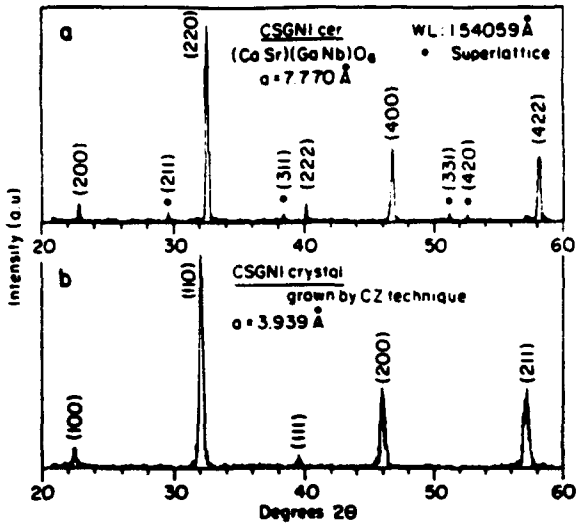

Fig. 1. XRD pattern of (a) $(CaSr)(GaNb)O_6$ ceramic (CSGN1 cer.) and (b) CSGN1 crystal grown by Czochralski technique.

Differential thermal analysis (DTA) (Perkin-Elmer DTA 1700) with 10°C/min heating–cooling rate and firing studies were utilized for CSGN melting characterization. Liquidus temperatures were determined in both a resistance-heated furnace, using a Pt crucible and air atmosphere, and an RF-heated crystal-growth chamber, using an Ir crucible and N_2 atmosphere.

3.3. Crystal growth of CSGN by Czochralski technique

Chemicals for crystal growth were weighed in two different compositions. One a 50:50 mol% CGN–SGN mixture (CSGN1) and the other a 35:65 mol% CGN–SGN mixture (CSGN2) were weighed for use as starting compositions. Identical chemicals were used as in CSGN ceramic preparation. After thorough homogenization, 1/2 mole batches of CSGN1 and CSGN2 mixtures were placed in alumina crucibles for sintering. After firing at 1100°C for 8 h the mixtures were ground and re-fired at 1250°C for 8 h for CSGN1 and 1300°C for 8 h for CSGN2.

Melting of these mixtures and subsequent crystal growth were carried out by a 35 kW RF heated Czochralski crystal growth unit (Crystalox-Stanelco). The 35 × 35 mm diameter cylindrical form (1.5 mm wall thickness) iridium crucible was heated under pure N_2 atmosphere with 0.5 l min^{-1} flow rate at 35 kPa pressure. The first growth runs for seed crystals were conducted using Ir wire. Crystal seeds (non-oriented) were selected and mounted on an alumina pulling rod. CSGN1 crystal growth was initiated at 1600°C, and CSGN2 crystal growth began at 1750°C. The temperature of the melt surface was measured by optical pyrometry (without correction). The pulling rates were 0.7–2 mm h^{-1}, and the rotation rate was 10 rpm for all cases. Crucible posi-

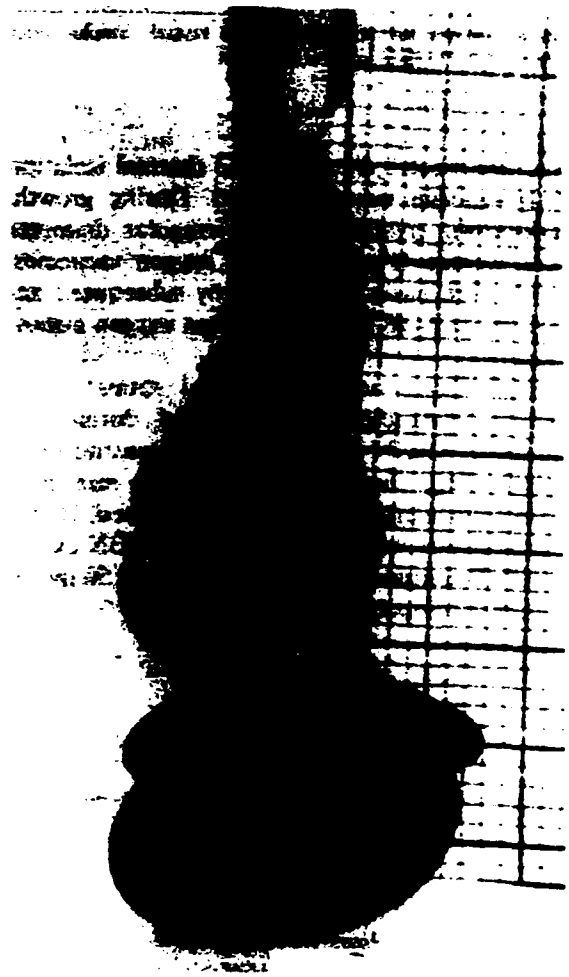

Fig. 2. CSGN1 crystal grown by Czochralski technique before annealing in O_2 (mm grid background).

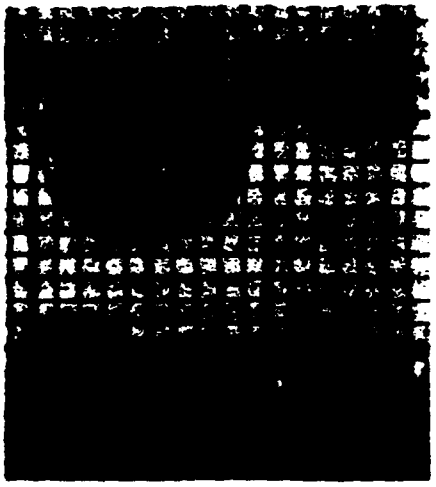

Fig. 3. CSGN1 (a) and CSGN2 (b) crystal samples after annealing in O_2 (mm grid background).

tion, afterheater elements, and thermal isolation of Ir crucible were optimized. During growth, dark-brown crystals with an irregular diameter were formed (Fig. 2) due to oxygen vacancies, which were easily eliminated by subsequent annealing for 6–46 h at 700°C in an oxygen atmosphere.

High Ga_2O_3 vaporization and strong supercooling tendencies were observed during the growth of CSGN crystals. Due to constitutional supercooling, the formation of large size high quality single crystals was severely limited. Better crystal quality was achieved with the SGN excess (CSGN2) composition than with the 50:50 mol% (CSGN1) composition melt (Fig. 3).

3.4. Characterization of CSGN crystals

Samples prepared from the upper third sections (least defective) of CSGN1 and CSGN2 crystals were annealed in O_2 for subsequent characterization. Energy dispersive spectroscopy (EDS) was utilized to analyze the incorporation of basic elements into the CSGN mixed perovskite crystals (Table 4). Ca^{2+}, Sr^{2+}, Ga^{3+} and Nb^{5+} cations in both CSGN1 and CSGN2 crystals were analyzed by a KEVEX 8000 Microanalyzer with ISI DS 130 Scanning Electron Microscope (SEM).

Crystal structures were identified by XRD (as in section 3.2) (Fig. 1b). Back-reflection Laue diffraction was used for crystallinity determination. Transmitted light optical microscopy (Zeiss Axioskop) was performed under crossed polars for characterization of polished CSGN crystals and determination of single and twin-free crystallinity. A defective CSGN1 crystal and cracked but good-quality twin-free CSGN2 single crystal can be seen in Figs. 4a and 4b, respectively.

Thermal expansion measurements for both CSGN crystal compositions were conducted from 23 to 800°C (Fig. 5): the difference between CSGN1 and CSGN2 crystals was indistinguishable. The heating rate was controlled at 3°C/min using microprocessor-based temperature controller.

Dielectric measurements were conducted on a CSGN2 single crystal specimen at 10 and 100 kHz from −50 to 120°C. The dielectric constant–temperature (K–T) dependence can be seen in Fig. 6.

Table 4
Incorporation of cations into CSGN1 and CSGN2 crystals (measured by EDS)

Sample	Starting composition in melt	Real composition in crystal	k_{eff}(cation)	
CSGN1	$(Ca_{0.5}Sr_{0.5})(Ga_{0.5}Nb_{0.5})O_3$	$(Ca_{0.18}Sr_{0.82})(Ga_{0.47}Nb_{0.53})O_3$	Ca^{2+}	0.36
			Sr^{2+}	1.64
			Ga^{3+}	0.94
			Nb^{5+}	1.06
CSGN2	$(Ca_{0.35}Sr_{0.65})(Ga_{0.5}Nb_{0.5})O_3$	$(Ca_{0.15}Sr_{0.85})(Ga_{0.45}Nb_{0.55})O_3$	Ca^{2+}	0.42
			Sr^{2+}	1.3
			Ga^{3+}	0.90
			Nb^{5+}	1.10

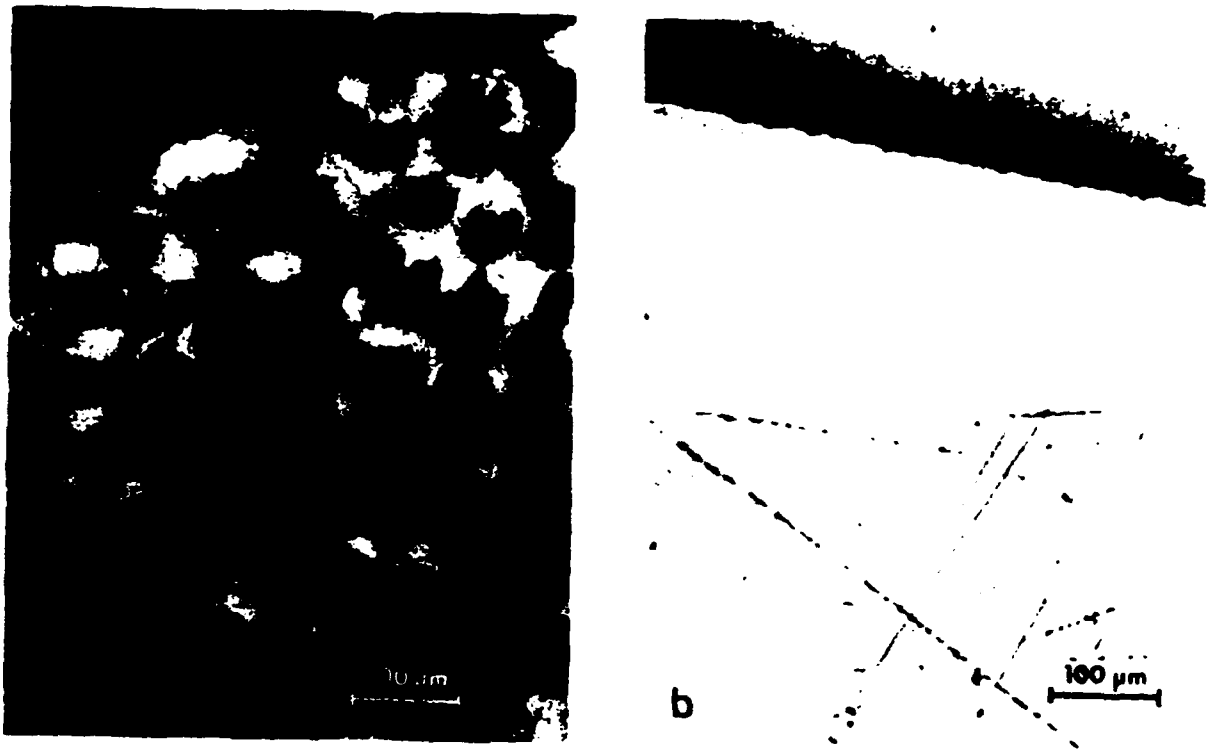

Fig. 4. Transmission optical micrograph of (a) CSGN1 sample showing defects which can be ascribed to constitutional supercooling and (b) twin-free transparent CSGN2 single crystal pieces.

4. Results and discussion

Mixed perovskite crystals with relatively low melting temperature, no twinning and low dielectric loss are required for HTSC substrate materials. The mixing of classified perovskite compounds promises to give a selection routine for alternative compositions.

This work presents a study of the mixing of

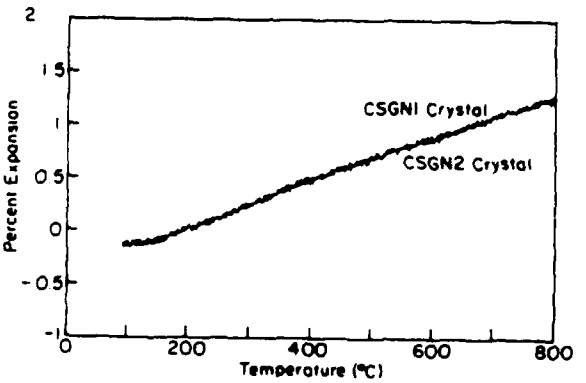

Fig. 5. Thermal expansion–temperature dependence for CSGN1 and CSGN2 samples.

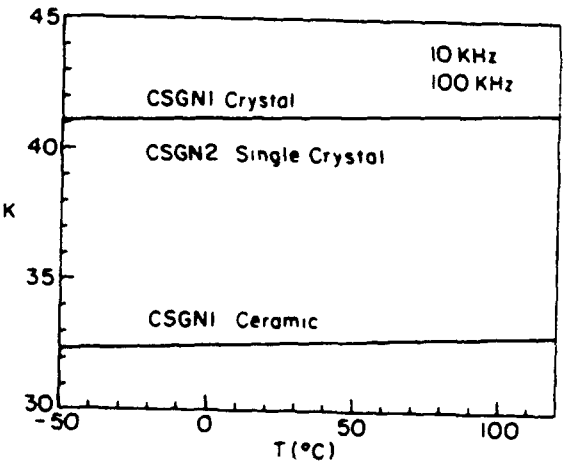

Fig. 6. Dielectric constant–temperature ($K-T$) dependence for CSGN1 cer., CSGN1 and CSGN2 crystals at 10 and 100 kHz.

Table 5
Some characteristic data for the CSGN system

Sample	Lattice parameter (cubic) (Å)	Density			Linear thermal coefficient expansion α ($\times 10^{-6}$ °C^{-1})	Dielectric constant (K) and tangent loss (tan δ) at 100 kHz and 23°C	
		Theoretical [a] (g/cm^3)	Measured (g/cm^3)	Relative (%)		K	tan δ ($\times 10^{-4}$)
CSGN1 cer. (ceramic)	7.770	5.47	4.8	88		32.5	3
CSGN1 (crystal)	3.939	5.67	5.14	91	18.5	41	≤ 3
CSGN2 (single crystal)	3.994	5.49	5.43	99	18.5	41	≤ 3
$YBa_2Cu_3O_{7-\delta}$	(orthorhombic)						
	a = 3.836 [b]				14 [c]		
	b = 3.883 [b]				9 [c]		
	c = 11.68 [b]				19 [c]		

[a] Calculated by XRD data.
[b] Ref. [41].
[c] Ref. [40].

two relatively low melting compounds of $A^{2+}(B^{3+}_{1/2}B'^{5+}_{1/2})^{4+}O_3$ complex perovskites group (No. 4), the $Ca(Ga_{1/2}Nb_{1/2})O_3$–$Sr(Ga_{1/2}Nb_{1/2})O_3$ (CSGN) system. Experiments on ceramic samples indicated that calcium gallate–niobate (CGN) excess mixtures do not form a single phase system, whereas samples with SGN concentrations ≥ 50 mol% form single phase cubic perovskites (see Fig. 1a). Weak superlattice diffraction peaks of the (211), (311), (331) and (420) crystallographic planes indicate the double-cubic lattice of (CaSr)(GaNb)O_6. This superstructure was also obtained on molten quenched samples of both Ca_2GaNbO_6 and Sr_2GaNbO_3 reported by Brandle and Fratello [23].

In the case of (CaSr)(GaNb)O_6 ceramics (CSGN1 cer.) formed by equal parts of CGN–SGN, the lattice parameter was 7.770 Å and the calculated theoretical density is 5.47 g/cm^3. The density of this sintered sample was 4.8 g/cm^3 (88% theor.) (Table 5), providing reasonably high density specimen for dielectric measurements. The superstructure in CSGN1 crystals grown from (CaSr)(GaNb)O_6 melt has been eliminated completely (see Fig. 1b) and a simple cubic lattice was formed, displaying only (100), (110), (111), (200) and (211) characteristic cubic XRD lines in the $2\theta = 20°$–$60°$ range. Since solid solutions were formed for SGN/CGN ≥ 1, lattice parameters of the grown crystals were larger than for ceramic specimens. The measured value for the CSGN1 crystal was 3.939 Å, an increase of 0.054 Å with respect to the ceramic sample. Lattice parameters were found to increase with increasing SGN concentration. Increasing the SGN content by 15% resulted in a 0.055 Å increase in lattice parameters for the CSGN2 composition. The lattice parameter obtained $a = 3.994$ Å, is close to the acceptable upper limit for YBCO substrates, as evident from the data of Fig. 7 compared with other ($SrTiO_3$, $NdGaO_3$, $LaAlO_3$) substrate materials [9]. Thermal expansion curves (Fig. 5) measured on CSGN1 and CSGN2 crystal samples were indistinguishable from each other. The linear thermal expansion coefficient obtained is $\alpha = 18.5 \times 10^{-6}\ °C^{-1}$, a very good match with YBCO. α_c (YBCO) $= 19 \times 10^{-6}\ °C^{-1}$ [40]. The values of lattice parameters, densities and thermal expansion coefficients can be seen in Table 5.

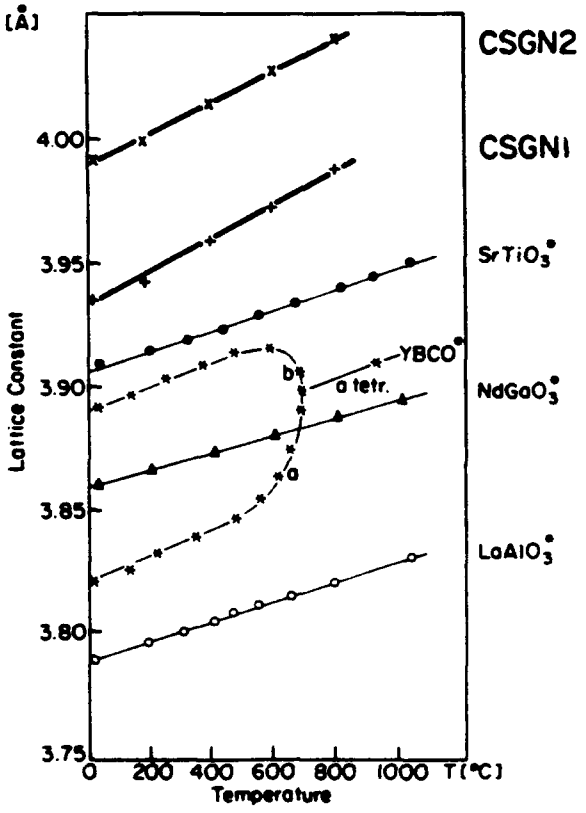

Fig. 7. Lattice parameter–thermal expansion dependence for CSGN1 and CSGN2 crystals compared with other published substrate materials; (•) after ref. [9].

The solidus temperature of CSGN1 ceramics was quite low (1350°C) as obtained by both DTA and firing experiments (where partial melting was first observed). The liquidus temperature was about 1580–1600°C (uncorrected values) as measured by optical pyrometry. Since the CSGN system with SGN/CGN ≥ 1 is a solid solution, the CSGN1 ceramic composition crystallizes in a different composition than that of the starting melt. DTA measurements on CSGN1 crystals indicated this change in connection with an increase in the solidus temperature (1435°C). This is related to the increase in lattice parameter of the CSGN1 crystal (compared to the ceramic), because higher solidus temperature indicates higher actual SGN concentration at solidification than in the starting melt compositions. The higher Ca concentration

at CSGN1 crystallization could cause the strong constitutional supercooling effect [43,44] observed during the Czochralski crystal growth processes.

During crystal growth the actual temperature at the solid–liquid boundary will be below the equilibrium temperature, creating an undercooling which is required to drive the kinetic processes of crystallization at the imposed rates. The constitutional supercooling as an undesired segregation can be caused by impurities, dopants [45,42] or lack of stoichiometry [46], producing different type characteristic defects, i.e. gas bubbles and cellular growth structures in the crystals. Similarly, in the growth of mixed oxides, the excess component segregates in the same manner as does an impurity [47]. In our case the unwanted segregation phenomenon can be ascribed to constitutional supercooling and can be minimized by such means as decreasing the critical impurity concentration, the pulling rates, and enhancement of the axial thermal gradient [44,45].

It was evident from EDS measurements that the observed constitutional supercooling effect is caused by the very low effective distribution coefficient of calcium (k_{eff}(Ca) = 0.36). Consequently, the Ca is a "critical impurity" for its own CSGN system. Although Ga_2O_3 vaporization was observed to be quite intensive, its effective distribution coefficient remained near unity (k_{eff}(Ga) = 0.94). EDS data for both CSGN1 and CSGN2 crystals can be seen in Table 4. In ideal or near-ideal cases the k_{eff} coefficient for all mixing cations should be $k_{eff} = 1$ or close to one ($k_{eff} \approx 1$) (mixing of $LaAlO_3$ and SAT or $LaAlO_3$ and SAN resulted in near-unity distribution coefficients for each cation as observed by Mateika et al. [11]). During crystal growth, a Ca^{2+}-rich boundary layer is formed before the crystallization front, which has lower melting and freezing temperatures than the liquidus and solidus temperature of the actual melt–crystal composition. Therefore, this Ca^{2+}-rich boundary layer will be supercooled and generate both uncontrollable growth rate and crystallization.

The critical k_{eff}(Ca) can be increased by decreasing the Ca (CGN) content of the starting melt composition. This means that the Ca^{2+} concentration in the boundary layer increases to the critical concentration level at a slower rate than previously. This favor effect is further enhanced by decreasing the pulling rate and increasing the axial thermal gradient. In the case of CSGN2 crystal grown from 35:65 mol% CGN–SGN starting melt composition, the effective distribution coefficient of calcium increased to k_{eff}(Ca) = 0.42, allowing the growth of transparent, single crystals in the upper third of the crystal (in ≈ 10 mm length at 7–8 mm diameter). An opaque CSGN1 crystal sample, containing defects which can be ascribed to constitutional supercooling [47,42] and a transparent CSGN2 single crystal sample can be seen in Fig. 3. Laue diffraction of the CSGN1 crystal sample did not indicate perfect single crystallinity due to the supercooled structure. Polarized transmitted-light optical micrographs of a supercooled CSGN1 sample and a good-quality, twin-free CSGN2 single crystal are presented in Fig. 4. In the CSGN2 specimen, no light transmission was observed between cross poles, proving the twin-free crystal structure.

Very similar constitutionally-supercooled structures were also observed in previously-investigated niobate (e.g., $LiNbO_3$:Si), where Si has a similarly low effective distribution coefficient (Erdei et al. [42]).

It is already known that SGN-excess compositions with increased k_{eff}(Ca) also formed cubic unit cells in CSGN crystals. The observation that the CSGN2 crystal is cubic with no twins is in agreement with previous studies [11]. Twin-free single crystals were also formed for other complex niobate (SAN) and tantalate (SAT) fibers grown by the LHPG technique [18]. However, it is not yet known whether this effect originated from the cubic perovskite structure or is a characteristic of niobates (or tantalates).

For realization of non-supercooled, twin-free CSGN2 single crystals, two sacrifices were required: (1) the growth temperature was increased to about 1750°C and (2) the lattice parameter increased to $a = 3.994$ Å, close to the acceptable size limit. Although more extensive vaporization resulted due to the increased growth temperature, decreasing k_{eff}(Ga); this effect is negligible because k_{eff}(Ga) remains at a value of 0.90. Since

unity or near-unity k_{eff} for all cations is required for growth of large crystals, reasonably large CSGN crystals can be grown as a small crystallized proportion of the melt from large crucibles with large batches of SGN-rich starting material using an optimized growth procedure (low pulling rate, high axial temperature gradient) for elimination of the constitutional supercooling caused by low k_{eff}(Ca).

Use of strontium (SGN) excess mixtures was also considered to have better dielectric properties, lower dielectric constant for CSGN crystals (i.e. Mateika et al. [11] reported higher dielectric constants in their mixed crystals containing Ca^{2+} than without it). The 23°C dielectric constant of high density (88%) ceramic was $K = 32.5$ at both 10 and 100 kHz. A slight linear temperature dependence can be seen in Fig. 6 between −50 and 120°C. The dielectric loss at 100 kHz (23°C) was tan $\delta = 3 \times 10^{-4}$. These same low values were obtained for both CSGN1 and CSGN2 crystals; however, the dielectric constant of these crystals, compared to ceramics, has increased by 30% ($K = 41$). A decrease in dielectric constant was not observed for the CSGN1 crystal with a slightly lower Sr concentration than CSGN2 (Tables 4 and 5).

5. Summary

In this work the CSGN system has been investigated as a possible low temperature crystallization, twin-free system for HTSG substrate applications. Numerous new HTSC substrate compositions can be derived by mixing of different perovskite compounds classified into 10 groups. From preliminary investigations on ceramic samples, the $Ca(Ga_{1/2}Nb_{1/2})O_3$–$Sr(Ga_{1/2}Nb_{1/2})O_3$ system was selected for study in more detail. It has been established that the effective distribution coefficient of calcium in CSGN crystal (k_{eff}(Ca)) is quite low (k_{eff}(Ca) = 0.36–0.42), which can easily promote the formation of defects, which can be ascribed to constitutional supercooling during the crystal growth process. This effect can be partly compensated for by using Sr-excess (35:65 mol% CGN:SGN starting composition) in the melt. Consequently, high-quality, twin-free, transparent single crystals with limited size were achieved in the upper 1/3 of CSGN2 crystals. The measured lattice parameter of the cubic unit cell was $a = 3.994$ Å, and the thermal expansion coefficient was $\alpha = 18.5 \times 10^{-6}$ °C^{-1}, providing excellent matching with YBCO in the c direction (α_c(YBCO) = 19×10^{-6} °C^{-1}). Dielectric properties with reasonably low loss ($K = 41$, tan $\delta \leq 3 \times 10^{-4}$) were observed for CSGN crystals.

In summation, the CSGN system has acceptably good physical properties for HTSC substrate applications; however, this system contains structural-type growth difficulties.

6. Acknowledgements

The authors are grateful to Professor Rustum Roy for his important comments, to Professor E.C. Subbarao, Drs. G. Harshe, R. Guo, P. Ravindranathan, and U. Selvaraj for their helpful scientific consultations as well as to Dr. R.P. Brodeur for his careful review of the manuscript. This work was supported by the Defense Advanced Research Project Agency (DARPA) under the contract DN 0014-90-J-4140.

7. References

[1] J.G. Bednorz and K.A. Müller, Z. Physik B64 (1986) 189.
[2] M.K. Wu, J.R. Ashburn, C.J. Torng, P.H. Hor, R.L. Meng, L. Gao, Z.J. Huang, Y.Q. Wang and C.W. Chu, Phys. Rev. Lett. 58 (1987) 908.
[3] H.J. Scheel, M. Berkowski and B. Chabot, J. Crystal Growth 115 (1991) 19.
[4] P. Choudhari, R.H. Koch, R.B. Laibowitz, T.R. McGuire and R.J. Gambino, Phys. Rev. Lett. 58 (1987) 2684.
[5] R.L. Sandstrom, E.A. Giess, W.J. Gallagher, A. Segmüller, E.I. Cooper, M.F. Chisholm, A. Gupta, S. Shinde and R.B. Laibowitz, Appl. Phys. Lett. 51 (1988) 1874.
[6] R.W. Simon, C.E. Platt, A.E. Lee, G.S. Lee, K.P. Daly, M.S. Wire, J.A. Luine and M. Urbanik, Appl. Phys. Lett. 53 (1989) 2677.
[7] H.M. O'Bryan, P.K. Gallagher, G.W. Berkstresser and C.D. Brandle, J. Mater. Res. 5 (1990) 183.
[8] F.S. Galasso, Structure, Properties and Preparation of Perovskite-type Compounds, (Pergamon, Oxford, 1969).
[9] H.J. Scheel, M. Berkowski and B. Chabot, Physica C 185–189 (1991) 2095.

[10] R. Uecker, P. Reiche, V. Alex, J. Doerschel and R. Schalge, J. Crystal Growth 137 (1994) 278.
[11] D. Mateika, H. Kohler, H. Laudan and E. Völkel, J. Crystal Growth 109 (1991) 447.
[12] M. Sasaura and S. Miyazawa, J. Crystal Growth 131 (1993) 413.
[13] D.B. Rogers et al., J. Appl. Phys. 37 (1966) 1431.
[14] G. Shirane, R. Newnham and R. Pepinsky, Phys. Rev. 96 (1954) 581.
[15] L.E. Cross and B.J. Nicholson, Phil. Mag. (Ser. 7) 46 (1955) 453.
[16] G.H. Jonker, Physica 22 (1956) 707.
[17] W.J. Merz, Phys. Rev. 75 (1949) 687.
[18] R. Guo, A.S. Bhalla, J. Sheen, F.W. Ainger, S. Erdei, E.C. Subbarao and L.E. Cross, J. Mater. Res., to be published.
[19] R. Guo, A.S. Bhalla and L.E. Cross, J. Appl. Phys., to be published.
[20] F. Galasso and J. Pinto, Nature 207 (1965) 70.
[21] F. Galasso and W. Darby, Inorg. Chem. 1 (1965) 71.
[22] R. Roy, J. Am. Ceram. Soc. 37 (1954) 581.
[23] C.D. Brandle and V.J. Fratello, J. Mater. Res. 5 (1990) 2160.
[24] S. Nomura, Ferroelectrics 49 (1983) 61.
[25] R.S. Roth, J. Res. Natl. Bur. Std. (US) RP 2736 (1957) 58.
[26] E.A. Wood, Acta Cryst. 4 (1951) 353.
[27] M. Wells and D. Megaw, Proc. Phys. Soc. (London) 78 (1961) 1258.
[28] I. Naray-Szabo, Müegyetemi Közlemények 1 (1947) 30.
[29] L.L. Quill, Z. Anorg. Allgem. Chem. 208 (1932) 257.
[30] P. Vousden, Acta Cryst. 4 (1951) 373.
[31] S. Geller, Acta Cryst. 10 (1957) 243.
[32] F. Galasso and J. Pinto, Inorg. Chem. 4 (1965) 255.
[33] M. German and L.M. Kovba, Russ. J. Inorg. Chem. 28 (1983) 586.
[34] J. Schwarzbach and H. Kralove, Czech. Patent 149524 (1973).
[35] P. Ravindranathan et al., to be published.
[36] K. Hayashi et al., Mater. Res. Bull. 21 (1986) 289.
[37] K. Hayashi et al., Mater. Res. Bull. 21 (1986) 523.
[38] V.S. Filip'ev and E.G. Fesenko, Sov. Phys.-Cryst. 10 (1965) 243.
[39] S. Erdei, $Sr(Ga_{1/2}Ta_{1/2})O_3$ fiber crystal grown by LHPG technique, unpublished data.
[40] H. You, U. Welp and Y. Fang, Phys. Rev. B 43 (1991) 3660.
[41] W. Wong-Ng, F.W. Gayle, D.L. Kaiser, S.F. Watkins and F.R. Fronczek, Phys. Rev. B 41 (1990) 4220.
[42] S. Erdei, Zs. Szaller, K. Raksányi and Gy. Matók, Crystal Res. Technol. 20 (1985) 1047.
[43] J.W. Rutter and B. Chalmers, Can. J. Phys. 31 (1953) 15.
[44] R.F. Sekerka, in: Crystal Growth: An Introduction, Ed. P. Hartman (North-Holland, Amsterdam, 1973) p. 403.
[45] W. Bardsley, J.M. Callan, H.A. Chedzey and D.T.J. Hurle, Solid State Electron. 3 (1961) 142.
[46] D.T.J. Hurle, O. Jones and J.B. Mullin, Solid State Electron. 3 (1961) 317.
[47] W. Bardsley and B. Cockayne, in: Crystal Growth, Ed. H.S. Peiser (Pergamon, Oxford, 1967).

Appendix 12.

"Candidate HTSC Film Substrates of Complex Oxide Perovskite Compositions," *Epitaxial Oxide Thin Films and Heterostructures, Proceedings of the MRS Spring Meeting* SPIE 1994 (Sept. 1994).

Ruyan Guo

A.S. Bhalla

Rustum Roy

L.E. Cross

CANDIDATE HTSC FILM SUBSTRATES OF COMPLEX OXIDE PEROVSKITE COMPOSITIONS

RUYAN GUO, A.S. BHALLA, RUSTUM ROY AND L.E. CROSS
Materials Research Laboratory, The Pennsylvania State University, University Park, PA 16802

ABSTRACT

The research focused upon generating new substrate materials for the deposition of superconducting yttrium barium cuprate (YBCO) has yielded several new hosts in complex perovskites, modified perovskites, and other structure families. New substrate candidates such as $Sr(Al_{1/2}Ta_{1/2})O_3$ and $Sr(Al_{1/2}Nb_{1/2})O_3$, $Ba(Mg_{1/3}Ta_{2/3})O_3$ in complex oxide perovskite structure family and their solid solutions with ternary perovskite $LaAlO_3$ and $NdGaO_3$ are reported. Conventional ceramic processing techniques were used to fabricate dense ceramic samples. A laser heated molten zone growth system was utilized for the test-growth of these candidate materials in single crystal fiber form to determine crystallographic structure, melting point, thermal, and dielectric properties as well as to make positive identification of twin free systems. Some of those candidate materials present an excellent combination of properties suitable for microwave HTSC substrate applications.

INTRODUCTION

There is great interest worldwide in the deposition of high quality thin films of high Tc superconductors (HTSC), using a whole variety of available deposition techniques. The selection of useful substrate materials is of first importance and is subjected to a number of constrains such as: thermal and chemical stability under the conditions used in the film processing and operating; suitable lattice parameter and ionic structure matching; thermal compatibility in terms of thermal expansion matching over the temperature range of film processing and operating; physical properties suitable for specific use (for instance the dielectric constant and loss for electronic devices and high thermal conductivity for high-power-density applications); commercial availability and if possible, low cost.

In addition to satisfy the general requirements, substrates to be used in microwave devices must be twin-free single crystals with potential to be grown in large size (2-4" wafer). Congruent melting compositions with modest melting temperatures are therefore favorable. The dielectric constant influences the propagation speed and the package dimensions therefore a moderately low dielectric constant (<25) is required. Because the conductor loss of the superconductor is diminished, the role of the dielectric loss becomes critically important. Very low dielectric loss ($<10^{-4}$) is therefore demanded.

The potential application of YBCO superconductor to the development of ultra high density interconnect systems for a new generation of high speed high density multichip modules dictates new requirements for the substrate design. An essential feature is the geometry of the X and Y layers of HTSC lines that must have geometries in cross section of order 2 x 1 μ meters thus necessitating a current carrying capability for the HTSC of $\sim 10^6$ A/cm^2. For this current capability clearly the YBCO must be highly grain oriented very near to single crystal, so that the whole multilayer structure is in the form of very highly oriented overgrowths on a single crystal substrate. Impedance characteristics for the interconnect structure dictate that the dielectrics used must be of low permittivity (ideally <10) if the geometry is to be preserved. Highly oriented thin films (2 μm or above) will be needed for the separation of strip line and ground plane structures. Dielectric loss requirements are a little less stringent than those required for the microwave applications; however, $\tan\delta < 0.001$ is highly desirable at the 77K working temperature.

The family of substrates with the perovskite structure is most important as those materials are among the most obvious candidates for epitaxial growth of YBCO films. Substrates of perovskite structure

This paper has been accepted for publication in Proceedings of MRS94 Spring Meeting.

usually have the ideal cubic (such as $SrTiO_3$), double cell cubic (such as Ba_2YSbO_6), hexagonal distorted pseudo cubic (such as $LaAlO_3$) or other pseudo cubic cells (such as $NdGaO_3$ that has the $[GdFeO_3]$ structure with orthorhombic symmetry). $SrTiO_3$ crystals of high quality and large sizes, though are readily available and yield the best epitaxial quality thin films (primarily due to their close interatomic structure matching to the HTSC), have high dielectric constant (>300) arising from the phase transition near the working temperature (~110K). Another probably the most used substrate currently, $LaAlO_3$, though good in lattice matching and of reasonable dielectric properties, is heavily twinned and goes through a ferroelastic phase transition at ~435°C.[1] These macroscopic defects in the crystals are not tolerable in substrates used for complex microcircuits.

In our ongoing search for substrates suitable for microwave device and integrated circuit applications, the focus has been upon developing and identifying new substrate materials primarily with perovskite structures for the deposition of superconducting yttrium barium cuprate (YBCO) films. It became increasingly clear to us that the demand on the substrates to have a close "lattice match" was in many cases less appropriate. Similarity in structure is a higher order criterion than simply lattice parameter matching though they are not independent. An ongoing wide range search for new low permittivity candidate materials using the predictive capability of the phenomenological ionic polarizability arguments is briefly described. The unique capabilities of a laser heated molten zone (LHMZ) growth system have been utilized for test-growth of candidate materials in single crystal fiber form to determine structure, thermal, and dielectric properties and make positive identification of twin free systems. This paper reports the combination of experimental and theoretical approaches in this field with focus on the complex oxide perovskites and related solid solutions.

CRYSTALS OF COMPLEX OXIDE PEROVSKITE COMPOUNDS

Ceramic samples were prepared by solid state reaction, using conventional techniques. X-ray diffraction technique was used extensively to characterize the crystallographic phases and to adjust the processing conditions. The laser heated molten zone growth method has been shown to be a powerful method for rapidly growing small diameter single crystals, particularly oxides of high melting temperature, for both property studies and fiber devices.[2,3,4] The LHMZ equipment used in this investigation consisted of a power source (water cooled, tunable flowing gas CO_2 55W laser), an optical layout, and a growth section. The molten zone temperature during a stable growth was monitored using an optical pyrometer.

Radio frequency dielectric constants and the tangent loss were measured using a General Radio 1621 Capacitance Measurement System. Dielectric properties at microwave frequency were measured using resonance techniques equipped with an HP8510A network analyzer. Post resonance technique (the Hakki and Coleman technique) was used to measure the dielectric constants of the ceramic samples. Cavity perturbation technique was used for the measurements on samples of thin rod (e.g., single crystal fiber samples) or bar-shaped. The Q factors (of microwave frequency) at liquid nitrogen temperature were measured by a transmission resonance technique.

$Ba(Mg_{1/3}Ta_{2/3})O_3$ (BMT)

Ceramics of complex perovskite oxides $A(B1_{1/3}B2_{2/3})O_3$ type have been explored previously as the candidate materials with excellent microwave dielectric properties.[5] $Ba(Mg_{1/3}Ta_{2/3})O_3$ (BMT), in particular, was reported to have a dielectric constant κ~25 and dielectric Q~16,800 (one of the highest in the oxide family) at 10.5 GHz, in samples with 1 mol% Mn additive as a sintering aid.[6] BMT compound is one of the most refractory oxides known thus the growth of single crystals is difficult. A single crystal of BMT was grown from a BaF_2 flux. It yielded a significantly higher dielectric constant (~200),[7] presumably attributable to the flux contamination.

BMT single crystal fibers were grown successfully using our LHMZ technique. It grows congruently from the melt in the temperature range of 2900-3100°C. A high temperature phase of simple cubic

perovskite was obtained at room temperature, in comparison to the hexagonal ordered perovskite structure usually obtained in ceramics. Dielectric properties of both the ceramic and the single crystal BMT were studied. BMT ceramic samples have ultra low dielectric loss ($<1x10^{-5}$ at 90K and 10kHz) and good thermal compatibility ($\alpha \sim 9.0x10^{-6}/°C$) with the YBCO superconductors. The single crystal BMT has a cubic lattice parameter a=4.0877Å. The dielectric constant increases and saturates as the bulk density approaches the theoretical density. Dielectric loss reduces with the enhancement of the ordering of the B-site. Single crystals of high temperature disordered cubic form preserve a moderate dielectric constant (26.0 at 10GHz) and low dielectric loss tanδ ($2.78x10^{-4}$ at room temperature and 10kHz and $<10^{-5}$ at 90K) that make this material unique for microwave device applications.

The BMT lattice parameter of a=4.0877Å, represents a lattice mismatch of 5.3% to the b-axis of YBCO (b=3.883Å); this seems less ideal as a substrate for YBCO. However, there has been no clear cut-off for lattice parameter matches for "epitaxial" (or highly oriented) film deposition of YBCO. "Epitaxial" YBCO thin films on MgO single crystals (with mismatch of 8.5%) have been reported.[8] A BMT single crystal has a twin-free cubic perovskite structure that is advantageous as a substrate compared to some of the heavily twinned substrates, e.g., $LaAlO_3$ and $NdAlO_3$. High temperature BMT single crystal grown by LHMZ is twin free, of moderate dielectric constant, low dielectric loss, and good thermal expansion matching and is therefore identified to be a potentially suitable substrate for the HTSC thin film deposition.

The application of BMT as a substrate, beside its fiber crystals' applications for microwave antenna, may be restricted by the fact that single crystals are difficult to grow. Skull melting growth techniques,[9] could presumably be used to grow BMT crystals of adequate sizes. The high melting temperature of BMT will not be a crucial issue, when the material is used as an insulating layer between the YBCO films in a multichip-module type of integrated structure, because vapor phase deposition techniques (e.g., laser ablation and metal-organic chemical vapor deposition) rather than liquid phase growth methods will be utilized.

$Sr(Al_{1/2}Ta_{1/2})O_3$ (SAT) and $Sr(Al_{1/2}Nb_{1/2})O_3$ (SAN)

The compounds of $Sr(Al_{1/2}Ta_{1/2})O_3$ (SAT) and $Sr(Al_{1/2}Nb_{1/2})O_3$ (SAN) were first prepared and tested to learn their crystallographic phases and melting behavior by the group at the AT & T Bell Labs.[10] Ceramic samples were identified to have double cell cubic perovskite structure with a=7.795Å and melting temperatures of 1900°C and 1790°C for SAT and SAN, respectively. On the basis of our understandings of the crystal chemistry-dielectric property relation of various oxide perovskites, and the reports by the Bell Labs group that showed both the SAN and SAT melt congruently and produce a single phase of the perovskite structure after melting, we selected the SAT and SAN as primary candidates in the $A(B1_{1/2}B2_{1/2})O_3$ complex oxide perovskite family for crystal growth and to investigate their properties in relation to substrate applications.

$Sr(Al_{1/2}Ta_{1/2})O_3$ (SAT) and $Sr(Al_{1/2}Nb_{1/2})O_3$ (SAN) are grown using the LHMZ growth technique. Their crystallographic structures are found to be simple cubic perovskite with lattice parameters a=3.8952Å (SAT) and a=3.8995Å (SAN) that are of close lattice matching to the YBCO superconductors. No structural phase transitions or twins have been found and the average coefficients of the thermal expansion are in good matching with the YBCO superconductor materials. SAT currently represents one of the best potential HTSC substrate materials for microwave applications. The unique feature of this material is that it has desired dielectric properties (dielectric $\kappa \sim 12$, loss factor $\tan\delta < 10^{-4}$) at the microwave frequencies with twin-free lattice and good thermal expansion matching along with chemical compatibility with the YBCO superconductors.

Our experimental results on the SAT composition along with the earlier report on the congruent melting nature of the SAT and SAN compounds, have stimulated research works in the thin film area. MOCVD-derived SAT films grown at 850°C on $LaAlO_3$ were found to have exclusively (001) growth with in-plane orientation.[11] Using SAT polycrystalline materials as targets in a pulsed laser deposition process, Findikoglu *et al.*[12,13] have reported high quality epitaxial (c-axis orientation) growth of thin films of SAT

and multilayers of YBCO/SAT on (001) $LaAlO_3$ and MgO substrates. Dielectric constants of the SAT films (~100-390nm thick), however, were reported to be ~23-30, notably higher than the value (κ~12) found in bulk ceramic materials. The deviations from perfect cation stoichiometry in films may be one of the causes for the discrepancy in value of the dielectric constants as the Al/Ta ratio in SAT films was found to be ~0.8 rather than the stoichiometric ratio of unity.[12,13] No dielectric loss data has been reported for the SAT films therefore direct comparison between the dielectric constants of the film and that of the bulk SAT sample is not intended.

SOLID SOLUTION OF TERNARY AND COMPLEX PEROVSKITE OXIDES

Further modification of the SAN and SAT compositions has been carried out to fine tune their properties, particularly reducing their melting temperatures (SAT: 1900~(1908±25), and SAN:1790~(1739±10))[10, 14] for easier fabrication of the crystals and better control of the reduction problem of the Nb^{5+} and Ta^{5+}. This modification was also an attempt to overcome the twinning problem and to stabilize the cubic phase at room temperature in $LaAlO_3$ crystals.

$LaAlO_3$ has a rhombohedrally distorted perovskite ($A^{3+}B^{3+}O_3$ type) structure. Although the La^{3+} ion generally prefers the 12-coordination-site, it has a tendency for 9-coordination. The distortion in the LaO_{12} polyhedron is brought about by a slight displacement of the oxygen atoms away from the ideal positions of the cubic perovskite-form, that is more clearly shown in other $[rear\text{-}earth]^{3+}AlO_3$ family members when the A-site cation radii become even smaller, e.g., in the case of $PrAlO_3$.[15, 16] In fact, no ideal cubic perovskite structure but the rhombohedral [$LaAlO_3$] and the orthorhombic [$GdFeO_3$] structure have been reported in ternary compounds of the $[A]^{3+}[B]^{3+}O_3$ type.[17] For aluminate compounds, rhombohedral symmetry is found when A-site is occupied by the largest A^{3+} cation, La^{3+}, and other $[A]^{3+}[Al]^{3+}O_3$ compounds have even lower symmetry.

Our approach following this direction was to introduce "balanced" cation substitution simultaneously in the A- and B-sites to increase the average cation size at the A-site, hence to stabilize the 12-coordination of that position and consequently the cubic perovskite structure. The solid solution of ternary $LaAlO_3$ and complex oxides of $Sr(Al_{1/2}Ta_{1/2})O_3$ or $Sr(Al_{1/2}Nb_{1/2})O_3$ was chosen for investigation.

By forming crystalline solutions with compounds of low melting temperatures, it was expected that the crystalline solution would result in lower melting temperature and consequently avoid the reduction problem and permit growth in platinum crucibles. $NdGaO_3$ was found to have a melting temperature of ~1484±24°C, and it was therefore selected as an end member of the crystalline solution series with SAT and/or SAN for the present studies. $NdGaO_3$ has the [$GdFeO_3$] structure with orthorhombic symmetry. No twinning problems are reported in this material. YBCO thin films deposited on $NdGaO_3$ were of better quality compared to those deposited on $LaAlO_3$ substrates. However, the high dielectric loss in the $NdGaO_3$ is a limiting factor for the YBCO film applications in microwave devices.

Single crystal fibers of modified strontium aluminum tantalum oxide $(1\text{-}x)Sr(Al_{1/2}Ta_{1/2})O_3{:}xLaAlO_3$ (SAT:LA) and $(1\text{-}x)Sr(Al_{1/2}Ta_{1/2})O_3{:}xNdGaO_3$ (SAT:NG), and modified strontium aluminum niobium oxide $(1\text{-}x)Sr(Al_{1/2}Nb_{1/2})O_3{:}xNdGaO_3$ (SAN:NG) and $(1\text{-}x)Sr(Al_{1/2}Nb_{1/2})O_3{:}xLaAlO_3$ (SAN:LA) were grown using a laser heated molten zone growth technique.[18] 0.7SAT:0.3LA grows congruently and remains twin free simple cubic perovskite structure (as the SAT) when cooled down to room temperature. 0.7SAT:0.3LA crystals have moderate dielectric constant (κ=21.7) and low dielectric loss ($\tan\delta=7.5\times10^{-5}$) at 10 kHz and 90K. The reduction problem of Ta^{5+} is eliminated (which is common in the case of SAT growth). 0.7SAT:0.3NG and 0.7SAN:0.3NG have lower melting temperatures and crystal growth is easier. $NdGaO_3$ addition to the SAT and SAN enhances the potential of SAT and SAN as large area substrates for HTSC growth. However, the dielectric constants increased from κ~12 to κ~16 (0.7SAT:0.3NG) and from κ~18 to κ~23 (0.7SAN:0.3NG) as a result of $NdGaO_3$ incorporation.

Our results further confirmed the report of Mateika *et al.*[19,20] that the ideal cubic phase can be formed in $(La,Sr)(Al,Ta)O_3$ compounds. It is interesting to notice that similar substitutions using [Ca,Ta] instead of [Sr,Ta] did not produce a compound with cubic structure. The average A-site cation radii of the

[Ca,Ta] substitution is smaller than that of $LaAlO_3$ (ionic radii of Ca^{2+}, La^{3+}, and Sr^{2+} are 1.14, 1.185, and 1.27Å, respectively),[21] therefore, no stabilization effect on 12-coordination A-site is expected.

The cubic symmetry for the compound of SAT-NG and SAN-NG may be due to the fact that Ga^{3+} is almost of the same cation size as Ta^{5+}/Nb^{5+}. Slight reduction in the A-site cation size is accompanied by the slight increase of the B-site cation size and thus the cubic structure of SAN or SAT stays intact.

The ideal cubic perovskite structure can be stabilized in the case of ternary $LaAlO_3$ by forming a crystalline solution composition with cubic $Sr(Al_{1/2}Ta_{1/2})O_3$ and $Sr(Al_{1/2}Nb_{1/2})O_3$. The mechanism of this type of stabilization is through introducing the compensated cation substitution in the form of $[2La^{3+}]+[Al^{3+}] \rightarrow [2A^{2+}]+[B^{5+}]$ with the A^{2+} cation having a radius larger than that of La^{3+} and therefore stabilizing the 12-coordinated A-site. Crystalline solutions of SAT-LA maintained or improved most of the dielectric and thermal properties of $LaAlO_3$ and gained the advantage of forming a twin-free simple cubic structure and improved lattice compatibility. $NdGaO_3$ is shown to be an effective end member to decrease the melting temperature of SAN and SAT without disturbing their simple cubic (twin-free) crystal structure. Dielectric constants of SAN and SAT with addition of the $NdGaO_3$ were increased; however, the dielectric loss factor still remained less than $5x10^{-4}$. The results suggesting that SAT-LA and SAN-LA are better candidates as substrate materials than $LaAlO_3$ because the latter is intrinsically twinned. The growth of SAT-NG and SAN-NG are comparatively convenient as they have relatively low melting temperatures together with the relatively lower dielectric constants and the ideal lattice constants and thermal compatibility with the YBCO superconducting materials.

Other substrate candidates such as $La(Mg_{2/3}Ta_{1/3})O_3$,[22] $La(Mg_{1/2}Ti_{1/2})O_3$,[23] $(Ca,Sr)(Ga,Nb)O_3$[24] and a family of materials of the magnetoplumbite structures[25] have also been fabricated and their dielectric properties studied. These crystals and their associated solid solutions provide several new options for ultra low loss, low permittivity, twin free oxides with low congruent melting temperature, matching thermal expansion and excellent chemical compatibility.

SUMMARY

Oxide crystals with the perovskite structure are major candidates for YBCO film epitaxial deposition particularly if large size cubic, twin free crystals become available. SAT has already shown promise in high quality epitaxial YBCO film growth. With improved growth capability, the SAT and particularly its modified solid solutions may be more useful than the intrinsically twinned $LaAlO_3$. Solid solutions between the known complex perovskite oxide and ternary end members, especially gallates, will provide large number of options to tailor the material for specific device applications. The property parameters of the newly proposed substrate materials of oxide perovskite family are summarized in Table I. $LaAlO_3$ and $NdGaO_3$ are also listed for comparison.

ACKNOWLEDGMENT

This work was supported by the Defense Advanced Research Projects Agency (DARPA) under the contract No. DN 00014-90-J-4140.

REFERENCES

1 E.A. Wood, *Amer. Min.* **36** 768 (1951).
2 J.S. Haggerty, W.P. Menashi and J.F. Wenckus, U.S. Patent No. 3 944 640 (16 March 1976); U.S. Patent No. 4 012 213 (15 March 1977).
3 R.S. Feigelson, *MRS Bull.* **13** 47 (1988).
4 J. Yamamoto and A.S. Bhalla, *Mat. Res. Bull.* **24** 761 (1989).
5 K. Wakino, *Ferroelectrics* **91** 69 (1989).

[6] S. Nomura, K. Toyama, and K. Kaneta, *Jpn. J. Appl. Phys.* **21**(10) L624 (1982).
[7] F. Galasso and J. Pinto, *Nature* vol. **207** No. 4992, 70 (1965).
[8] e.g., T. Terashima, K. Iijima, K. Yamamoto, K. Irata, Y. Bando, and T. Takada, *Jpn. J. Appl. Phys.* **28**, L987 (1989).
[9] H.R. Harrison and J.M. Honig, *Bull. Mater. Sci.* **3**(3), 247 (1981).
[10] C.D. Brandle and V.J. Fratello, *J. Mater. Res.* **5**(10), 2160 (1990).
[11] B. Han, D. A. Neumayer, B.H. Goodreau, T. J. Marks, H. Zhang, and V.P. Dravid, *Chem. Mater.* (in press).
[12] A.T. Findikoglu, C. Doughty, S. Bhattacharya, Qi Li, X.X. Xi, T. Venkatesan, R.E. Fahey, A.J. Strauss, and J. M. Phillips, *Appl. Phys. Lett.* **61** 1718 (1992).
[13] A.T. Findikoglu, S. Bhattacharya, C. Doughty, M.S. Pambianchi, Qi Li, X.X. Xi, S.M. Anlage, R.E. Fahey, A.J. Strauss, J.M. Phillips, and T. Venkatesan, *IEEE Trans. Appl. Superconductivity*, **3**(1) 1425 (1993).
[14] R. Guo, A.S. Bhalla, J. Sheen, F. Ainger, E.C. Subbarao, S. Erdei, and L.E. Cross, *J. Mat. Res.* (in press, 1994).
[15] R.D. Burbank, *J. Appl. Cryst.* **3** 112 (1970).
[16] O. Muller and R. Roy, in "*The major ternary structural families*" (Springer-Verlag, Berlin, Heidelberg, New York 1974) p.215.
[17] F.S. Galasso, in "*Structure, properties and preparation of perovskite-type compounds*" (Pergamon Press, Oxford, London, Edinburgh, New York, Toronto, Sydney, Paris, Braunschweig 1969) p.10.
[18] R. Guo, P. Ravindranathan, U. Selvaraj, A.S. Bhalla, L.E. Cross, and R. Roy, *J. Mater. Sci.* (in press, 1994).
[19] S. Haussühl and D. Mateika, *Crystal. Res. Technol.* **26**(4) 481 (1991).
[20] D. Mateika, H. Kohler, H. Laudan and E. Völkel, *J. Cryst. Growth* **109** 447 (1991).
[21] R.D. Shannon and C.T. Prewitt, *Acta Cryst.* **B25** (1969) 925; *Acta Cryst.* **B26** 1046 (1970).
[22] P. Ravindranathan and A.S. Bhalla *et al.* (to be published).
[23] G. Harshe, A.S. Bhalla, and L.E. Cross, *Materials Letters* (in press, 1994)
[24] S. Erdei, L.E. Cross, F.W. Ainger, and A.S. Bhalla, *J. Cryst. Growth* (in press, 1994).
[25] R. Guo and A.S. Bhalla (to be published).

TABLE I. Properties of Some Newly Proposed Oxide Perovskite Substrate Materials

Composition	symmetry	Lattice Constant (Å)	κ 10kHz 90K	tanδ 10kHz 90K	α (x10-6/°C) (@~300K)	Melting Point (°C) *
BMT (crystal)	Cubic	4.0877	25.9	$<10^{-5}$	9.0	(>2800)
SAT	Cubic	3.8952	11.8	4.2×10^{-5}	9.7	1908±25
SAN	Cubic	3.8995	18.7	2.2×10^{-4}	8.5	1739±10
SAT-LA	Cubic	3.8727	21.7	7.5×10^{-5}	7.7	1830±22
SAN-LA	Cubic	3.8634	25.7	2.8×10^{-4}	9.5	1705+20
SAT-NG	Cubic	3.8866	16.0	4.3×10^{-4}	8.8	1767±31
SAN-NG	Cubic	3.8790	23.0	5.2×10^{-4}	10.8	1582±20
$LaAlO_3$ (crystal)	Rhomb.	a=3.789 a=90.12°	23	7.5×10^{-5}	8.2//[1 $\bar{1}$ 0] 6.4//[001]	2040±9
$NdGaO_3$ (crystal)	Ortho.	a=5.426 b=5.502 c=7.706	23 (77K,10GHz)	3.2×10^{-4}		1484±24

*The melting point was determined rather simply using a strip furnace, with two operators using two separate optical pyrometers and averaging several readings per sample.